Author:
Cooper, Samson

Title:
Identification and Validation of Non-linearities in Vibrating Structures

Identification and Validation of Non-linearities in Vibrating Structures

By

SAMSON BIDEMI COOPER

Department of Mechanical Engineering

School of Civil, Aerospace and Mechanical Engineering

UNIVERSITY OF BRISTOL

A dissertation submitted to the University of Bristol in accordance with the requirements of the degree of DOCTOR OF PHILOSOPHY in the Faculty of Engineering.

AUGUST 2019

Word count: 95000 Approximately

Abstract

Most engineering sectors are going through an era of digital transformation or transition, where they are becoming more dependent on simulation models to make decisions about the design of engineering structures. However, there still exist several engineering problems that have significant lack of confidence associated with simulation-based engineering designs. An example of such problem is the issue of modelling local non-linearities between joints and assembled structures, a core topic of this thesis. An approach for solving this challenge is based on exploiting the advantages of combining experimental and simulation data to produce a validated and verified design, an initial step in the digital twin concept. Modal testing and analysis has been an established method used for connecting experimental models with simulation models for linear vibrating structures using the notion of vibration modes, where a simulation model is often a Finite Element model of the physical structure. However, operational performance of recent engineering structures have been acknowledged to exhibit complex nonlinear phenomena which can no longer be handled by the current linear techniques. In addition, strong emphasis is now devoted to account for non-linearities for current and future designs.

The objective of this thesis is motivated by the industrial needs to progress the development of integrating experimental test and simulation methods for nonlinear vibrating structures. The demonstration of the test and simulation integration approach adopted in this thesis is founded on three different complementary model types, namely, white, black and grey box models. The first part of the thesis presents a black-box data driven approach for modelling local non-linearities. In this case, the entire non-linear identification and simulation is derived from experimental data with no prior knowledge or assumption of the non-linear characteristics with demonstration done on measured data obtained from the experimental campaign of an aero-engine casing structure.

The second part of this thesis is devoted to the requirement for quantifying and associating physics-based parameters to each non-linear characteristic observed in an engineering structure. A novel method for non-linear system identification based on revising an existing black-box oriented state space model technique is presented. The proposed time-domain method is formulated based on converting a black-box oriented state space model algorithm for a nonlinear system to a grey-box state space model. The advantage of this method is the ability to extract a lower number of parameters with physics based interpretation. This method is tested and validated on simulated data and experimental data obtained from an aerospace structure. The final part of this thesis addresses the current challenge of predicting the vibration response and validating simulated models of assembled engineering structures with identified non-linearities. This challenge is investigated through a framework strategy that permits simulation model parameters to be updated and upgraded based on experimental observations, to constitute a white-box model approach. This is achieved by embedding the current linear modal analysis technique into a test-simulation integration framework for non-linear systems.

ACKNOWLEDGEMENTS

I would like to recognise the Engineering Physical Science and Research Council (EPSRC) for the financial support received through the University of Bristol. Part of this research was also funded by the Atomic Weapon Establishment (AWE) which is gratefully acknowledged.

Sincere gratitude to my supervisors, Dr Branislav Titurus, Dr Dario DiMaio and Professor David Ewins for their constant guidance and encouragement provided during the course of this research. Special thanks to Dr Branislav for his continuous stream of ideas on the presentation of the results from this research and his meticulous reading of the thesis draft.

I am grateful to Professor Matthew R. W. Brake for inviting me to participate at the summer 2016 edition of the Nonlinear Mechanics and Dynamics Research (NORMAD) Institute organised by Sandia National Laboratory. It was a great opportunity to collaborate with other like minded researchers. I would like to express my profound gratitude to Sandia National Laboratories for sponsoring my travel and accommodation cost during the summer institute.

My sincere appreciation goes to Dr Koen Tiels at Uppsala University and Dr Ludovic Renson at Bristol University for their helpful discussions on some of the methods and results presented in this research. Thanks to many researchers and friends at the BLADE laboratory in Bristol University, for their constructive feedback on my experimental activities.

I would also like to express my gratitude to Professor David Wagg from University of Sheffield and Professor Nicholas Lieven from University of Bristol for accepting to serve on my examination committee, review this thesis and provide valuable comments.

My most love and gratitude are expressed to my wife, (Esosa Elizabeth Cooper) and my son, (Joshua Cooper) for their infinite support and patience during the research.

Finally, I would like to thank the almighty God for giving me the wisdom and excellent spirit to complete this research.

AUTHOR'S DECLARATION

I declare that the work in this dissertation was carried out in accordance with the requirements of the University's Regulations and Code of Practice for Research Degree Programmes and that it has not been submitted for any other academic award. Except where indicated by specific reference in the text, the work is the candidate's own work. Work done in collaboration with, or with the assistance of, others, is indicated as such. Any views expressed in the dissertation are those of the author.

SIGNED: ..... DATE: .....

TABLE OF CONTENTS

Page

List of Tables **xiii**

List of Figures **xv**

Nomenclature **xxiii**

1 Introduction **1**

1.1 Objectives and Contribution of the Thesis 5

1.2 Thesis Outline 7

1.3 List of Publications 9

2 Literature Review **13**

2.1 Introduction 14

2.2 Modelling Non-linearities in Structural Dynamics 16

2.2.1 Theoretical Modelling 17

2.2.2 Numerical Modelling 18

2.2.3 Experimental Testing 19

2.3 Sources of Non-linearities in Engineering Structures 20

2.3.1 Geometric Non-linearity 20

2.3.2 Material Non-linearity 21

2.3.3 Non-linearity From Governing Equations of Motion 22

2.3.4 Damping Dissipation and Friction 23

2.3.5 Boundary Condition Effects 24

2.4 Overview of Non-linear System Identification Methods 25
2.4.1 Linearisation Methods 27
2.4.2 Time Domain Methods 28
2.4.3 Frequency Domain Methods 30
2.4.4 Modal Methods 33
2.4.5 Time-Frequency Methods 35
2.4.6 Structural Model Updating Methods 36
2.4.7 Black-Box Methods 39
2.5 Non-linear System Identification Process 41
2.5.1 Detection of Non-linearity 42
2.5.2 Location of Non-linearity 44
2.5.3 Characterisation of Non-linearity 44
2.5.4 Parameter Estimation of Non-linearity 45
2.6 Representation of Non-linear Systems 46
2.7 Limitations of Current Identification Methods and Processes 48

3 Identifying Nonlinearities based on State Space Models 51
3.1 Introduction 52
3.2 State Space Models 54
3.2.1 Linear and Non-linear State Space Model 55
3.2.2 Bilinear State Space Models 55
3.2.3 Other Types of State Space Models 56
3.3 Polynomial Non-linear State Space Model 58
3.3.1 Approximation Behaviour 59
3.3.2 Model Structure 59
3.3.3 Model Stability 60
3.4 A PNLSS Approach to Identification of Structural Non-linearities 61
3.4.1 Best Linear Approximation 62
3.4.2 Non-linear Optimisation of a Linear Model 66

3.4.3 Estimation of a Full Non-linear Model 67
3.4.4 Validation of the Non-linear Model 72
3.5 Demonstration on an Aero-Engine Casing 73
3.5.1 Description of the Aero-Engine Casing 73
3.5.2 Linear Finite Element Modal Analysis 74
3.5.3 Experimental Campaign and Linear Modal Analysis 76
3.5.4 Best Linear Approximation of the Casing Assembly 81
3.5.5 Non-linear Identification of the Casing Assembly 87
3.5.6 Identifying a Parsimonious Data Data Driven Model 90
3.5.7 Model Validation Based on Sine-Sweep and Broadband Excitation 96
3.6 Remarks on PNLSS Approach for Non-linear Identification 101
3.7 Conclusions 102

4 Grey-box State Space Identification of Non-linear Vibrating Systems. 105
4.1 Introduction 106
4.2 Time Domain Grey-box State Space Identification Method 108
4.2.1 Step 1 - Nonlinear Model Formulation in the physical domain 109
4.2.2 Step 2 - Continuous-time Model Discretisation 110
4.2.3 Step 3 - Approximation of the Discretised Model 112
4.2.4 Step 4 - Formulation of a Discrete Grey-box PNLSS Model 114
4.2.5 Step 5- Estimation of the Discrete-time Non-linear Feedback Model 119
4.2.6 Step 6 - Estimation of the Continuous-Time Model 123
4.2.7 Grey-box PNLSS Identification Process 124
4.3 Numerical Demonstration on a Duffing Oscillator 127
4.3.1 Problem Description 128
4.3.2 Best Linear Approximation of the Duffing Oscillator 130
4.3.3 Linear Grey-box State Model of the Duffing Oscillator 131
4.3.4 Nonlinear Initialisation of the Duffing Oscillator Model 132
4.3.5 Estimation of the Nonlinear Coefficients of the Duffing Oscillator 134

4.3.6 Improving the Stiffness and Damping Estimates . . . 137
4.4 Validation of the Non-linear Feedback Model . . . 139
4.4.1 Multi-sine Data Validation . . . 141
4.5 Conclusions . . . 144

5 Grey-box Identification of an Aerospace Structure. 147
5.1 Introduction . . . 148
5.2 The Aerospace Test Structure . . . 150
5.2.1 Linear Finite Element Model of the MTS . . . 151
5.3 Experimental Test and Linear Modal Analysis of the MTS . . . 154
5.3.1 Low Level Test Campaign . . . 155
5.4 Non-linear Detection and Analysis . . . 155
5.4.1 Time Series and FRF Inspection . . . 157
5.4.2 Time Frequency Analysis using the short time Fourier transform . . . 160
5.5 Non-linear Identification Based on Grey-box PNLSS . . . 165
5.5.1 Best Linear Approximation of the Aerospace Test Structure . . . 165
5.5.2 Linear and Nonlinear Initialised Model . . . 166
5.5.3 Estimation of a Full Nonlinear Model of the MTS . . . 169
5.6 Conclusions . . . 172

6 Validation of Nonlinear Vibrating Structures. 175
6.1 Introduction . . . 176
6.2 Integration of FE and test-based identification for nonlinear structures . . . 178
6.3 Demonstration on Cantilever Beam Assembly . . . 181
6.3.1 Description of the Test Structure . . . 181
6.3.2 Linear model validation (phase I) . . . 181
6.3.3 Non-linear identification (phase II) . . . 193
6.3.4 Non-linear FE modelling and validation (phase III) . . . 206
6.4 Conclusions . . . 223

7 Conclusion **227**

7.1 Suggestions and Future Direction of the Research 232

Bibliography **235**

List of Tables

Table **Page**

3.1 Estimated natural frequencies and damping ratios based on low-level excitation . . . 78

3.2 Overview of the polynomial order implemented in the PNLSS identification 87

3.3 *Estimation results for different monomial combination experiments* 92

3.4 Validation results for different monomial combination experiments 96

4.1 *Linear and nonlinear parameters of the Duffing oscillator* 129

4.2 *True and estimated polynomial coefficients of the nonlinear stiffness and nonlinear damping curve of the grey-box PNLSS model. The relative estimation errors on the non-zero true coefficients are indicated in orange.* 137

5.1 *Estimated resonance frequencies and damping ratios based on low-level random data* 157

5.2 *Estimated nonlinear parameters of the Missile Test Structure for Mode 4* 171

6.1 Dimensions of the cantilever beam assembly 181

6.2 Estimated linear resonance frequencies and damping ratios based on low-level excitation183

6.3 Updated FE Model Natural Frequencies and MAC Values for the linear-assembly in Figure 6.2a 186

6.4 Estimated Linear resonance frequencies and damping ratios based on low-level random data for the nonlinear assembly in Figure 6.2b 188

6.5 Updated FE Model Natural Frequencies and MAC Values for the FE model of the nonlinear assembly in Figure 6.2b. 190

6.6 Final Material Properties obtained from the model calibration 190

6.7 Validation Results Using FDAC Values for the FE model of the nonlinear assembly in Figure 6.2b. 192
6.8 Identified parameters 201
6.9 Non-linear Stiffness Elements included in the FE Model of the nonlinear assembly in Figure 6.2 209
6.10 Updated Non-linear Stiffness Coefficient 216
6.11 Error and objective function values (%) for the Non-linear Stiffness updated FE model 216
6.12 Updated Non-linear Damping Coefficient 218
6.13 Error distribution across the Upgraded non-linear FE model 220
6.14 Validation and Error Results Using FDAC and Normalised Error Values 222

LIST OF FIGURES

FIGURE **Page**

2.1 Basic skill sets for an effective structural dynamics solution 16

2.2 Practical Application of Current Identification Methods, sub-categorised by small and large structures 49

3.1 Schematic of the identification procedure 63

3.2 *Aero-engine casing and the attached Aluminium plate on the bottom right corner* . . . 73

3.3 *Selected mode shapes obtained from the 3D FE modal analysis. (a) Mode 1: 83.95 Hz, (b) Mode 2: 87.12 Hz, (c) Mode 11: 233.27 Hz, (d) Mode 14:246.85 Hz.* 75

3.4 *Experimental set-up of the Engine casing suspended on a TRL-6 frame. (a) Test Set-up,(b) Instrumented section of the casing* 77

3.5 *Acceleration response function obtained from low-level broadband excitation performed on the non-linear assembly. (a) Bottom centre of the first cylinder (b) Drive point.* . . . 78

3.6 *Force controlled stepped sine acceleration response: (a) Mnode 2 FRF for frequency range 230-242Hz, (b) Drive point FRF for frequency range 230-242Hz (c) Mnode 2 FRF for frequency range 282-296Hz (d) Drive point FRF for frequency range 282-296Hz.* . . 79

3.7 *Sine-sweep acceleration responses measured on two different locations of the assembly. (a) and (b) Drive point (b) and (d) Mnode2* 80

3.8 *The difference of the sine sweep input DFT spectrum* $(U(k)-U(k-1))$ *of the interested bandwidth. (a) Frequency range 70-93Hz, (b) frequency range 200-260Hz* 82

3.9 *nonparametric FRFs and total distortions in the form of a discrete fourier transform spectrum: (a) Mnode 2 for 70-93Hz (b) Drive point for 70-93Hz.* 84

3.10 *nonparametric FRFs and total distortions in the form of a discrete fourier transform spectrum: (a) Mnode 2 for 200-260Hz (b) Drive point for 200-260Hz.* 84

3.11 *Comparison of initial linear model against measured data: (a) time domain signal for drive point, (b) amplitude of the corresponding discrete time fourier transform for drive point, (c) time domain signal for Mnode, (d) amplitude of the corresponding discrete time fourier transform for Mnode.* 86

3.12 *Comparison of the identified PNLSS model against measured data: (a) time domain signal for drive point, (b) amplitude of the corresponding discrete time fourier transform for drive point, (c) time domain signal for Mnode, (d) amplitude of the corresponding discrete time fourier transform for Mnode.* 89

3.13 *Time and Frequency domain estimated model error for simulated PNLSS model using monomial combination of 2,4 and 3, 5,7: (a) time domain error signal of the drive point, (b) amplitude of the corresponding discrete time fourier transform error of the drive point, (c) time domain error signal of Mnode, (d) amplitude of the corresponding discrete time fourier transform error of Mnode.* 91

3.14 *Decrease of the NRMS estimation error over 120 Levenberg-Marquardt successful iteration for the seven simulated PNLSS models based on different monomial degree combination.* 93

3.15 *Time and frequency domain comparison of the final estimated PNLSS model against measured data based on polynomial order 3, 5 and 7. (a) and (b) Time domain and amplitude of the corresponding discrete time fourier transform for the Bolted connection closest to the drive point between the casing and the plate, (c) and (d) Time domain and amplitude of the corresponding discrete time fourier transform for the Drive point.* . . 95

3.16 *Validation of PNLSS model against measured data for 3-5-7 monomial combinations. (a) Time domain response of the drive point, (b) amplitude of the corresponding discrete time fourier transform of the drive point (c) Time domain response of Mnode 2 (d) amplitude of the corresponding discrete time fourier transform of Mnode 2* 97

3.17 *NRMS Validation error over 120 Levenberg-Marquardt successful iteration for the seven simulated PNLSS models based on different monomial degree combination.* . . 98

3.18 *Time-domain performance of the validated model for the monomials of degree 3-5-7 based on the measured broadband data. (a) Time domain response of the drive point, (b) Zoomed-in time domain response of the drive point, (c) Time domain response of Mnode 2 (d) Zoomed-in time domain response of Mnode 2.* 99

4.1 *Flowchart describing the steps in the Grey-box state space identification algorithm.* . . 109

4.2 *Block-oriented feedback representation of the continuous-time system.* 111

4.3 *Block-oriented feedback representation of the approximated discretised system.* 113

4.4 *Simple input and output mechanical system.* 127

4.5 *A nonlinear mass-spring-damper system.* 128

4.6 *Feedback representation of the mass-spring-damper system.* 128

4.7 *Generated sine-sweep time series and frequency domain response for the SDOF system:(a) Time domain response, (b) amplitude of the corresponding discrete time fourier transform* 129

4.8 *Estimated BLA and non-linear distortions for different force values: (a) amplitude of the discrete time fourier transform of the BLA FRF, (b) amplitude of the discrete time fourier transform of the nonlinear distortions.* 130

4.9 *Estimated Linear model compared with original data and error: (a) time domain response of the SDOF, (b) corresponding displacement amplitude of the discrete time fourier transform of the SDOF.* 131

4.10 *comparison of estimated initial nonlinear model against true nonlinear data. (a) Time domain data response (b) corresponding displacement amplitude spectrum of the discrete time fourier transform.* 132

4.11 *comparison of estimated initial nonlinear model against true nonlinear data. (a) stiffness curve (b) damping curve* 133

4.12 *comparison of the identified nonlinear model against true nonlinear data. (a) time domain data response (b) corresponding displacement amplitude spectrum of the discrete time fourier transform.* 134

4.13 *comparison of the identified nonlinear model against true nonlinear data. (a) nonlinear stiffness curve (b) nonlinear damping curve* 135

4.14 NRMS estimation error over successful Levenberg-Marquardt iterations. 136

4.15 *comparison of estimated optimised nonlinear model against true nonlinear data. (a) stiffness (b) damping* 139

4.16 *comparison of validated nonlinear model against true data. (a) time domain data response (b) corresponding displacement amplitude spectrum of the discrete time fourier transform.* 140

4.17 NRMSE validation error over successful Levenberg-Marquardt iterations. 141

4.18 *Comparison of simulated multi-sine time and frequency domain data at different force levels. (a) time domain data response (b) corresponding amplitude spectrum of the discrete time fourier transform.* 142

4.19 *Comparison of multi-sine estimated model errors against true nonlinear data. (a) time domain data response (b) corresponding magnitude spectrum of the discrete time fourier transform.* 143

4.20 *NRMSE error over successful Levenberg-Marquardt iterations for the multisine data.* 143

5.1 *Missile Test Structure.* 151

5.2 *Individual CAD parts and assembly of the Missile Test Structure.* 152

5.3 *Mesh model of the Missile Test Structure.* 152

5.4 *Linear FE Modes of the Missile Test Structure. (a) mode 1 (b) mode 2* 153

5.5 *Linear FE Modes of the Missile Test Structure.(a) mode 4 (b) mode 5* 153

5.6 *Missile Test Structure Experimental Set-up.* 154

5.7 *FRFs and Coherence responses obtained from low-level broadband excitation.(a) and (b)FRF and coherence response for the centre tube of the Missile, (c) and (d) FRF and coherence response for the far-end of the Hanger.* 156

5.8 *Nonlinearity detection based on envelope time series inspection.(a) measured time signals at different force levels for mode 2 (b) measured time signals at different force levels for mode 4* 158

5.9 *Non-linearity detection based on FRF inspection. (a) MTS Nose, (b) (Hanger)* 159

5.10 *Estimated spectrogram maps obtained for sweep frequency (120-400 Hz) at 1N. (a) and (b) spectrogram of 2 sensors located at the front and rear tube of the MTS. (c) and (d)spectrogram of 2 sensors located at connections between the tube and the launch rail.* 161

5.11 *Estimated spectrogram map obtained for sweep frequency (120-400 Hz) at 3N.(a) and (b) spectrogram of 2 sensors located at the front and rear tube of the MTS. (c) and (d)spectrogram of 2 sensors located at connections between the tube and the launch rail.*162

5.12 *Estimated spectrogram map obtained for sweep frequency (120-400 Hz) at 5N. (a) and (b) spectrogram of 2 sensors located at the front and rear tube of the MTS. (c) and (d)spectrogram of 2 sensors located at connections between the tube and the launch rail.*163

5.13 *Estimated non-parametric BLA FRFs and total distortions for (mode 4). (a) amplitude of the discrete time fourier transform of the BLA FRF, (b) amplitude of the discrete time fourier transform of the nonlinear distortions* 166

5.14 *Estimated Linear grey-box model compared with measured data and error (mode 4). (a) time domain data response (b) corresponding displacement amplitude spectrum of the discrete time fourier transform* 167

5.15 *Estimated nonlinear initialised stiffness and damping curve (mode 4)* 168

5.16 *Comparison of estimated initial nonlinear model against measured data. (a) Time domain data (b) spectrum (mode 4)* 168

5.17 *comparison of the identified nonlinear model against true nonlinear data for mode 4. (a) time domain data response (b) corresponding displacement amplitude spectrum of the discrete time fourier transform.* 170

5.18 *Final estimated nonlinear stiffness and damping curve (mode 4)* 170

5.19 *NRMSE error over successful Levenberg-Marquardt iterations.* 171

6.1 *Data flow scheme of FE and test-based identification integration procedure showing the steps in each phase Courtesy of Arnaldo DelliCarri, University of Bristol, United Kingdom.* 180

6.2 *photograph of the cantilever beam structure.* 182

6.3 *Linear acceleration response function and coherence measured at low-level excitation for the linear assembly. a (drive-point acceleration response) and b (Coherence)* 183

6.4 *Comparison of acceleration response functions at three excitation levels for the linear assembly in figure 2a. (a) Magnitude and (b) coherence: (blue) measured form 0.5N, (d-blue) measured form 3N, and (red) measured from 5N excitation.* 184

6.5 *Finite Element mode shapes of the cantilever beam for the linear assembly in Figure 6.2a. (a) Mode 1, (b) Mode 2, (c) Mode 3 and (d) Mode 4.* 185

6.6 *Comparison between measured data and FE simulated response at the driving point for the first vibration mode of the linear assembly in Figure 6.2a.* 187

6.7 *Acceleration response function and Coherence obtained from low-level broadband excitation performed on the non-linear assembly. (a) Acceleration response and (b) Coherence.* 188

6.8 *Linear Finite Element Mode shapes of the Non-linear Cantilever Assembly in figure 2b. (a) Mode 1 and (b) mode 2.* 189

6.9 *Comparison between measured data and FE simulated response at node 1 and driving point for the first and second modes of the nonlinear assembly. (a) node 1 and (b) drive point.* 191

6.10 *Sine-sweep acceleration data measured on node 1 of the non-linear assembly in Figure 6.2. (a) sine-sweep for mode 1, (b) sine-sweep for mode 2* 195

6.11 *Force controlled Stepped Sine acceleration response measured at Node 1of the non-linear assembly. (a) Mode 1 sweep up, (b) Mode 1 sweep down, (c) Mode 2 sweep up and (d) Mode 2 sweep down.* 196

6.12 *Acceleration Surface plot across the non-linear connection.* 198

6.13 *Qualitative Stiffness curve obtained across the beam connection of the non-linear assembly . Mode 1 (a), Mode 2 (b).* 199

6.14 *Measured vs Polynomial fit stiffness curve of the nonlinear assembly . (a) Mode 1, (b) Mode 2* 200

6.15 *Hilbert Transform based Identified non-linear stiffness and damping curves for the non-linear assembly. (a) Mode 1, (b) mode 2* 203

6.16 *Experimental backbone curves identified from sine-sweep data for the non-linear assembly. (a) Mode 1, (b) Mode 2* 204

6.17 *Experimental damping curves identified from sine-sweep data for the non-linear assembly. (a) Mode 1, (b) Mode 2* 205

6.18 *Schematic diagram of the FE model with non-linear element..* 209

6.19 *Comparison of measured and FE simulated acceleration responses for modes 1 and 2 of the non-linear assembly. (a) driving point and (b) node 1 at 2N (blue) and 5N (red) force levels. Dotted lines are from experiments, continuous lines are from upgraded FE model, before updating (using starting coefficients).* 211

6.20 *Comparison of Stiffness updated acceleration responses with measured data for modes 1 and 2. (a) node 1 and (b) driving point across two force levels. Dotted lines are from experiments, continuous lines are from the updated upgraded FE model.* 215

6.21 *Comparison of Damping and Stiffness updated acceleration responses with measured data for modes 1 and 2.(a) Node 1 and (b) drive point across three force levels. Dotted lines are from experiments, continuous lines are from the updated upgraded FE model.* 219

6.22 *Comparison of measured and FE predicted acceleration responses for mode 3 of the non-linear assembly. (a) Node 1 at 1N and 3N force level; (b) drive point at 1N and 3N ;(c) Node 1 at 4N, 6N and 7N force level; (d) drive point at 4N, 6N and 7N force level. Dotted lines are from experiments, continuous lines are from the predicted FE model.* . 221

NOMENCLATURE

Abbreviations & Acronyms

ANN Artificial Neural Network

ARMA Auto-Regressive Moving Average

ARX Auto-Regressive with exogenous inputs

ASM Acceleration Surface Method

BLA Best Linear Approximation

CNM Complex Non-linear Mode

CRP Conditioned Reverse Path

DDS Dynamic Design Solution

DFT Discrete Fourier Transform

DOF Degree-of-Freedom

DUT Device Under Test

EMA Experimental Modal Analysis

EMD Empirical Mode Decomposition

FANS Force Appropriation of Nonlinear Systems

FD Frequency Domain

FDAC Frequency Domain Assurance Criterion

FE Finite Element

FEA Finite Element Analysis

FEM Finite Element Model

FFD Forward Finite Difference

FFT Fast Fourier Transform

FNSI Frequency domain Nonlinear Subspace Identification

FRF Frequency Response Function

FSR Frequency Sampling Rate

FT Fourier Transform

GN Gaussian Noise

HOFRF Higher-Order Frequency Response Function

LTI Linear Time Invariant

MAC Modal Assurance Criterion

MDOF Multiple-Degree-of-Freedom

MIMO Multiple Input Multiple Output

MISO Multiple Input Single Output

NARX Nonlinear Auto Regressive with eXternal input

NIFO Nonlinear Identification through Feedback of Outputs

NLRD NonLinear Resonant Decay

NLS Nonlinear Least Squares

NNM Nonlinear Normal Mode

NRMSE Normalised Root Mean Squared Error

OMA Operational Modal Analysis

PISPOT Periodic Input, Same Periodic OuTput

PNLSS Polynomial NonLinear State Space

POD Proper Orthogonal Decomposition

POM Proper Orthogonal Mode

RFS Restoring Force Surface

RMS Root Mean Square

RMSE Root Mean Square Error

ROM Reduce Order Model

SDOF Single-Degree-of-Freedom

SIMO Single Input Multiple Output

SISO Single Input Single Output

SNR Signal-to-Noise Ratio

STFT Short Time Fourier Transform

SVD Singular Value Decomposition

TMA Theoretical Modal Analysis

ULM Underlying Linear Model

WLS Weighted Least Squares

CHAPTER 1

INTRODUCTION

Vibration in engineering structures is still regarded as a critical feature when determining the performance of an engineering design, especially in the aerospace and automotive sectors. As such, engineers and researchers are constantly developing methods capable of reducing or eliminating extreme vibration phenomena, mainly because of the associated damage and negative consequences on the final product design. Excessive vibrations experienced by structural components in an aerospace or automotive design can often result in severe disturbance leading to catastrophic consequences or overall failure of the product.

In the last few decades, different studies and techniques for characterising and obtaining the underlying physics of linear vibration phenomena have been developed, where advanced methodologies have been developed to predict and monitor excessive vibration behaviour in structural components. An example is the effective use of modal testing and analysis [1] for identifying linear resonance frequency and damping properties of engineering structures. Other classical techniques for analysing vibration characteristics in the linear domain have also been developed and implemented. Examples are the poly-reference least-squares complex frequency-domain method in [2], the subspace deterministic-stochastic algorithm [3], the eigen-system realisation algorithm [4]. A unified matrix polynomial approach to modal identification was also introduced in [5] and many more linear identification methods which can be found in existing literature.

However, with the continuing interest in increasing the functional performance such as range, reduced fuel consumption for engineering designs and most importantly for each designed product to meet the CO2 emission targets and reduced environmental pollution footprint set by regulating bodies, structural components are now being designed to have certain features such as flexibility, light-weight, adaptation, active control, inter-connectivity and modularity. The presence of these features in engineering designs can often expose structural components to reach high vibration levels resulting from large displacement and introduce or reinforce the presence of nonlinear behaviour in the entire design with examples illustrated in the recent extensive survey [6]. For example, the recently adopted use of composite materials in aerospace and automotive design yields light-weight structures, but their vibration performance can become significantly nonlinear. The use of composite materials in structural engineering also introduces new failure methods which are different from the existing traditional metal materials, one of these failures is delamination failure found in most laminated composites structures [7]. Delamination is a serious failure mode in composite materials not only as a result of the damage it causes to structure but it also separates the composite material into different layers which can lead to a reduction of the section strength and material stiffness [8]. Another example is the increased frequency in the design of engineering structures with inter-connected components leading to the creation of different types of jointed interfaces with complex nonlinear behaviours. In addition, as both linear experimental and simulation results become more accurate, the presence of nonlinear features can become a significant influence limiting the vibration performance of structure.

As a result, engineers are frequently being challenged and confronted by the presence of non-linear behaviour in modern day structures during a typical vibration or certification test particularly in the aerospace sector. Examples of case studies where non-linearity have been noticed in aerospace structures can be found in [9] where non-linearity was detected at the elastomeric mounts supporting the four turboprop engines of the aircraft during the Ground Vibration Test (GVT) of the Airbus A400M aircraft designed for military purposes. The F-16 fighter aircraft also showed some non-linear behaviour at the wing-to-payload mounting interface when a similar GVT was conducted [10]. Non-linearities were also detected on the Cassini spacecraft due to the presence of gaps in the support of the Huygens probe [11]. Hence the development of nonlinear

identification and modelling techniques has become an active research area of vibrations and structural dynamics.

To investigate this on-going challenge, the last two decades have witnessed the advancement and development of many new methods and technologies based on theoretical modelling, numerical analysis and experimental testing to address the wide variety of nonlinear phenomena, in particular those caused by large vibration amplitude [12, 6]. Some of these have been successfully applied to address specific challenges, for example, identification of weak non-linearities in engineering structures was investigated and reported in [13], identification of nonlinear softening behaviour on a vibration mode of an helicopter was also studied in [14]. Methods for analysing vibrating structures with localised non-linearites were considered and implemented in [15, 16] and a multi-degree-of-freedom system based on lumped mass nonlinear stiffness parameter modelling was examined in [17–19].

Even though different theoretical, numerical and experimental tools and methods are now readily available to improve our ability of tackle challenges arising from nonlinear vibration, the complementary role of experimental testing and simulation still remains an important aspect when determining the vibration performance of a validated engineering structure. Aside from the complexity associated with non-linearity, an important aspect of successful investigation of a nonlinear vibration problem is the ability to characterise the type of nonlinear behaviour and also attribute a parameter value to such nonlinear behaviour. The *characterisation* and *parameter estimation* can be considered as the most important aspect of nonlinear system identification. In addition, these two tasks are often required when developing a virtual nonlinear model of the system under consideration.

In this work, it is recognised that in order to successfully achieve these two tasks and effectively develop a validated virtual model of a nonlinear structure, the complementary role of test and simulation or a test-simulation integration strategy is inevitable. In this case, the complementary role of test and simulation is defined as the ability to use a set of measurement test campaign to improve the simulation or modelling activities and vice-versa. An important subject of this thesis is the development of physics-based methodology for characterising and estimating nonlinear parameters from vibration measurements. Further, the importance and requirement to have

the right balance and integration between experimental testing and simulation for the effective analyses of nonlinear vibrating structures is another topic investigated in this research. Where tests can complement or be used as a guide for simulation and, equally, when simulation can be used to determine required experimental tests. Particular attention is devoted to practical and industrial applications.

1.1 Objectives and Contribution of the Thesis

Whilst many new methods for theoretical modelling, numerical analysis and experimental testing of nonlinear systems have been developed, it is rather surprising that their practical applications on industrial structures or case studies are limited and not commonly used by practising industrial engineers. In addition, in this era of supercomputers and simulation-based designs, effective verification and validation remains an important role in the design phase of an engineering structure. In particular, the emerging "digitilisation paradigm" [20] is becoming more widespread across most industries, where major aerospace and automotive industries are expected to be using the "digital-twin concept" by 2025 [20]. A digital twin is a virtual representation of an engineering system, product or production process built from a combination of simulation models and data [21, 22] developed to create steady augmentation and reduce failure rates. From a structural dynamics perspective, verification and validation of linear structures using modal testing and analysis have been widely adopted as an active step in developing a early stage digital-twin concept for underlying linear initial design of engineering structure. However, the extension of this early stage digital-twin concept to structures with non-linearites remains an active area of research.

To this end, this doctoral thesis is aimed at creating an early stage digital-twin process for vibrating structures exhibiting non-linear behaviour, based on a combination of test and simulation models to generate nonlinear predictive tools and models. This is mainly established in this doctoral thesis by progressing further the development of a selected nonlinear identification technique and by demonstrating an approach for extending current modal testing and analysis techniques from linear to nonlinear systems using a test-to-simulation integration strategy. Three types of modelling approaches were considered in this thesis, namely white-box, black-box and grey-box modelling. Here, white-box modelling is based on using approximately accurate knowledge of the physics, black-box modelling is based on using data-driven models without adequate knowledge of the physics and grey-box modelling is based on a combination of both white and black box models. To achieve the main aim, three objectives were determined:

1. *Develop a black-box data-driven approach for detection and characterisation of nonlinearities for large structures with multiple nonlinear sources and dynamic modes*.

   Large sets of data are often acquired during the experimental test campaign of mechanical structures. The measured data are either in the time or frequency domain, or a combination of both for convenient use during the linear identification stage. However, once nonlinear behaviour have been detected from the measured data, characterisation and identification of parametric models from measured data is always a challenging task. Most importantly, this is problematic for large assembled structures with several nonlinear vibration modes and multiple nonlinear sources. Therefore, the first contribution of this thesis is aimed at the development of a black-box data driven approach for characterising and identifying structural nonlinearities from measured data only without any assumed knowledge of the system's nonlinear physics. The developed data-driven approach is proposed to have the flexibility to build nonlinear models capable of representing the non-linearities observed on assembled large structures with multiple nonlinear modes.

2. *Propose an effective time-domain grey-box algorithm for experimental identification of nonlinear parametric models.*

   A black-box modelling approach has the flexibility for fitting and extracting models from data only, without making use of nonlinear physics related information of the structure under consideration but some underlying linear information and dynamic assumptions are used. The final outcome of this approach often posses several limitations, such as the large number of parameters obtained from the identified model and the challenges associated with extracting the physics-based parameters from the resulting model. Therefore, the second contribution of this thesis is to propose a novel time-domain algorithm for the identification of nonlinear parameters and coefficients from experimental data. Here, the resulting identified parameters and coefficients have physics-based quantification of the nonlinearities in the structure or system under consideration. The theoretical principle of the proposed method is developed from the data-driven black box identification approach implemented in the first objective, in addition with an assumption of treating

non-linearities as internal feedback forces to the underlying linear model of the system under consideration, results in a grey-box identification algorithm. The grey-box algorithm is applied to simulation and experimental case studies.

3. *Demonstrate a pre-digital-twin framework for nonlinear vibrating structures using a white-box modelling approach.*

   Given the continual increase in the development of High-Performance Computing (HPC), most engineering sectors are aiming to build high fidelity simulation models to make design decision and also to account for uncertainties. However, there are many challenges related to this, one of which is the level of trust that can be given to a specific simulation result and associated uncertainties. As such, the combined use of simulation models and test data is still of vital importance, where data obtained from the physical twin can be used to update or validate the digital twin of the structure under consideration. The final contribution of this thesis is to demonstrate a pre-digital-twin framework for structures exhibiting structural non-linearities. This is achieved through the combined use of test and simulation and by extending the established linear modal testing and analysis methods to nonlinear structures. In this case, the implemented test and simulation integration strategy take the form of a white-box modelling approach, where a series of steps are put together in the coherent framework to obtain improved validated non-linear model. In this thesis, validation is defined as solving the correct equations, i.e., formulating a mathematical model and selecting the coefficients such that physical phenomenon of the nonlinear behaviour is described to an adequate level of fidelity while verification is solving the equations correctly, i.e., performing the computations in a mathematically correct manner.

1.2 Thesis Outline

An extensive review on non-linearity with particular attention to the context of structural dynamics is presented in Chapter 2. To start with, a brief description of the term "non-linearty" from the perspective of the superposition principle, linear resonance and mode shapes is presented.

This is followed by a survey of the recent advances in numerical analysis, experimental testing and theoretical modelling for non-linear structural dynamics. In addition, an overview of the root sources of non-linearities in structures is presented and a detailed description of current non-linear identification methods is also given. The last section of this chapter addresses the advantages and limitations of the current methods.

Chapter 3 addresses the first objective of this thesis where a black-box data driven approach is developed. Here, the main aim is pivoted at developing a computational and predictive model capable of characterising and identifying the non-linearities observed in the structure under consideration. The black-box data driven approach is established based on the existing black-box oriented nonlinear state space model identification method. Particular attention is devoted to selecting the most suitable polynomial degree and order required for the nonlinear model identification. The developed approach is demonstrated in the experimental identification exercise of a large assembled aerospace structure containing several bolted connections, where the identified non-linear models are derived entirely from the measured data obtained from the extensive experimental campaign.

In Chapter 4, a novel time-domain grey-box method for the identification of non-linear parameters is proposed. Given the limitations of the nonlinear state space identification method implemented in Chapter 3 where the identified models possess a large number of parameters with limited physics-based interpretation, the proposed method is aimed at developing an algorithm capable of estimating nonlinear parametric models with lower number of parameters and improved potential for physics-based interpretation of the system under consideration. The proposed identification method stems from the existing black-box oriented polynomial nonlinear state space model method which considers the non-linearites as internal feedback forces to the underlying linear system. The proposed grey-box state space identification method is demonstrated numerically on a Single Degree of Freedom (SDOF) example with a non-linear stiffness and damping element.

Chapter 5 demonstrates and challenges the identification abilities of the proposed time domain grey-box state space method in chapter 4. In this chapter,a lab demonstrator of an aerospace structure with multiple parts assembled using bolted connection is studied. A Finite

Element model of the structure is designed for a pre-test and modal analysis. Subsequently, a range of different experimental data sets were acquired for increasing force levels for further use in non-linear detection and identification. The full nonlinear identification was conducted on experimental data, where complex polynomial behaviours were successfully identified at local joint regions. In addition, data acquired at local bolted regions of the aerospace structure under consideration is shown to exhibit interesting nonlinear responses such as Jump phenomena.

The final chapter focuses on a test-simulation integration strategy suitable for the development of an early stage digital twin of a nonlinear structure. This chapter proposes a holistic approach for designing and validating assembled structures with identified non-linear phenomena. The combined use of the established non-linear analysis techniques, both for the experimental identification and response simulation, is used to achieve an improved knowledge and understand of the physics of any vibrating structure under consideration. The key to the strategy illustrated in this chapter is ability to obtain an optimum balance and integration between test and simulation, where major attention is dedicated to growing the importance of including nonlinear elements into already validated linear finite element models for effective modelling, response prediction and cross validation with experimental data at the same corresponding force levels. This holistic approach is demonstrated on a cantilever beam assembly where polynomial functions are identified and validated for both stiffness and damping characteristics.

The concluding chapter summarises the research, revisits the most important findings and evaluates the research objectives. It also states the main original contributions of the presented research work. Lastly, the avenues for the future research in integrating experimental test and simulations for nonlinear systems in structural dynamics are suggested.

1.3 List of Publications

The work results in this thesis have either been published or under review for publication by the the time of submission.

Journal Papers

- **S.B.Cooper**, K.Tiels, B.Titurus and D.DiMaio (2019) (Accepted with revision) Polynomial

Nonlinear State Space Identification of an Aero-Engine Structure. Accepted at the *Journal of Computers and Structures*.

- **S.B.Cooper**, D.DiMaio and D.J.Ewins (2018) Integration of system identification and finite element of nonlinear vibrating structures. *Journal of Mechanical Systems and Signal Processing*,102,401-430.

- **S.B.Cooper** and D.DiMaio (2018) Static load estimation using artificial neural network: Application on a wing rib. *Journal of Advances in Engineering Software*,125,113-125.

Conference Papers

- **S.B.Cooper**, S.Manzato, A.Borzacchiello, L.Bregan, B.Peeters (2019) Investigating Nonlinearities in a Demo Aircraft Structure Under Sine Excitation. *In R.Barthorpe (Ed.), Nonlinear Dynamics Volume 1: Proceedings of the 37th IMAC, A Conference and Exposition on Structural Dynamics 2019* (pp. 41-57).

- **S.B.Cooper**, K.Tiels and D.DiMaio (2018) Nonlinear Identification of an Aero-Engine Component Using Polynomial Nonlinear State Space Model.*In G. Kerschen (Ed.), Nonlinear Dynamics Volume 1: Proceedings of the 36th IMAC, A Conference and Exposition on Structural Dynamics 2018* (pp. 260-273).

- **S.B.Cooper**, D.DiMaio, (2018) An Experimental Case Study for Nonlinear Model Validation: Effect of Nonlinearities in an Aero-Engine Structure.*In R.Barthorpe (Ed.), Validation and Uncertainty Quantification, Volume 3: Proceedings of the 36th IMAC, A Conference and Exposition on Structural Dynamics 2018* (pp. 37-47).

- **S.B.Cooper**, D.DiMaio, D.J.Ewins (2017) Nonlinear Vibration Analysis of a Complex Aerospace Structure. *In G. Kerschen (Ed.), Nonlinear Dynamics Volume 1: Proceedings of the 35th IMAC, A Conference and Exposition on Structural Dynamics 2017* (pp. 55-68).

- **S.B.Cooper**, M.Rosatello, A.T.Mathis, K.Johnson, M.R.W.Brake, M.S.Allen, A. A.Ferri, D.R.Roettgen, B.R.Pacini, R.L.Mayes (2017) Effect of Far-Field Structure on Joint Properties.

In M.S.Allen, R.L.Mayes, D.Rixen (Ed.), Nonlinear Dynamics Volume 4: Proceedings of the 35th IMAC, A Conference and Exposition on Structural Dynamics 2017 (pp. 63-77).

- **S.B.Cooper**, (2016) Nonlinear vibration analysis of a complex aerospace structure. *In proceedings of the Defence and Security Doctoral Symposium*. https://doi.org/10.17862/cranfield.rd.4288874.v2.

- **S.B.Cooper**,and D.DiMaio (2016) Experimental and Numerical Modelling of Nonlinear Complex Assembled Structures. *Proceedings of the 27th ISMA, An International Conference on Noise and Vibration 2016* (pp. 2597-2612).

- **S.B.Cooper**, A.DelliCarri and D.DiMaio (2016) Model upgrading T0 augment linear model capabilities into nonlinear regions. *In G. Kerschen (Ed.), Nonlinear Dynamics Volume 1: Proceedings of the 34th IMAC, A Conference and Exposition on Structural Dynamics 2016* (pp. 203-217).

- **S.B.Cooper**, D.DiMaio and A.DelliCarri (2015) Direct matrix updating method for structural models based on measured response. *In M.Boltezar M.Wieciegoch, (Ed.), Conference Proceeding: Proceedings of ICOeV2015, International Conference on Engineering Vibration*.

- **S.B.Cooper** and D.DiMaio (2015) A Neural network approach to load identification on a wing rib. *In Y.Tsompanakis, J.Kruis, B.H.V.Topping (Ed.), Conference Proceeding: Proceedings of the Fourth International Conference on Soft Computing Technology in Civil, Structural and Environmental Engineering*.Paper 34, 2015. doi:10.4203/ccp.109.34.

- **S.Cooper**, R.Amali and S.Noroozi (2014) Application of artificial neural network to predict the static load on an aircraft rib. *In L.Iliadis, I.Maglogiannis, H.Papadopoulos (Ed.), Conference Proceeding: Proceedings of the Artificial Intelligence Applications and Innovations. AIAI 2014*.Advances in Information and Communication Technology, vol 436.

CHAPTER 2

LITERATURE REVIEW

Abstract

Nonlinear dynamics is now regarded as a wide research topic with a significant level of interest from a wide range of researchers and engineers in the structural dynamics community. In this chapter, a broad review on non-linear dynamics and key developments within the research field is presented. Firstly, the concept of non-linear dynamics is introduced followed by further discussions on the effects and sources of non-linearities in structural dynamics. An extensive review on current methods and approaches to identification and modelling of structural non-linearities is presented, avenues on prospective development with regards to the objectives of this thesis are also highlighted. Finally, non-linear identification methods and process are grouped based on their analysis approach and specific features with further discussions on the strengths and limitations of each method.

2.1 Introduction

Non-linearity is an extensive term which could have various meaning in the mathematical and engineering discipline. From the context of a structural dynamicist, non-linearity occurs when a system violates the homogeneity principle i.e the absence of the superposition principle. This means that for any combination of loads applied simultaneously to a system does not yield the same response as the sum of the individual responses to each of the loads acting separately. Currently the superposition principle is said to be the benchmark of linear vibration which also provides an explanation to the failure of current linear identification tools when exposed to non-linearity. From a mathematical perspective, non-linear systems are usually represented by a set of differential equations with non-linear terms included in the overall equation. The corresponding resonance frequencies and mode shapes of such system are considered as the functions of the operating conditions [23] .

Another important feature of a non-linear system is the fact that their natural frequencies and mode shapes can vary with respect to the excitation amplitude, in this case, the presence of non-linearities can easily invalidate results based on linear simulations. In addition, the dynamic response or behaviour of a strongly non-linear system are usually significantly different from the response of a linear system as shown in [24] and [25]. It is therefore important to define methodologies that would accurately predict the behaviour of a non-linear system. Non-linear systems also exhibit behaviours such as bifurcation, chaos and quasi-periodicity [26]. Aside from the specific and different features of non-linear system, one of the major challenges or characteristics is the requirement to have a preceding knowledge of the functional form that maps the input onto the output for the system under consideration, a typical example is a cubic polynomial non-linear function established in the Duffing oscillator case study [27].

The selection of various non-linear functions in the process on non-linear system identification also adds more complexity when compared to linear system identification.Currently, a typical process of modelling non-linearity in structural dynamics is by including some corresponding non-linear elements in the mathematical models which describes the non-linear system. For this type of case study the parameters of these non-linear elements are usually specific and can

only be obtained from an experimental test or through an updating process. As such in [12], the authors defined nonlinear identification as the process of identifying non-linear parameters or constructing a mathematical model representation of a system under consideration.

Non-linear system identification has received a great level of attention over the last few decades, where it is fair to acknowledge that a high level of maturity and achievements have been attained with this research field. For example, continuous structures with localised geometrical non-linearity illustrated in [28, 15], identification of non-linear multi-degree-of-freedom (MDOF) lumped parameters was also presented in [19, 18]. The identification of weak non-linearities was also studied on more complex structures, example of this can be found [29] where a strategy for non-linear modal identification of weak non-linear effects on large aircraft structures was presented. An aluminium plate attached with two stores used to illustrate the behaviour of a wing and an engine suspended by a means of non-linear pylon also displayed a presence of weak non-linearities during a vibration test, the results obtained illustrated some hardening characteristics as shown in [13]. Similar study was also carried out on a large helicopter with the identification of a weak non-linear softening behaviour on one of the vibration modes as shown in [30]. A detailed review on the types of non-linearity and methods of non-linear system identification can be found in [12].

However the identification and modelling of systems with complex and strongly non-linear behaviour still remains an area of challenge and active research in structural dynamics [6]. The use of black box to model strongly non-linear behaviour has also received some attention, one of the major advantage of the black-box modelling method is its mathematical approach to the identification of non-linearities in a system irrespective of the type and strength of the non-linearity in the system [31]. The method has also successfully been used to model complex joints and friction dynamics as shown in [32, 33], despite the advancement of the use of black box modelling in non-linear identification there still appears to be some major drawbacks. One of the major disadvantage with black box models is their practical application and usefulness, black box models are also not able to give any physical quantity or information for a structure under vibration test which can cause a limitation to its usefulness.The comprehensive literature on nonlinear structural dynamics presented in this chapter are classified in different groups. These

classifications are Sources of non-linearities, non-linear Identification Methods and non-linear Identification Process.The aim of this chapter is to present a brief overview on current literature, where major attention of the review is tailored to recent development on non-linear identification and modelling in structural dynamics.

2.2 Modelling Non-linearities in Structural Dynamics

In structural dynamics, the study of non-linearities can be defined as the identification of the mechanical forces and motion related to the nonlinear phenomena exhibited by a mechanical system or component of interest. From a mathematical perspective, nonlinear dynamics can be referred to as the investigation of a nonlinear system represented by a set of nonlinear differential equations [34]. For linear mechanical structures, the dynamics characteristics namely natural frequencies, damping ratios and mode shapes are often extracted using the well known modal analysis approach. These modal parameters are determined either through mathematical models using (Theoretical Modal Analysis TMA) or from an inverse approach based on experimental data (Experimental Modal Analysis EMA). The development of super computers and advance

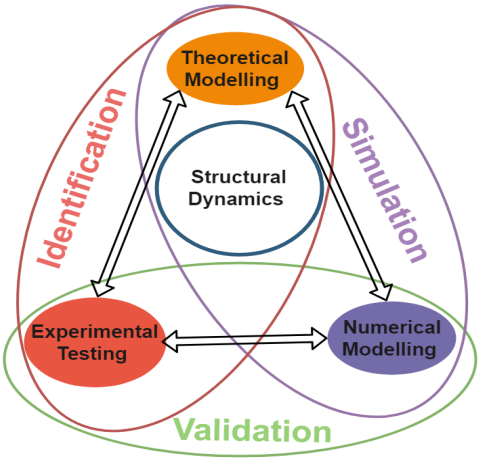

Figure 2.1: Basic skill sets for an effective structural dynamics solution

algorithms also introduced the concept of Finite Element Models (FEM), which are used to

generate simulated modal natural frequencies and mode shapes. These three approaches have been well developed for understanding and modelling linear structural dynamics for over 40 years [35].

For nonlinear structures, a linear representation of the system is constructed with the addition of internal nonlinear restoring forces to represent the nonlinear effects. These nonlinear forces often depend on specific functions attributed to the mechanics of the system under consideration which can be described using a range of different parameters. As such, to effectively model and gain deeper understanding into a particular nonlinear structural challenge, a combination of different analysis approach are required. According to two technical surveys conducted in [6] and [36], three primary skills sets/approaches required for a successful solution of a nonlinear structural dynamic challenge was reviewed in detailed with a range of applications and examples. A schematic diagram of these skill sets are described in Figure 2.1 which are often referred to as theoretical modelling, experimental testing and numerical modelling. In addition, Figure 2.1 shows labelled connecting arrows between the three skills sets, these are classified as techniques that can be used when combining the skills sets for specific application. The literature on these skills sets and techniques are briefly reviewed in the subsections below.

2.2.1 Theoretical Modelling

Theoretical modelling in nonlinear structural dynamics is an approach often used for constructing and obtaining thorough understanding of the underlying physics and defining sets of equations that represents the nonlinear system under consideration. The theory of nonlinear dynamics have been well developed by mathematicians using the fundamentals developed in Poincare's theorem. For example, the perturbation method was used in studying the nonlinear characteristics of single and multiple degree of freedom systems in [37]. In structural dynamics, the theoretical concept of Linear Normal Modes (LNM) and its nonlinear extension Nonlinear Normal Modes (NNM) introduced by Rosenberg and Shaw in [38, 39] and [40] are now seen as classical techniques used in modelling non-linearities.

In recent years, more advanced theoretical techniques such as bifurcation theory [41, 42] and isolated response analysis [43] have also been adopted to gain useful insight into complex

nonlinear behaviour observed in some real-life application. The advantage associated with a theoretical modelling approach is the ease of use to describe discretised nonlinearites and the ability to conveniently analyse simple scaled geometry structures such as beam, shells and plate models. Other types of techniques used in theoretical modelling approach includes, polynomial approximation [44, 45], cubic splines [46, 47] and non-integer exponents [48, 49]. The challenge with this type of modelling approach is its in-ability to effectively solve large sets of equations of motion under multiple specified performance conditions. To tackle this challenge, the combination of theoretical and numerical modelling (section 2.2.2) is used and this is referred to as simulation as shown in Figure 2.1

2.2.2 Numerical Modelling

Numerical modelling is used to provide accurate and competent computational algorithms required for solving both small and large scale challenges associated with nonlinearities. In structural dynamics, both theoretical and numerical modelling are grouped as simulation tool sets as shown in Figure 2.1, the computational algorithms developed based on numerical methods are often used to solve the nonlinear system of equations of motion derived based on theoretical modelling. The correct combination of both theoretical and numerical modelling tool sets is always of major importance as even the most advanced numerical algorithm can be unproductive if the given theoretically formulated equations of motion is not a true representation of the nonlinear system under consideration.

Different algorithms and numerical methods for the computation of nonlinear systems have been developed over the last 15 years, most of them are based on a continuation procedure [50] and are used for studying the periodic solution of a nonlinear system with respect to the frequency of the harmonic forcing or design parameter. Examples of these numerical methods includes the shooting method [51] which is based on Newmark time integration, orthogonal collocation methods such as COLSYS [34], AUTO [52], MATCONT [53] and most recently developed COCO [54], all of which are also useful for bifurcation detection and tracking. Another powerful numerical method in the frequency domain is the Harmonic Balance (HB) method. It is often used to compute the periodic solution of finite element models (FEM), with the main advantage

on the use of truncated and low order Fourier approximations to obtain an accurate solution for a nonlinear system. The HB method has been applied to several mechanical and vibration problems, examples of these applications are found in the subsonic flow of an aerofoil motion with strong cubic nonlinear restoring force [55], unsteady aerodynamic prediction of helicopter rotors [56], modelling of friction interface elements [57] and the prediction of nonlinear dynamic response of mechanical structures [58, 59]

2.2.3 Experimental Testing

In this era of super computers and simulation based designs, experimental measurement and testing still remain an important tool in nonlinear structural dynamics. Till date and according to Figure 2.1, experimental testing and numerical modelling play complementary and often matching roles in the development of advanced structures, machines and vehicles. Experimental testing and measurements are mainly used to uncover uncertainties during design process and most importantly used for the final verification of the structural design. There exist a wide range of established modal and linear testing techniques in the literature [60, 61, 1] including the use of advanced hardware and software such as the Scanning Laser Doppler Vibrometer (SLDV) [62, 63] for non-contactless measurement. However, experimental testing of nonlinear structures requires more demand and post-processing techniques such as selecting the right Frequency Sampling Rate (FSR) and number of harmonics during post processing.

To cope with the challenges and demands that come with the experimental testing of nonlinear structure, new methods that can capture the unique complex behaviours of non-linearities are constantly being developed. Methods such as stochastic technique in ref [64, 65] used for measuring global dynamics and mapping basin of attractions. As developed in the numerical modelling approach, experimental continuation as in ref [66] techniques are also used to track unique features such as stable and unstable regions as shown in [67], and further advanced developed method used in [68] for bifurcation analysis and backbone tracking.

2.3 Sources of Non-linearities in Engineering Structures

Most fields of engineering such as civil, structural, aerospace, automobile and mechanical engineering experience some form of non-linearity. Before proceeding to the identification of these non-linearities it is also important to recognise where these non-linearities originate from, a large majority of the causes of non-linearities in engineering can be traced to (i) The geometric of the structure. i. e Geometrical Non-linearity (ii) The type of energy going in to the system. i.e Inertia Non-linearity. (iii) The behaviour/ properties of material under test. i.e Non-linear Material behaviour (iv) Damping dissipation or characteristics of the structure. (v) The experimental or simulation set-up. i.e Boundary conditions. Non-linearities can arise from a combination of all these sources and can easily nullify any results based on linear simulations, it is therefore important to be able to accurately identify and understand the contributing sources of non-linearities. The following subsections gives a brief overview of the common sources of non-linearities in structural dynamics.

2.3.1 Geometric Non-linearity

This source of non-linearity is mainly based on the type of experiment or analysis that is being carried out on the structure, geometric non-linearity occurs when the structure is subjected to a large displacement which arises from the potential energy. An example of identifying a non-linear term due to large deformation or displacement is to consider the equation of a simple pendulum which is $\ddot{\theta} + \omega_0^2 \sin\theta = 0$; which models large angular motion. The non-linear term in the equation $\omega_0^2 \sin\theta$ represents geometric non-linearity. Geometric non-linearities can also be found in large deformation of flexible elastic continuum structures such as shell, beams and plate. The vibration of shell structures with geometrical non-linearity was considered in [69] where the shell is immersed in a fluid, the shell and fluid interaction was defined by a linear hyper-singular equation. The method of the Lagrange equations was then used to derive the non-linear finite-degree-of-freedom models of the shells vibrations.

The effects of geometrical non-linearities were also encountered in flexible steel cables used in the design of bridges and flexible connected beams [70]. Prediction of large displacements and

dynamic response of panels exhibiting localised geometric non-linearity effect was also studied in [71] using Reduced Order Model (ROM) and Finite Element Analyses (FEA). A change in the geometric parameters of a structure also causes an effect in the non-linear behaviour of the structure, in [72] the non-linear hardening and softening resonance of a cantilever beam designed with intentional geometric non-linearity was studied. Geometric non-linearity can also be encountered in composite structures and some components of today's aircraft structures, an example of the effects of geometrical structural non-linearity on flutter and limit oscillations of high aspect ratio wings is presented in [73]. A detailed survey on structural geometrical non-linearity and its applications are presented in [74].

2.3.2 Material Non-linearity

A material is categorised to have a non-linear behaviour when the law relating the stress and strain is non-linear, an example of this feature can be found in resilient mounting systems such as rubber isolators [48]. For linear elastic analysis the stress- strain relationship is defined through the modulus of elasticity (E) but for the case of non-linear material analysis, the modulus of elasticity only serves as first point of definition of the overall behaviour. A characteristic property and analysis in the non-linear material domain involves one of the post-yeild point behaviour, i.e. the plasticity behaviour. A typical elasto-plastic material characteristics under tensile loading is studied in [47]. This type of problem involves approximating the non-linear section of the stress-strain curve with a series of piece-wise linear function to obtain a suitable solution.

Inelastic behaviour is also characterised by a force-deformation relationship which is often referred to as a backbone curve, it measures the strength against translational or rotational deformation. There are different types of force-deformation relationships which are used to characterise material non-linearity, examples of these relationships include monotonic curve, hysteresis cycle and interaction surface. The use of new materials in structural engineering also introduces new failure methods which are different from the existing traditional metal materials, one of these failures is found in the delamination failure found in most laminated composites structures [7]. Delamination is a serious failure mode in composite materials not only as a result of the damage it causes to structure but it also separates the composite material into different

layers which can lead to a reduction of the section strength and material stiffness [8].

2.3.3 Non-linearity From Governing Equations of Motion

This source of non-linearity is obtained from the non-linear terms in the equation of motion of the system, most of the non-linear terms can be found in the velocities, accelerations or displacement terms which takes its source in the kinetic energy of the system. Methods for solving non-linear differential equation is an important aspect of analysis mechanical systems or structures associated with non-linearities. Conventional analytical methods have been developed for solving non-linear equations which includes perturbation methods and generalised averaging methods [26, 75], A classic example of a differential equation used in the perturbation method for analysing linear system is written in the form as shown in Equation 6.1:

$$m\frac{d^2x}{dt^2} + c\frac{dx}{dt} + kx = 0 \tag{2.1}$$

Where m, c and k denotes the mass, damping and stiffness properties of the system. However the usefulness of the perturbation methods in non-linear identification is limited as they are primarily applied when the non-linear terms in the differential equation is rather small when compared with the linear terms.

Other available methods used for solving weakly and strongly non-linear equations includes the describing function [76], the power series method [77], equivalent linearisation method [78] and the harmonic balance [79, 80]. All these listed methods have their own advantages and limitations and any deviation in parameters can cause errors in the predicted response either qualitatively or quantitatively. For example the harmonic balance method is very useful for solving strongly non-linear vibration problems, however the construction of higher order approximation to the solution can be very difficult and tedious. This is as a result of the level of complicated non-linear algebraic equations that must be solved for higher-order approximations. Some major disadvantages associated with both perturbation and non-perturbation methods of solving non-linear differential equation is that the methods are not able to correct the convergence region and the rate of given approximate series [81].

To overcome some of these challenges, a method that provides accurate solution for analysing

non-linear free vibrations of a conservative oscillator with inertia and static cubic non-linearities was presented in [82], the solution obtained is based on the Homotopy Analysis Method (HAM) which was formulated by [83] to overcome the traditional analytical methods. The HAM is able to correct the convergence region and the rate of approximation series, it is also easy to use and is able to solve strongly non-linear differential equations analytically. The efficiency and precision of the HAM have also been tested and proven in the analysis of some non-linear problems [84, 85], results from these research show that the solutions obtained using the HAM is quickly convergent and the its coefficients can easily be calculated. The accuracy of the results obtained from using the HAM also indicates that this method is very valuable for solving problems with strong non-linearities. It should be noted that there are also other powerful methods used for solving strongly non-linear problems which are referenced in [81].

2.3.4 Damping Dissipation and Friction

The dissipation of energy in vibrating structures is often referred to as damping which can be related to a number of mechanisms that operate inside or outside of the vibrating structure. Internal damping can be allied with the material properties of the structure as shown in [86] while the external damping is often associated with dry friction at any joints within the structure and any other form of fluid structure interaction surrounding the structure [87]. Unlike the mass and stiffness properties of a structure, the damping characteristics of a structure cannot easily be determined from the finite element method, the mathematical formulation of non-linear damping requires some experimental knowledge of damping for the structure under test. The challenge behind this principle is that for a real structure under test, the type of experiment conducted on the structure is at relatively low amplitude which can only give little or less information about the non-linear damping behaviour of the structure.

The effects of non-linear damping force on the dynamics of slender structures under flapping motion was investigated in [88], where linear and non-linear, internal and external damping force models in different functional forms are incorporated into a non-linear, in-extensible beam theory. The theory behind damping dissipation is basically a non-linear concept which has not fully been understood, examples of non-linear damping can be found in dry friction effects such

as bodies in contact sliding with respect to each other. Hysteretic damping is another example of non-linear damping effect, an illustration of this can be found in an article written by Tomlinson and Hibbert, 1979 where a technique, based upon the in-phase and quadrature power dissipated when exciting a normal mode, is presented which allows the magnitude of the non-linear friction force and the hysteretic damping constant to be evaluated [89]. Joints and Interfaces are another major source of non-linearities in structural dynamics, a range of research have been conducted on methods for modelling joints with several applications referenced in [90–92], in [93], Ewins suggested the need to review and change the design of joints and structural interfaces to reduce the effect of non-linearities.

2.3.5 Boundary Condition Effects

Non-linearity can also arise from the boundary condition set-up during an experiment or simulation, examples of such boundary conditions are rigid constraints, free surfaces in fluids imperfectly bonded bodies, clearances, and vibro-impacts due to loose joints. Non-linearities that arises as a result of the boundary conditions sometimes require special treatment compared with other types of non-linearities, non-linear vibration analysis of doubled layered nano-plates with different boundary conditions was studied in [94] where the results observed indicated that weak non-linearities are observed in boundary conditions with clamped movable edge when non-local effects are neglected.

Furthermore results shows that the type of non-linearity is substantially different from clamped immovable edge. Clearance and vibro-impact due to loose joints are considered as the major types of non-linearities associated with the problem boundary condition, typical static test results associated with these types of non-linearities possesses non-smooth force-displacement characteristics. Largely, these types of non-linearities are treated specially compared with other forms of non-linearities.

2.4 Overview of Non-linear System Identification Methods

The main purpose of any system identification is to obtain specific parameters from a mathematical model which represents the physical model of the system under consideration. These parameters are acquired by making use of the relationship that describe the input and output data function. It can be concluded that the identification of linear system which uses vibration measurement data to determine the mathematical models of linear dynamic system is an established area. Linear tools such as modal testing and analysis [95, 1] are available and widely used by researchers and industries for linear system identification. In structural dynamics the transfer function relating the input and output of linear system is always constant for all level of excitation, this implies that the mathematical model obtained through the identification at an operating force level can be used for the prediction of a model at a different operating level provided the system is still observed as linear.

However it is difficult or sometimes impossible to obtain a generic mathematical model for a non-linear system by performing a system identification from a vibration test, thus the identification of non-linear system is largely different from the conventional linear system identification. The continual interest of increasing the performance of today's engineering structures where lighter and more flexible structures are constantly being designed consequently leads to more non-linear vibration problems on structural components. The present challenge is that the theory behind the identification of non-linear dynamical system is not as established compared to linear systems, in addition systems that are considered to have weak non-linearities can display some interesting complex behaviour which today's linear identification methods cannot accommodate.

Examples of such complex behaviours includes bifurcations, sub-harmonics, jumps, internal resonance, saturation, super-harmonics, modal interaction, chaos and resonance capture. A detailed review of these complex non-linear behaviours can be found in textbooks and technical surveys presented in [6, 12, 26, 27, 96, 97]. The old conventional technique used in studying non-linear system was the linearisation approach introduced in [98, 99], further non-linear theories have since then been developed. The perturbation theory [100] was used to analyse weakly non-linear system, perturbation methods includes the Lindstedt-Poincare technique [100]

and the multiple scale method [101, 102]. However, there has also been an evolution from weakly non-linear structures to strongly non-linear structures, thus a need to extend the current methods used for analysis of weak non-linearities to accommodate strong non-linearities is required.

The aspect of system identification and extraction of model parameters from experimental measurement in the presence of non-linearity still remains an area that is not yet fully developed, according to the present literature it is possible to admit that there is currently no general analysis method that is applicable to the identification of non-linear system. One of the major reason for this challenge is that the functional which maps the input and output of a non-linear system is unknown beforehand which makes the overall identification process generally more difficult. Several research teams in Europe and across the world have devoted time and effort in the development of non-linear system identification for over thirty years with examples such as the (COAST) Action F3 structural dynamics project [103] and other benchmark research which was carried out by research institutions. The Ecole Centrale de Lyon (ECL) benchmark [104] and the VTT Technical Research Centre benchmark in Finland [105] are examples of frame work projects which have been devoted to non-linear system identification. In addition to this, several papers have also been published in conjunction with these projects and research teams [106–108].

Research into non-linear identification methods have proven that the nature of the problem of the considered non-linear system can greatly determine the type of method or approached that would be used in analysing the system. As such, In a comprehensive review presented by Kerschen.,et., al, in [6, 12], seven methods have been identified and categorised as the key important methods and domain used in the analysis of non-linear system. These methods are:

- Time domain methods
- Frequency domain methods
- Modal methods
- Linearisation methods
- Time-frequency methods
- Black-box modelling

- Structural model updating methods

These methods have been cited and used in many published papers and textbook such as in [109–111]. A brief overview on these methods are described in the following subsections with major attention devoted to their advantages and limitations.

2.4.1 Linearisation Methods

To test for linearity, modal analysis has been the most sophisticated theory used [95, 1], however it is only restricted to linear system and attempts to apply the same process directly to non-linear system with some modification such as the curve fitting algorithms has been reached. A method used for linearising non-linear equations of motion with harmonic forcing referred to as the harmonic balance method is another linearisation method, it is based on the assumption that sub- and super harmonics are negligible compared to the fundamental harmonic and it also provides a process of approximating the FRFs of a non-linear system which for this case the harmonic balance method is often referred to as the describing function method [1].

The harmonic balance method has been the underlying foundation for several non-linear system identification, (Meyer and Link.,2002) applied the harmonic balance method to identify local non-linear stiffness and damping parameters from dynamic response data in [112]. The investigation was to model the local non-linear effects using a frequency domain representation which is based on a FE model description in the time domain and also leads to a parametrisation of the non-linear model which can be used to solve the inverse problem. The equivalent linearisation method is another technique developed based on replacing non-linear oscillator with external Gaussian excitation by a linear one with the same excitation such that the mean-square error between the actual non-linear and linearised systems is minimised in a statistical sense. (Kimura et al., 1983) applied the same technique for calculating the non-stationary responses of a system with bilinear hysteresis subjected to non-white random excitations, the method was based on writing an approximate equation of motion describing the hysteretic behaviour by introducing an additional state variable and non-linear functions [113].

Another popular linearisation technique which is often associated with the equivalent linearisation method is the statistical linearisation technique which is also used for determining

the response characteristics of non-linear dynamic system, the statistical method is developed mainly to replace non-linear elements in a model by linear forms, where the coefficients of linearisation can be found using the specific criterion of linearisation and is often used to define the characteristic response of a stochastic dynamic system. (Socha and Pawleta., 2001) presented a comparison between the statistical and equivalent methods in [114] to determine if in general both methods are the same for analysing non-linear dynamical system excited by a stationary Gaussian white noise, the presented argument concluded that the differences between both linearisation techniques in application to the determination of the response characteristics of a dynamical system, are eliminated by iterative procedures and can therefore conclude that statistical linearisation and standard equivalent linearisation are exactly the same methods.

2.4.2 Time Domain Methods

Non-linear identification can also depend on the type of data that is made available during the identification process, a method is categorised as a time domain method if the data measured during the identification process is in a time series format. For example the force and acceleration data obtained from a standard vibration test are classic examples of time series data, the signals for this type of test are directly provided by the measurement devices. Several applications of the time domain identification method have been published in papers referenced in [115–119]. A successful technique used in the time-domain identification method is the Restoring Force Surface techniques (RFS) which was used to initiate the analysis of non-linear structural system in terms of their internal RFSs, this technique was introduced by (Masri and Caughey,1979),(Masri et al.., 1982 [120]).

The RFS technique was initially developed for Single Degree of Freedom (SDOF) system, an extended generalised approach used to analyse multiple degree of freedom (MDOF) system was later developed by (Masri et al.., 1982 [121]). This nonlinear identification technique has enjoyed a variety of applications from experimental investigations proposed in [117, 122], the technique was also used for non-linear system identification in the absence of measured data in [123] the curve fitting approach was also avoided in [124] to make use of the RFS technique for identification of non-linear MDOF system. Extensive research was also carried to extend

the RFS method to the frequency domain analysis which involved applying force-state mapping, a numerical application of this method can be found in [125] where a method of identifying non-linear joint properties of a structure through its connection points from measured frequency response function (FRF) is proposed.

A rather more mathematical technique which is mainly applied in the frequency-domain is the Hilbert Transform (HT) used famously for the detection of non-linearity, the Hilbert transform provides some additional information about amplitude, frequency and instantaneous phase from the signal of a mechanical vibrations [126]. Some methodologies where the HT has been applied in the time-domain is cited in [127] where a typical inverse problem approach is used for the identification of non-linearity on a SDOF dynamic system with unknown restoring and damping force. The HT can also be used to construct non-linear damping and stiffness curves of large non-linear system with mono-component signals [12]. Further work was carried out on the decomposition of signals with multiple components into a collection of mono-component signals which is termed intrinsic mode function (IMFs) by Huang et al. and it is represented as the Huang-Hilbert transform [128], it consist of two steps which are the Empirical Mode Decomposition (EDM) algorithm and the Hilbert spectral analysis.

Contrary to the previous methods, HHT is intuitive, direct, a posteriori, and adaptive, with the basis of the decomposition based on and derived from the data. It is a new time–frequency analysis technique that can not only offer higher frequency resolution and more accurate timing of transient events and non-stationary data than conventional methods, but also provide physically meaningful interpretations. Even though its theoretical base has not been fully established, HHT has been tested and validated empirically, and has been applied to various fields of scientific research and industries [129]. Although the HT technique is fast and operational at testing for non-linearities based on a single measured frequency response function (FRF), however its form of detection method is based on the level of distortion of the measured FRF and the distortion of an FRF isn't always the best way to classify a system as non-linear especially when there is the presence of weak non-linearities. Another drawback to using the HT is that the test for non-linearity is based on individual judgement which does not always provide an established solution to the problem.

An alternative technique used in the time-domain method is the time-series analysis which is regularly used in structural dynamics but initiated by control system engineering, it is based on the linear variant approach of the ARMA model (Auto-Regressive Moving Average) [130]. This method has long been existence in the world of modelling and prediction purpose and there has been attempts to generate a similar model for non-linear identification of structures.Currently the most adaptable and continuing model under the time-series analysis which has been designed for non-linear case is the NARMAX method (Non-linear ARMA with eXogeneous input models) introduced by Billings and Leontaritis, examples of cases where the NARMAX model has been used in conjunction with the non-linear output frequency response function and other methods in the detection of non-linearity are seen in articles related to structural damage detection [131], identification of non-linear structures [132], predicting the hysteric behaviour of passive control systems [133].

There has also been prominent research of using the NARMAX method to estimate model parameters successively in order to allow a reasonable control of the model which is been analysed with the aid of an orthogonal estimation. It can be stated that the NARMAX method is now been enjoyed in both theoretical and experimental aspect of structural dynamics and in several application it can be used to investigate an established linear system with non-linear parameters. Irrespective of its usefulness, the NARMAX does not give a direct understanding to the physics of the system that is being modelled. This often causes a difficult validation stage of the non-linear system as there would not be any form of correlation test.

2.4.3 Frequency Domain Methods

If the data measured during the identification process take the form of a spectra or FRF, then that particular identification method is classified as a frequency domain method. Previous investigation has been carried out by several authors on developing frequency domain methods by using FRF or spectra data which are classified as frequency domain data for the purpose of non-linear system identification methods. The method of using frequency domain data was obtained through functional series –the Volterra and Wiener series [134]. One of the practical application of the Volterra and Wiener series is the non-linear bearing stiffness parameter estimation in

flexible rotor-bearing systems by (Khan and Vyas) [135]. Where a frequency domain was adopted for the identification of higher order Volterra and Wiener kernel from the response of the system to a Gaussian white noise excitation, the Volterra and Wiener series also helps to generalise the idea behind the application of impulse response function and FRF to nonlinear system.

The High Order Frequency Response Function (HOFRFs) has received a lot of attention in the area of system identification with its first application in the field of structural dynamics focused on the extraction of non-linear parameters by fitting surface to the HOFRFs, a work carried out by Gifford 1989 in his PhD thesis. (Khan and Vyas 1998) explored the prospect of non-linear parametric estimation using Volterra and Wiener theories. If one has measured input and output time data, it is possible to evaluate the FRF's by carrying out many multi-dimensional Fast Fourier Transforms and averaging the results, in much the same way as one would evaluate a standard linear transfer function. An engineering application of a SDOF system with a cubic stiffness non-linearity which involved using a HOFRF to obtain the first and third order kernels for the estimation of the non-linear parameters is also presented in [136].

The extension of modal analysis linear tool to study non-linear structures using the Volterra and wiener series was carried out by (Tawfiq and Vinh) [137], it explains how the functional series generalises the superposition principles included in the definition of each term of the Volterra series which constitute the basis of non-linear modal analysis and also allows to get the impulse responses and transfer function of various orders [137]. Despite the practicality involved in using the HOFRF and Volterra Kernel transforms, the major limitation to this techniques is the level of series convergence present in the analysis. Major challenges can be encountered if the approach is applied to practical engineering with discontinuous or non-smooth non-linearities as the systems have a demonstration of the Volterra technique. If the system under consideration includes non-linear behaviours like bifurcation, the Volterra technique might loss its validity due to the single-value associated to the Taylor series of which Volterra series is a functional of Taylor series.

A new method for estimating parameters of non-linear parametric models that uses internal feedback to account for non-linearities was proposed by (Adams and Allemang, 1999), it was founded on the integration of non-linear systems as linear in the open loop with non-linear

feedback in the closed loop. Previous work on using the feedback to derive a new formulation of frequency response function matrices of non-linear system which is called the modulation of nominal linear system was investigated by the same authors. The advantage of this new method which is commonly called the non-linear identification through feedback of the output (NIFO) is its simplicity and how it can be easily applied to estimating the linear frequency response matrix and non-linear parameters at forced and unforced single and multiple degrees of freedom systems which can either be linear or non-linear [109].

This method also instigated further development of a new method for non-linear system identification of mechanical systems, in the absence of an input measurement, using a combination of time and frequency domain techniques [138], where the restoring force plots are used to characterise the frequency and amplitude characteristics of non-linearities in the time domain. The experimental non-linearities are then used in the output-only formulation of the non-linear identification through feedback of the outputs frequency domain, which can be used to predict the response of the system.

A different method of non-linear system identification using the frequency domain is the harmonic balance method which is used in an inverse way to estimate parameters in non-linear system. Authors such as (Kamyia and Yasuda,2005) investigated and applied these method to identifying non-linear boundary conditions of machines [139], the analytical technique involved modelling the boundary as a spring and damper system with effective mass and moment inertia. The harmonic balance-based identification method was in cooperated into non-linear system with chaotic behaviour [140], the method is based on extraction of parameters of periodic orbits from a chaotic sets in an experiment.

A generalised non-iterative approach using reverse spectral analysis technique for the identification of linear and non-linear multiple degrees of freedom was proposed by (Rice and Fitzpatrick, 1990 [141]), the method is appropriate for highly coupled non-linear systems and systems with substantial damping effects. It also helps to define the coefficients of the non-linear terms as well as the physical model of the linear structure and requires excitation signals at each location of the response. (Richard and Singh) [48] also proposed a further method that estimates the non-linear coefficient and the FRF-based model of the primary linear structure called the

conditioned reverse path method CRP, this method does not take into consideration the excitation pattern. The formulation is based on utilising multiple-input/multiple-output data from non-linear system when excited by Gaussian random excitation [110]. The underlying linear system is also identified without any use of the non-linear terms. (Richard and Singh,2000) supplementary provided a comparison between reverse path and the CRP methods to illustrate the similarities and difference that exist between these two methods [142], the evaluation creates a core difference between both methods.

However a possible limitation that was noticed in the CRP method is that there is a measurement requirement of the structural response at the location of the non-linearity which can be some worth difficult in reality. Arguably, the reverse path and the condition reverse path techniques are more advantageous when compared to other techniques within the identification methods since physical properties are identified, and typically physical domain properties are preferred over modal domain properties since modal properties can be determined from physical properties but the opposite is not always true. It is worth commenting that a further integration of the reverse path and the conditioned reverse path method might be able to provide better results in terms of the localisation, characterisation, and parametric quantification of non-linearities.

2.4.4 Modal Methods

The theory of modal analysis is based on the form of the modal parameters which are the natural frequencies, damping ratios and mode shapes of a particular system, these parameters are able to describe the behaviour of a system with a range of input and output type. Numerous research has been conducted on the application of modal analysis to non-linear modal structure with the assumption of weak non-linearities in the system (see, e.g.,(platen et al., 2007 [13]) where a novel concept of non-linear identification for large system of 5DOF is introduced. Laxalde and Thouverez also proposed a complex non-linear modal analysis method on a turbo-machinery blade which also gives a description of a two-dimensional frictional motions by complex variables [143].

A new direct simultaneous modal approximation method to improve the accuracy of all eigenvalues and eigenvectors was also introduced by (Chalko et al., 1996) with the adoption of

current techniques of curve fitting in modal analysis [144]. A new concept of extending modal analysis to non-linear system identification was first introduced by (Rosenberg, 1962), called the Non-linear Normal Modes (NNM). The concept is based on the development of a non-linear model in modal space, the NNMs demonstrates a theoretical background for extending modal analysis to non-linear system which therefore brings about the development of non-linear system identification techniques based on non-linear modes [1]. The analysis of NNMs is often more challenging compared to linear normal modes theory based on the fact that NNMs and their periods depends on the amplitude of the vibrating system, however the mode of vibration in resonant conditions can be regarded as an estimate of the NNM. An example on the theoretical derivation of NNM applied to a two degree of freedom (DOF) system is extracted from [50].

The modified single non-linear mode method presented in [145] which is based on the assumption that the mode of vibration in resonant conditions is assumed to be the same as the normal mode (or eigenfunction) of the corresponding linear system i.e. the system with the rejected non-linear term, which in turn is assumed to be known proves the idea behind the estimation of NNM from the mode of vibration. However to determine if the single non-linear mode method would give a satisfactory result, the sensitivity of the normal modes to the amplitude of vibration has to be examined using the Ritz method to check if they vary slightly or significantly with the amplitude.

The drawback to the approach is that a general criterion, which would enable one to predict the “sensitivity” of the normal mode shapes to the amplitude before carrying out the calculation of them, is not available. Other methods of non-linear modes for identification of non-linear system includes a process which involves modes extraction often referred to as the proper orthogonal modes (POMs) and are readily obtained from the decomposition of the response matrix. Instantaneous modes shapes can also be extracted using wavelet transforms, although all these modes don’t have direct theoretical formulation of the NNMs they can still provide useful information for non-linear system identification.

2.4.5 Time-Frequency Methods

The time-frequency methods are often used in the analysis of non-linear oscillatory systems, the time-frequency analysis is made up of the decomposition of a signal into simpler components which later add up to produce the original signal. The time-frequency analysis have been used to study linear system mainly for the estimation of their natural frequencies and damping properties, examples of these applications are cited in [146–148]. Several techniques have been developed and studied in structural dynamics using time-frequency method, for example non-linear oscillations were investigated using the Gabor transforms in [149, 150].

Time-frequency methods offer a different perception to the dynamics of the system, one of its major advantage is that the decomposition of time-frequency signals permits the storage of time history data into a section that allows the separation of individual components of the signal which can help in signal filtering stage. A detailed review on the analysis of non-stationary signals using time-frequency methods is presented in [151], these methods have now been applied in most application of structural dynamics. Further techniques have also been developed in the time-frequency domain for analysing inverse problems, for example a combination of the Hilbert and Gabor transform was proposed in [149] for the extraction of parameters from measured data. The Gabor transform was used to detect the time-variant matrix which is able to predict the spatial behaviour of the system, the matrix is also able to decouple the transient solution into sets of quasi-harmonic components. The Hilbert transform is then used to identify the elastic restoring force associated with each component.

The Gabor transforms was also used for the computation of coupled non-linear modes from measured data in [152] for the extraction of non-linear modal parameters. The wavelet transform is another approach used in non-linear system identification, the technique involves the expansion of the system excitation and response in terms of scaling functions, the tangent stiffness of the structural system is then conveyed as a series of wavelets. A detailed review on the use of wavelet transform in non-linear structural dynamics is presented in [153], approaches cited in the review includes non-linear identification techniques associated with wavelet ridges and skeletons, damping estimation procedures, wavelet-based frequency response function, cross-wavelet analysis, self-similar signals, coherent structures and chaos.

Other techniques on the identification of non-linear systems using time-frequency analysis is presented in [154, 155] which includes the Winger-Ville distribution and the time-frequency distribution. Although the time-frequency analysis method is suitable for problems with different non-linear vibration systems, however a major concern with the time-frequency analysis is that it's only appropriate for mono-component signals such as systems with a single dominant frequency. Another minor disadvantage is that the change in amplitude must be slow in relation to the phase change.

2.4.6 Structural Model Updating Methods

Analysis of complex structures with many DOF in a wider range of frequency can be extremely difficult, this would require a new estimation or modelling method compared to structures which are analysed with small DOF system. But the extraction of the required parameters from experimental measurement can often be a process which is not flexible, however a common solution to this problem is to use the popular computational technique often referred to as structural modelling which involves a process of computing the structural model parameters using the information from the mechanical and geometrical properties of the structure that is being analysed.

The process behind structural model updating often starts with a creating a finite element model of the structure with the aid of popular software packages such as MSC Nastran-Patran, Ansys, Abaqus etc. Where most of the packages are able to give the desired output of a structural compute in the form of displacement, stress, strain and many more, the structural model update of the computed model is regularly regarded as finite element model updating. The use of structural modelling is however not fully accurate as there still proves to be some discrepancies between structural modelling and practical application, the error is often noticed from a usual percentage difference between the experimental results and the model prediction. The sources of these errors can be from improper modelling assumptions or boundary condition, mechanical parameter errors such as damping constant, young's modulus and errors that might occur during the event of conducting the experiment. Thus it is therefore important to correct and improve the accuracy of the structural model by comparing with measurements obtained from the experimental stage,

this process is often denoted as structural model updating.

Finite element model updating was introduced to linear structures in the 1990s to improve the design, construction and maintenance of mechanical systems, (Goge.,2002) demonstrated the use of finite element model updating on a large aircraft model as shown in [156]. The presented method uses experimental data from a ground vibration test to perform the computational model updating (CMU), the CMU procedure involved fitting parameters of a given initial analytical model i.e the stiffness and mass matrices that corresponds very closely to the measured behaviour [156]. Other application of finite element updating to linear structures have been published in several papers for example (Lee and Dobson.,1990 [157]) and (Sheinman., 1996 [158]) and many more which have all proven that the majority of structural model updating methods are perfectly suited for linear structures.

On the other hand, updating of non-linear structures or models can sometimes come with some mathematical and computation challenge because tools such as modal analysis which are suitable for analysing linear system cannot be applied directly to non-linear system. Schmidt proposed a method of updating non-linear components with local non-linearities such as coulomb friction and local plasticity in [159], it involves updating the parameters of non-linear elements in the input file of a FE code by fitting simulated time history function and its corresponding measured data. The method of modal state observers was used to overcome the problem encountered in estimating the initial values and the error between the simulated and time history function. (Meyer and Link.,2002) formulated a modelling technique based on the harmonic balance method for the linearisation of the non-linear equilibrium equation of a structure. The technique involved identifying local non-linear stiffness and damping parameters from dynamic response data, the non-linearity is being taken into account by assembling non-linear two-degree-of-freedom elements into larger linear finite element models. The model is linearised using the harmonic balance method to obtain an appropriate model description in the frequency domain and the response is calculated iteratively using the dynamic condensation for the linear part of the structure [112].

A two-step methodology for analysing non-linear system was proposed by (Kerschen and Golinval) [160], where it decouples the estimation of the linear and non-linear parameters. The

method enjoys the application of the reverse-path method and a numerical simulation applied to an aeroplane like structure [160]. In the absence of non-linear identification tools which are able to identify parameters or variables used for test correlation, structural model updating of non-linear structures becomes more challenging. Several research has been made to define features (i.e., variables or quantities identified from the structural response that give useful insight into the dynamics of interest) that facilitate correlation [160].

Proper orthogonal decomposition (POD) technique, also known as Karhunen-Loeve (K-L) decomposition is also a developing tool for non-linear identification in dynamics and vibration, it functions by extracting spatial information from a set of time-series data available in a domain. (Lenaerts et al.,2000) investigated the use of proper orthogonal modes of displacements for the identification of parameters of non-linear dynamical structures with an optimisation procedure based on the difference between the experimental and simulated POM. POM is mainly an empirical system of modes with the application of POD to measured displacement of a discrete structure with a known mass matrix leading to an estimation of the normal modes. A finite element update of a beam with a local non-linear component was used as an example for this analysis [161]. Although it is frequently applied to non-linear problems, it should be stated that the POD only gives the optimal approximating linear manifold in the configuration space represented by the data [12]. A further work was also carried out by (Kerschen., 2002) in his thesis on finite element model updating using the features extracted from a non-linear generalisation of the POD termed non-linear principal component analysis [162].

Aside from the iterative process involved in structural model updating, there are some other limitations and unresolved issues with structural model updating. One of the major concerns with structural model updating is the difficulty in correlation between the analytical and the experimental test. It is generally assumed that the analytical model would have a close formulation of the actual physical structure, this can pose a challenge when dealing with large DOF of freedom systems also isolation of non-active DOF from the analytical model requires a detailed level of attention in order not delete information of the active DOF.

Another disadvantage with structural model update is that it is dependent on the accuracy the measurement obtained from an experimental test, a current challenge in vibration testing is

that the majority of the transducer and sensors which are currently available have limitations with obtaining 3 dimensional measurement data i.e (X,Y and Z) data expect when using a laser scanner which is not currently a fully developed technology in vibration testing. In the aspect of non-linear structural updating it obvious from the literature that there are different types and levels of non-linearities therefore the implementation of structural model updating in non-linear system can sometimes be a difficult or impossible task as there are no universal features applicable to all types on non-linearities. Nevertheless structural model updating in totality can be classified as an important aspect of nonlinear structural dynamics and it is also an essential aspect of the verification and validation process of a system.

2.4.7 Black-Box Methods

For most non-linear system, the functional which maps the input $x(t)$ to the output $y(t)$ is usually unknown in advance which is seen as a major challenge in non-linear system identification but the movement to non-linear black-box modelling has instigated some new methods. A non-linear black-box structure is a model structure designed to define the non-linear dynamics behaviour of a system with the use of data only [12]. Non-linearity is caused by various mechanism and phenomena which can therefore make the black-box modelling approach an aspiring one, with current theories available to support the approach. Artificial Neural Network (ANN) as a black-box method in data mining has proven to be an effective tool for system approximation, Cybenko, 1989 discussed the approximation of possible types of non-linearities that can be realised by artificial neural network and also established that the finite linear combinations of compositions of a fixed, univariate function and a set of affine functional can uniformly approximate any continuous function of n real variables with support in the unit hypercube; only mild conditions are imposed on the univariate function [163].

Non-linear black box modelling is also described as a concatenation of a mapping previously seen data to a regression vector and a non-linear mapping from the regressor space to the output space, with several applications as illustrated in [32, 61, 164–166]. There has also been interest in black-box modelling and non-linear mapping with methods based on artificial neural network, radial basis network, wavelet network and hinging hyperplanes, wavelet-transforms methods and

fuzzy sets and fuzzy rule based methods [31]. Various application of ANN for system identification and modelling have been published with examples from (Jagannathan and Lewis, 1996) where a novel multilayer discrete-time neural network paradigm was presented for the identification of multi-input multi-output (MIMO) of a non-linear dynamical system with major attention on identification error and convergence that shows the constraint for a new identifier structure and non-standard weight tuning algorithms [167]. Other use of ANN in non-linear identification can also be noticed in experimental studies with much attention drawn to processing of excitation signals (Doherty et al ., 1995) worked on how the design configuration such as choice of process excitation signal, data sampling time, neural network structure can contribute to the successful reliability of how well a neural network can approximate the non-linear dynamic behaviour of a system. The method observes the effect of these configuration with the use of a multi-layered perceptron neural network to identify the non-linear dynamics of a simulated chemical reaction process, it also proved that the general classification of neural network as a black-box model does not prevent engineers and experimentalist from applying a certain degree of influence over the outcome of a non-linear identification experiment [168].

Multilayer perceptron neural network can also denote a comprehensive range of non-linear SDOF systems with continuous or discontinuous non-linearities, the application of Volterra Wiener neural network to the identification of non-linear hysteretic dynamic system with more focus on predicting the response of hysteretic systems with discrete degrees-of-freedom under known force excitations also proves this concept of representing SDOF as multilayer perceptron neural network. ANN can be said to be the most established method compared to wavelets network, neuro-fuzzy models and the use of splines function which are the other forms of black-box modelling in the field of structural dynamics. However black-box modelling also has some limitations which can border the usefulness of the method in practical applications, the parameters obtained from the identification model does not directly provide any information about the physical properties of the structure under consideration and also how to contract with simulation of non-linear system where there are large number of parameters to handle which may lead to over fitting during the training process therefore cause a later error of the parameter estimation.

2.5 Non-linear System Identification Process

Another way of classifying the research on non-linear identification is based on the processes or steps implemented in achieving a successful identification of a non-linear system. In this context Identification process can defined as the number of steps or procedures required for the complete identification of a non-linear system. In the field of structural dynamics, the identification process of non-linear system are often developed based on individual non-linear problem which is being encountered by the structure. However there are some popular processes which are commonly used by researchers and engineers in this field. One of the popular process frequently used in the identification of non-linear system is Non-linear Modal Analysis (NMA) procedure which involves extending linear modal analysis theory to non-linear system. In a brief overview the modal model of the underlying linear system is determined based on low level excitation of the structure during a vibration test. The modal model is than extended by directly adding non-linear terms to the modes that behave non-linearly and a couple of non-linear coupling terms to any non-linear mode interaction in the system. A systematic approach and a numerical application of this process is presented in [17, 13].

A similar flow chart process was proposed by (Fuellekrug and Goege., 2011) in [29], the process was developed mainly for the identification of weak non-linearities in a large aerospace structure during ground vibration testing. Likewise, the theory behind this process is based on the extension of linear modal analysis to non-linear system. Another practical process based on the restoring force approach was introduced by (Goege.,et.,al) in [32], the process involves eight different steps where the first three steps are similar to identification process based on the NMA strategy. The later steps of the restoring force approach includes calculation and plotting of the non-linear restoring force, curve-fitting of non-linear terms and creation of linearity plots from fitted non-linear restoring force using the harmonic balance method. Although these identification processes have successfully been applied to practical problems, one can argue the fact that these identification process are only applicable to some type of structures and non-linear identification problems.

A more generic identification process was proposed in [12] and it is still frequently used

till date according to a recent survey in [6]. Recently, the location of nonlinearity was added to the already existing steps, the revised identification process is broken down into four different activities in [169] namely :

1. *Detection of non-linearity in the system*
2. *Location of non-linearity in the system*
3. *Characterisation of non-linearity i.e type of non-linearity*
4. *Parametric estimation i.e calculate the non-linear parameter*

The implementation of this identification process has now been adopted by many researchers and engineers in the field of structural dynamics, one of the major advantage of this process is the universal systematic approached which the process accommodates. An advantage of the three-step identification process is that it is often implemented in most of the of newly developed nonlinear identification codes and analysis tool sets. To a certain degree, it can be regarded as a bench-marking process for a successful identification of a non-linear system.

2.5.1 Detection of Non-linearity

The first stage in identification process of non-linearity is the detection of structural non-linearity according to the flow diagram above, in general it can be said that almost all practical structures have a certain degree of non-linearity so it is therefore important to detect the presence and level of non-linearity in a structure. For a system under test, there are questions which provide a forward direction to the detection of non-linearity. Examples of such questions are:

- *Is the system under test linear or non-linear?*
- *What is the evolution of non-linear distortions present in the system with increase in excitation level*

Several approaches to the detection of non-linearity in a test structure was described in [12], (Zhang et al., 2010) also proposed a method for the fast detection and quantification of non-linear distortion in the output of a dynamic system [170]. The basic idea behind the proposed approach is

the use of a non-stationary excitation which makes the non-linear distortions also non-stationary, thus making it possible to differentiate from their stationary plant noise. The non-stationarity of the excitation allows the evolution of the system non-linearity to be assessed in one single analysis, greatly accelerating the experiment. An alternative methodology that is based on the principal component analysis and uses time responses obtained with a random excitation was presented by (Hot et al., 2012), the method is based on using two criteria to quantify the difference between two response sub-spaces, based on the angle between them and the residual error resulting from the projection of one on the other. The concept of limit of linearity and design decision margins is also addressed in this paper [171].

The literature on non-linearity detection is broad, a summary of the literature is presented in the text-book by Worden and Tomlinson [61]. Referring back to the fundamental principle of classifying if a system is linear or non-linear which is the principle of superposition, the breakdown of this principle can also be used to detect the presence of non-linearity effect in a system. However the direct application of this principle to the detection of non-linearity is somewhat limited in practical situation. The test for homogeneity which is a constrained form of the superposition principle is one of the most often applied method in the detection of non-linearity in a system, according to (kershen et al., 2006) homogeneity violation is best visualised in the frequency domain through distortions of FRFs. However, because a weaker condition is enforced, this linearity test is not reliable [12].

Another proven method of non-linearity detection is by using well-designed excitation signals which have the ability to disclose the odd and even nature of the non-linearity and also quantify the non-linearity level based on response, an example of this application is described in [172]. A more practical diagnosis method is the Hilbert transform approach introduced in [173], the method is based on the fact that the FRF of a system are invariant under a Hilbert transformation, the Hilbert transform of an FRF for a non-linear system will return a distorted version of the FRF. However there are some disadvantage with using the Hilbert transform for detection purposes, a major concern with using Hilbert transform in line with measured FRF data is when the data that is being used does not start with a zero frequency value and the problem of neglecting the outbound data usually occur.

2.5.2 Location of Non-linearity

The second step in the identification process is the location phase, the aim of this step is to identify the location of the non-linearity in the structure. Location refers to determining exactly where the nonlinear features are positioned in the spatial description of the structure. In mathematical terms, this means identifying which of the DOFs in the model are closely located to the source of the nonlinear behaviour.

Discrete nonlinearities are located at the interface between two components and are responsible for the majority of their nonlinear behaviour (e.g. joints). These can be modelled by spring/damper elements with higher-order characteristics and are differentiated in the 'grounded' or 'non-grounded' variety, depending of the number of degrees of freedom they involve. A grounded nonlinearity is a function of the absolute displacement/velocity of a single degree of freedom, while a non-grounded nonlinearity is function of the relative displacement/velocity of one degree of freedom with respect to another. Grounded nonlinearities are mostly found between the test structure and its fixture while in general the nonlinearities can be regarded as non-grounded (e.g. acting across a joint between two components of the structure).

It is important to be aware that no method can provide reliable location information if the test geometry does not contain DOFs near and/or across the cause of the nonlinearity. Although this might seem a major issue, the engineer can usually narrow the range of possible locations in which nonlinearities are expected to be found, based on experience or common assumptions (e.g. joints play an important role in nonlinear behaviour for assembled structures). In this specific case, we were aware of the location of the nonlinearities, since the structure comprised primitive elements coupled through a carefully designed joint.

2.5.3 Characterisation of Non-linearity

The third step in the identification process is characterisation stage, the aim of this step is to establish the type of non-linearity and functional form of all the non-linearities in the system. This step can be argued as the most critical or important step in the identification process, a detailed review on the available techniques for characterisation of non-linearity is presented in [6, 12]. The characterisation process is concerned with establishing the main source of non-

linearity in the system and also point out the order of non-linear features in the system. A typical characterisation process would provide information related to:

- *The aspect of motion that drives the non-linear behaviour. (e.g., either displacement or velocity).*
- *The effect and functional description of the level of non-linearity in the system. (e.g. bilinear, multi-linear or polynomial)*
- *The parametric forms of the functional (e.g. order of the polynomial)*

For an accurate characterisation process, it important to determine the behaviour of the non-linear elastic and dissipative behaviour of the physical structure, the characterisation process often involve a variety of experimental test and trials to obtain some form of graphical plot which are in turn used to characterise the system.

The literature on characterisation based on experimental applications are available in [28, 118, 174]. The aim of the characterisation step is to form the fundamental nature of the non-linearity, it is also very important to have an understanding of the behaviour of the physical structure which would be useful in the parameter estimation stage of the identification process. The characterisation step is also able to describe the deviation of the structure once it fails the linearity principle, this function or description is often obtained by conducting a static test experiment on the structure. Typical results from this type of test often display a softening or hardening property for the stiffness of the structure, it could also be presented in the form of an increase or decrease in the damping of the structure. Characterisation can often be a challenging task due to the variety of phenomena present in the entire identification of non-linearity.

2.5.4 Parameter Estimation of Non-linearity

The last step in the identification process is parameter estimation, this step aims to quantify the correct numerical values for the coefficients of the terms that were obtained in the characterisation stage either through iteration or by direct means. This part of the identification process is majorly to express or deliver the most important information about the structure or system under test

by providing the closest numerical values for the stiffness and damping of the structure. There are several established techniques for parameter estimation of non-linear system either through experimental or numerical simulation are available in the literature with common examples cited in [121]. The restoring force technique used in [91, 161], the non-linear identification through feedback of the output is also presented in [109], other established techniques are also cited in [6].

The direct parametric techniques such as the reverse path methods in time and frequency domain is also presented in [175] and [110, 176]. A time-domain subspace technique based on assuming nonlinearities as internal feedback forces was also introduced in [116], another SDOF method designed for non-linear quantification referred to as CONCERTO was introduced and applied to a real structure in [177]. Further direct parametric techniques like the non-linear resonant decay is also is presented in [178], the corresponding variants technique is also available in [29]. Despite the level of developed and available estimation techniques, there is a common limitations which is associated with these techniques. The required experimental response at all non-linear DOF can sometimes have a disadvantage in a simulation case study.

2.6 Representation of Non-linear Systems

The representation of non-linear system is also a way to classify the literature on non-linear system identification, the identification of non-linear system are often presented based on the type of coordinates in which the analysis takes place. There are two forms in which non-linear system identification are present in the literature, the result of any non-linear identification are presented using physical coordinate or modal coordinate. The analysis of a non-linear system is regarded in a physical coordinate if the systems matrices are obtained through spatial discretisation [12]. i. e. The direct manipulation of the mass and stiffness of the structure are mainly used during the non-linear identification calculation. One of the major advantages associated with using the physical coordinate is the direct estimation of the physical response of the structure, any solution obtained from a non-linear identification using this coordinate will always produce a physical meaning of the entire system.

However, using the physical coordinate can sometimes come with some limitation depending on the level of discretisation and the amount of DOF used during the simulation. For a large structure the system matrices/DOF could be in range of thousands which means solving differential equations with thousands of coefficient. This process is time consuming and also involves using super-fast computers which are often expensive. Another disadvantage with using physical coordinates is the use of reduced order modelling which does not represent the actual dynamics of the system and can in turn lead to errors in the non-linear identification results. The use of modal parameters such as eigen values and eigen vectors are directly used during the identification of a non-linear system is often regarded as a modal space analysis. It often referred to as generalised coordinates, the use of this approach involves using some set of modes obtained from initial testing to reproduce new sets of response for the system.

A significant advantage of working in the modal space is based on the principle that the orthogonal property of the eigen vectors for a DOF is fully described by its own eigenvector [35, 36], this leads a massive reduction in the level of algebraic manipulation required to generate a non-linear response. The disadvantage associated with this approach is that the modal response obtained during a non-linear analysis does not provide adequate physical meaning of the structure in consideration. This can cause further problems during the structural model updating and the response correlation between simulated response and the experimental response. In summary it is arguable that analysis conducted using physical coordinates often generate meaningful results compared to analysis done using modal coordinates, in addition modal properties can easily be determined from physical properties by calculating the eigen values of the mass and stiffness matrices. However the extraction of physical properties from modal coordinates is not always feasible.

2.7 Limitations of Current Identification Methods and Processes

It is clear from the literature on nonlinear system identification that there exists a variety of nonlinear identification methods and techniques, however for this purpose of this research only the methods which have been applied in structural dynamics have been cited. From the review on the seven identification methods which have been highlighted in this report, one can draw a conclusion that there are multiple techniques or approaches which are available in each identification method. In a search to understand the applicability of these seven methods, a statistical analysis on the practical application of these methods most especially in the field of structural dynamics was conducted. In the analysis small structures are categorised as examples of simulation or experimental work which has been carried out on beams, plates, lap joints and small masses connected together with a nonlinear device using the associated technique. Large structures are categorised as automotive shock absorbers, full scales shear wall structures, helicopter blades, aircraft wings, ailerons, SmallSat Spacecraft, and a full-scaled small aircraft. For clarity the chart is intended to show a comparison of how each individual methods have been applied to different types of engineering structure in the field of structural dynamics, other theoretical and academic applications of these techniques are also available in the literature.

Despite the level of development in nonlinear identification methods, the chart presented in Figure 2.2 indicates that only a small percentage of these methods are practically suitable for structures modelled with large degrees of freedom (DOF) and localised nonlinearity. An important criterion in the industrial environment is that a method is acknowledged as a good method if it can be applied to a real life structure or system. In most cases the direct application of these methods are not always straightforward due to the level of mathematical algorithms that these methods are founded upon. Furthermore one can admit that techniques such as Gabor transform, Wigner-Ville distribution, ANN, Neuro-Fuzzy models and Wavelet networks which all fall under black box modelling are practically not being applied to large structure but they produce understandable numerical result. From the chart a conclusion can be drawn based on the level of published papers in the literature that the following identification methods: Time Domain

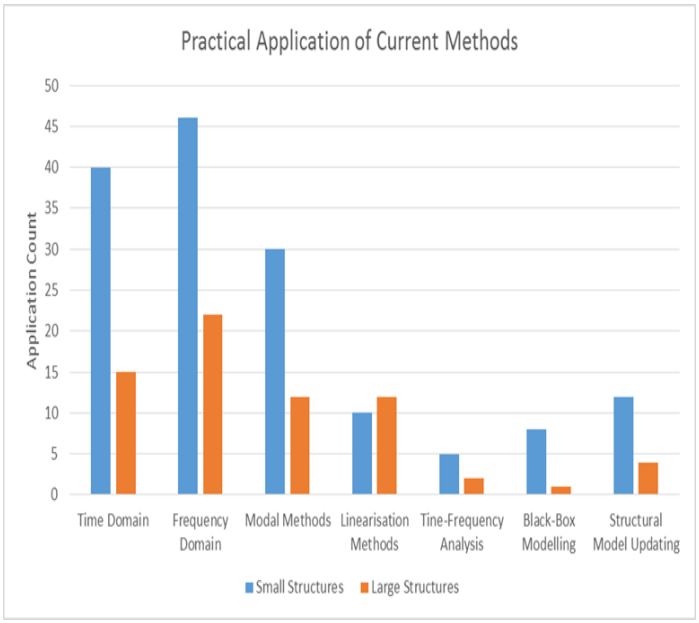

Figure 2.2: Practical Application of Current Identification Methods, sub-categorised by small and large structures

method, Frequency Domain method, Modal method, Linearisation method and Structural model updating method are popularly used more often to generate reliable nonlinear identification results that match closely with the real experimental measurement of the structure from a vibration test.

In the field of structural dynamics, the basic concept behind nonlinear identification is that every structure is considered to have an underlying linear model (ULM) where the response of a structure obeys the homogeneity principle up to a certain level before shifting into nonlinear region where superposition is no longer valid. Regardless of the extensive literature on linear and nonlinear identification, there is little or no work on developing methodologies that are capable of enhancing validated linear structural models to accommodate structures with distributed and localised nonlinearities. In the aspect of the current available nonlinear identification techniques, it is obvious that some of these popular techniques like the RFS technique can be applied and used across the seven identification methods listed above, this suggests that future work can be done on integrating some of the available techniques together to obtain better nonlinear identification tool boxes. However even if there are better upcoming identification methods or techniques, it should be noted that a general universal approach or simulation method is far

from being reached in the field of structural dynamics. Therefore the literature can be concluded that the current challenge that is being encountered in nonlinear system identification would continue to receive solution or concepts based on individual verdict.

CHAPTER 3

IDENTIFYING NONLINEARITIES BASED ON STATE SPACE MODELS

Abstract

This chapter proposes the use of a black-box data driven approach based on Polynomial Non-linear State Space (PNLSS) models for identifying structural non-linearities from measured time series data. In this investigation, a PNLSS model capable of describing a Single Input Multiple Output (SIMO) representation of a system and its corresponding non-linearities is developed. An identification procedure is stated and implemented with the procedure exploiting the great flexibility of the PNLSS model to investigate the non-linear characteristics observed at measured local regions of the structure. The developed approach is demonstrated on an Aero-Engine casing assembly with multiple joints, where the use of measured sine-sweep and broadband data obtained from the experimental campaign are used to access the validity of the proposed PNLSS model estimation.

3.1 Introduction

Most non-linear identification methods reviewed in section 2.4 of the previous chapter require prior knowledge or an initial assumption of the mathematical law (model) of the type of non-linearities present in a system, i.e. they require the functional form or depend on a proposition that the measured data obey a certain non-linear function. However, research has proven that such assumptions are only possible for specific applications due to the individualistic nature of non-linear systems and the fact that non-linear effects can be caused by several sources, therefore acquiring preceding knowledge can be difficult or sometimes practically impossible. In many cases, the detection of non-linearity from measured data can easily be achieved by using simple techniques such as those described in section 2.5.1. After non-linearity has been detected in measured data, identification of parametric or non-parametric models from such data is still regarded as a challenging task.

Black-box modelling has proven to be a successful way of tackling non-linear system identification as reviewed in section 2.4.7, especially for case studies where the functional forms and mathematical law governing the non-linearities are challenging to obtain prior to the final parameter estimation. Other black-box modelling techniques which were not cited in section 2.4.7 are the Volterra models [135–137] and state space models [179–181]. Obtaining prior knowledge of the non-linear functional form or non-linear characteristics of large assembled structures with joints can be very challenging due to their individualistic non-linear behaviour such as stick-slip behaviour at macro- and micro-scopic levels and hysteresis damping. As such, black-box identification methods are often considered as a reasonable approach to gaining useful insights into the characteristics and nature of non linearities in the system based on measured input and output data.An emerging black-box modelling method utilised in non-linear system identification is the state space modelling approach. Most importantly, non-linear state space models based on their flexibility and capacity to capture different types of non-linear phenomena. Recent work and contributions in this research area including applications are demonstrated in [181–184].

Relying on the flexible nature of state space models, this chapter introduces the use of a selected type of state space model to identify the structural non-linearities observed in measured

data. Major attention is drawn towards the extraction of useful physical information on the nature of non-linearities present in the system under consideration. A novel identification approach based on Polynomial Non-linear State Space (PNLSS) method is applied to a Single Input Multiple Output (SIMO) experimental system with multiple bolted connections, without any preceding knowledge on the type of non-linearities present in the system. The PNLSS identification strategy implement in this chapter adopts the great flexibility of nonlinear state space models to investigate the non-linear characteristics observed at local regions of the test structure. Furthermore, a study on the trade off between the flexibility of a fitted non-linear model and its parsimony is illustrated in this chapter.

The chapter is structured as follows. The theoretical context and derivation of the PNLSS model is described in great detail from Section 3.2 to Section 3.3. The proposed PNLSS identification procedure including implemented techniques such as the Best Linear Approximation (BLA) and the full non-linear identification based on Levenberg-Marquardt (LM) optimisation is described in Section 3.4. In Section 3.5, the PNLSS identification is implemented on measured data obtained from a test campaign conducted on an aero-engine casing. A parametric and non-parametric study of the total distortions (noise and non-linear distortions) observed in the test data are presented. In addition, further analysis on deriving a flexible PNLSS model capable of capturing the observed non-linearities is presented based on sine-sweep and Frequency Response Function (FRF) data. The validity of the identified model using new set of measured Sine Sweep and broadband data is tested and illustrated in this section, while discussions and concluding remarks are presented in Section 3.7.

Part of this chapter is based on the following journal and conference papers:

S.B.Cooper, K.Tiels, B.Titurus and D.DiMaio (Accepted with revision) Polynomial Nonlinear State Space Identification of an Aero-Engine Structure. Accepted at the *Journal of Computers and Structures*.

S.B.Cooper, S.Manzato, A.Borzacchiello, L.Bregan, B.Peeters (2019) Investigating Nonlinearities in a Demo Aircraft Structure Under Sine Excitation. *In R.Barthorpe (Ed.), Nonlinear Dynamics Volume 1: Proceedings of the 37th IMAC, A Conference and Exposition on Structural*

Dynamics 2019 (pp. 41-57).

S.B.Cooper,K.Tiels and D.DiMaio (2018) Nonlinear Identification of an Aero-Engine Component Using Polynomial Nonlinear State Space Model.*In G. Kerschen (Ed.), Nonlinear Dynamics Volume 1: Proceedings of the 36th IMAC, A Conference and Exposition on Structural Dynamics 2018* (pp. 260-273)

3.2 State Space Models

State space models are presented in different approaches as observed in the literature, this section of the chapter provides a brief overview on various existing types of state space models and there remarkable properties. A state space representation can conveniently model a system with multiple inputs and multiple outputs [6]. For this research, discrete-time models are adopted as opposed to continuous-time models which are computationally intensive due to calculations of time derivatives and integrals of non-linear functions. A discrete-time state space model in a general form is expressed as:

$$\begin{cases} x(t+1) = f(x(t), u(t)) \\ y(t) = g(x(t), u(t)) \end{cases} \tag{3.1}$$

where $u(t) \epsilon \mathbb{R}^{n_u}$ is a vector containing the n_u input values at time instant t, note that $n_u = 1$ in this study, while $y(t) \epsilon \mathbb{R}^{n_y}$ is the vector of the n_y outputs. The state vector $x(t) \epsilon \mathbb{R}^{n_a}$ represents the memory of the system and stores the collective dynamics present in the different outputs. The first line of 3.1 represents the state equation which describes the evolution of the states as a function of the inputs and the previous states. The second line of 3.1 is called the output equation and it relates the system's output with the states and the inputs [185]. For an accurate mathematical representation, a discrete time state space model is often represented with x_{k+1}. However, there is some abuse of notation in this chapter of the thesis where the symbol t denotes both the continuous time variable and the number of samples in a discrete-time model. It should be clear from the context which meaning is intended, in continuous time, the state equation has a time-derivative whereas in discrete time, the state equation has a one sample forward time shift.

3.2.1 Linear and Non-linear State Space Model

For a linear system, the model equations for its corresponding state space model are given by

$$\begin{cases} x(t+1) = Ax(t) + Bu(t)) \\ y(t) = Cx(t) + Du(t)) \end{cases} \tag{3.2}$$

with the state space matrices denoted by $A \in \mathbb{R}^{n_a \times n_a}$, $B \in \mathbb{R}^{n_a \times n_u}$, $C \in \mathbb{R}^{n_y \times n_u}$ and $D \in \mathbb{R}^{n_y \times n_a}$ and the transfer function $G(z)$ that corresponds to Equation 3.2 is given by

$$G(z) = C(ZI_{n_a} - A)^{-1}B + D \tag{3.3}$$

where I_{n_a} is the identity matrix of dimension n_a [185]. From 3.3, it is possible to determine the poles of $G(z)$ based on the eigenvalues of A. using a similarity transformation technique, the sets of state space matrices ABCD can be converted into a new set of $A_T B_T C_T D_T$ that have the same input/output behaviour [186]. The similarity transform $x_T(t) = T^{-1}x(t)$ with an arbitrary non-singular square matrix $\dot{T}$ yields

$$A_T = T^{-1}AT, B_T = T^{-1}B, C_T = CT, D_T = D \tag{3.4}$$

For a non-linear system, the state space model equation is defined as a classical linear state space model with the addition of non-linear functions f_{NL} and g_{NL} to the state and output equations. A discrete time model of a non-linear state space model is described in 3.5

$$\begin{cases} x(t+1) = Ax(t) + Bu(t)) + f_{NL}(x(t), u(t)) \\ y(t) = Cx(t) + Du(t)) + g_{NL}(x(t), u(t)) \end{cases} \tag{3.5}$$

where the functions f_{NL} and g_{NL} can be a set of basis functions of different types such as wavelets, sigmoid functions, polynomials, hyperbolic tangents or radial basis functions [186]. In this chapter, polynomial non-linear state space models are selected based on their ability to provide enough flexibility to cover the problem of interest.

3.2.2 Bilinear State Space Models

A bilinear state space model for a continuous-time system is defined as

$$\begin{cases} \frac{dx_c(t)}{dt} = Ax_c(t) + Bu_c(t) + Fx_c(t) \bigotimes u_c(t) \\ y_c(t) = Cx_c(t) + Du_c(t) \end{cases} \tag{3.6}$$

where $A \in \mathbb{R}^{n_a \times n_a}$, $B \in \mathbb{R}^{n_a \times n_u}$, $C \in \mathbb{R}^{n_y \times n_a}$, $D \in \mathbb{R}^{n_y \times n_u}$, and $F \in \mathbb{R}^{n_a \times n_u n_a}$, are the bilinear state space matrices. These models are classified as extension of linear state space models with the capabilities to handle non-linear systems. Bilinear state space models are seen as universal approximators for continuous-time non-linear systems and can approximate any causal function within a bounded time interval [185]. A discrete-time bilinear state space model is given by

$$\begin{cases} x(t+1) = Ax(t) + Bu(t)) + F(x(t) \bigotimes u(t)) \\ y(t) = Cx(t) + Du(t)) \end{cases} \tag{3.7}$$

normally, it is expected that the discrete-time state space models would preserve the approximation capabilities of continuous-time models, however this is not always possible for all non-linear discrete-time systems. This is as a result of the fact that the set of discrete-time bilinear systems is not closed with respect to the product operation, where the product of the outputs of two discrete-time bilinear state space systems is not essentially a bilinear system as shown in [187]. In order to maintain a universal approximation property for discrete-time systems, a more generic model formulation is required. This generic models are referred to as state affine models introduced in [188]

3.2.3 Other Types of State Space Models

Aside from linear, bilinear and non-linear state space models, state space models also exist in other forms which are not often used in similar mechanical or aerospace applications. State affine model [189] is a more generic way of describing a state space model, a single input, single output state affine model of degree r is written as

$$\begin{cases} x(t+1) = \sum_{i=0}^{r-1} A_i u^i(t) x(t) + \sum_{i=1}^{r} B_i u^i(t) \\ y(t) = \sum_{i=0}^{r-1} C_i u^i(t) x(t) + \sum_{i=1}^{r} D_i u^i(t) \end{cases} \tag{3.8}$$

state affine models were introduced in [188] and can be used to model sampled continuous-time and bilinear systems. They are also good approximators for continuous and discrete-time systems with finite time interval and bounded inputs. The Linear parameter Varying (LPV) [190] model is another form of representing state space models, they are used to create linear and time-variant models. The parameters are a function of any user-chosen vector $p(t) \in \mathbb{R}^s$ which are used to

characterise the operating point of the system and are assumed to be measurable. The state space equation for LPV models are an affine function of $p(t)$:

$$\begin{cases} x(t+1) = A \begin{bmatrix} x(t) \\ p(t) \bigotimes x(t) \end{bmatrix} + B \begin{bmatrix} u(t) \\ p(t) \bigotimes u(t) \end{bmatrix} \\ y(t) = C \begin{bmatrix} x(t) \\ p(t) \bigotimes x(t) \end{bmatrix} + D \begin{bmatrix} u(t) \\ p(t) \bigotimes u(t) \end{bmatrix} \end{cases} \tag{3.9}$$

where $A = [A_0 A_1 A_2 .... A_s]$, and $A_i \in \mathbb{R}^{n_a \times n_a}$. Other state space matrices B, C, and D are partitioned in a similar way. LPV models are applied in two special cases, the bilinear and state affine approach. When $p(t)$ is chosen equal to $u(t)$, and $B_i = 0, C_i = 0$, and $D_i = 0$ where i=1, ... ,s, then the model equations become identical to the bilinear model equations as expressed in 3.7. When $p(t)$ is equal to a vector that contains all distinct non-linear combinations of $u(t)$ up to degree $r-1$, then the state affine model is obtained. The LPV state space model structure is particularly useful for non-linear control as it enables the use of different linear controllers at different operating points. Another type of state space model is the Local Linear Model (LLM) [190], the principle behind this type of state space model is based on partitioning the input space and the state space into operating regions in which a particular linear model dominates. The LLM state space matrices are defined as a sum of weighted local linear models:

$$\begin{cases} x(t+1) = \sum_{i=1}^{s} p_i(\phi_t)(A_i x(t) + B_i u(t) + O_i) \\ y(t) = \sum_{i=1}^{s} p_i(\phi_t)(C_i x(t) + D_i u(t) + P_i) \end{cases} \tag{3.10}$$

The scalar weighting functions $P_i(.)$ generally have local support, such as radial basis functions. The scheduling vector ϕ_t is a function of the input $u(t)$ and the state $x(t)$. The last type of state space listed in this section is the deterministic Neural State Space model [191, 192], this type of state space model is based on the parametrisation of the general non-linear equation expressed in (3.1). The non-linear equation is parametrised by multi-layer feed-forward neural networks using hyperbolic tangents as activation functions:

$$\begin{cases} x(t+1) = W_{AB} \tanh(V_A x(t) + V_B u(t) + \beta_{AB}) \\ y(t) = W_{CD} \tanh(V_C x(t) + V_D u(t) + \beta_{CD}) \end{cases} \tag{3.11}$$

The model expressed in (3.11) can be viewed as a multi-layer recurrent neural network with one hidden layer. It is also a specific type of NL_q system, for which sufficient conditions for global asymptotic stability were derived in [191].

3.3 Polynomial Non-linear State Space Model

The state space approach implemented in this thesis is based on a first principle of a general model illustrated as:

$$\begin{cases} x(t+1) = f(x(t), u(t), \theta) \\ y(t) = g(x(t), u(t), \theta) \end{cases} \tag{3.12}$$

with a functional expansion of the functions $f(.)$ and $g(.)$. In this case, a set of basis functions need to be selected from the many available possible functions such as wavelets, radial basis, hyperbolic tangents, sigmoid and polynomial functions. A polynomial non-linear state space approach is adopted in this thesis. A main advantage of polynomial basis functions is the ability to easily compute them and also directly apply these functions in a multi-variable framework. In the polynomial non-linear state space (PNLSS) approach, the non-linear functions f_{NL} and g_{NL} in 3.5 are expanded using basis functions by extending the state and the output equation with polynomials in the states and the input:

$$\begin{cases} x(t+1) = Ax(t) + Bu(t) + E\zeta(x(t), u(t)) \\ y(t) = Cx(t) + Du(t) + F\eta(x(t), u(t)) \end{cases} \tag{3.13}$$

where the vectors ζ and η contains all non-linear monomials with user-chosen degrees larger than one, and the matrices $E \in \mathbb{R}^{n_x \times n_\zeta}$, $F \in \mathbb{R}^{n_x \times n_\eta}$ contain the corresponding monomial coefficients. Here $x(t) \in \mathbb{R}^n$ is the state vector at time instant $t, u(t) \in \mathbb{R}^{n_u}$ is the input (excitation) vector at time instant t, and $y(t) \in \mathbb{R}^{n_y}$ is the output vector at time instant t.The vectors $\zeta(x(t), u(t))$ and $\eta(x(t), u(t))$ contain all possible monomials in $x(t)$ and $u(t)$ of user-chosen degrees. The sizes of the state space matrices are configured in a form where matrices A, B, and E have n rows, the matrices C, D, and F have n_y rows. The matrices A and C have n columns, the matrices B and D have n_u columns, and E and F have a number of columns that corresponds to the total number of monomials of the user-chosen degrees. Non-linear dynamics are captured because of the inclusion of the non-linear terms $E\zeta$ and $F\eta$. In particular, the monomials $\zeta(t)$ and $\eta(t)$ are formed by all

possible products of the input and the state variables raised to a chosen degree [179] e.g. for an element in $\zeta(t)$:

$$\zeta_{k,1_1...,...,1_{ni}}(t) = u^k(t) \prod_{i=1}^{n_i} x_i^{1i}(t) \tag{3.14}$$

Where the total degree of monomial fulfils the conditions: $k + \sum_{i=1}^{n_x} l_i \in 0,2,3,...,p$, where k is the exponents of the inputs . The use of polynomial expansions are very useful because they are linear in parameters, hold universal approximation properties and can easily be extended to multivariate cases.

3.3.1 Approximation Behaviour

when a full polynomial expansion of (3.5) is carried out, all monomials up to a chosen degree r must be taken into account. In addition, all monomials of different degrees are placed in groups of increasing degree. The concatenation of the state vector and the input vector $\xi(t)$ is defined as:

$$\xi(t) = [x_1(t)...x_{n_a}(t)u_1(t)...u_{n_u}(t)]^T \tag{3.15}$$

where the dimensions of the vector $\xi(t)$ is given by $n = n_a + n_u$. Therefore $\zeta(t)$ and $\eta(t)$ in equation 3.13 is defined as:

$$\zeta(t) = \eta(t) = \xi(t)_{[r]} \tag{3.16}$$

In this case the total number of parameters required by the model in 3.13 is given by:

$$\left(\binom{n+r}{r} - 1\right)(n_a + n_y) = \left(\binom{n_a + n_u + r}{r} - 1\right)(n_a + n_y) \tag{3.17}$$

When all non-linear combinations of the state are present in $\zeta(t)$ and $\eta(t)$ for a given degree, then the above mentioned model structure is invariant under a similarity transform.

3.3.2 Model Structure

A data driven non-linear black-box modelling often requires a flexible model structure capable of uncovering all the non-linearities observed in an interested case study. A benefit of using state space models is the suitability for modelling a variety of system configurations such as Multiple-Inputs and Multiple-Outputs (MIMO), Single-Input and Multiple-Output (SIMO) and

Single Input and Single Output (SISO) systems. In this chapter, the SIMO configuration is used in deriving a data driven non-linear model for the application case study. Although a PNLSS model can capture many non-linear effects, it is important that an appropriate model structure is selected to reduce and manage the effects on the increasing number of parameters based on a combination of the polynomial degree and number of variables in the inputs and states. For a full PNLSS model with any polynomial degree combination $d_1, d_2, \ldots, d_D$, the number of columns in the matrices E and F can be computed using the expression in:

$$s = \left(\sum_{i-1}^{r} \frac{(n_a + n_u - 1 + r_i)^!}{(n_a + n_u - 1)^! r!} \right) (n_a + n_y) \tag{3.18}$$

While the number of non-linear terms in Equations 3.13 for a full PNLSS model with consecutive polynomial degrees 2, 3, ..., r are determined based on the following expression [183]

$$s_{full} = \left(\frac{(n_a + n_u + r)^!}{(n_a + n_u)^! r!} - (n_a + n_u) - 1 \right) (n_a + n_y) \tag{3.19}$$

This number is also dependent on the type of model structure used in developing the PNLSS model. The model structures considered in this thesis are classified as full model and state only model [183]. For a full model structure all elements in the matrices E and F of equations 3.13 are taken into consideration during the optimisation process, while a state only model structure only takes into account the elements in $E\zeta(x(t))$ and $F\eta(x(t))$ i.e. no input terms are considered, in this case, the number of parameters is reduced with n_u in (3.19) being considered to be zero. The state only model parameters are calculated based on

$$s_{state} = \left(\frac{(n_a + r)^!}{(n_a)^! r!} - (n_a) - 1 \right) (n_a + n_y) \tag{3.20}$$

The PNLSS models can also be expressed in a modal model, but this model structure is not investigated in this thesis.

3.3.3 Model Stability

The only recursive relation present in the general state space model in 3.12 is the state equation. Therefore, the Stability of the model depends on the initial conditions of the state, the properties of the input signal and the function f. Hence when analysing the stability of a general state

space equation such as 3.12, it is important to consider the function:

$$x(t+1) = f(x(t), u(t)) \tag{3.21}$$

Where $x(0) = x_0$. The concept of input-to-state stability (ISS) is reflected in this idea and was first introduced for continuous-time systems in [188], it was subsequently extended to discrete-time systems in [185]. In general, a system is ISS if every state trajectory corresponding to a bounded input remains bounded, and if the trajectory eventually becomes small when the input signal becomes small independently of the initial state.

3.4 A PNLSS Approach to Identification of Structural Non-linearities

This section of the chapter describes the identification procedure that was implemented in developing a data driven polynomial non-linear state space model for the practical case study implemented in this thesis. The state space identification approach used in this chapter is fundamentally based on four different steps. These steps are listed below with a brief description and summarised schematically in Figure 3.1.

1. To obtain the PNLSS model of a system, it is often beneficial that the initial linear state space parameters (A, B, C D) of the non-linear system are first identified. To do this, a non-parametric best linear approximation (BLA) of the system is determined here using the local polynomial method (LPM) [193]. Additionally, an estimate of the total variance (i.e. the sum of the noise and non-linear variance) is obtained.

2. A linear state space parametric model (A, B, C, D) is identified from the BLA using a frequency domain subspace method [194]. The weighted mean square difference between the estimated FRF of the BLA and the FRF of the linear state space model is minimised. This weighting is used to select a frequency band of interest and is typically the inverse of the total variance estimated in the previous step.

3. The linear state space model is then extended with polynomial terms in the states. The corresponding polynomial coefficients, together with those of the linear state space model

are optimised using the Levenberg-Marquardt method [195]. The linear parameters are optimised again because the initial guess is biased due to nonlinear distortions. During this optimisation the nonlinear effects are taken care of in this step by extending the state space model with polynomial terms. Re-estimating the linear coefficients improves the input/output fit. A cost function is defined to minimise the weighted mean square difference between the measured and the modelled output spectra of the Polynomial Nonlinear State Space (PNLSS) model. The weighting is used here to focus on a frequency band of interest. A fixed number of Levenberg-Marquardt iterations is performed. The models obtained after a successful Levenberg-Marquardt iteration (i.e. one for which the cost function evaluated on the estimation data decreases) are retained as candidate models. Models obtained after an unsuccessful iteration are discarded.

4. This last step involves validating the identified nonlinear model on a new data set that was not used in the identification process. This cross-validation step is done to avoid over-fitting. The model among the candidate models that achieves the lowest cost on the validation data is selected as the final model estimate. The candidate models are selected based on applying a parameter update evaluating the cost function on the initial parameter guess. If the new cost function value is lower than the previous value, then the iteration is classified successful and the parameter update is included as a candidate model. Here, new swept-sine and broadband data are introduced to measure the performance of the identified nonlinear model.

3.4.1 Best Linear Approximation

Linear models have proven to possess many attractive properties and therefore can be useful for approximating non-linear systems, the approximation results can often be employed to gain useful insight into the level of non-linear distortion present in the system. The Best Linear Approximation (BLA) of a non-linear system for a given class of input signals is defined as the linear model $G_{BLA}(k)$ which produces the best approximation of the system's output in

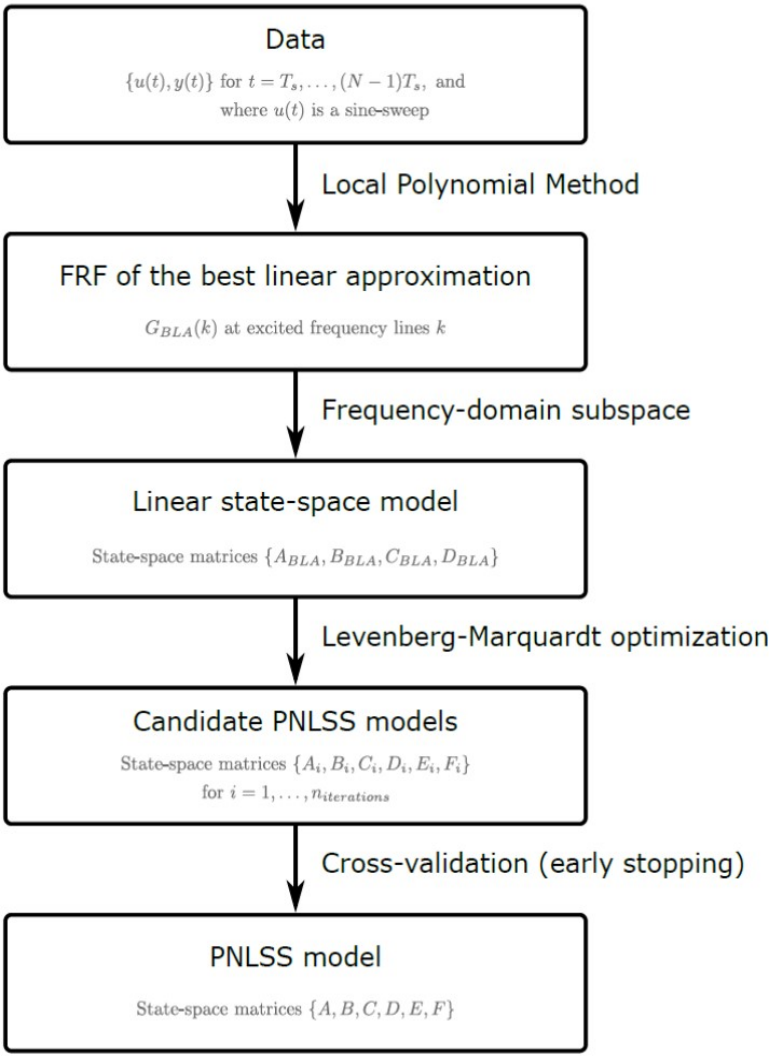

Figure 3.1: Schematic of the identification procedure

least-square sense [196]:

$$G_{BLA}(k) = \arg min E_u[\|Y(k) - G(k)U(k)\|_2^2] \tag{3.22}$$

Where G_{BLA} is the frequency response function (FRF) of the BLA, E_u. is an ensemble average over the considered class of input signals, $Y(k)$ and $U(k)$ are the discrete Fourier spectra of the output and the input at frequency line k, and G is the FRF of a linear system. The BLA generally varies with the input frequency content and the root mean squared (RMS) values, it can be measured by performing several experiments and acquiring the steady-state periods of the input-output data [197]. To keep the notation simple, the single input single output case of the

BLA estimation procedure is described in this section while a generalisation for multiple input and multiple output non-linear systems is presented in [198, 197]. Usually, the BLA framework is introduced for period in same period out (PISPO) systems [196], which means that the response of the system to a periodic input is itself periodic with the same period length, and for (extended) Gaussian input signals [196]. With this condition obeyed, then the BLA of such system is definite to exist. The output spectrum of the system can then be written as:

$$Y_k = G_{BLA}(k)U(k) + Y_S(k) + V(k) + T(k) \tag{3.23}$$

where the term $Y_S(k)$ accounts for non-linear distortions, $V(k)$ accounts for additive measurement noise, and $T(k)$ accounts for leakage due to system and noise transients. To estimate the BLA and to significantly reduce the effect of leakage, the Local Polynomial Method (LPM) [199, 193] is often adopted.

The LPM exploits the smoothness over frequencies of $G_BLA(k)$ and $T(k)$, and the roughness over frequencies of $U(k), Y_S(k)$, and $V(k)$. The basic idea of the LPM is to model the $G_{BLA}(k)$ and $T(k)$ as polynomials in a local frequency band around frequency line k:

$$Y(k+r) = G_{BLA}(k+r)U(k+r) + Y_s(k+r) + V(k+r) + T(k+r) \tag{3.24}$$

with

$$\begin{aligned} G_{BLA}(k+r) &= \hat{G}_{BLA}(k) + \textstyle\sum_{s=1}^{R} \alpha_s r^s \\ T(k+r) &= \hat{T}(k) + \textstyle\sum_{s=1}^{R} \beta_s r^s \end{aligned} \tag{3.25}$$

for $r = -n, -n+1, ..., 0, ..., n-1, n$ with $n > R+1$.

Putting all unknown coefficients $\hat{G}_{BLA}(k), \hat{T}(k), \alpha_1, ..., \alpha_R, \beta_1, ..., \beta_R$ in a parameter vector θ_{LPM}, and collecting all variables in Equations 3.24 for $r = -n, -n+1, \ldots, 0, \ldots, n-1, n$ results in a linear regression formulation:

$$Y_n = K_n \theta_{LPM} + V_n \tag{3.26}$$

Solving for θ_{LPM} in least squares sense provides an estimate $\hat{G}_{BLA}(k)$ of the FRF of the BLA. From the residuals, the LPM can also provide an estimate of the covariance matrix of the noise V_n, which in this case includes the random noise and the non-linear distortions.

3.4.1.1 Estimating the Linear State Space Model

Once a non-parametric FRF model has been estimated, a parametric model is often required to get better understanding of the system's behaviour. To achieve this, a linear state space parametric model (A B C D) is fitted to the estimated non-parametric FRF $\hat{G}_{BLA}$ (k) in first part of Equation 3.25. The fitted linear state space model is attained using the frequency domain subspace identification introduced in [200]. The subspace identification algorithm is is used to transform the estimated non-parametric BLA ($\hat{G}(k)$) into a parametric model. The purpose is to estimate a linear discrete-time state space model from the estimated ($\hat{G}(k)$), taking into account the covariance matrix ($\hat{C}_G(k)$).

For this, the frequency domain subspace algorithm allows the incorporation of the covariance information for non uniformly spaced frequency domain data. In addition, the quality of the fit for the subspace identification is assessed by introducing a weighted least-squares cost function in the form:

$$V_L = \sum_{k=1}^{n_F} \epsilon_L^H(k) W_L(k) \epsilon_L(k) \tag{3.27}$$

where n_F is the number of processed frequencies, superscript H represents the Hermitian transpose while the weighting function is$W_L(k)$. The transfer function of the linear subspace model used in obtaining the FRF of the parametric BLA is calculated using the expression:

$$G_L(k) = C(z_k I^n - A)^{-1} B + D \tag{3.28}$$

where $Z_k = e^{j(\frac{2\pi k}{N})}$ represents the Z-transform variable, $I^n \epsilon \mathbb{R}^{n \times n}$ is an identity matrix with n being the most suitable model order required to achieve the lowest fitting error from the cost function minimisation.

Further minimising the cost function with respect to all the linear state space parameters in (A,B,C,D) with a Levenberg-Marquardt optimisation method often improves the quality of the fitting results obtained for the linear model.The main aim of the BLA and the subspace identification algorithm is to identify a linear model from the non-linear model of the device under test (DUT). The actual system will definitely not adhere to the linear representation, however, it is important to note at this stage that the goal is to retrieve a parametric model for the best linear approximation of the system. From the point of the view BLA, the non-linear behaviour of the

DUT can only result in two types of effects. First, through a bias contribution which can change the dynamic behaviour of the BLA while the second effect is through a stochastic contribution which act as disturbing noise. In general, the Best Linear Approximation G_{BLA} of a non-linear system depends on the amplitude distribution, the power spectrum and the higher order moments of the stochastic input.

3.4.2 Non-linear Optimisation of a Linear Model

During the estimation of the Linear model, a Weighted least square cost function VL shown in 3.27 to measure the quality of the model. According to this measure, it turns out that the subspace algorithm generates acceptable model estimates. However, in practical application the cost function V_L strongly depends on the dimensions of the selected parameter r. To improve the quality of the linear model estimate, the subspace algorithm can be applied for different values of r, for example $r = n_a + 1, ..., 6n_a$ while the model that corresponds to the lowest V_L is selected. Another way of obtaining better modelling result is to introduce the cost function:

$$V_{WLS} = \sum_{k=1}^{n_F} \epsilon^H(k) C_G^{-1}(k) \epsilon(k) \tag{3.29}$$

with

$$\epsilon(k) = vec(G_{SS}(A,B,C,D,k) - G(k)) \tag{3.30}$$

to minimise V_{WLS} with respect to all the parameters of (A B C D). This is classified as a non-linear optimisation problem which can be solved using the Levenberg-Marquardt (LM) algorithm.

This process requires the computation of the Jacobian of the model error $\epsilon(k)$ with respect to all model parameters. Based on Equations 3.30 and 3.28, the Jacobian of the model error are computed using the expressions:

$$\begin{cases} \frac{\partial \epsilon(k)}{\partial A_{ij}} = vec(C(z_k I_{n_a} - A)^{-1} I_{ij}^{n_a \times n_a} (z_k I_{n_a} - A)^{-1} B) \\ \frac{\partial \epsilon(k)}{\partial B_{ij}} = vec(C(z_k I_{n_a} - A)^{-1} I_{ij}^{n_a \times n_u} \\ \frac{\partial \epsilon(k)}{\partial C_{ij}} = vec(I_{ij}^{n_y \times n_a} (z_k I_{n_a} - A)^{-1} \\ \frac{\partial \epsilon(k)}{\partial D_{ij}} = vec(I_{ij}^{n_y \times n_u}) \end{cases} \tag{3.31}$$

In this case, the subspace algorithm is used to generate a number of initial linear models (e.g. $r = n_a + 1, ..., 6n_a$), which are used as initial starting values for the non-linear optimisation

procedure. The model that corresponds to the lowest cost function is finally selected. It is worth stating that there is a higher probability of ending up in a global minimum or at least a good local minimum due to the high number of different initial models employed during the optimisation. This is a consequence of fully parametrising the linear state space representation. In addition, the unstable models estimated with the subspace algorithm during the non-linear optimisation can be stabilised using methods such as the one described in [196].

3.4.3 Estimation of a Full Non-linear Model

The third step in the identification process is to estimate the full non-linear model

$$\begin{cases} x(t+1) = Ax(t) + Bu(t) + E\zeta(t) \\ y(t) = Cx(t) + Du(t) + F\eta(t) + e(t) \end{cases} \tag{3.32}$$

with the initial state given as $x(1) = x_0$ and $e(t)$ being the output noise. To achieve this, a second weighted least squares cost function is utilised. To make the estimates of the model parameters unbiased, it is often assumed that the input signal $u(t)$ of the model in 3.32 is noiseless. However, in practical situation, the assumption is not often fulfilled. When the Signal to Noise Ratio (SNR) at the input is high ($> 40dB$), the resulting bias in the estimated model parameter is negligible.If the SNR is too low, it can be increased by using periodic signals.i.e by measuring a sufficient number of periods and averaging over time or frequency. The second weighted least squares cost function that would be minimised with respect to the model parameters $\theta = [vec(A); vec(B); vec(C); vec(D); vec(E); vec(F)]$ is :

$$V_{WLS}(\theta) = \sum_{k=1}^{n_F} \epsilon^H(k,\theta) W(k) \epsilon(k,\theta) \tag{3.33}$$

Where $W(k) \in \mathbb{C}^{n_y \times n_y}$ is a user-chosen frequency domain weighting matrix.

Typically, this matrix is chosen equal to the inverse covariance matrix of the output $\hat{C}_Y^{-1}(k)$. This matrix can easily be obtained when periodic signals are used to excite the DUT. If the weighting matrix is selected appropriately, it is also possible to put more weight at specific frequency band of interest. When no covariance information is available and no specific weighting is required by the user, a constant weighting ($W(k) = 1$, for $k = 1, ..., F$) is utilised. The model error

$\epsilon(k,\theta) \in \mathbb{C}^{n_y}$ is defined as:

$$\epsilon(k,\theta) = Y_m(k,\theta) - Y(k) \tag{3.34}$$

where $Y_m(k,\theta)$ and $Y(k)$ are the DFT of the modelled and the measured output respectively. It worth stating that $Y_m(k,\theta)$ should be calculated with the correct initial conditions to avoid leakage problems if using non periodic data since the leakage terms in Equation 3.34 $Y_m(k,\theta)$ and $Y(k)$ cancel each other.

3.4.3.1 Non-linear Optimisation Methods

To minimise the cost functions introduced in Equations 3.27, 3.29 and 3.33, an iterative non-linear optimisation algorithm is required. This section provides a summary of the optimisation methods that could be used to minimise $V(\theta,Z)$ with respect to all parameters of θ. Given the iterative nature, the methods mentioned in this chapter all have a common computation of a parameter update $\Delta\theta$.

1. The Gradient Descent Algorithm

   The first algorithm is the Gradient Descent method. It is the most intuitive method to find the minimum of a function. In this iterative procedure, the parameter update $\Delta\theta$ is proportional to the negative gradient ∇V of the cost function

   $$\Delta\theta = -\lambda \nabla V \tag{3.35}$$

   with λ the damping factor. The main advantages of the gradient method are its theoretical simplicity and its large region of convergence to a local minimum. However, a drawback to this method is its slow convergence during the optimisation.

2. The Gauss-Newton Algorithm

   This method is very useful when a quadratic cost function $V(\theta,Z)$ needs to be minimised:

   $$V(\theta,Z) = e^T(\theta,Z)e(\theta,Z) = \sum_{k=1}^{N} |e_k(\theta,Z)|^2 \tag{3.36}$$

   with $e(\theta,Z)\epsilon\mathbb{R}^N$ being a residual. The iterative procedure in this method makes explicit use of the quadratic nature of the cost function. This results in a faster convergence compared

to the gradient descent method. The parameter update $\Delta\theta$ for this method is given by

$$\Delta\theta = -(\nabla^2 V)^{-1}\nabla V \tag{3.37}$$

This approach requires the knowledge of the Hessian matrix ($\nabla^2 V$) (i.e., the matrix containing the second derivatives) and the gradient (∇V) of the cost function, both with respect to θ.The convergence rate of the Gauss-Newton algorithm depends on the assumption that the residuals $e_k(\theta, Z)$ are small. In this case, the convergence rate can either be quadratic or become supra-linear. A major drawback to the Gauss-Newton algorithm is its smaller region of convergence compared to the gradient method.

3. The Levenberg-Marquardt Algorithm.

The last optimisation algorithm or method mention in this chapter is the Levenberg-Marquardt algorithm [185, 188]. This method combines the large convergence region of the gradient descent method with the fast convergence of the Gauss-Newton method. In this method the columns of the Jacobian matrix need to be normalised prior to the computation of the parameter update. This helps to increase the numerical stability and also avoids like for like comparison with the two previous algorithms. The normalised Jacobian matrix $J_N(\theta, Z)$ is given by

$$J_N(\theta, Z) = J(\theta, Z)N \tag{3.38}$$

where the diagonal normalisation matrix $N \epsilon \mathbb{R}^{n_\theta \times n_\theta}$ is defined as

$$N = diag\left(\frac{1}{rms(J_{[:,1]}(\theta, Z))}, ..., \frac{1}{rms(J_{[:,n_\theta]}(\theta, Z))}\right) \tag{3.39}$$

In most cases, the normalisation yields a better condition number (i.e., the ratio between the largest and smallest non zero singular value) for $J_N(\theta, Z)$ compared with $J(\theta, Z)$. For this method, the parameter update $\Delta\theta_N$ is computed by solving the equation

$$(J_N^T(\theta, Z)J_N(\theta, Z) + \lambda^2 I_{n_\theta})\triangle\theta_N = -J_N^T(\theta, Z)e(\theta, Z) \tag{3.40}$$

Where the damping factor λ determines the weight between the two methods. For a scenario where λ has a large numerical value, the second term in 3.40 is important which makes the gradient descent method dominate the optimisation. but for a scenario where λ is small,

the Gauss-Newton method takes over. To compute equation 3.40 in a numerically stable manner, the Singular Value Decomposition (SVD) of $J_N(\theta,Z)$ needs to be calculated first. If the Jacobian is singular, the SVD is calculated based on

$$J_N(\theta,Z) = U diag(\sigma_1,\sigma_2,...,\sigma_{n_{\tilde{\theta}}},0,...,0)V^T \tag{3.41}$$

The parameter update $\Delta\theta_N$ is then calculated using a truncated SVD resulting in the expression

$$\triangle\theta_N = V \wedge U^T e(\theta,Z) \tag{3.42}$$

The last step involves de-normalisation of the parameter update using the expression

$$\triangle\theta = N\triangle\theta_N \tag{3.43}$$

The largest singular value of $J_N(\theta,Z)$ from the first iteration can be used as initial values for λ, the λ, value is then adjusted based on the success of the parameter update. Different stop criteria can be used to bring the iterative Levenberg-Marquardt algorithm to an end. For example, the optimisation can be stopped when the relative decrease of the cost function becomes smaller than a user-chosen value or when the relative update of the parameter vector becomes too small. However, a simple approach is to stop the optimisation once a sufficient high number of iterations i_{max} is exceeded.

3.4.3.2 Calculation of the Jacobian

Since the minimisation of the cost function $V_{WLS}(\theta)$ is performed by means of a combination of the non-linear optimisation methods described in previous subsection. It is required to compute the Jacobian $J(k,\theta)$ of the modelled output with respect to all the model parameters. To compute this, the expression below is used

$$J(k,\theta) = \frac{\partial\epsilon(k,\theta)}{\partial\theta} = \frac{\partial Y_m(k,\theta)}{\partial\theta} \tag{3.44}$$

Given the non-linear relationship in Equation 3.32, it is often practically impossible to calculate the model output and the Jacobian directly in the frequency domain. Hence, the calculation can be carried out in the time domain followed by a DFT post processing to obtain $Y_m(k,\theta)$ and

$J(k,\theta)$. The explicit expression used in calculating the Jacobian in the time domain is based on considering a discrete-time non-linear model of the form

$$\begin{cases} x(t+1) = f(x(t),u(t),a) \\ y(t) = g(x(t),u(t),b) \end{cases} \tag{3.45}$$

Where a and b are the model parameters present in the state and output equation. The partial derivatives of the output $y(t)$ with respect to a and b are given by

$$\begin{cases} \frac{\partial x(t+1)}{\partial a} = \frac{\partial f(x(t),u(t),a)}{\partial x(t)} \frac{\partial x(t)}{\partial a} + \frac{\partial f(x(t),u(t),a)}{\partial a} \\ \frac{\partial y(t)}{\partial a} = \frac{\partial g(x(t),u(t),b)}{\partial x(t)} \frac{\partial x(t)}{\partial a} \\ \frac{\partial y(t)}{\partial b} = \frac{\partial g(x(t),u(t),b)}{\partial b} \end{cases} \tag{3.46}$$

The above equations can be rewritten in a simpler format expressed as

$$\begin{cases} x_a(t+1) = f_x(x(t),u(t),a)x_a(t) + f_a(x(t),u(t),a) \\ y_a(t) = g_x(x(t),u(t),b)x_a(t) \\ y_b(t) = g_b(x(t),u(t),b) \end{cases} \tag{3.47}$$

Hence the simplified expression that define the calculation of the Jacobian in Equations 3.47 can be regarded as a new dynamic discrete-time non-linear model. The inputs of this Jacobian are the inputs and the simulated states of the original model, these states are obtained by simulating the original model with the estimated parameters of the previous Levenberg-Marquardt iteration. Furthermore, due to the polynomial nature of Equation 3.32, the Equations in 3.47 are also in a polynomial form, hence, it is possible to obtain a PNLSS model based on the calculation of the elements of the Jacobian.

3.4.3.3 Initialisation of the Non-linear Model

In Equation 3.47, the simulated states are used to calculate the Jacobian. Hence, it is important to consider the initial state x_0 of the PNLSS model Equation in 3.32 when computing the state sequence.To achieve this, there are different possible approaches. But the simplest approach is to calculate the Jacobian for the full data set and then discard the first N_{trans} transient samples of both the Jacobian and the model error. With this approach, a part of the data is not used

for the model estimation. The last step that needs to be cleared before starting the non-linear optimisation is the selection of good starting values for θ.

A good starting value for θ is to use the values estimated from the parametric Best Linear Approximation for matrices A, B, C, and D. The other state space matrices E and F can be set to have zero initial starting values. Using the parametric BLA as initial values for the non-linear optimisation comes with two main advantages, first, it gives an assurance that the estimated non-linear model performs at least as good as the best linear model of the system under consideration. The second advantage is the ability to obtain a rough estimate of the model order n_a for a typical PNLSS model structure as illustrated in Equation 3.32.

3.4.4 Validation of the Non-linear Model

To achieve an optimum PNLSS model, the non-linear parametric search should be pursed until the cost function in Equation 3.33 stops decreasing. However, in the search for the best optimisation result, over-fitting can occur during the optimisation as it is often the case for model structures with many parameters. The over-fitting phenomena can be visualised by applying a fresh data set to the models obtained from the iterations of the non-linear search. In the case of over-fitting, the model quality first increases to an optimum and then deteriorates as a function of the number of iterations. This is as a result of the fact the important parameters are quickly pulled to minimising values at the start of the optimisation, while the bias error diminishes.

As the minimisation continues, the insignificant parameters are drawn close to reach minimising values. Hence, the number of parameters grow rapidly and the variance on the parameter estimate increases. To the growing number of parameters effect, a stopped search approach [31] is often implemented. This is used to evaluate the model quality of every estimated model on a test set, with the possibility of selecting the model that achieves the best result. Note that there is often no optimisation required in the validation step (no computation of Jacobian, step sizes, etc), just an evaluation of all the estimated models (this only requires simulating the estimated models with the validation input, and comparing the measured validation output with the simulated output). *It is worth stating that all equations used in deriving the PNLSS identification theory in this chapter are already available in the literature with references provided/cited at relevant*

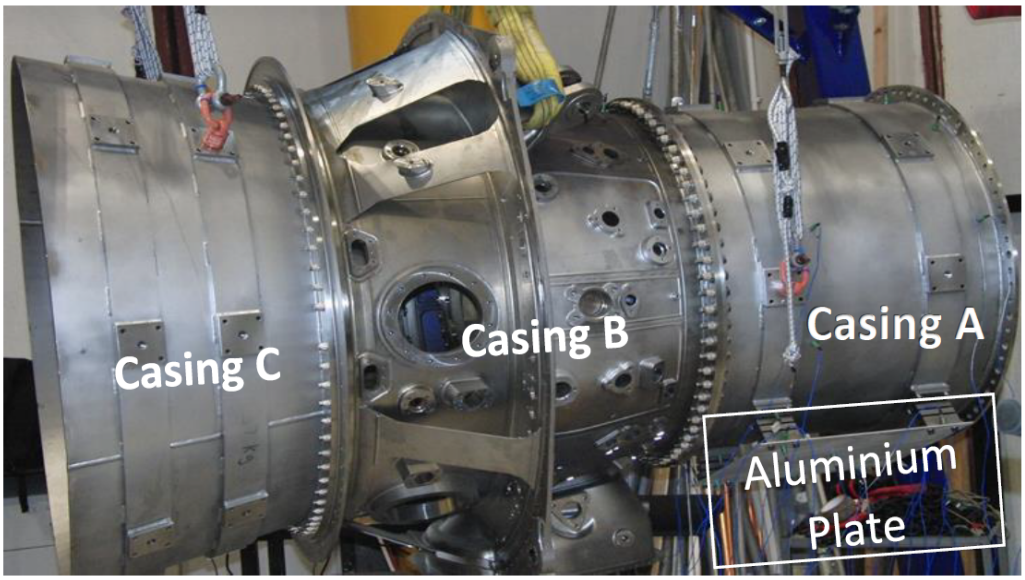

Figure 3.2: *Aero-engine casing and the attached Aluminium plate on the bottom right corner areas.*

3.5 Demonstration on an Aero-Engine Casing

3.5.1 Description of the Aero-Engine Casing

The application presented in this chapter was performed on an aero engine casing assembly structure presented in Figure 3.2. This type of aircraft engine casing assembly is often used for powering a typical commercial aircraft. The structural configuration of the casing assembly considered in this paper is a three-layer architecture without any internally attached accessories such as blades, shafts and other rotating components. The aero-engine casing assembly is made of three components comprising of casing A, casing B and casing C as shown in Figure 3.1 The entire assembled casing has structural features that are typical of a full-size assembled system e.g. multiple body sections and bolted joints.

The total mass of this casing assembly is 461kg. Additionally, the first cylindrical section of the casing (Casing A) has an aluminium plate with four low stiffness shaped steel blocks

mounted on it as shown in 3.2. Based on an experimental campaign and initial analysis of the aero-engine casing demonstrated in [201], the mounted plate forms an additional source of non-linear behaviour in the entire casing assembly. It introduces localised non-linearities from the bolted joints and large deformation of the plate depending on the mode of interest and also reflects on typical operational measurement limitations. To study the nonlinear phenomena exhibited by the entire assembly in a rather simplified approach, only the first cylindrical section of the casing (Casing A) was instrumented to obtain measured data during the experimental campaign as shown in experimental set-up.

3.5.2 Linear Finite Element Modal Analysis

Pre-test analysis is a vital step of Experimental modal testing and analysis, it often has direct effect on the accuracy and results of test and analysis. A detailed Finite Element (FE) model of the casing assembly was developed using the commercial ABAQUS FE package, all parts of the casing and the plates were modelled using shell elements. A linear FE modal analysis was conducted to extract the FE mode shapes. The linear FE analysis was conducted with the aim of getting better insight into the selection of appropriate measurement locations, sensor placement and the test excitation point. In addition, the initial FE analysis was used to determine the number of expected modes in a given frequency range. Most importantly, since the test was being conducted on a large aerospace structure with multiple joints and localised non-linearities, the results from the FE mode shapes were used to quickly and reliably identify the frequency ranges where the joints and additional localised nonlinear source were actively excited. The FE analysis highlighted 20 mode shapes between 0-350 Hz. A complete summary of the FE modal analysis is not included in this chapter. However, it is sufficient to state that the modes of vibration that engaged the entire casing assembly and the plate were calculated to have FE natural frequencies of 83.95 Hz and 87.12 Hz as shown in Figures 3.3a and 3.3b.

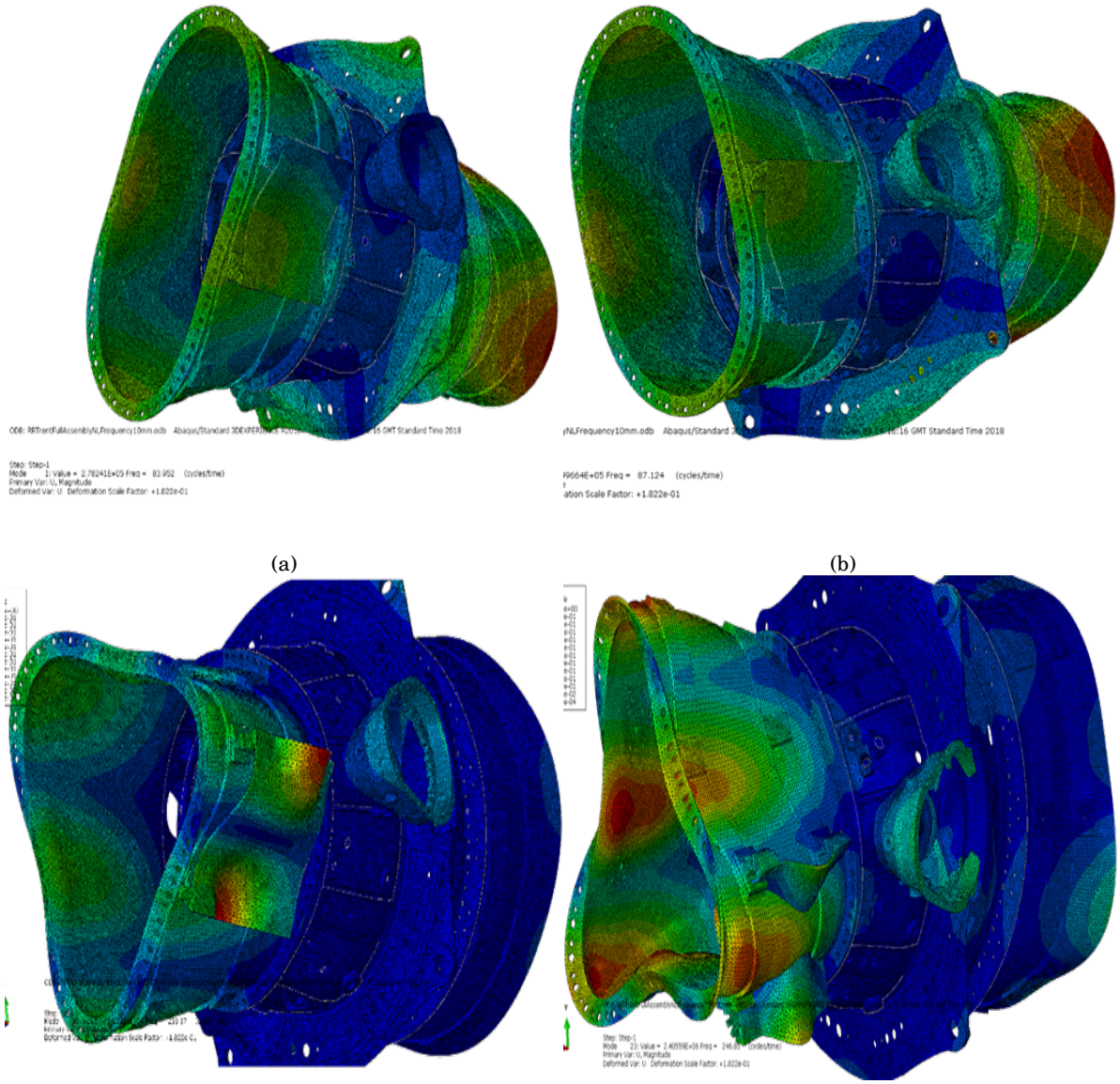

(a) (b)

(c) (d)

Figure 3.3: *Selected mode shapes obtained from the 3D FE modal analysis. (a) Mode 1: 83.95 Hz, (b) Mode 2: 87.12 Hz, (c) Mode 11: 233.27 Hz, (d) Mode 14:246.85 Hz.*

In addition, an area of interest on the casing assembly is the bolted connection between casing A and the aluminium plate. One of the main reasons for this interest is to understand the influence of connected devices on the casing and their potential introduction of local and geometrical nonlinearities to the entire structure. The FE model was also able to highlight the modes of vibration of casing A and plate with natural frequencies ranging between 180 to 300 Hz. Of all modes of vibration highlighted by the FE model, only those that are prone to stimulate all joints and plate connections are further investigated in the nonlinear identification section of this chapter. Figures 3.3c and 3.3d illustrate a selection of modes of vibration where the joints and local nonlinear sources are stimulated.

3.5.3 Experimental Campaign and Linear Modal Analysis

The casing was suspended horizontally from a test frame using four elastic chords as shown in Figure 3.4a. The test frame used in this research is classified as a Technology Research Level (TRL6) structure developed under the Highly Innovative Technology Enablers for Aerospace (HiTEA) project while the elastic chords are used to represent a free-free boundary test condition. The experimental set-up was designed to replicate the traditional horizontal configuration of such component when attached to an aircraft. A total of 32 Integrated Circuit Piezoelectric (ICP) type single-axis acceleration sensors were employed to instrument the structure. For this investigation, only the first subassembly section casing A where the plate is bolted to the engine casing, as illustrated in Figure 3.4b, was fully instrumented. A large shaker visible in Figure 4a was used to apply the excitation inputs to the casing in a vertical direction. The first stage of the experimental investigation involved conducting a set of traditional modal tests on the casing and plate assembly to obtain the natural frequencies and damping ratios at low amplitude of vibration. In addition, a force controlled stepped-sine test at high excitation levels was carried out on the assembly to check for the symptoms of non-linearity that could be present in the instrumented section of the casing. A preliminary experimental study highlighting non-linearities observed at the high amplitude of vibration was already conducted on the engine casing assembly in [200]. There, the linear FE mode shapes were used to gain an insight into the regions of the assembly that could potentially show some form of nonlinear behaviour. The first measurements

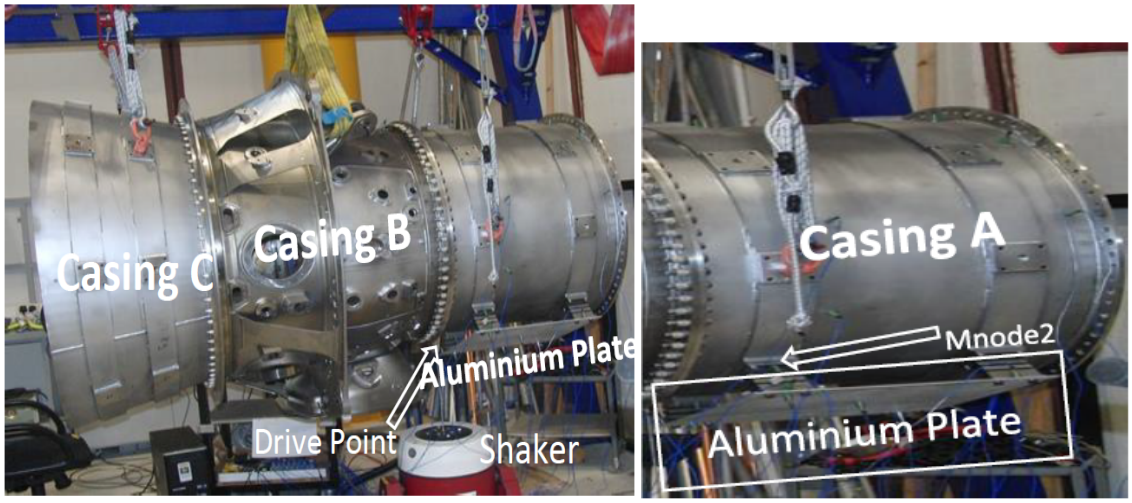

(a) (b)

Figure 3.4: *Experimental set-up of the Engine casing suspended on a TRL-6 frame. (a) Test Set-up,(b) Instrumented section of the casing*

obtained from the test comprised of several low-amplitude responses which were acquired based on the broadband random excitation. The choice of the broadband excitation was made based on its conventional use in modal testing. The low level random excitation test was performed using the Spectral Test module in LMS Test Lab. The test structure was excited near the flange connecting the casing B with casing A as shown in Figure 3.4a. The structure was excited using burst random excitation ranging between 30 and 320Hz and the applied random excitation had an RMS value of 45N. The Frequency Response Functions (FRFs) obtained from the test were used to identify the linear modal parameters of the entire assembly. Figure 3.5 shows a selection of the FRFs obtained from the low-level test. A linear modal analysis based on the FRFs obtained from the low-level random test was conducted using the PolyMAX method [2]. Table 3.1 presents the corresponding natural frequencies and damping ratios of the casing A with the aluminium plate bolted to it.

Mode Number	Natural Frequency (Hz)	Damping Ratio (%)	Mode Number	Natural Frequency (Hz)	Damping Ratio (%)
1	82.17	0.29	9	179.68	0.19
2	84.34	0.19	10	237.51	0.34
3	87.17	0.09	11	238.68	0.12
4	158.42	0.13	12	243.45	0.28
5	163.41	0.39	13	247.01	0.39
6	167.29	0.57	14	285.51	0.42
7	169.98	0.46	15	287.72	0.37
8	172.05	0.46	16	312.51	0.29

Table 3.1: Estimated natural frequencies and damping ratios based on low-level excitation

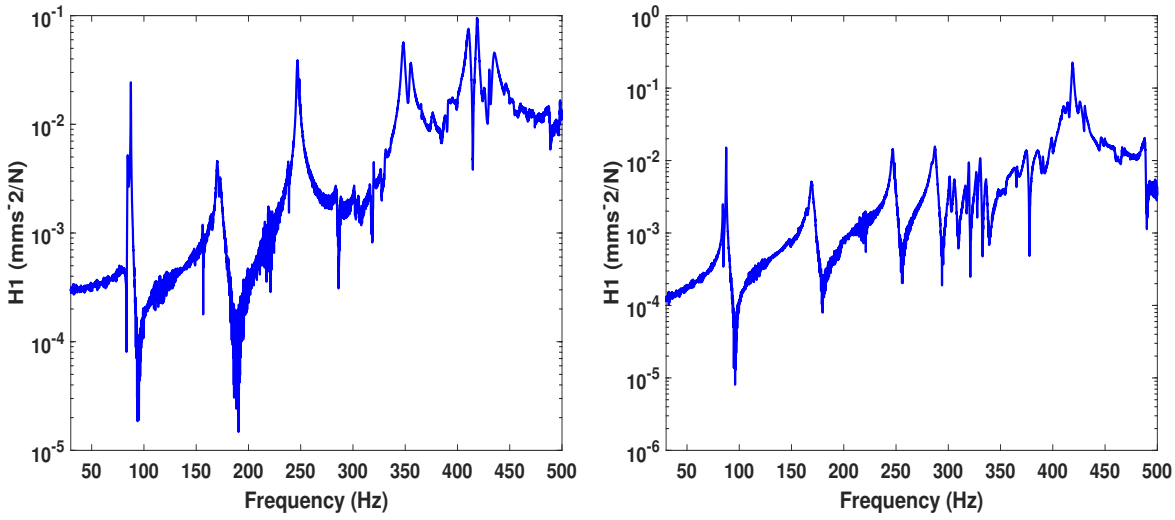

(a) (b)

Figure 3.5: *Acceleration response function obtained from low-level broadband excitation performed on the non-linear assembly. (a) Bottom centre of the first cylinder (b) Drive point.*

3.5.3.1 Non-linear Detection Based on Distortion of Measured Data

To check for symptoms of non-linear behaviour in the casing and plate assembly, several tests were conducted on the entire assembly using two different types of excitation signals. In this chapter, stepped and swept-sine excitations were used for investigating the non-linear effects observed in the measured response of the assembly from low to higher excitation levels. Stepped and swept sine excitation signals were selected based on their deterministic nature. For a linear system or structure, the output response would produce a pure sine wave and for a non-linear

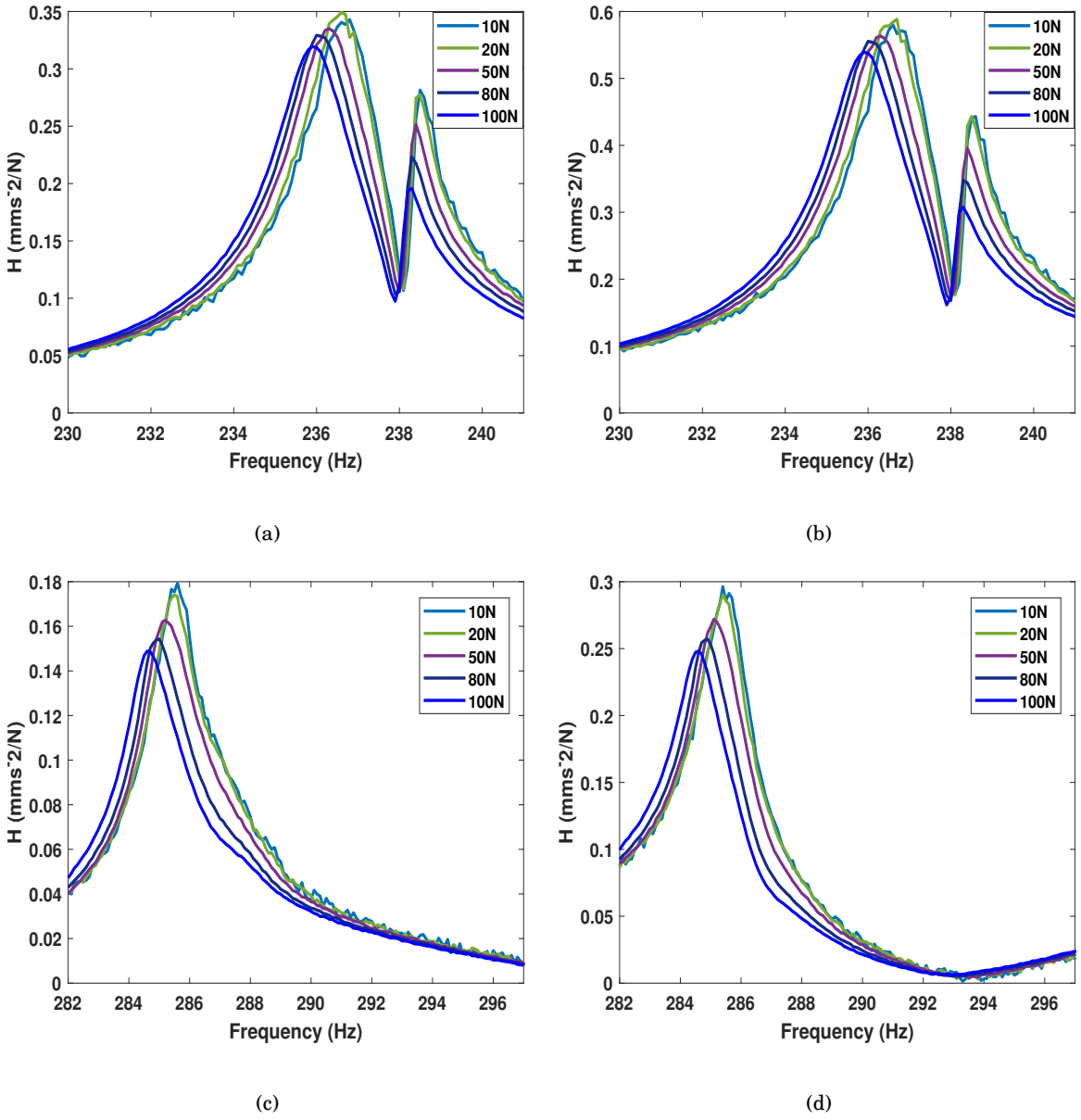

Figure 3.6: *Force controlled stepped sine acceleration response: (a) Mnode 2 FRF for frequency range 230-242Hz, (b) Drive point FRF for frequency range 230-242Hz (c) Mnode 2 FRF for frequency range 282-296Hz (d) Drive point FRF for frequency range 282-296Hz.*

case, distortions are easily detected by visualising the output response of the sine wave. In Figure 3.6 stepped-sine FRFs are presented for the test concentrated around each vibration mode of interest ranging from the lowest (10N) to the highest (100N) input levels of excitation. These stepped-sine FRFs only consider the first harmonic and neglect all other higher-order harmonic components in both input and output [202]. Figure 3.6 shows the lack of homogeneity in the

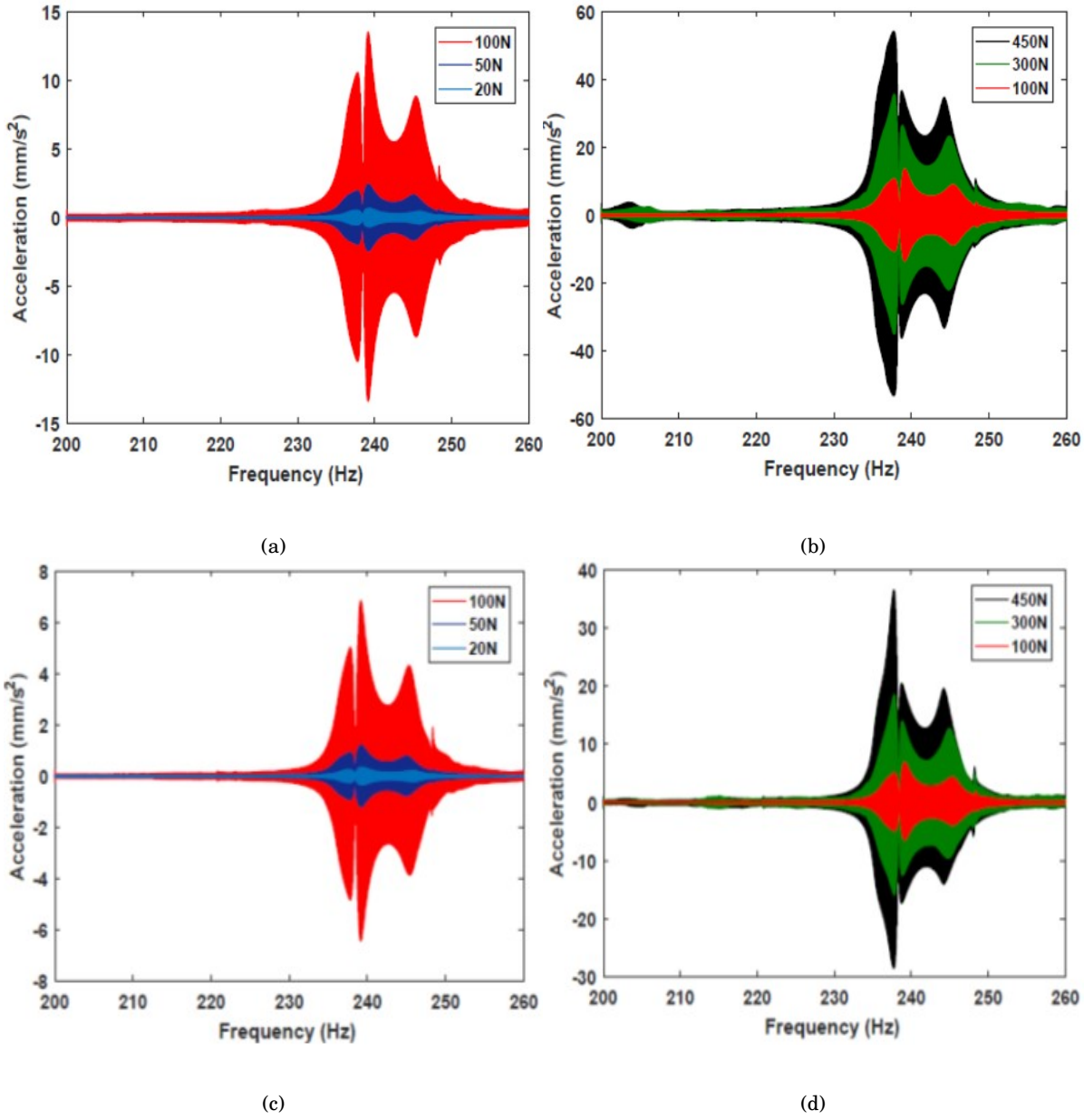

Figure 3.7: *Sine-sweep acceleration responses measured on two different locations of the assembly. (a) and (b) Drive point (b) and (d) Mnode2*

measured FRFs over different excitation levels, this is a clear breakdown of the superposition principle coming from linear theory. Evidence of non-linearity is observed based on the shift in frequency and maximum amplitude for the measured frequency bandwidth of 230-241Hz and 282-298Hz. In addition to the observed frequency and amplitude shifts, the resonant peaks also lean to the left as shown in Figure 3.6, causing a sudden transition (jump) down to a lower energy

state when increasing in frequency, and a smaller transition (jump) up to a higher energy state when decreasing in frequency in the result presented in Figure 3.6. This is most evident in the FRFs illustrated in Figure 3.6a and 3.6b for frequency bandwidth of 237-241Hz.

Sine-sweep test was also conducted on the casing assembly at multiple excitation levels to gain some insight into the time series data, the sine-sweep test was conducted to cover a frequency bandwidth of 200-260 Hz. Accelerations at selected locations of the assembly were measured at 20N, 50N, 100N, 300N and 450N excitation levels. Figure 3.7 (a-d) shows selected plots of the measured acceleration against sweep frequency for the modes of the assembly in that bandwidth.

Symptoms of non-linearity are visible in the plots presented in Figure 3.7 where a frequency shift is observed for all modes when the amplitude of vibration is increased. The lack of symmetry feature is also observed around the resonance peak of 238Hz for high amplitude of vibration, this is more obvious in Figure 3.7b and 3.7d. Skewness of the signal envelop is also observed around the resonance peaks at high excitation level, resulting to a jump phenomenon and non-smoothness of the signal envelop.

In practice, many non-linearities exhibit a degree of amplitude dependence and most of these become more prominent at higher levels of vibration rather than low levels. In this case of the aero-casing assembly, non-linear behaviour is clearly observed at higher excitation amplitude using a variety of excitation signals. Therefore, it is important to conduct further analysis on the casing assembly to gain further insight on the type of non-linearities detected from the measured data. This includes estimating a Best Linear Approximation (BLA) model based on measured data and also derive a data driven non-linear model using PNLSS method. All these are described in following sections below.

3.5.4 Best Linear Approximation of the Casing Assembly

To calculate the BLA of the casing assembly, sine-sweep input and output data sets were acquired at different excitation levels and different locations of the whole assembly. Although a sine-sweep is a deterministic signal instead of a random one, the initial linear state space and the FRF of

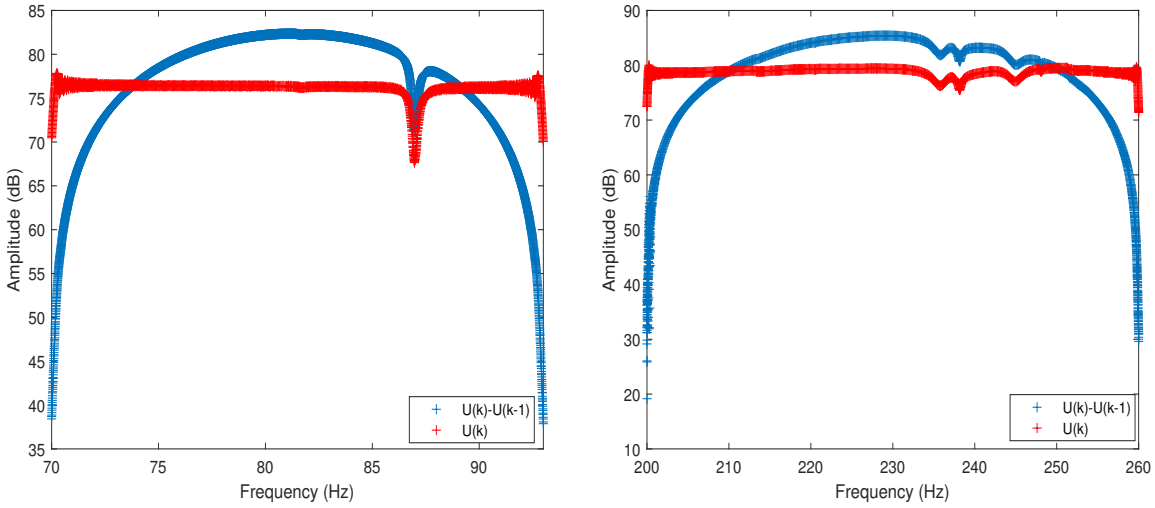

(a) (b)

Figure 3.8: *The difference of the sine sweep input DFT spectrum* $(U(k)-U(k-1))$ *of the interested bandwidth. (a) Frequency range 70-93Hz, (b) frequency range 200-260Hz*

the BLA can still be obtained using the expression given by:

$$G_{BLA}(k) = \frac{Y(k)}{U(k)} \tag{3.48}$$

at the excited frequency lines k. The fact that the spectrum $U(k)$ of a sine-sweep is not rough at all frequencies could pose a challenge in the calculation [199], however the LPM can still be applied based on calculating the difference between the input at two consecutive frequencies i.e, $(U(k)-U(k-1))$. The results obtained from the difference in spectrum calculation are presented in Figure for frequency bandwidth of interest. As shown in Figure 3.8, the spectrum $(U(k)-U(k-1))$ remains the same or at least within the same order of magnitude as U(k) in a large part of the frequency band of interest and only become extinct to zero at 70Hz and 93Hz for Figure 3.8a and 200 Hz and 260 Hz for Figure 3.8b.

This means that the spectrum $U(k)$ is sufficiently rough in the frequency band of interest. Therefore indicating that the LPM will be able to locally smooth the FRF for the BLA estimation With the FRFs and the BLA estimated based on the procedure described in section 3.4.1, a parametric model $(ABCD)$ is fitted on the non-parametric estimated model of the $G_{BLA}(k)$ using the frequency-domain subspace identification described in [196, 2]. The accuracy of the fitted

state space model is evaluated using a similar weighted least squares cost function expressed in Equation 3.27. In this case, the inverse of the estimated total variance of $G_{BLA}(k)$ is chosen as a weighting function

$$V_L(k) = \sum_{k=1}^{n_F} \frac{\left|G_{BLA}(K) - \hat{G}_{BLA}(K)\right|^2}{\sigma^2_{BLA(k)}} \tag{3.49}$$

Where $\sigma^2_{BLA(k)}$ represents the total distortions observed in the model. The model fitting error is then calculated based on the difference between the parametric and non-parametric BLA:

$$\epsilon_L = G_L(k) - G_{BLA}(k) \tag{3.50}$$

Figure 3.9 shows the corresponding estimated FRFs and total distortions for the parametric and non-parametric BLA for two main frequency bandwidth of interest (70-93Hz) and (200-260Hz), the selected FRFs and total distortion (= noise + non-linear) levels are based on excitation levels ranging from 20N to 100N. In this thesis, the time-domain signal is transformed to the frequency domain using the FFT algorithm, meaning that the time domain signal is written as a sum of sine waves. The amplitude spectrum shows the amplitudes of the frequency components in the Fourier series also known as the Discrete Fourier Transform (DFT) spectrum in vibration analysis of signals. An accurate fit is observed between the parametric and non-parametric estimation of the BLA based on a selected model order of 6, little discrepancies are only noticed at the start and end frequencies of the bandwidth of interest. The noise and non-linear distortion levels across the input band mostly lie averagely below -20dB most especial for the distortion estimation illustrated in Figure 3.9. To get an initial understanding into the non-linearities observed in the measured sine sweep in preparation for the full non-linear identification, a parametric and non-parametric BLA model was also estimated for different excitation levels ranging from an RMS value of 20N to 100N. Figures 3.9 and 3.10 shows an illustration of the estimated amplitudes and total distortion levels across the different excitation levels and frequency bandwidth of interest. Slight shift in the resonance peaks and reduction in amplitude is observed across the FRFs obtained from the multiple forcing level BLA estimation as shown in Figures 3.9 and 3.10 at higher excitation level. Similarly, it is evident that the total distortion (noise + non-linear distortions) also affect the response of the structure.

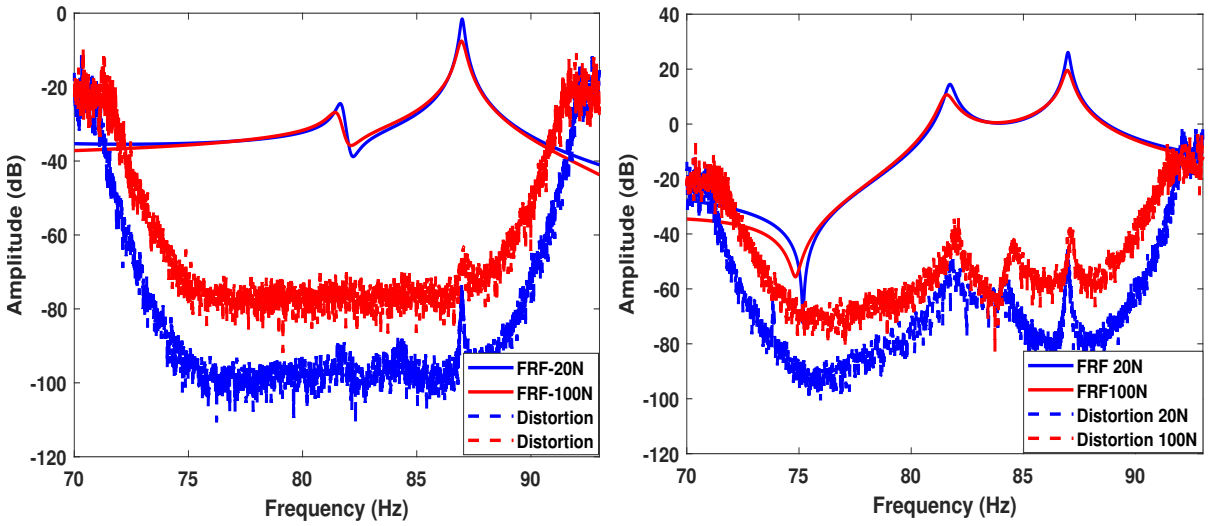

(a) (b)

Figure 3.9: *nonparametric FRFs and total distortions in the form of a discrete fourier transform spectrum: (a) Mnode 2 for 70-93Hz (b) Drive point for 70-93Hz.*

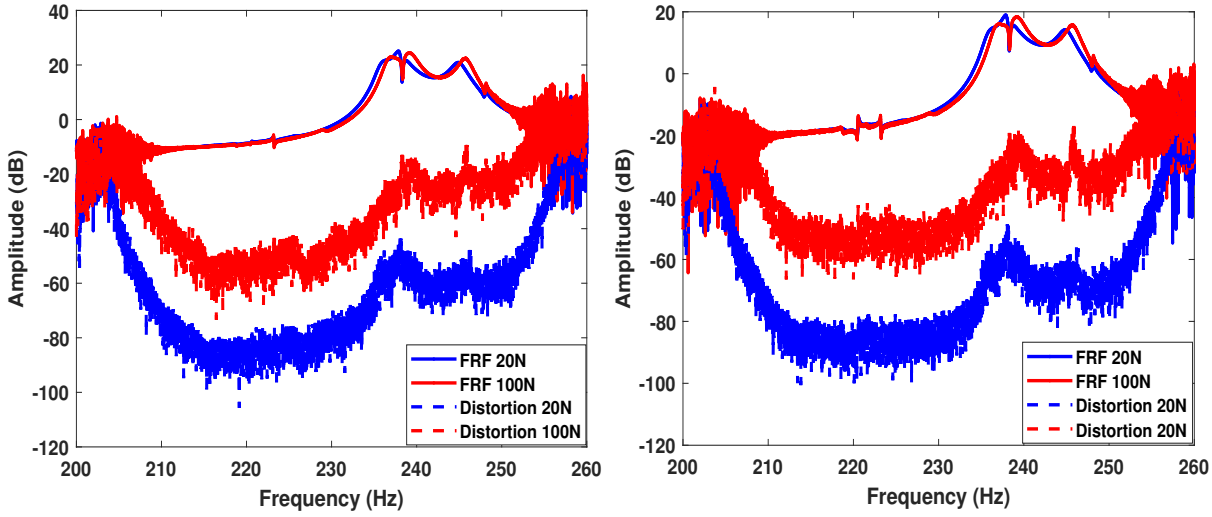

(a) (b)

Figure 3.10: *nonparametric FRFs and total distortions in the form of a discrete fourier transform spectrum: (a) Mnode 2 for 200-260Hz (b) Drive point for 200-260Hz.*

In Figures 3.9 and 3.10, the level of total distortions increases as the forcing changes from 20N to 100N for each frequency bandwidth of interest. The results obtained from the multiple forcing BLA estimation shows clear signs of non-linearity in the measured data and thus require

inclusion of non-linear terms in the state space modelling.In this case of the casing assembly, the increase in total distortion response at higher excitation levels as shown in Figures In this case of the casing assembly, the increase in total distortion response at higher excitation levels as shown in Figures 3.9 and 3.10 for the selected frequency ranges is a clear indication of the presence of non-linearities in the measured sine-sweep data. Furthermore, linear approach or technique can no longer be used to produce a true representation of the characteristics observed in the measured data illustrated in Figure 3.7

3.5.4.1 Linear State Space Model of the Casing Assembly

Before developing a PNLSS model, a linear state space model of the system under consideration is required, in this chapter, the linear state space model for the casing assembly is identified from the previously estimated BLA using the frequency domain subspace method [196]. A time domain least squares cost function which calculates the squared error between the simulated model outputs and the measured data was implemented to evaluate the accuracy of the linear state space model. The cost function expressed in Equation 3.30 is introduced to assess the quality of the fit for the linear subspace identification.

Figure 3.11 depicts the comparison between the simulated results obtained from the linear state space identification and the measured data, the time-domain signal is transformed to the frequency domain using the FFT algorithm, meaning that the time domain signal is written as a sum of sine waves. The amplitude spectrum shows the amplitudes of the frequency components in the Fourier series, plotted as a discrete time fourier transform. These results are identified based on using the non-parametric BLA estimated model parameters i.e (A, B, C, D) as initial starting values while the parameters in the E, and F matrices are set to have zero initial values. Judging from the time and frequency domain results presented in Figure 3.11, the results show that the initial identified linear model has a reasonable agreement with the measured data. However large errors and discrepancies are observed mainly around the resonance region which shows a clear indication that the non-linear dynamics are not yet captured.

The acceleration values at the resonance region are larger and in this case, may mean that the non-linearities are stronger in those section of the measured data, it therefore evident that the

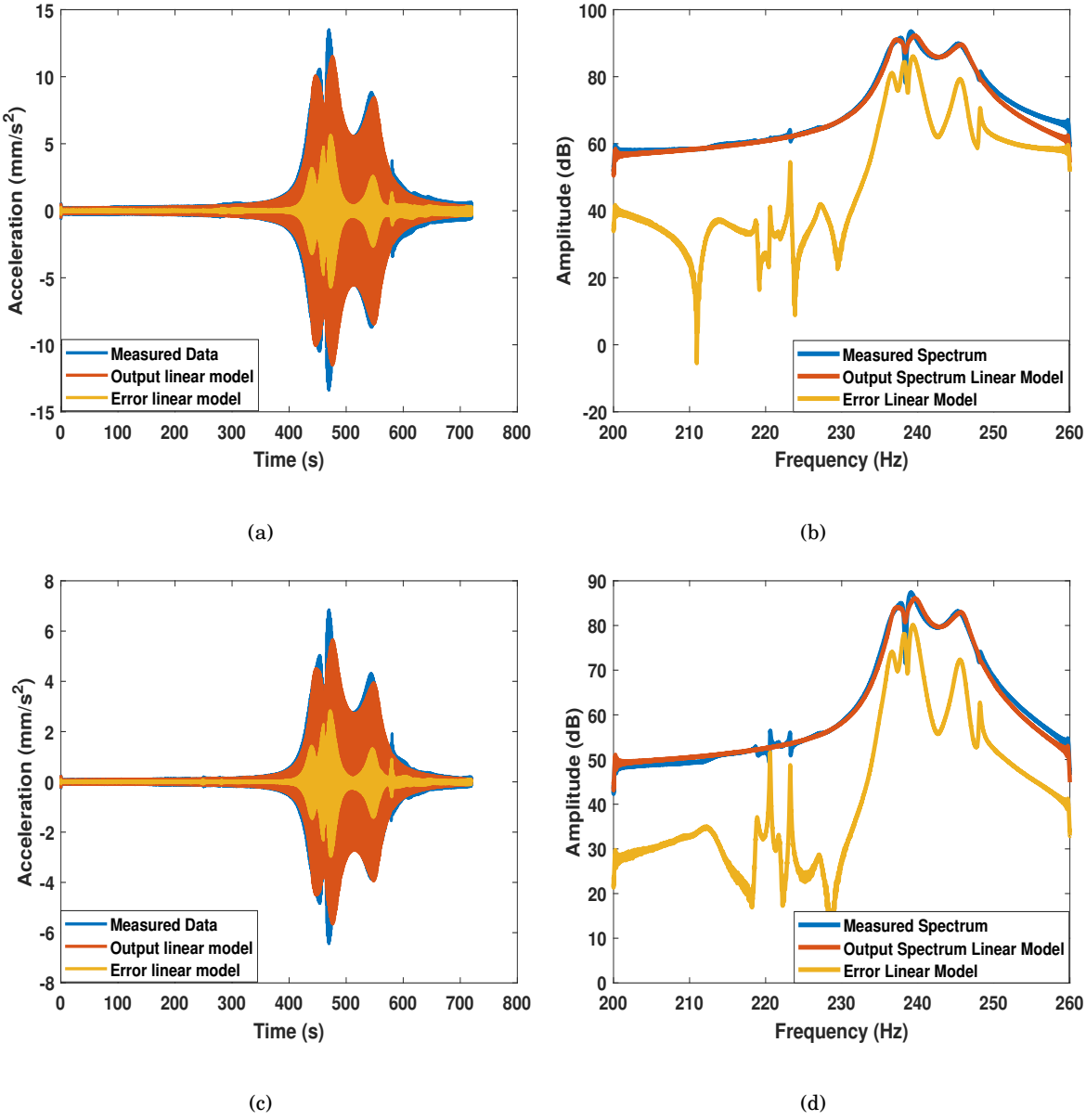

Figure 3.11: *Comparison of initial linear model against measured data: (a) time domain signal for drive point, (b) amplitude of the corresponding discrete time fourier transform for drive point, (c) time domain signal for Mnode, (d) amplitude of the corresponding discrete time fourier transform for Mnode.*

non-linear behaviour that cannot be captured by a linear model and as such a full identification is required to accurately capture the non-linear dynamics in the measured data. Similarly, the normalised Root Mean Squared (RMS) error of the linear model on the estimation data-set was 52.6%. Such a relatively high RMS percentage value is also an indication that the proposed linear

PNLSS Model Study	Polynomial Degrees
1	2-3
2	2-3-4-5
3	2-3-4-5-6-7
4	2-4
5	2-4-6
6	3-5
7	3-5-7

Table 3.2: Overview of the polynomial order implemented in the PNLSS identification

model is not sufficient and thus require further identification and minimisation of the selected cost function.

3.5.5 Non-linear Identification of the Casing Assembly

Referring back to the schematic of the identification procedure illustrated in Figure 3.1, this section focuses on developing a data driven non-linear model to model the non-linearities observed in the aero-engine casing assembly based on PNLSS model. Here, sine-sweep excitation at 100N RMS are used as the estimation data set for the PNLSS identification, while the non-linear identification is focused around the frequency bandwidth of 200-260 Hz. Furthermore, a study on using different monomial combination shown in Table 3.2 for the polynomial degrees selection such as consecutive, non-consecutive, even and odd was conducted.

3.5.5.1 Full Non-linear Model

To begin this stage, the linear state space parameters for (A, B, C, and D) estimated in the previous section was used as an initial starting value while the matrices (E and F) in Equation 3.33 are initialised as zero. The PNLSS model is evaluated by defining the weighted least-squares cost function $V_{WLS}(\theta_{NL})$ expressed in Equation 3.33. The final estimate of the non-linear state space parameters (A, B, C, D, E, F) are obtained by minimising the cost function $V_{WLS}(\theta_{NL})$. Here, the parameters in the matrices E and F that correspond to a term in which the input is raised to a non-zero power, is not optimised, but kept at its initial zero value. In other words, polynomial terms in the states only are considered.

A unit weighting $W(K)$ is applied as shown in Equation 3.33 for focusing on the frequency band 200-260 Hz during the minimisation of weighted least-squares cost function in the frequency domain. Unit weights are chosen in the frequency band of interest, while weights of 0.05 are chosen outside this band. It is important to give a non-zero weight to the data outside the frequency band of interest, since not using the information at those frequencies would lead to an ill-conditioned optimisation problem (with more unknown parameters than data samples used). The cost function is minimised with a Levenberg-Marquardt algorithm. In this research, the Levenberg-Marquardt method is initialised with $\lambda = 200$. This relatively large number is selected to make the optimisation process more robust.

This iterative algorithm can be seen as a mixture of the gradient-descent and the Gauss-Newton algorithm where the trade-off is determined by the Levenberg-Marquardt parameter λ. The limiting cases $\lambda = +\infty$ and $\lambda = 0$ correspond to gradient-descent with a zero step-size (the step-size decreases for increasing values of λ) and Gauss-Newton, respectively. Close to a local minimum, the Gauss-Newton method can converge faster, but there is no guarantee of convergence, especially if the current parameter guess is far away from a local minimum. In contrast, the gradient-descent method is more robust (under some conditions it is guaranteed to converge to a local minimum of the cost function), but convergence in the vicinity of a local minimum can be slow.

When an iteration is successful (i.e. the cost function decreased on the estimation data), the Levenberg-Marquardt parameter λ is adjusted to half of its previous value in order to make the optimisation algorithm lean more towards the Gauss-Newton method. This further improves the speed of the iterative process. While in the case of an unsuccessful iteration, the Levenberg-Marquardt parameter λ is multiplied with a factor $\sqrt{1}0$ to make the method lean more towards a gradient-descent algorithm with a decreased step-size for further optimisation improvement and robustness. The sine sweep data obtained at 100N level of excitation during the experimental campaign was used for the PNLSS model estimation. The estimated PNLSS model was developed using a state only model structure with a model order of 6 where no input terms were considered, while polynomial degrees of the order (2,3,4,5 and 7) was selected for the PNLSS estimation.

By minimising the second cost function in Equation 3.33, the results obtained from running

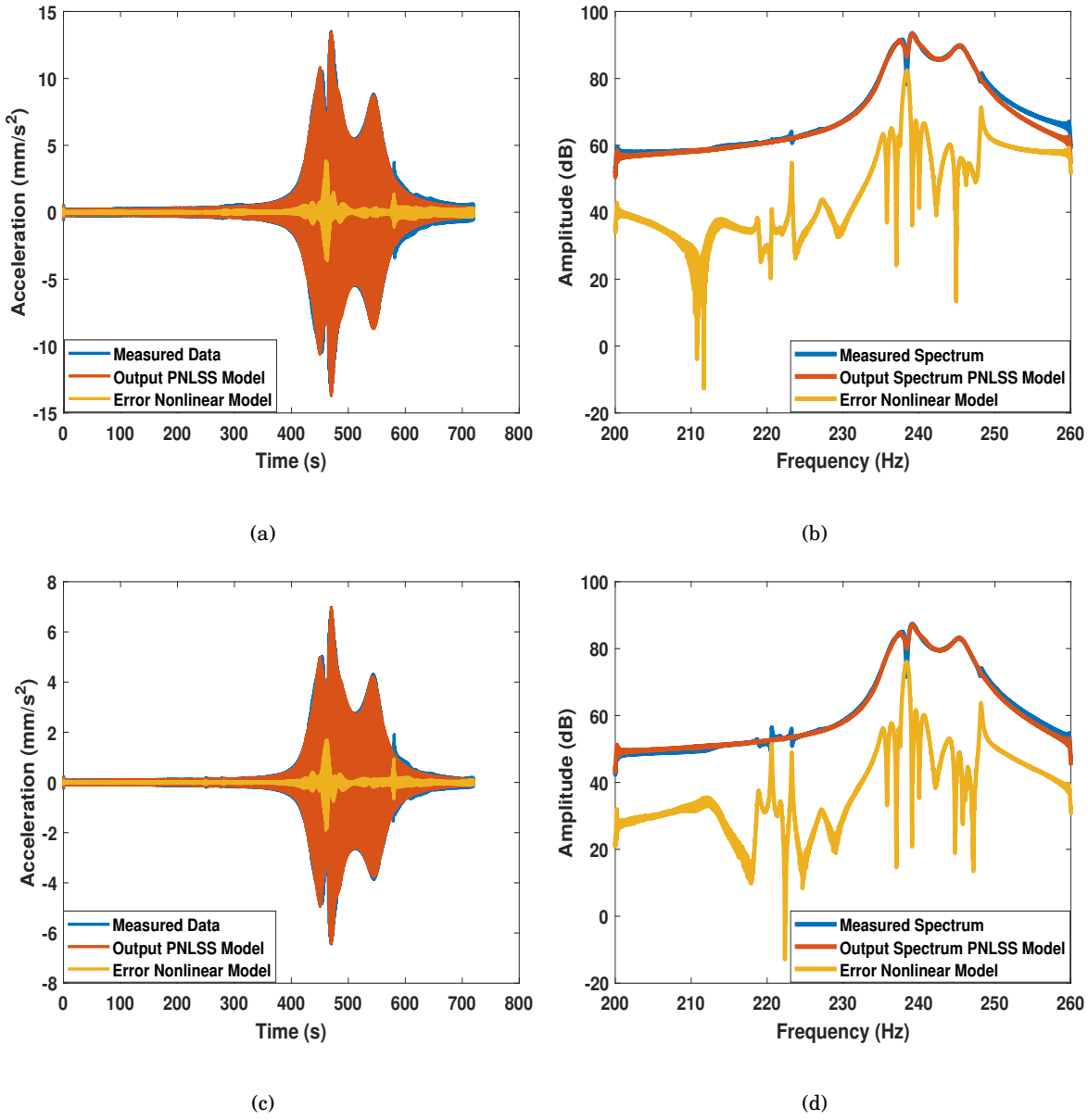

Figure 3.12: *Comparison of the identified PNLSS model against measured data: (a) time domain signal for drive point, (b) amplitude of the corresponding discrete time fourier transform for drive point, (c) time domain signal for Mnode, (d) amplitude of the corresponding discrete time fourier transform for Mnode.*

the second optimisation problem are presented in Figure 3.12. Comparing the full PNLSS results with the initial estimated results in Figure 3.12, one can observe a great improvement in the PNLSS model compared to the initial linear model. The optimised PNLSS model improves on the results of the initial linear model, most especially around the resonance frequencies as

shown in Figure 3.12 (a-d). This is a clear indication that the PNLSS model has successfully been able to capture a large portion of the non-linear dynamics that was not captured in the initial linear model presented in Figure 3.11. A significant improvement was also observed in the RMS percentage value after running the optimisation. Compared to the initial estimated model, a much lower RMS value of 7.2% was obtained for the PNLSS model. This shows a strong improvement of about 45% RMS reduction between the identified linear state model and the final estimated PNLSS model, validation of the identified PNLSS model on a new set of sine sweep data also yield RMS error of 9.1%. With this important improvement, it is evident that a discrete PNLSS model that describes the non-linear dynamics observed in the measured data has been successfully modelled without imposing any prior knowledge of the non-linearities in the measured data.

3.5.6 Identifying a Parsimonious Data Data Driven Model

Although the results achieved in previous section 3.5.5.1 indicated high degree of accuracy that the identified PNLSS model order of (2, 3,4,5,6 and 7) was able to capture the non-linear phenomena observed in the measured data, the total number of estimated parameters for the identified model is very large in the region of 13,728 parameters. The large number of estimated parameters can be narrowed down to the number of terms in a polynomial growing combinatorially with the degree of the polynomial. In addition, the combination of both even, odd and high monomial degrees in developing a suitable PNLSS model can be disadvantageous for some cases where the non-linear phenomena exhibited by the system are dominated by either even or odd polynomial degrees.

Hence in this section, a study on deriving a suitable PNLSS model using a series of different monomial combinations is conducted. The aim is to develop the best PNLSS model with the lowest number of parameters capable of modelling the non-linearities observed in the measured data of the aero-engine casing. Seven different PNLSS models were developed based on the monomial combination and order shown in Table 3.2, sine sweep measured data at 100N was utilised as the data set for the estimation of each PNLSS model while another set of sine sweep data at 50N was used for the validation of each estimated PNLSS model. Each monomial combination simulation

experiment was based on measured sine sweep data with signal sizes of (1474561x1) for the input and (1474561x2) for the output. The signal sizes are based on the Single Input Multiple Output (SIMO) configuration which is being considered in this chapter. For quality measures, the

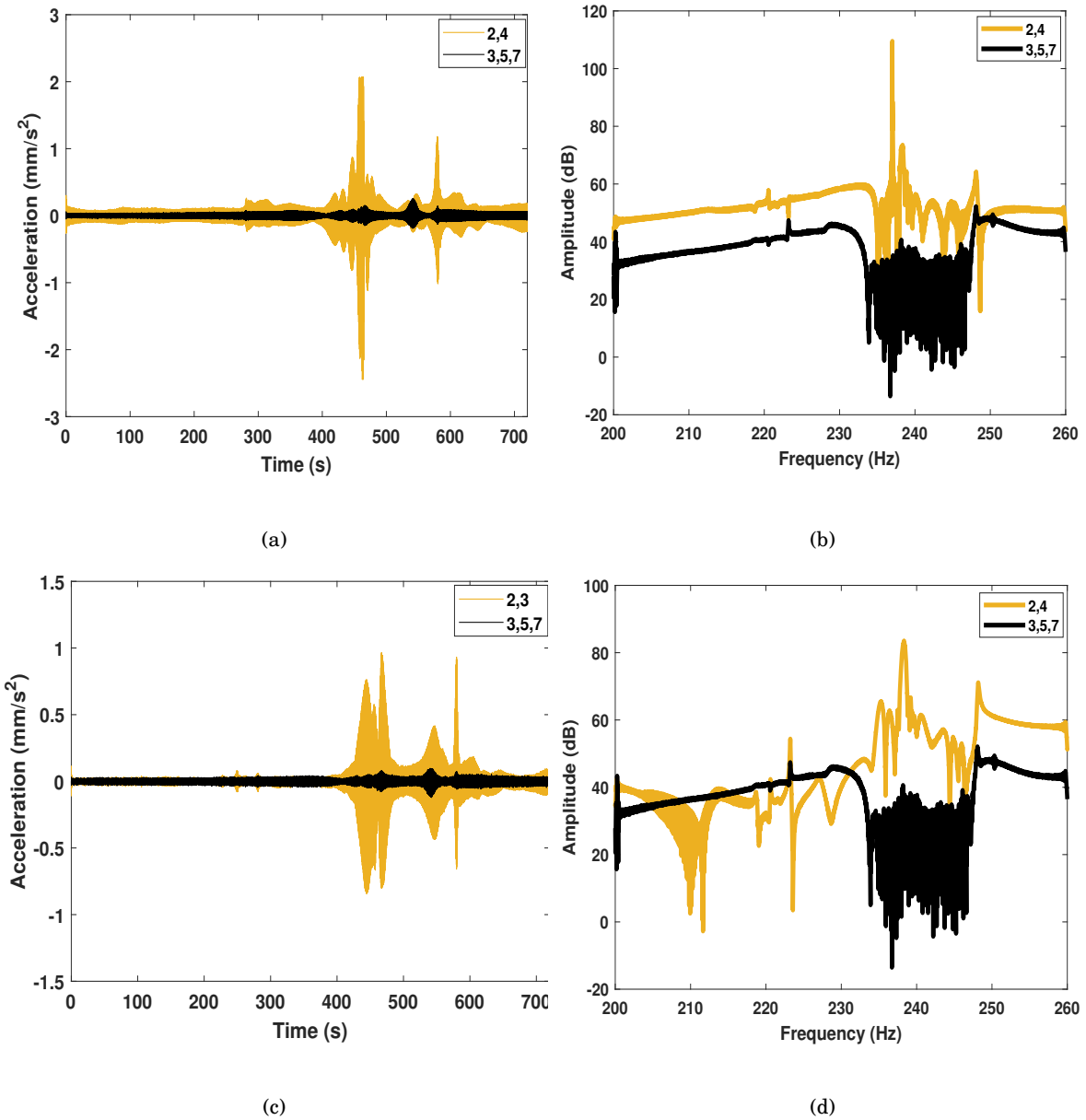

Figure 3.13: *Time and Frequency domain estimated model error for simulated PNLSS model using monomial combination of 2,4 and 3, 5,7: (a) time domain error signal of the drive point, (b) amplitude of the corresponding discrete time fourier transform error of the drive point, (c) time domain error signal of Mnode, (d) amplitude of the corresponding discrete time fourier transform error of Mnode.*

Polynomial Degrees	Estimation RMS Error (%)	Total Number of Parameters	Simulation Time (Hours)
2-3	15.91	672	8.37
2-3-4-5	4.89	3696	41.52
2-3-4-5-6-7	1.72	13728	121.29
2-4	16.04	1232	11.74
2-4-6	11.87	4928	63.81
3-5	5.01	2520	34.26
3-5-7	1.58	8856	101.65

Table 3.3: *Estimation results for different monomial combination experiments*

relative RMS error in the time and frequency domain and the NRMSE of the successful iteration of the LM optimisation were computed for each estimated PNLSS model. The performance of each simulated PNLSS model structure in Table 3.2 is calculated based on the expression in Equation 3.51

$$NRMSE = \frac{\sqrt{\frac{1}{N_t}\sum_{t=1}^{N_t}(y_{model}(t) - y_{measured}(t))^2}}{\frac{1}{N_t}\sum_{t=1}^{N_t}(y_{measured}(t))^2} \tag{3.51}$$

Where y_{model} and $y_{measured}$ are the PNLSS output and measured data, while N_t is the total number of data points. Transforming the error to the frequency domain was also another criteria used in judging the performance of each simulated monomial degree combination, the amplitude plot of the frequency domain error helps to show in which frequency bands the model performs well, and in which frequency bands it performs poor, based on the order of magnitude of the error which is classified as the amplitude.

Figure 3.13 shows the time and frequency domain error plots obtained for two PNLSS simulation results out of the seven PNLSS simulations that was conducted. For all the different PNLSS models that were estimated, the RMS error of the time and frequency domain is seen to decrease for increasing model complexity, in particular within the frequency band where nonlinear distortions are observed as shown in Figure 3.13 and Figure 3.14. The estimation errors for each PNLSS simulated model is presented in Table 3.3 with an approximate value of the time taken to compute each simulated PNLSS model. The lowest error value of 1.58% and 1.44% is achieved for monomial combination of the order (3, 5 and 7) as shown in 3.3. In addition, judging from the time and frequency error comparisons in Figure 3.13, it is possible to conclude that the monomial combinations with odd degrees can be used to reproduce better fitting PNLSS

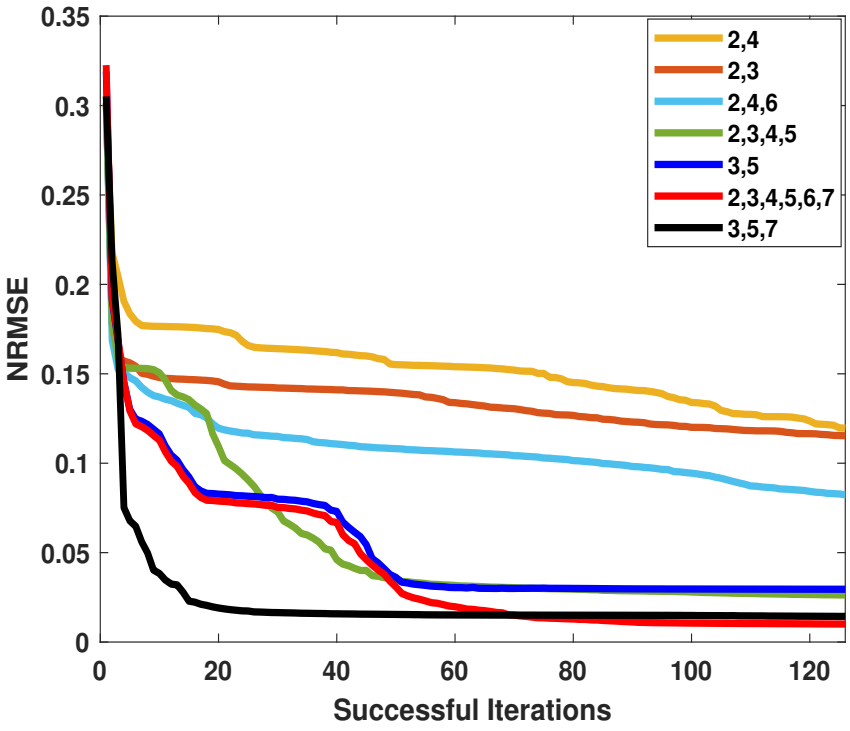

Figure 3.14: *Decrease of the NRMS estimation error over 120 Levenberg-Marquardt successful iteration for the seven simulated PNLSS models based on different monomial degree combination.*

models compared to the PNLSS model with even monomial degree combination.

In terms of obtaining a parsimonious model, Table 3.3 shows how the effect of increasing the complexity of the monomial degrees can cause a drastic growth in the total number of parameters estimated by each PNLSS model. In this case a parsimonious model is defined as a monomial combination with the lowest percentage error value between the PNLSS model and the measured data whilst using the least number of parameters or variables to obtain best PNLSS model prediction. For a performance perspective, selecting monomial of degrees 3, 5 and 7 yields estimation and validation errors of 1.58% and 1.44% with total number of 8856 estimated parameters. Compared to the first identified PNLSS model with monomial degrees of (2, 3, 4, 5, 6, and 7) and 13728 parameters which took just over 5 days on a standard desktop to complete all the computations, one can conclude that a PNLSS model with monomial degrees of 3 and 5 or 3, 5 and 7 can be used to correctly reproduce or model the non-linearities observed in the measured data to a high degree of accuracy.

Using either of these two proposed PNLSS model configurations has not only shown an advantage in terms of obtaining a reasonable parsimonious model, the computational burden and time involved in minimising the cost functions for these two models were considerably lower than the initial identified PNLSS model in Figure 3.12. Figure 3.14 shows the behaviour of the NRMSE for all simulated PNLSS cases, it is worth stating that for Figures 3.14 and 3.17, there are more than 120 Levenberg-Marquardt iterations. However, only the successful iterations (i.e. the iterations for which the cost function decreased during the optimisation process) are plotted. By plotting the normalised root mean squared error against the number of successful iterations of the LM optimisation, it is also possible to get some information on the monomial degree combination that produces the best PNLSS model capable of modelling the non-linearities based on the error magnitude and convergence rate during optimisation.

In Figure 3.14, the NRMSE with odd monomial degrees generally show significantly better and faster convergence versus error curve compared to the ones with even and odd monomial degree combination. The model with monomial degrees 3, 5, and 7 reaches the one but lowest NRMSE (after the model with monomial degrees 2, 3, 4, 5, 6, and 7), but converges faster and uses significantly less parameters. Since the obtained NRMSE values with both models are fairly close, the model with monomial degrees 3, 5, and 7 is retained because of the trade-off between performance and parameter parsimony as illustrated in the results presented in Table 3.3. From Figure 3.14, it is apparent that the PNLSS model with monomials of degree (3, 5 and 7) performs better than the other six different monomial combinations that were simulated.

Comparing the measured data and the simulated PNLSS model in the time domain for monomial degree 3, 5 and 7 as shown in Figure 3.15a and 3.15c, it is evident that the model was practically able to accurately reproduce the maximum amplitude of each mode in the envelope of the time series. In Figures 3.15b and 3.15d, the simulated PNLSS model was able to replicate correctly the frequency spectrum and also the characteristics for each mode of the measured data. The non-linear distortions observed in the envelope of the time series at higher excitation level was also well captured by the simulated PNLSS model as shown in Figures 3.15a and 3.15c.

Based on all these observations it is possible to draw a conclusion that the non-linearities observed during the experimental campaign of the aero-engine casing assembly are best modelled

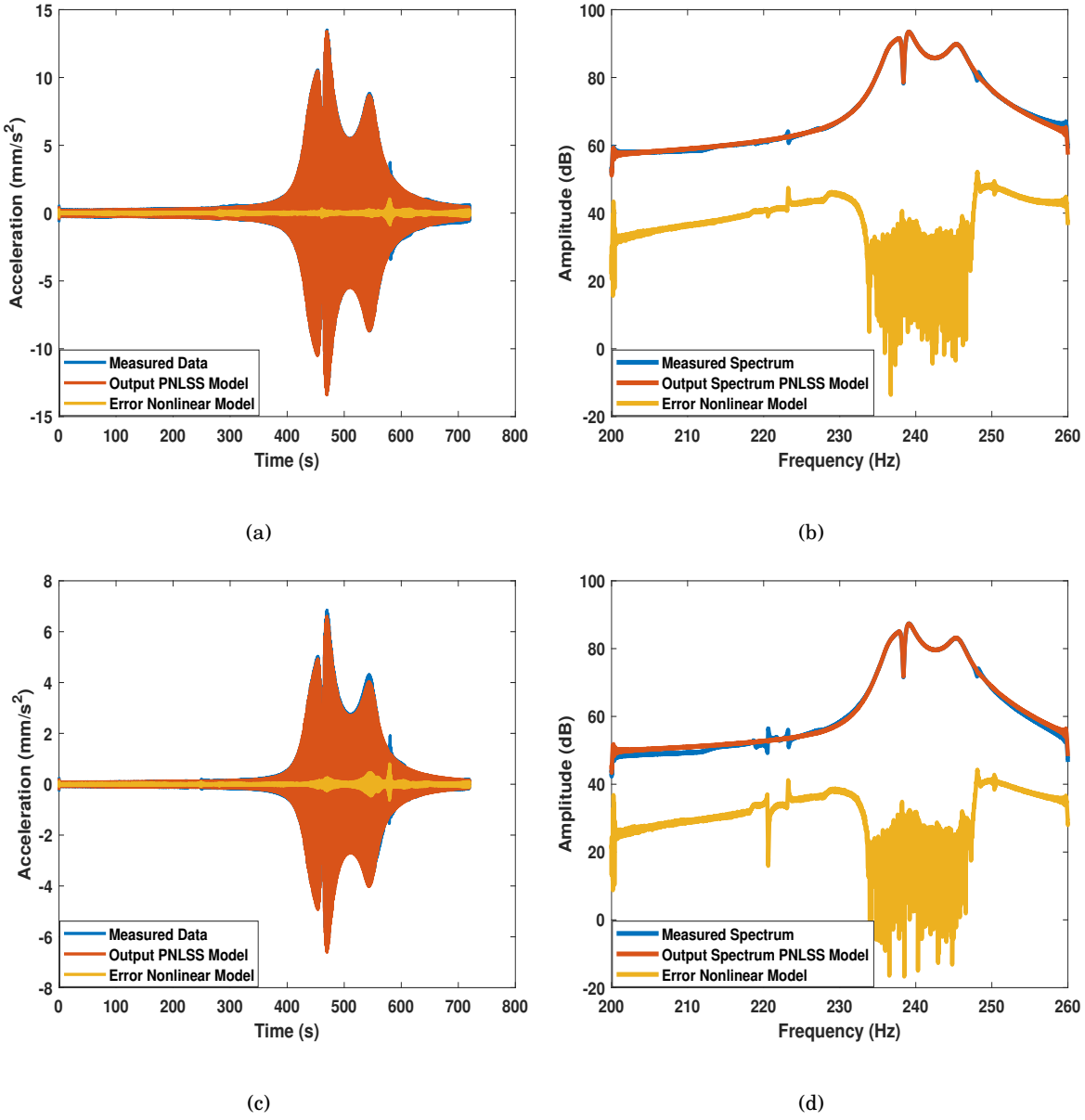

Figure 3.15: *Time and frequency domain comparison of the final estimated PNLSS model against measured data based on polynomial order 3, 5 and 7. (a) and (b) Time domain and amplitude of the corresponding discrete time fourier transform for the Bolted connection closest to the drive point between the casing and the plate, (c) and (d) Time domain and amplitude of the corresponding discrete time fourier transform for the Drive point.*

using polynomial with odd degrees. Both the error values and the LM iteration curves demonstrate the success of how well PNLSS models could be used to model the non-linearities observed in the experimental data without prior assumptions. Most importantly, this section of the chapter

Polynomial Degrees	Validation Error (%)
2-3	10.83
2-3-4-5	4.71
2-3-4-5-6-7	1.67
2-4	11.69
2-4-6	6.34
3-5	2.13
3-5-7	1.44

Table 3.4: Validation results for different monomial combination experiments

has also shown some advantages and the possibility of obtaining an optimal parsimonious model with a low percentage error by running several simulation studies using different monomial degree combinations.

3.5.7 Model Validation Based on Sine-Sweep and Broadband Excitation

To examine the domain of validity for the different simulated PNLSS models, each model is subjected to a validation experiment by introducing new measured data. In the estimation step, the models obtained after a successful Levenberg-Marquardt iteration are retained as candidate models. In the validation step, the model among the candidate models that achieves the lowest cost on the validation data is selected as the final model. Note that there is no optimization in this validation step (no computation of Jacobians, step sizes, et cetera), just an evaluation of all the candidate models by simulating the candidate models with the validation input and comparing the measured validation output with the simulated output.The validation experiment was intended to measure the performance of the identified PNLSS models under similar practical conditions based on the frequency and amplitude range of interest.

However, since the system under consideration is non-linear then it is advisable to use experimental data with lower excitation levels to avoid extrapolation. In this case, measured sine-sweep data at 50N was introduced to each identified PNLSS model in Table 3.3, the RMS error in the time and frequency domain were also used as quality measures to judge the performance of each validation experiment. Seven different PNLSS model validation experiments were conducted and a comparison between the measured data and the reconstructed PNLSS model at excitation level of 50N was used to visualise the performance of each validation experiment. The percentage

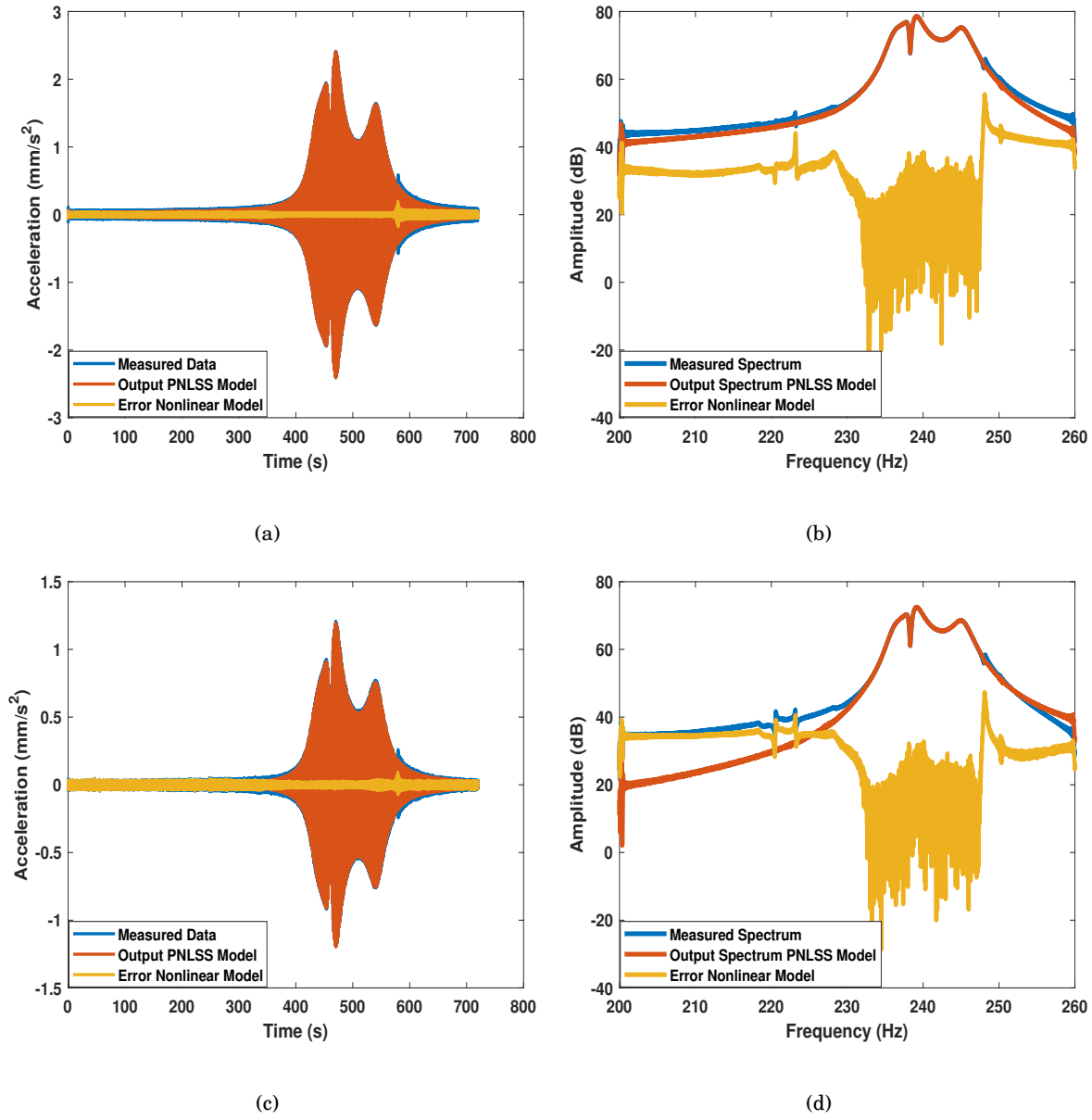

Figure 3.16: *Validation of PNLSS model against measured data for 3-5-7 monomial combinations. (a) Time domain response of the drive point, (b) amplitude of the corresponding discrete time fourier transform of the drive point (c) Time domain response of Mnode 2 (d) amplitude of the corresponding discrete time fourier transform of Mnode 2*

error of the non-linear PNLSS model for each validation experiment is illustrated in Table 3.4, where the RMS errors for the validation experiment were generally lower than the errors for the estimation results.

Amongst all the PNLSS models of the validation experiment, the PNLSS model with monomial

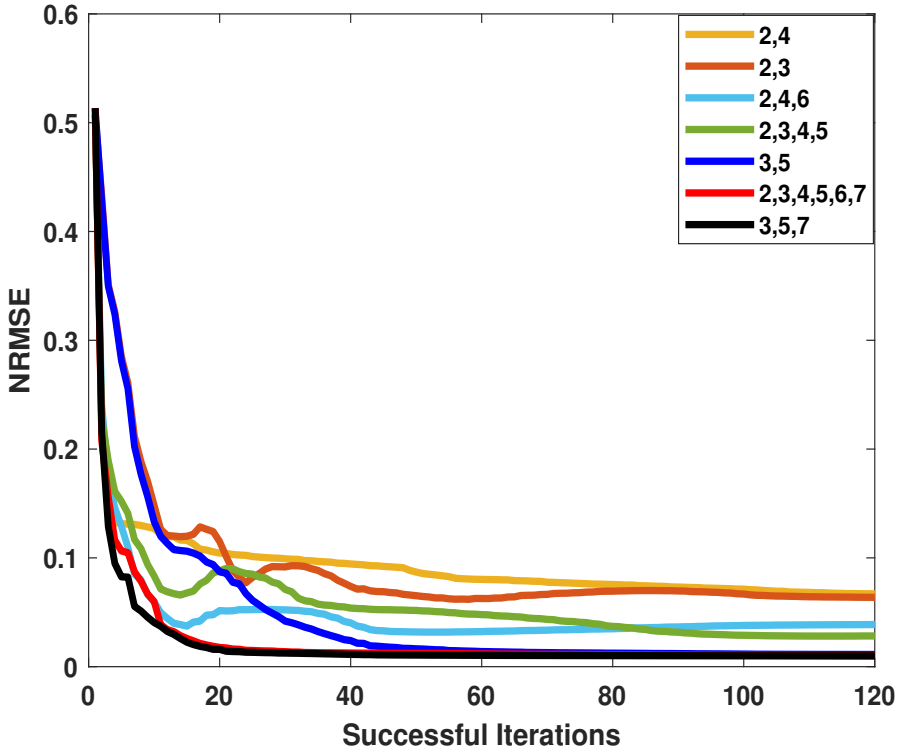

Figure 3.17: *NRMS Validation error over 120 Levenberg-Marquardt successful iteration for the seven simulated PNLSS models based on different monomial degree combination.*

degrees of 3, 5 and 7 had the lowest RMS error value. Figure 3.16 illustrates the time series envelope and the spectrum for this PNLSS model compared with experimental data at 50N for two different location on the aero-engine casing, the PNLSS results presented in Figure 3.16 show good agreement with the measured data most especially around regions of the three dominant resonance peaks. Although minor discrepancies are still observed between the PNLSS model and measured data, these discrepancies are outside the resonances/ frequencies of interest and can be narrowed to errors generated from the flexibility of the PNLSS models. Similar to the identification results, the normalised root mean squared error (NRMSE) against the number of successful iterations of the LM optimisation was plotted for each model in the validation experiment. Results of the NRMSE curve for the seven validation models are illustrated in Figure 3.17. For all the models, the final NRMSE is less than 10%, indicating that the PNLSS model structure seems reasonable to capture the non-linear dynamics of the aero-engine casing. Moreover, the NRMSE is relatively low already after 20 iterations and keeps being small. The

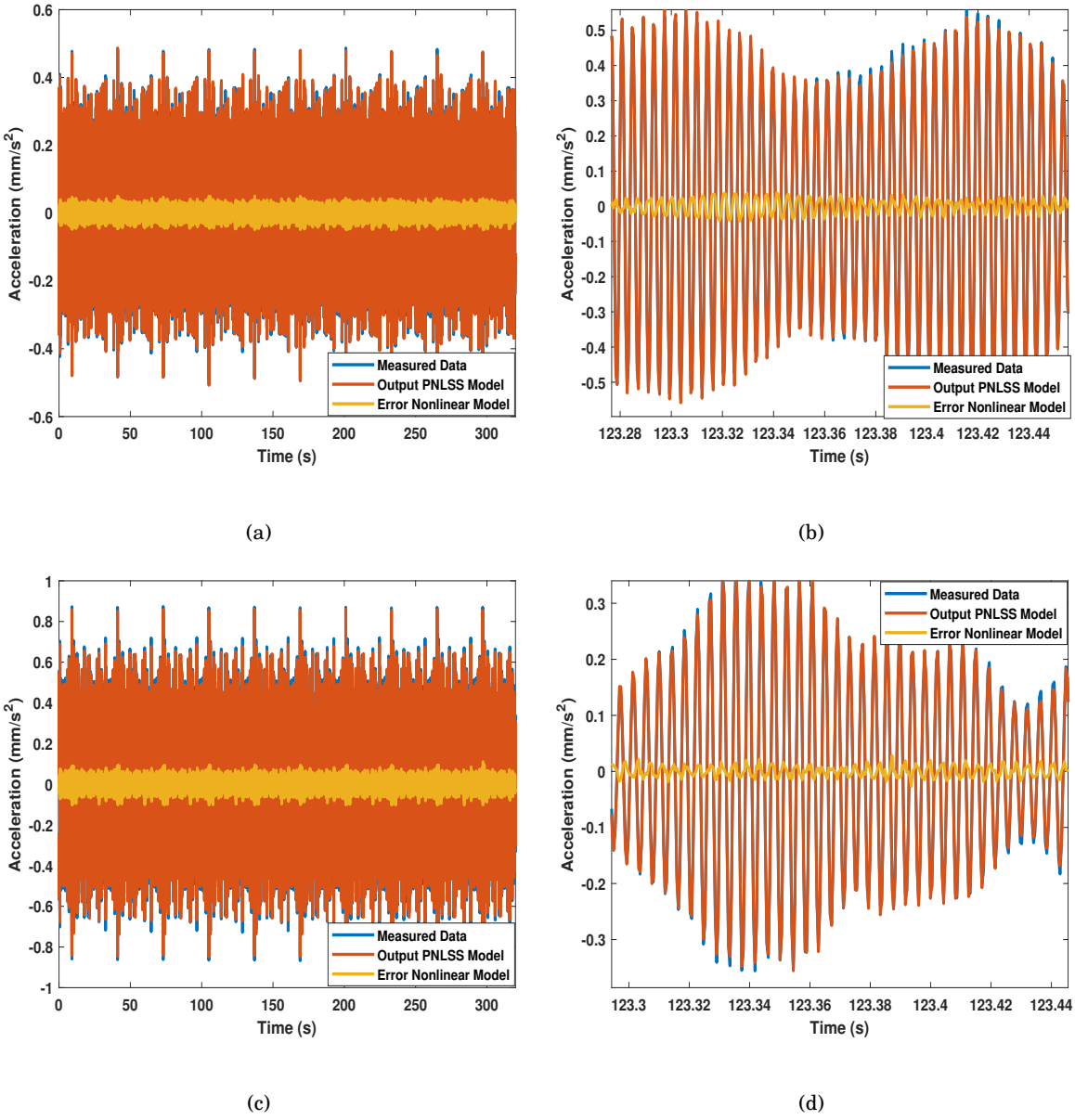

Figure 3.18: *Time-domain performance of the validated model for the monomials of degree 3-5-7 based on the measured broadband data. (a) Time domain response of the drive point, (b) Zoomed-in time domain response of the drive point, (c) Time domain response of Mnode 2 (d) Zoomed-in time domain response of Mnode 2.*

performance of the model is thus robust to the model selection process as it does not seem to matter too much which of the models between iterations 20 and 120 actually got selected as the best one on the estimation data. Comparing the NRMSE for all validation models, two different monomial degree combinations namely (3, 5, 7) and (2, 3, 4, 5, 6, 7) had almost the same decreasing

NRMSE curve and RMS error values as shown in Figure 3.17 and Table 3.4. Compared to the identification results, the PNLSS models with monomial combinations (3, 5, 7) and (2, 3, 4, 5, 6, 7) proved the best performance on the RMS error criterion. Whilst the Levenberg-Marquardt has proven very effective in this case study based on it's ability to successfully adjust the optimisation step size to lean to either of the Gauss-Newton and Gradient-descent algorithms when required during the optimisation, the Levenberg-Marquardt may sometimes not find the global minimum during optimisation which can yield inaccurate optimisation results. For optimisation processes with global minimum challenges, other optimisation algorithm such as simulated annealing [203] which uses probabilistic method for finding global minimum of a cost function with several local minima and genetic algorithm [204] which is based on intelligent exploitation of random search provided with historical data to direct the search into the region of better performance in solution space. The genetic algorithm is often used for solving both constrained and unconstrained optimisation problems that is based on natural selection.

To further test the domain of validity of best performed PNLSS model, the PNLSS model was subjected to another validation test. In this case, broadband data measured at 40N excitation level was introduced to the PNLSS model with monomial degree combinations of (3, 5, 7). Figure 3.18 shows a time domain comparison of the measured data and reconstructed data by the PNLSS model. The RMS value of the error on this validation data set is $0.05mm/s^2$. Figure 3.18 agreeably demonstrates the significance and validity of the PNLSS model using a different type of excitation signal, where the minimal RMS value can be seen as a way of enhancing the predictive confidence of the PNLSS model with monomial degree combinations of (3, 5, 7). From a user point of view, having minor errors between the measured data and the reconstructed PNLSS models in many cases be tolerable, given that a good estimate of the maximum amplitude, the frequency of the response and the features of the signals are obtained. Most importantly, for such a black-box application, the results have shown a great degree of accuracy based on the error values between the simulated PNLSS model and measured data. It is also worth stating that a price to pay for the large modelling flexibility implemented in non-linear state space models is the systematic and variance errors which are sometimes unavoidable depending on the problem which is being investigated.

3.6 Remarks on PNLSS Approach for Non-linear Identification

The Polynomial state space approach can often have a number of drawbacks, some of which are the explosive behaviour of polynomials outside the estimation region and the stability issues during estimation and validation. On experimental data, it often possible that the estimated model becomes unstable on the validation set, to overcome this problem an empirical method is implemented. This is based on passing the validation input signal on to the non-linear optimisation algorithm, with this, the validation output of the updated model with parameters θ_{test} can be computed in every iteration using the LM algorithm. When the validation output is unstable, the optimisation algorithm reacts as if the cost function has increased. This approach guarantees that the model is stable for the validation set.

Secondly, the PNLSS model is only suitable to handle low order systems such as ($n_a < 10$). For higher order systems, the combinatorial explosion of the number of parameters poses a big restriction in getting a good identification result. This problem can be overcome by restricting the number of states included in the polynomial expansion or by imposing a linear relation for a part of the states. Another disadvantage of the PNLSS approach occurs in the non-linear search stage of the estimation of the model parameters, the challenge of getting stuck in a local minimum is imminent. However, this can be seen as a generic burden for most non-linear identification methods and even some linear modelling techniques. Lastly, the stability of the estimated model can be difficult to ascertain, though, the risk of instability is inherent to any recursive model. One can override the instability by adding constraints to keep the model stable. But this may have a negative influence on the modelling performance.

On positive notes, the PNLSS model can be used to derive a general black box model of a non-linear system or structure as demonstrated on the aero-engine casing assembly. In addition, PNLSS models have extreme flexibility and capabilities to cope with multi-variable systems most especially if the user is not interested in physical interpretation of the model parameters. Additionally, the PNLSS identification procedure is straightforward and can easily be achieved in three steps: (1) The Best Linear Approximation computation, (2) Linear model estimation, and (3) compute a standard non-linear optimisation problem. Another significant advantage of the

PNLSS approach is the fact that there are no difficult identification settings such as number of input and output time lags, number of neurons or hyper-parameter values to select by the user during the non-linear identification. An estimate of the model order is determined in the BLA estimation step. Although a PNLSS model can be improved by tweaking the non-linear state and output equations, the standard full PNLSS model often delivers satisfactory results.

Finally, one can conclude that the PNLSS approach to non-linear identification has the Keep it Simple,Stupid (KISS) principle [205]) embedded. This is based on the assumption that the user is not interested in overwhelming and complicated mathematical models or cumbersome identification procedure. But in a rather simple and robust tool that can be used to model a broad range of non-linear systems. All of which is encompassed in this PNLSS approach.

3.7 Conclusions

In this chapter, a black-box method has been used to gain useful insight into the non-linearities observed in an aero-engine casing during an experimental campaign. A discrete-time PNLSS model was used for the identification and validation of the non-linear phenomena observed in the measured data obtained from a vibration test conducted on a large aerospace structure. The whole PNLSS model was investigated using Sine-Sweep data, the PNLSS model was initialised using the best linear approximation and a local polynomial method for local smoothing of the FRFs. Subsequently, a weighted least-squares minimisation approach was used to estimate the PNLSS model parameters. The success of the PNLSS model was judged based on RMS errors between the data simulated from the PNLSS model and the true measured data.

Based on the RMS values of 1.58% and 1.44% on the identification and validation models, one can conclude that the PNLSS method was able to successfully model the non-linear dynamics observed in the measured data without any prior knowledge or physical insight to the nature of the non-linearities. Several drawbacks are associated with polynomial non-linear state space application, one of which is the explosive behaviour of polynomials outside the estimated region. A polynomial has a characteristic of attaining large numerical values when its arguments are large, compared to the behaviour of other basis functions when used in similar application. However,

it should also be noted that extrapolating with an estimated model is never a good idea most importantly for non-linear systems.

To overcome the limitation of the great number of parameters involved in the construction of the multivariate polynomials, tensor techniques can be used to prune the non-linear parameters in the state space identification.. Based on linearisation of the multivariate polynomial in a PNLSS model and a tensor decomposition, the non-linear function $E\zeta(x(t),u(t))$ and $F\eta(x(t),u(t))$ in the state space equation can be represented by decoupled polynomials [182]. This representation further helps to reduce the number of parameters to be estimated by removing the cross-terms in the multivariate polynomials. In summary, results presented in this chapter have shown the strength of using a black-box method to model the non-linearities observed in a large aerospace structure.

CHAPTER 4

GREY-BOX STATE SPACE IDENTIFICATION OF NON-LINEAR VIBRATING SYSTEMS.

Abstract

This fourth chapter introduces a grey-box nonlinear state space identification method based on insights developed from the existing black-box PNLSS identification algorithm implemented in the previous chapter. The proposed time-domain identification method is capable of describing a Single Input Single Output (SISO) nonlinear system, expressing the nonlinearity as internal feedback forces. An identification theorem is stated and implemented with major attention on extracting physics-based understanding when using a standard black-box oriented PNLSS identification algorithm. The proposed grey-box algorithm assumes that the non-linearities are localised in the physical domain. The method is demonstrated on a Duffing oscillator example with non-linear stiffness and damping elements. Simulated sine-sweep and multi-sine data were used for the model estimation and validation.

4.1 Introduction

In Chapter 3, the advantages of black-box oriented state spaces models and polynomial nonlinear state space model (PNLSS) were extensively discussed, with a practical demonstration of the identification capabilities on an Aero-Engine casing. Whilst the practical application proved successful, the number of estimated model parameters was too large to obtain tangible physics based parametric models. This makes the approach limited or practically impossible to use for applications where the identified nonlinear parameters are required for simulating and validating virtual models such as a Finite Element Models (FEM) of the structure under consideration. An approach to overcoming this limitation is the use of grey-box 1D modelling concept, a grey-box approach uses a known model structure with the addition of mathematical functions that can model a variety of non-linear behaviours.

Grey-box models contain sets of stochastic differential equations used to describe the dynamics of a system in continuous time and a set of discrete time measurement equations. They provide a way of combining the advantages of both white and black-box model types, through the use of prior physical knowledge to be incorporated in a black box statistical method for effective parameter estimation. In grey-box modelling, the model structure is often dependent on the Newton's law governing the dynamics of the system while a black-box approach uses abstract mathematical model structures that are adequate and rich to capture all the appropriate dynamics governing the non-linearities of a given system. The use of grey-box models in mechanical systems application has been in existence for several years with examples originating from rotating system applications [206] to control systems application [207].

In nonlinear structural dynamics the use of grey-box models for nonlinear identification has also been adopted, where an identified model structure is enhanced with a suitable mathematical functions capable of describing a range of nonlinear phenomena. The most common examples are the use of high order functions such as Chebyshev polynomials [120], polynomial functions [13],[5], cubic splines [208]. An alternative approach of identifying nonlinearities adopted by structural dynamicist is the use of feedback models. The feedback modelling principle is based on treating the nonlinearities in the system as additional internal forces applied to the underlying

linear structure under consideration.

The use of Nonlinear Identification through Feedback of the Outputs (NIFO) methods in structural dynamics was first introduced by Adams and Allemang in [209], [109], with further frequency domain applications in [210], [211], [138]. The time domain version of the NIFO method was also introduced by Marchesiello and Garibaldi in [116] referred to as Time Domain Nonlinear Subspace Identification (TNSI). Demonstration of the TNSI method on simple and complex systems were highlighted in [212] and [213]. While the TNSI method makes good use of the subspace algorithm to compute the final system parameter matrix and also has the benefit of simultaneously handling several non-linear terms, the frequency domain NIFO method also has an advantage on its lighter computational effort and theoretical concept. More specifically, the method uses spatial data in addition to temporal input and output data to resolve the individual contributions that the linear and non-linear elements contribute to the system dynamics.

However, the successful implementation of both NIFO and TNSI methods does require a prior knowledge or characterisation of the type of non-linearity present in the system under consideration. This means that the if the non-linearities are not well characterised, the parameter estimation will not be well suited for both TNSI and NIFO formulation because it involves a correlated source of noise which can produce biased parametric estimates. Obtaining prior knowledge or performing accurate non-linear characterisation can be difficult or impossible for certain identification problems due to the highly specific nature of practical non-linearities. Therefore,the non-linear characterisation pre-requisite for the NIFO method makes it challenging or limited for its application to large structure or complex systems where the non-linearities are difficult or impossible to calculate from measured input and output data.

In this chapter, a grey-box identification algorithm is proposed. The proposed algorithm is based on combining the existing PNLSS method used in Chapter 3 with the concept of interpreting nonlinearities as internal feedback forces to the underlying linear model of the system to develop a grey-box state space identification algorithm. The whole nonlinear parametric identification is conducted using the force and displacement data measured at equidistantly spaced sampling times. The advantage of the proposed grey-box state space identification algorithm is the adaptation of the current optimisation techniques used in the PNLSS method in Chapter

3 are adopted and taken into account in the identification procedure. The chapter begins with a description of the proposed grey-box state space identification method in Section 4.2, with further illustration on the adaptation of the previous chapter's black-box PNLSS identification procedure in the proposed time domain grey-box state space identification method. A numerical demonstration of the proposed method applied to a SDOF Duffing oscillatory system with nonlinear stiffness and damping is presented in Section 4.3. Validation of the proposed identification method on data obtained from a different type of excitation is demonstrated in Section 4.4 while the conclusions and future suggestions on the method are detailed in Section 4.5.

4.2 Time Domain Grey-box State Space Identification Method

The proposed time domain grey-box identification method consist of a set of steps to obtain a successful nonlinear parametric model . This section of the chapter describes a brief overview implemented in the time domain grey-box state space identification method for identifying structural nonlinearities. The fundamental principle behind the proposed grey-box method is based on writing the equations of motion of a discretised nonlinear system in the form of a black-box PNLSS model with structured state space matrices. In this case the term structured refers to the imposed sparsity patterns and relationships between elements of the state-space matrices. The black-box PNLSS model equation is then turned into a grey-box model by modifying and incorporating sparsity patterns into the state space matrices during the computation of the Jacobian.

Another important feature of the proposed algorithm is the fact the it is developed using a block-oriented formulation of nonlinearities in structural dynamics, where the nonlinearities are considered as additional external feedback forces into the underlying linear model of the structure. Theoretically, the algorithm is formulated with the assumption that the nonlinearity in the structure under consideration can be modelled as a localised nonlinear element in the physical domain and only uses the force and the displacement measured at equidistantly spaced sampling times. To simplify the computation involved, a continuous-time model representation of system under consideration is first converted to a discrete-time model in the physical domain.

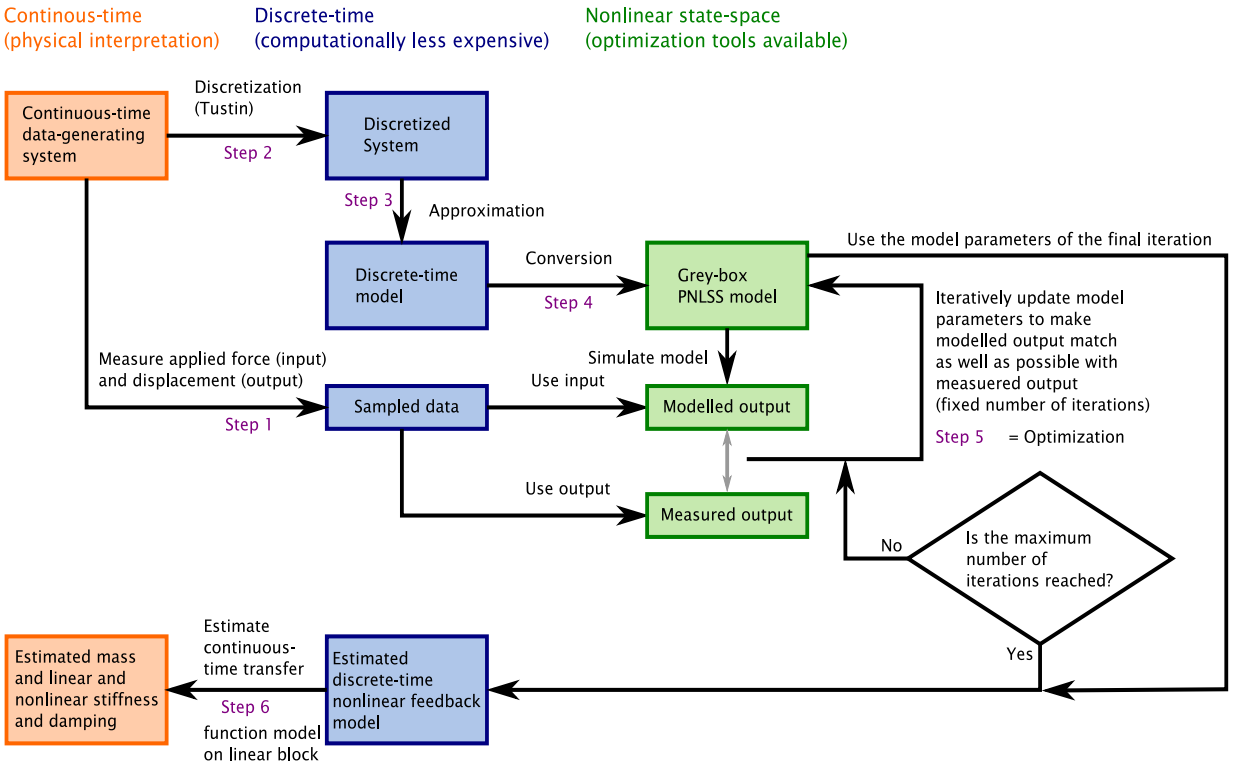

Figure 4.1: *Flowchart describing the steps in the Grey-box state space identification algorithm.*

The discrete time model is further approximated using Tustin approximation method [214]. Next, the discrete-time model is converted / formulated as a polynomial non-linear state-space (PNLSS) model with structured state-space matrices. Using the PNLSS identification process introduced in the previous chapter with modification to the Jacobian of the PNLSS optimisation algorithm implemented, a discrete-time model can be identified. Once the discrete-time model is identified, the non-linear stiffness and damping curve estimates can be obtained. The corresponding mass, linear stiffness, and linear damping can be estimated by fitting a continuous-time transfer function to the estimated discrete-time transfer function that is present in the identified discrete-time model.Figure 4.1 shows a flow-chart illustration of all the steps included in the identification algorithm. A description of each required step is detailed in the following sections.

4.2.1 Step 1 - Nonlinear Model Formulation in the physical domain

The proposed grey-box nonlinear identification algorithm is here developed for the class of nonlinear vibrating systems that can be modelled as a single degree of freedom (sdof) mass spring

damper system with localised nonlinear stiffness and damping. The vibration characteristics of such continuous-time nonlinear systems are assumed in the following form.

$$M\ddot{y}(t) + d\dot{y} + ky(t) + f_d(\dot{y}(t)) + f_k(y(t)) = u(t) \tag{4.1}$$

Where M, d, k are the mass, linear viscous damping and linear stiffness constants respectively; the generalised displacement and applied force are represented by $y(t)$ and $u(t)$. The nonlinear stiffness and damping are expressed by $f_k(\cdot)$ and $f_d(\cdot)$. The first step in the algorithm involves generating input and output data for the continuous-time model of the expression in Equation 4.1. In this case only the input force and displacement are required further for the nonlinear identification. To obtain the required data, standard time-domain differential equation solvers such as the Runge-Kutta Method [215], Newmark-time integration method,Central Difference Method and many more methods discussed in [216] can be used to numerically acquire the force and displacement data at equidistant sampling times. In the case of an experimental application, the measured input force and measured acceleration are directly obtainable during the test, while the acceleration can be integrated to get the velocity and further integrated to get the displacement signal.

4.2.2 Step 2 - Continuous-time Model Discretisation

Once the force and displacement data for continuous-time model of the nonlinear system have been obtained, the next step is to construct a discrete-time model from the continuous time model of the system under consideration. The discretisation step is considered based on its efficient computational advantages over the continuous-time model. Considering the single degree of freedom (sdof) single input single output (SISO) continuous-time system in Equation 4.1, assuming zero initial conditions taking the Laplace transform of model equation results in

$$\left(Ms^2 + ds + k\right)Y(s) + U_d(s) + U_k(s) = U(s) \tag{4.2}$$

where $U_d(s)$ and $U_k(s)$ are the Laplace transforms of $f_d(\dot{y}(t))$ and $f_k(y(t))$, respectively. Based on representing the non-linearities as internal feedback forces as introduced by Adams and Allemang in [209], [109] and Marchesiello in [116], the non-linear damping and stiffness can be

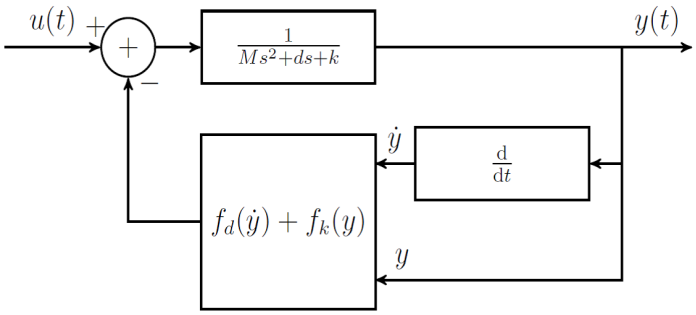

Figure 4.2: *Block-oriented feedback representation of the continuous-time system.*

thought of as additional internal feedback forces. Together with the applied force u, they act as an input to a linear mass-spring-damper system and can be demonstrated by rearranging Equation 4.2:

$$Y(s) = \frac{1}{Ms^2 + ds + k}(U(s) - U_d(s) - U_k(s)). \tag{4.3}$$

A corresponding block-oriented feedback representation of the system is provided in Figure 4.2. Given that the measured data (force $u(t)$ and displacement $y(t)$) are only available at sampling instances $t = 0, T_s, \ldots, (N-1)T_s$, where T_s is the sampling period and N is the length of the data record. Since these data are only available at the equidistantly spaced time instances, it is possible to identify a discrete-time model that maps the measured inputs $u(0), u(T_s), \ldots, u((N-1)T_s)$ to the measured outputs $y(0), y(T_s), \ldots, y((N-1)T_s)$ at the sampling instances only. Identifying such a discretised model is computationally less expensive than identifying a continuous-time model (illustrated in Equation 4.1) that maps the complete input signal $u(t)$ to the output signal $y(t)$ at all times t.

Discretising a continuous-time system can be narrowed down to approximating the time derivatives with the finite difference approximations. Several approximation schemes exist, such as forward and backward Euler approximation [217], Tustin approximation [218], and other types of approaximation techniques cited in [219]. In this thesis, the Tustin approximation is selected based on its simplicity and modelling convenience in MATLAB. A Tustin approximation corresponds to an approximation $\dot{y}(t) \approx v(t)$ [220], where

$$\frac{v((k+1)T_s) + v(kT_s)}{2} = \frac{y((k+1)T_s) - y(kT_s)}{T_s}, \tag{4.4}$$

i.e. the average of $v(t)$ at two consecutive sampling instances kT_s and $(k+1)T_s$ is put equal to a finite difference approximation of the time derivative of y, where this finite difference approximation involves samples of y at the sampling instances kT_s and $(k+1)T_s$. Taking the z-transform of Equation 4.4 results in

$$\frac{z+1}{2}V(z) = \frac{z-1}{T_s}Y(z), \tag{4.5}$$

and thus

$$V(z) = \frac{2}{T_s}\frac{z-1}{z+1}Y(z). \tag{4.6}$$

Comparing this with the Laplace transform of $v(t) \approx \dot{y}(t)$, namely $V(s) \approx sY(s)$, it is clear that a Tustin approximation corresponds to approximating the Laplace variable s with $\frac{2}{T_s}\frac{z-1}{z+1}$. A Tustin approximation of a linear mass-spring-damper system $G_{\text{CT}}(s) = \frac{1}{Ms^2+ds+k}$ under consideration is given by

$$\begin{aligned} G(z) &= G_{\text{CT}}\left(\frac{2}{T_s}\frac{z-1}{z+1}\right) \\ &= \frac{1}{M\left(\frac{2}{T_s}\frac{z-1}{z+1}\right)^2 + d\left(\frac{2}{T_s}\frac{z-1}{z+1}\right) + k} \\ &= \frac{T_s^2(z+1)^2}{4M(z-1)^2 + 2d(z-1)T_s(z+1) + kT_s^2(z+1)^2} \\ &= \frac{T_s^2z^2 + 2T_s^2z + T_s^2}{(4M + 2dT_s + kT_s^2)z^2 + (-8M + 2kT_s^2)z + 4M - 2dT_s + kT_s^2}. \end{aligned} \tag{4.7}$$

Note that even though the continuous-time representation $G_{\text{CT}}(s)$ is strictly proper (the degree of the numerator is strictly smaller than the degree of the denominator), however, this is not the case for the discretised system.

4.2.3 Step 3 - Approximation of the Discretised Model

One of the challenges encountered in nonlinear identification of structures is the ability to obtain a balance between model representation and selection of an appropriate algorithm. The model representation is associated with ensuring that the selected representative model of the structure does include sufficient nonlinear parameters and elements capable of describing the structural behaviour. Selecting the right computational algorithm is very essential to solving the equations of motion of the model efficiently. This step is included in the grey-box identification algorithm

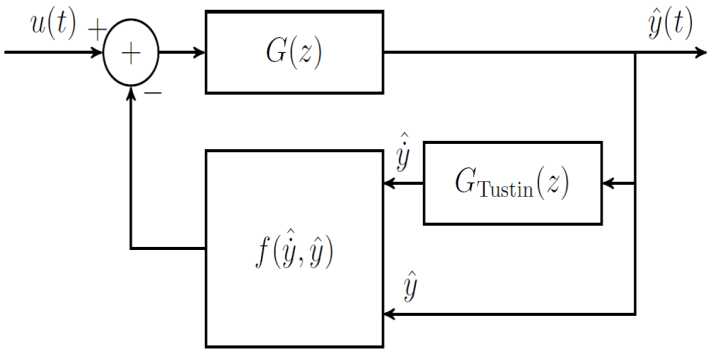

Figure 4.3: *Block-oriented feedback representation of the approximated discretised system.*

mainly to avoid heavy computational burden when solving the equations of motion by developing an approximate model requiring less computational effort whilst maintaining a representation of the nonlinear behaviour. Since the Tustin approximation of the linear model $\frac{1}{Ms^2+ds+k}$ is not strictly proper, replacing the feedback representation of the continuous-time mass-spring-damper system in Figure 4.2 by its Tustin approximation in Equation 4.7 leads to an algebraic loop when solving for y. This means that a non-linear algebraic equation needs to be solved at each time step. To avoid this algebraic loop, and also to simplify the computations, the continuous-time mass-spring-damper system in Figure 4.2 and Equation 4.3 is approximated by a strictly proper discrete-time transfer function [214].

$$G(z) = \frac{b_1 z^{n-1} + \ldots + b_n}{z^n + a_1 z^{n-1} + \ldots + a_n} \tag{4.8}$$

The discrete-time approximation introduces a one-sample delay to properly approximate the continuous-time system as long as the sampling period T_s is small enough. In Figure 4.3, a new feedback representation of the approximated discretised system is presented with the time derivative of the modelled displacement $\hat{y}$ being approximated by its Tustin approximation, i.e. the block $G_{\text{Tustin}}(z)$ in Figure 4.3 is a first-order Tustin approximation of a differentiator

$$G_{\text{Tustin}}(z) = \frac{2}{T_s}\frac{z-1}{z+1}. \tag{4.9}$$

and the model order n in Equation 4.8 is assumed to be known. In practice, the model order n can be determined using a model order selection criterion (e.g. Akaike [221], MDL [222]). The non-linear functions from the original continuous-time system are grouped together in a function

f in Figure 4.3 as a feedback forces to the linear system. The function (f) contains the non-linear stiffness and damping. In this case, a polynomial expansion of the form shown in Equation 4.10 is assumed:

$$f(\hat{y},\hat{y}) = \sum_{\ell=1}^{r_y} p_\ell \hat{y}^\ell + \sum_{m=1}^{r_{\dot{y}}} q_m \hat{\dot{y}}^m + c. \tag{4.10}$$

These polynomial expansions are implemented further as state variables during the derivation of the grey-box state space model. It is worth emphasising the fact that polynomial functions are assumed in this thesis based on their universal abilities of handling smooth nonlinearities. Other non-smooth nonlinear functions such as piecewise and tri-linear functions can be implemented.

4.2.4 Step 4 - Formulation of a Discrete Grey-box PNLSS Model

Building on from the approximated discretised feedback model in Figure 4.3, an important assumption in the proposed grey-box algorithm is addressed in this step. The hypothesis stated in this grey-box formulation is the possibility of representing the block-oriented feedback model of the approximated discretised system in Figure 4.3 as a black-box PNLSS model of the form:

$$\begin{cases} x(t+1) = Ax(t) + Bu(t) + E\zeta(x(t),u(t)) \\ y(t) = Cx(t) + Du(t) + F\eta(x(t),u(t)) \end{cases} \tag{4.11}$$

with matrices A, B, C, D, E, and F. The functions ζ and η are vectors of monomials in the states $x(t)$ and the input $u(t)$. The discrete non-linear state space model in Equation 4.10 was successfully implemented as a black-box PNLSS identification method in Chapter 3. In this step, the black-box PNLSS model equation is modified to a grey-box formulation with the objective of extracting lesser parameters with physics-based interpretation of the identified model.

The discrete-time non-linear state-space form in Equation 4.11 has non-linear functions ζ and η that depend on the states x and the input u. The approximated discrete-time model in the physical space, however, has non-linear function f in Equation 4.10 that depends on the modelled displacement $\hat{y}$ and modelled velocity $\hat{\dot{y}}$. Therefore, to express the feedback representation of the approximated discrete-time system of Equations 4.8 – Equation 4.10 into a black-box PNLSS state-space of the form of Equation 4.11, then, the outputs of the approximated physical discrete-time system are required to be the states in the black-box PNLSS model equation. This means

that the displacement and velocity in the feedback representation of the approximated physical system in Figure 4.3 $\hat{y}$ and $\dot{\hat{y}}$ must be converted to the two states x in Equation 4.11.

4.2.4.1 Converting the Displacement ($\hat{y}$) to a State (x)

To convert the displacement ($\hat{y}$) in Figure 4.3 to a state x in Equation 4.11, the function $G(z)$ in Equation 4.8 is written in an observer canonical form [223]. In this form, the resulting modelled output $\hat{y}$ becomes one of the states x in Equation 4.11. Writing $G(z)$ in observer canonical form results in

$$\begin{bmatrix} x_1(t+1) \\ x_2(t+1) \\ \vdots \\ x_{n-1}(t+1) \\ x_n(t+1) \end{bmatrix} = \begin{bmatrix} -a_1 & 1 & 0 & \cdots & 0 \\ -a_2 & 0 & 1 & \ddots & \vdots \\ \vdots & \vdots & \ddots & \ddots & 0 \\ -a_{n-1} & 0 & \cdots & 0 & 1 \\ -a_n & 0 & \cdots & 0 & 0 \end{bmatrix} \begin{bmatrix} x_1(t) \\ x_2(t) \\ \vdots \\ x_{n-1}(t) \\ x_n(t) \end{bmatrix} + \begin{bmatrix} b_1 \\ b_2 \\ \vdots \\ b_{n-1} \\ b_n \end{bmatrix} (u(t) - f(\hat{y}(t), \hat{y}(t))) \tag{4.12}$$

and

$$\hat{y}(t) = \begin{bmatrix} 1 & 0 & \cdots & 0 & 0 \end{bmatrix} \begin{bmatrix} x_1(t) \\ x_2(t) \\ \vdots \\ x_{n-1}(t) \\ x_n(t) \end{bmatrix} \tag{4.13}$$

With the expression in Equations 4.12 and 4.13, the displacement in the physical domain of Figure 4.3 is now a state of the form $\hat{y} = x$.

4.2.4.2 Converting the Velocity ($\dot{\hat{y}}$) to a State ($\dot{x}$)

In parallel with the displacement, the velocity of the approximated discrete-time system must also be converted to form the second state x in Equation 4.11. To convert the velocity ($\dot{\hat{y}}$) in Figure 4.3 to a state, the $G_{\text{Tustin}}(z)$ is first written in state-space form:

$$x_{\text{Tustin}}(t+1) = -1x_{\text{Tustin}}(t) - \frac{4}{T_s}\hat{y}(t) \tag{4.14}$$

$$\dot{\hat{y}}(t) = \quad 1x_{\text{Tustin}}(t) + \frac{2}{T_s}\hat{y}(t) \tag{4.15}$$

Next, the x_{Tustin} needs to be eliminated from the state-space equations to choose $\hat{y}$ as a state instead. To select $\hat{y}$ as a state, the time update ($\hat{y}(t+1)$) must be written as a function of the states and the input at time t. From Equation 4.15, this results in

$$\hat{y}(t+1) = 1x_{\text{Tustin}}(t+1) + \frac{2}{T_s}\hat{y}(t+1) \tag{4.16}$$

Replacing the first term on the right hand side by its expression in Equation 4.14, and the second term by an expression found from combining Equations 4.12 and 4.13, results in

$$\hat{y}(t+1) = -x_{\text{Tustin}}(t) - \frac{4}{T_s}\hat{y}(t) + \frac{2}{T_s}\left(-a_1\hat{y}(t) + x_2(t) + b_1\left(u(t) - f\left(\hat{y}(t), \hat{y}(t)\right)\right)\right) \tag{4.17}$$

x_{Tustin} can now be eliminated by replacing it by its expression obtained from Equation 4.15, and plugging in the expression in Equation 4.10 for $f(\hat{y}, \hat{y})$ results in:

$$\begin{aligned}\hat{y}(t+1) = &-\left(\hat{y}(t) - \frac{2}{T_s}\hat{y}(t)\right) - \frac{4}{T_s}\hat{y}(t) \\ &+ \frac{2}{T_s}\left(-a_1\hat{y}(t) + x_2(t) + b_1\left(u(t) - \sum_{\ell=1}^{r_y} p_\ell \hat{y}^\ell(t) - \sum_{m=1}^{r_{\dot{y}}} q_m \hat{y}^m(t) - c\right)\right)\end{aligned} \tag{4.18}$$

Rearranging the terms, it is possible to observe that $\hat{y}(t+1)$ is a function of the states $\hat{y}(t)$, $\hat{y}(t)$, and $x_2(t)$, and the input $u(t)$:

$$\hat{y}(t+1) = \alpha_1\hat{y}(t) + \frac{2}{T_s}x_2(t) + \alpha_2\hat{y}(t) - \frac{2}{T_s}b_1\left(\sum_{\ell=2}^{r_y} p_\ell \hat{y}^\ell(t) + \sum_{m=2}^{r_{\dot{y}}} q_m \hat{y}^m(t) + c\right) + \frac{2}{T_s}b_1 u(t) \tag{4.19}$$

where the coefficient of the linear term in $\hat{y}(t)$ is

$$\alpha_1 = -\frac{2}{T_s}(1 + a_1 + b_1 p_1) \tag{4.20}$$

and the coefficient of the linear term in $\hat{y}(t)$ is

$$\alpha_2 = -\left(1 + \frac{2}{T_s}b_1 q_1\right). \tag{4.21}$$

Since $\hat{y}(t+1)$ is a function of the states and input at time t, it fits in the state-space representation that is being sought after and can indeed choose $x_{n+1}(t) = \hat{y}(t)$ to be a state.

4.2.4.3 Grey-box PNLSS Model

Now that the displacement and velocity ($\hat{y}(t)$, $\hat{y}(t)$) of the approximated physical discrete-time system in Figure 4.3 has been represented as the states in the PNLSS model equation in the form

$x_1(t) = \hat{y}(t)$ and $x_{n+1}(t) = \hat{y}(t)$, it is now possible to formulate a grey-box PNLSS model equation. This is achieved by putting the newly formulated states of Equations 4.12, 4.13 and 4.19 together in an original black-box PNLSS model structure. This yields

$$\begin{bmatrix} x_1(t+1) \\ x_2(t+1) \\ \vdots \\ x_{n-1}(t+1) \\ x_n(t+1) \\ x_{n+1}(t+1) \end{bmatrix} = \begin{bmatrix} -a_1 & 1 & 0 & \cdots & 0 & 0 \\ -a_2 & 0 & 1 & \ddots & \vdots & 0 \\ \vdots & \vdots & \ddots & \ddots & 0 & \vdots \\ -a_{n-1} & 0 & \cdots & 0 & 1 & 0 \\ -a_n & 0 & \cdots & 0 & 0 & 0 \\ \alpha_1 & \frac{2}{T_s} & 0 & \cdots & 0 & \alpha_2 \end{bmatrix} \begin{bmatrix} x_1(t) \\ x_2(t) \\ \vdots \\ x_{n-1}(t) \\ x_n(t) \\ x_{n+1}(t) \end{bmatrix} + \begin{bmatrix} b_1 \\ b_2 \\ \vdots \\ b_{n-1} \\ b_n \\ \frac{2}{T_s} b_1 \end{bmatrix} u(t) \tag{4.22}$$

$$- \begin{bmatrix} b_1 \\ b_2 \\ \vdots \\ b_{n-1} \\ b_n \\ 0 \end{bmatrix} \begin{bmatrix} p_1 & 0 & \cdots & 0 & 0 & q_1 \end{bmatrix} \begin{bmatrix} x_1(t) \\ x_2(t) \\ \vdots \\ x_{n-1}(t) \\ x_n(t) \\ x_{n+1}(t) \end{bmatrix}$$

$$- \begin{bmatrix} b_1 \\ b_2 \\ \vdots \\ b_{n-1} \\ b_n \\ \frac{2}{T_s} b_1 \end{bmatrix} \begin{bmatrix} p_2 & \cdots & p_{r_y} & q_2 & \cdots & q_{r_y} & c \end{bmatrix} \begin{bmatrix} x_1^2(t) \\ \vdots \\ x_1^{r_y}(t) \\ x_{n+1}^2(t) \\ \vdots \\ x_{n+1}^{r_y}(t) \\ 1 \end{bmatrix}$$

$$\hat{y}(t) = \begin{bmatrix} 1 & 0 & \cdots & 0 & 0 & 0 \end{bmatrix} \begin{bmatrix} x_1(t) \\ x_2(t) \\ \vdots \\ x_{n-1}(t) \\ x_n(t) \\ x_{n+1}(t) \end{bmatrix} \tag{4.23}$$

From the expression in Equations 4.22 and 4.23, the feedback representation of the approximated physical discrete-time system can now be written in the form of a grey-box PNLSS model equation

$$x(t+1) = Ax(t) + Bu(t) + E\zeta(x_1(t), x_{n+1}(t)) \tag{4.24}$$

and

$$y(t) = Cx(t) \tag{4.25}$$

where the structured matrices A, B, C and E are of the form

$$A = \begin{bmatrix} -a_1 & 1 & 0 & \cdots & 0 & 0 \\ -a_2 & 0 & 1 & \ddots & \vdots & 0 \\ \vdots & \vdots & \ddots & \ddots & 0 & \vdots \\ -a_{n-1} & 0 & \cdots & 0 & 1 & 0 \\ -a_n & 0 & \cdots & 0 & 0 & 0 \\ \alpha_1 & \frac{2}{T_s} & 0 & \cdots & 0 & \alpha_2 \end{bmatrix} - \begin{bmatrix} b_1 \\ b_2 \\ \vdots \\ b_{n-1} \\ b_n \\ 0 \end{bmatrix} \begin{bmatrix} p_1 & 0 & \cdots & 0 & 0 & q_1 \end{bmatrix} \tag{4.26}$$

$$B = \begin{bmatrix} b_1 \\ b_2 \\ \vdots \\ b_{n-1} \\ b_n \\ \frac{2}{T_s} b_1 \end{bmatrix} \tag{4.27}$$

$$C = \begin{bmatrix} 1 & 0 & \cdots & 0 & 0 & 0 \end{bmatrix} \tag{4.28}$$

$$E = - \begin{bmatrix} b_1 \\ b_2 \\ \vdots \\ b_{n-1} \\ b_n \\ \frac{2}{T_s} b_1 \end{bmatrix} \begin{bmatrix} p_2 & \cdots & p_{r_y} & q_2 & \cdots & q_{r_{\dot{y}}} & c \end{bmatrix} \tag{4.29}$$

and

$$\zeta(x_1(t), x_{n+1}(t)) = \begin{bmatrix} x_1^2(t) \\ \vdots \\ x_1^{r_y}(t) \\ x_{n+1}^2(t) \\ \vdots \\ x_{n+1}^{r_y}(t) \\ 1 \end{bmatrix} \tag{4.30}$$

The new expression in Equations 4.24 and 4.25 is referred to as the grey-box PNLSS model equations with its corresponding model parameters formulated in Equations 4.26 to 4.30. Compared to the state space matrices of the original black-box PNLSS model in Equation 3.13, the state space matrices of the newly formulated grey-box PNLSS model (Equations 4.24-4.25) correspond to the parameters of the approximated discretised system in Figure 4.3. The parameters of the non-linear stiffness and non-linear damping characteristics are obtainable from the A and E matrices of estimated grey-box PNLSS model. The mass, linear stiffness, and linear damping can be estimated by fitting a continuous-time transfer function to the estimated discrete-time transfer function $G(z)$. Based on this adjusted formulation of black-box PNLSS model Equation, it is therefore possible to adapt the existing black-box PNLSS optimisation procedure for the newly formulated grey-box PNLSS model.

4.2.5 Step 5- Estimation of the Discrete-time Non-linear Feedback Model

The next step after the grey-box PNLSS model formulation is the estimation of the model parameters. In this case, the parameters of the grey-box PNLSS model are the coefficients of the transfer function of the linear subsystem $a_1,\ldots,a_n,b_1,\ldots,b_n$ of elements in matrices A,B and E, in Equation 4.24, and the parameters of the nonlinear stiffness and damping characteristics, $p_1,\ldots,p_{r_y},q_1,\ldots,q_{r_y}$, and c in matrices A,B and E, of Equation 4.24. These parameters are associated with the elements in the grey-box state space matrices A,B,C and E, and are estimated by minimising the difference between the measured and the modelled output in (weighted) mean-square sense. Similar to the black-box PNLSS identification method,

the minimisation exercise in this grey-box method is also a nonlinear optimisation problem. Therefore the optimisation routine implemented in the black-box PNLSS model can also be used in this case. The only difference between the optimisation routine of the black-box PNLSS model and the grey-box model is the expression of the Jacobian.

This step provides the expressions of the Jacobian corresponding to the considered grey-box model structure. To keep the notation compact, $\zeta(x_1(t), x_{n+1}(t))$ is denoted by $\zeta(t)$. The Jacobians are of the form

$$J_\theta(t) = \frac{\partial \hat{y}(t)}{\partial \theta} = C\frac{\partial x(t)}{\partial \theta} \tag{4.31}$$

where θ is a free parameter ($a_1,\ldots,a_n,b_1,\ldots,b_n,p_1,\ldots,p_{r_y},q_1,\ldots,q_{r_{\dot{y}}}$, or c).

These partial derivatives can be computed from the state equation which generally results in an expression for $\frac{\partial x(t+1)}{\partial \theta}$ as a function of $\frac{\partial x(t)}{\partial \theta}$, i.e. a recursion, which can be seen as the state equation of another state-space model. The specific results are as follows:

$$\frac{\partial x(t+1)}{\partial a_1} = \left(A + E\frac{\partial \zeta(t)}{\partial x(t)}\right)\frac{\partial x(t)}{\partial a_1} + \begin{bmatrix} -1 & 0 & \cdots & 0 \\ 0 & 0 & \cdots & 0 \\ \vdots & \vdots & & \vdots \\ 0 & 0 & \cdots & 0 \\ -\frac{2}{T_s} & 0 & \cdots & 0 \end{bmatrix} x(t) \tag{4.32}$$

$$\frac{\partial x(t+1)}{\partial a_i} = \left(A + E\frac{\partial \zeta(t)}{\partial x(t)}\right)\frac{\partial x(t)}{\partial a_i} + \begin{bmatrix} 0 & 0 & \cdots & 0 \\ \vdots & \vdots & & \vdots \\ 0 & 0 & \cdots & 0 \\ -1 & 0 & \cdots & 0 \\ \vdots & \vdots & & \vdots \\ 0 & 0 & \cdots & 0 \end{bmatrix} x(t) \tag{4.33}$$

for $i = 2,\ldots,n$ and where the -1 in the matrix in front of $x(t)$ appears in the ith row.

$$\begin{aligned}\frac{\partial x(t+1)}{\partial b_1} &= \left(A + E\frac{\partial \zeta(t)}{\partial x(t)}\right)\frac{\partial x(t)}{\partial b_1} \\ &+ \begin{bmatrix} -p_1 & 0 & \cdots & 0 & -q_1 \\ 0 & 0 & \cdots & 0 & 0 \\ \vdots & \vdots & & \vdots & \vdots \\ 0 & 0 & \cdots & 0 & 0 \\ -\frac{2}{T_s}p_1 & 0 & \cdots & 0 & -\frac{2}{T_s}q_1 \end{bmatrix} x(t) + \begin{bmatrix} 1 \\ 0 \\ \vdots \\ 0 \\ \frac{2}{T_s} \end{bmatrix} u(t) \\ &- \begin{bmatrix} p_2 & \cdots & p_{r_y} & q_2 & \cdots & q_{r_{\dot{y}}} & c \\ 0 & \cdots & 0 & 0 & \cdots & 0 & 0 \\ \vdots & & \vdots & \vdots & & \vdots & \vdots \\ 0 & \cdots & 0 & 0 & \cdots & 0 & 0 \\ \frac{2}{T_s}p_2 & \cdots & \frac{2}{T_s}p_{r_y} & \frac{2}{T_s}q_2 & \cdots & \frac{2}{T_s}q_{r_{\dot{y}}} & \frac{2}{T_s}c \end{bmatrix} \zeta(t)\end{aligned} \tag{4.34}$$

$$\begin{aligned}\frac{\partial x(t+1)}{\partial b_i} &= \left(A + E\frac{\partial \zeta(t)}{\partial x(t)}\right)\frac{\partial x(t)}{\partial b_i} \\ &+ \begin{bmatrix} 0 & 0 & \cdots & 0 & 0 \\ \vdots & \vdots & & \vdots & \vdots \\ 0 & 0 & \cdots & 0 & 0 \\ -p_1 & 0 & \cdots & 0 & -q_1 \\ 0 & 0 & \cdots & 0 & 0 \\ \vdots & \vdots & & \vdots & \vdots \\ 0 & 0 & \cdots & 0 & 0 \end{bmatrix} x(t) + \begin{bmatrix} 0 \\ \vdots \\ 0 \\ 1 \\ 0 \\ \vdots \\ 0 \end{bmatrix} u(t) \\ &- \begin{bmatrix} 0 & \cdots & 0 & 0 & \cdots & 0 & 0 \\ \vdots & & \vdots & \vdots & & \vdots & \vdots \\ 0 & \cdots & 0 & 0 & \cdots & 0 & 0 \\ p_2 & \cdots & p_{r_y} & q_2 & \cdots & q_{r_{\dot{y}}} & c \\ 0 & \cdots & 0 & 0 & \cdots & 0 & 0 \\ \vdots & & \vdots & \vdots & & \vdots & \vdots \\ 0 & \cdots & 0 & 0 & \cdots & 0 & 0 \end{bmatrix} \zeta(t)\end{aligned} \tag{4.35}$$

for $i = 2,\ldots,n$ and where the non-zero rows in the matrices are the ith rows of those matrices.

$$\frac{\partial x(t+1)}{\partial p_1} = \left(A + E\frac{\partial \zeta(t)}{\partial x(t)}\right)\frac{\partial x(t)}{\partial p_1} + \begin{bmatrix} -b_1 & 0 & \cdots & 0 \\ \vdots & \vdots & & \vdots \\ -b_n & 0 & \cdots & 0 \\ -\frac{2}{T_s}b_1 & 0 & \cdots & 0 \end{bmatrix} x(t) \tag{4.36}$$

$$\frac{\partial x(t+1)}{\partial p_i} = \left(A + E\frac{\partial \zeta(t)}{\partial x(t)}\right)\frac{\partial x(t)}{\partial p_i} - \begin{bmatrix} 0 & \cdots & 0 & b_1 & 0 & \cdots & 0 \\ \vdots & & \vdots & \vdots & \vdots & & \vdots \\ 0 & \cdots & 0 & b_n & 0 & \cdots & 0 \\ 0 & \cdots & 0 & \frac{2}{T_s}b_1 & 0 & \cdots & 0 \end{bmatrix} \zeta(t) \tag{4.37}$$

for $i = 2,\ldots,r_y$ and where the non-zero column in the matrix in front of $\zeta(t)$ appears in the $(i-1)$th column.

$$\frac{\partial x(t+1)}{\partial q_1} = \left(A + E\frac{\partial \zeta(t)}{\partial x(t)}\right)\frac{\partial x(t)}{\partial q_1} + \begin{bmatrix} 0 & \cdots & 0 & -b_1 \\ \vdots & & \vdots & \vdots \\ 0 & \cdots & 0 & -b_n \\ 0 & \cdots & 0 & -\frac{2}{T_s}b_1 \end{bmatrix} x(t) \tag{4.38}$$

$$\frac{\partial x(t+1)}{\partial q_i} = \left(A + E\frac{\partial \zeta(t)}{\partial x(t)}\right)\frac{\partial x(t)}{\partial q_i} - \begin{bmatrix} 0 & \cdots & 0 & b_1 & 0 & \cdots & 0 \\ \vdots & & \vdots & \vdots & \vdots & & \vdots \\ 0 & \cdots & 0 & b_n & 0 & \cdots & 0 \\ 0 & \cdots & 0 & \frac{2}{T_s}b_1 & 0 & \cdots & 0 \end{bmatrix} \zeta(t) \tag{4.39}$$

for $i = 2,\ldots,r_{\dot{y}}$ and where the non-zero column in the matrix in front of $\zeta(t)$ appears in the $(r_y - 1 + i - 1)$th column.

$$\frac{\partial x(t+1)}{\partial c} = \left(A + E\frac{\partial \zeta(t)}{\partial x(t)}\right)\frac{\partial x(t)}{\partial c} - \begin{bmatrix} 0 & \cdots & 0 & b_1 \\ \vdots & & \vdots & \vdots \\ 0 & \cdots & 0 & b_n \\ 0 & \cdots & 0 & \frac{2}{T_s}b_1 \end{bmatrix} \zeta(t) \tag{4.40}$$

In all these expressions, the term $\frac{\partial \zeta(t)}{\partial x(t)}$ is given by

$$\frac{\partial \zeta(t)}{\partial x(t)} = \begin{bmatrix} 2x_1(t) & 0 & \cdots & 0 & 0 \\ 3x_1^2(t) & 0 & \cdots & 0 & 0 \\ \vdots & \vdots & & \vdots & \vdots \\ r_y x_1^{r_y-1}(t) & 0 & \cdots & 0 & 0 \\ 0 & 0 & \cdots & 0 & 2x_{n+1}(t) \\ \vdots & \vdots & & \vdots & \vdots \\ 0 & 0 & \cdots & 0 & r_{\dot{y}} x_{n+1}^{r_{\dot{y}}-1}(t) \\ 0 & 0 & \cdots & 0 & 0 \end{bmatrix} \tag{4.41}$$

The Jacobians can then be computed as $J_\theta(t) = \frac{\partial \hat{y}(t)}{\partial \theta} = C \frac{\partial x(t)}{\partial \theta}$. It's worth stating that in the black-box PNLSS model, the elements of the A, B, C, D, E, and F matrices are the free parameters, while in the grey-box model, the parameters of the nonlinear feedback model are the free parameters. The parameter updates are computed in the same way for both models, the only difference is the expression for the Jacobian as illustrated above.

4.2.6 Step 6 - Estimation of the Continuous-Time Model

The final step in the grey-box PNLSS identification algorithm involves estimating the continuous time model from the discrete-time nonlinear feedback model. It is important to note that the identified nonlinear stiffness and damping models are polynomials, i.e. static function. As such, the identified grey-box model can be expressed in either a discrete-time or continuous-time form, since these functions are the same in both models. The only model that needs to be estimated from the discrete time model is the continuous time model of the linear block $G(z)$. The result of this estimation gives a continuous-time model of the mass m , linear damping d, and linear stiffness k . The linear continuous time model $G(z)$ can be estimated from the FRF of the discrete time model.

To perform this estimation, the inverse operation of the discrete frequency response is required. The inverse (FRF) operation calculates a continuous-time transfer function that corresponds to a given complex frequency response. This is done by using a minimisation error

function illustrated in Equation 4.42 to estimate the best model given FRF data of the discrete time model.

$$\sum_{k=1}^{n} wt(k)|h(k)A(w(k)) - B(w(k))|^2 \tag{4.42}$$

Where $A(w(k))$ and $B(w(k))$ are the Fourier transform of the polynomials at frequency $w(k)$, and n is the number of frequency points associated with the length of the data (h and w). This estimation method is was developed by Levi and demonstrated in [224].

4.2.7 Grey-box PNLSS Identification Process

The formulated grey-box identification method estimates its parameters based on an optimisation routine, where the output of the grey-box non-linear state-space matrices is non-linear in the parameters. Minimisation of the least squares cost function or simulation error in mean-square sense will generally result in a non-convex optimisation problem [225]. To avoid getting stuck in a bad local optimum of the cost function, a good parameter initialisation is often required.

In this case, a linear and non-linear initialisation was considered. The standard linear initialisation the best linear approximation (BLA) implemented in the previous chapter was also applied in this chapter. The non-linear initialisation implemented here is tailored to a non-linear feedback structure with similar concept with the method developed by Johan Paduart in [179]. In this case, the BLA is estimated, followed by the opening of feedback loop, and estimation of the non-linearity as a linear least-squares problem. In addition, the estimation of non-linear damping models is incorporated.

4.2.7.1 Best Linear Approximation of a Grey-box PNLSS Model

To initially understand the nonlinear effects and observe the distortions introduced in the data, the BLA of the system is first estimated. The BLA of a system with input $u(t)$ and output $y(t)$ is defined for a class of input signals as the linear system whose output approximates the system's output best in mean-square sense around the operating point, i.e.

$$G_{\mathrm{BLA}}(k) = argmin_{G(z)} E_u \left\{ \|\tilde{Y}(k) - G(k)\tilde{U}(k)\|_2^2 \right\} \tag{4.43}$$

with

$$\begin{cases} \tilde{u}(t) = u(t) - E\{u(t)\} \\ \tilde{y}(t) = y(t) - E\{y(t)\} \end{cases} \tag{4.44}$$

where G_{BLA} is the frequency response function (FRF) of the BLA, $\tilde{Y}(k)$ and $\tilde{U}(k)$ are the discrete Fourier transform (DFT) spectra of $\tilde{y}(t)$ and $\tilde{u}(t)$, and the expected value $E_u\{\cdot\}$ in Equation 4.43 is the ensemble average over the given class of input signals. In the remainder of this chapter, it is assumed that the mean values are removed from the signals when a BLA is calculated. The notations u and y will be used, instead of $\tilde{u}$ and $\tilde{y}$. If the BLA exists, the minimising parameter in Equation 4.43 can be obtained as

$$G_{\mathrm{BLA}}(k) = \frac{S_{YU}(k)}{S_{UU}(k)}, \tag{4.45}$$

where the expectation in the cross-power and auto-power spectra S_{YU} and S_{UU} is again an ensemble average over the considered class of input signals. Note that for periodic excitations, Equation 4.45 reduces to [226]

$$G_{\mathrm{BLA}}(k) = E_u\left\{\frac{Y(k)}{U(k)}\right\}. \tag{4.46}$$

The invariance of the BLA is very useful. It means that the BLA can be estimated by averaging Equations 4.45 or 4.46 over a number of realisations of signals belonging to the same Riemann-equivalence class. This is the main idea in the robust method [226], which provides non-parametric estimates of the BLA, the noise variance, the non-linear variance, and the total (= noise + non-linear) variance.

After obtaining a non-parametric estimate of the BLA, a parametric rational transfer function model is typically estimated on top of the non-parametric estimate. Nevertheless, since the linear block $G(z)$ in Equation 4.8 is assumed to be strictly proper (in order to avoid an algebraic loop in the feedback model), the Output Error (OE) model starting from the time domain data is immediately estimated, with this estimation, it is then possible to easily impose strict approximation of the transfer function and at the same time have the same estimation procedure for both periodic and non-periodic inputs.

4.2.7.2 Initialisation of the Non-linear Model

Since the nonlinear parameters of discrete-time grey-box model are estimated using an optimisation, it is important to select an initial state x_0 of the grey-box PNLSS model equation when computing the state sequence of the Jacobian. To achieve this, the non-linear initialisation starts with an estimation of the BLA. Again, since the linear block is assumed to be strictly proper, the linear block is estimated as an Output Error model starting from the time domain data. Next, an initial estimate for the non-linear block is obtained by cutting the feedback loop (and thus using the measured output as an input to the model).

The path from the measured input to the output only contains the linear block, of which already have estimated parameters. The output of this path is removed from the output of the model:

$$v(t) = y(t) - \hat{G}(q)u(t) \tag{4.47}$$

The path from the measured output (which is temporarily used as an input to the model) to the output of the model contains the unknown non-linear block as well as a known time-derivative approximation block G_{Tustin} and the already estimated linear block. By expanding the non-linear block in terms of basis functions (in this case polynomials, see Equation 4.10, the parameters of the non-linear feedback (the polynomial coefficients $p_1,\ldots,p_{r_y},q_1,\ldots,q_{r_{\dot{y}}}$ and c) are estimated using linear least squares computation.

4.2.7.3 Estimation of the Nonlinear Grey-box Model Parameters

To estimate the nonlinear parameters in the state space matrices of the grey-box model, a weighted least squares cost function is minimised through an optimisation. The weighted least squares cost function V_{LS} that would be minimised with respect to the model parameters $a_1,\ldots,a_n,b_1,\ldots,b_n$ and $p_1,\ldots,p_{r_y},q_1,\ldots,q_{r_{\dot{y}}}$ in the grey-box state space matrices $\theta = [vec(A);vec(B);vec(C);vec(E);]$ is:

$$V_{LS}(\theta) = \sum_{k=1}^{n_F} \epsilon^H(k,\theta)\epsilon(k,\theta) \tag{4.48}$$

Compared to the parameter estimation method for the black-box PNLSS model where the model parameters are the elements in matrices $\theta = [vec(A); vec(B); vec(C); vec(D); vec(E); vec(F)]$. In the grey-box model, the model parameters are not the elements in the matrices A, B, C, D, E, and F. Instead, the free parameters are the numerator and denominator coefficients of G(z), and the polynomial coefficients of the stiffness and damping curve.

4.3 Numerical Demonstration on a Duffing Oscillator

In this section, the newly formulated grey-box PNLSS model identification process is demonstrated on a simple generic mechanical system where only a set of input (force) $u(t)$ and output (displacement) $y(t)$ measurements are available for $t = 0, \ldots, N-1$. Figure 4.4 shows an illustration of the system considered for this demonstration. To give a structural dynamics interpretation of

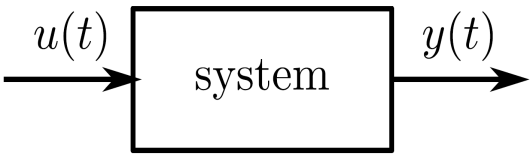

Figure 4.4: *Simple input and output mechanical system.*

the system under consideration,the objective of the demonstration is to examine the performance of the proposed grey-box PNLSS identification procedure on a model that can be represented as a SDOF mass-spring-damper system, with non-linear stiffness and non-linear damping as illustrated in Figure 4.5. Here, M is the mass, k the linear stiffness, d is the linear damping, k_{NL} is the nonlinear stiffness and d_{NL} is the nonlinear damping. Since the one of the assumptions in deriving the grey-box is based on considering the non-linearities as feedback internal forces to the original linear, the single degree-of-freedom mass-spring-damper system with non-linear damping and stiffness can also be represented as a feedback model. The block-oriented feedback model of SDOF system in Figure 4.5 can be represented as a linear system in the feed-forward branch and the non-linear damping and stiffness in the feedback. The block $G_{\text{Tustin}}(z)$ in Figure 4.6 represents a first-order transfer function of a discrete-time approximation of the time-derivative.

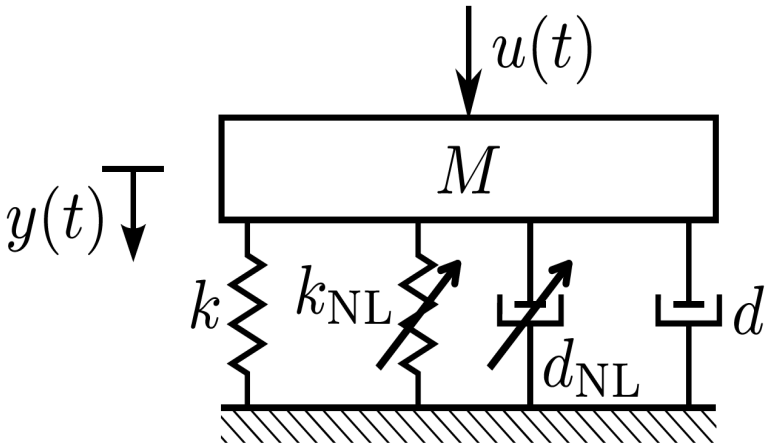

Figure 4.5: *A nonlinear mass-spring-damper system.*

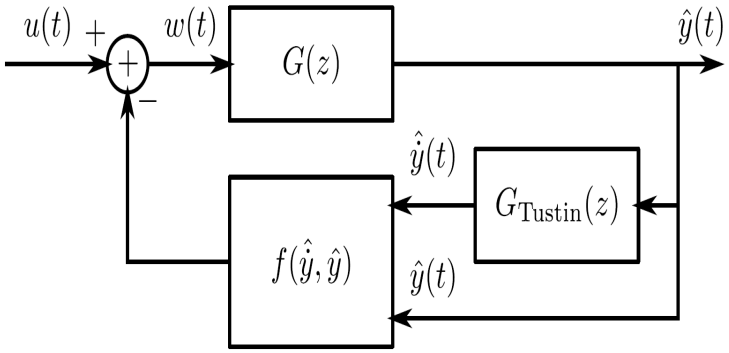

Figure 4.6: *Feedback representation of the mass-spring-damper system.*

4.3.1 Problem Description

The vibration characteristics of the considered Duffing oscillator system illustrated in Figure 4.5 are governed by Newton's second law of motion described in Equation 4.49. The linear and non-linear parameters selected for the system under consideration are listed in Table 4.1 with the corresponding natural frequency (ω_0) and damping ratio (η).

$$M\ddot{y}(t) + C_v\dot{y}(t) + Ky(t) + f_{nl}(\dot{y}^3, y^3) = u(t) \tag{4.49}$$

The system was simulated in time-domain using standard MATLAB ODE45 function with acceptable Relative and Absolute error tolerances. The relative and absolute tolerance values were set to $1e-3$ and $1e-6$ while the sampling frequency (fs) was set to 2800 Hz to obtain a better and accurate integration. The excitation selected for $u(t)$ was a sine-sweep, a sine-sweep

Linear	$M(Kg)$	$C(Ns/m)$	$K(kN/m)$	$\omega_0(Hz)$	ϵ	
Coefficients	3	155.81	7.61	253.57	1.63	
Nonlinear	$p_1(N/m)$	$p_2(N/m^2)$	$p_3(N/m^3)$	$q_1(Ns/m)$	$q_2(Ns/m^2)$	$q_3(Ns/m^3)$
Coefficients	$7.04 \cdot 10^4$	$-2.38 \cdot 10^8$	$1.75 \cdot 10^{15}$	-3.66	-39.96	$7.92 \cdot 10^3$

Table 4.1: *Linear and nonlinear parameters of the Duffing oscillator*

also referred to as a chirp signal is a type of sine-wave signal where the frequency increases upwards or decreases downwards depending on the direction of the chirp or sweep. One of the advantages of using sine-sweep is the capability of exciting the nonlinearities present in the test structure or system under consideration. Furthermore, its is also very useful for describing the vibration of an Oscillatory motion. A linear sine-sweep excitation with sweep rate of 100 Hz/min in 210 - 280 Hz was chosen, the RMS amplitude of the signal was ranged from 1 -5 N and total data sample of 117601. The simulated sine-sweep time series and corresponding FRFs are plotted in Figure 4.7, it also shows a comparison of the amplitude for different RMS levels. From both the time series and FRF plots, it can be seen that when varying the RMS value, the shape of the amplitude changes, also indicating a significant level of distortion for both envelope of the time series and the distortions observed at the resonances peak for RMS values of 3N and 5N.

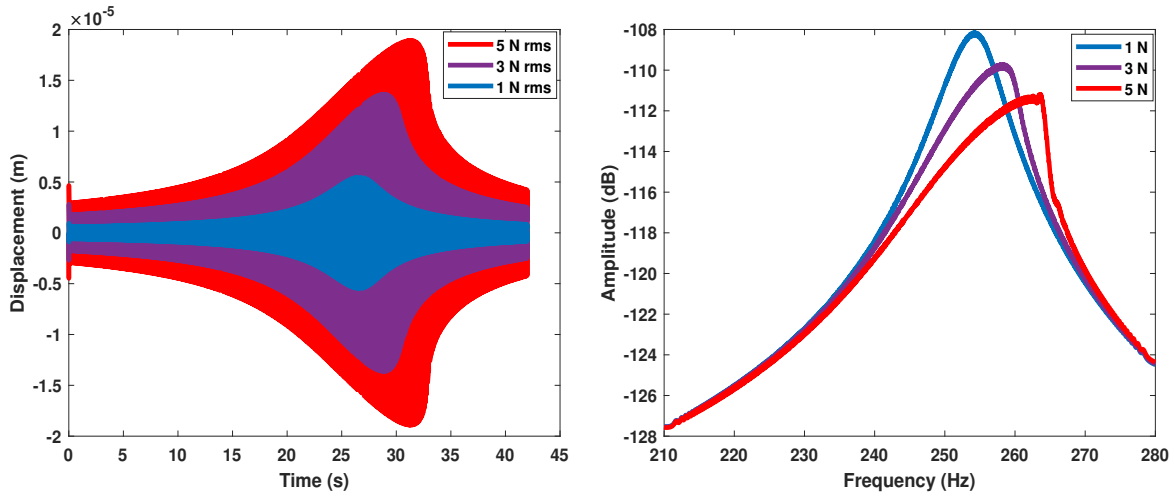

(a) (b)

Figure 4.7: *Generated sine-sweep time series and frequency domain response for the SDOF system:(a) Time domain response, (b) amplitude of the corresponding discrete time fourier transform*

4.3.2 Best Linear Approximation of the Duffing Oscillator

Similar to the black-box PNLSS identification procedure, the first step in this proposed Grey-box PNLSS identification is the estimation of the parametric and non-parametric BLA of the duffing oscillatory system in Figure 4.5. The BLA of the simulated sine-sweep input $u(t)$ and output $y(t)$ for $t = 1,...N$ was estimated using the LPM method [27] that was applied in the previous chapter. A model order of 2 was selected for the estimation based on a single mode analysis. A parametric linear model is then estimated in the frequency domain using the frequency subspace identification algorithm [220], it is worth noting that the linear behaviour of the nonlinear feedback model is included in this BLA estimation. In addition to the estimating BLA FRFs, total standard deviation (including the noise and non-linear distortion) of the BLA was also calculated. The amplitude and total distortions of the G_{BLA} are plotted in Figure 4.8 for different force levels where Figure 4.8a is the FRF and 4.8b is the total distortion (noise + non-linear distortion). From

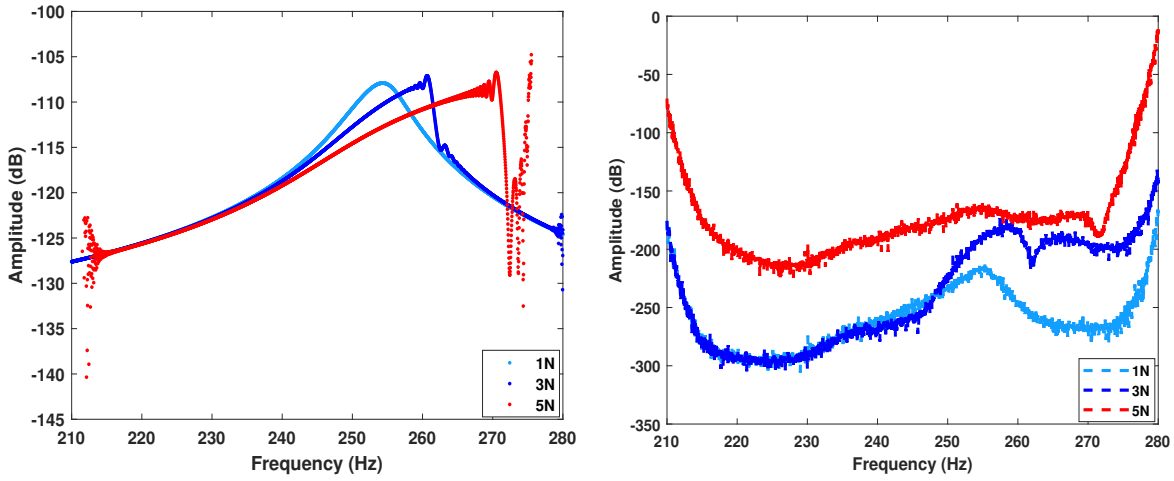

(a) (b)

Figure 4.8: *Estimated BLA and non-linear distortions for different force values: (a) amplitude of the discrete time fourier transform of the BLA FRF, (b) amplitude of the discrete time fourier transform of the nonlinear distortions.*

the plots in Figure 4.8, it is possible to observe that varying the RMS amplitude value changes both the BLA FRF and the calculated distortion, a shift to the right for higher force value is observed on both the FRF and the total distortions. Furthermore, in Figure 4.8a for higher input excitation, the FRF of the G_{BLA} becomes less smooth at the resonance peak. This is as a result

of the fact that the non-linearites in the system become more excited and dominant requiring further identification investigation.

4.3.3 Linear Grey-box State Model of the Duffing Oscillator

Before constructing the nonlinear grey-box PNLSS model, a linear state space model of the system under consideration is required, a linear state space model of the SDOF system in Figure 4.5 is constructed in an approximated discretised grey-box form of Equations 4.24 and 4.25 using the sine-sweep data at 5N excitation level. Based on the physical description of the SDOF system given in Equation 4.49, nonlinear terms in the state are selected as polynomial functions with quadratic and cubic functions of the output displacement. The approximated discrete-time linear

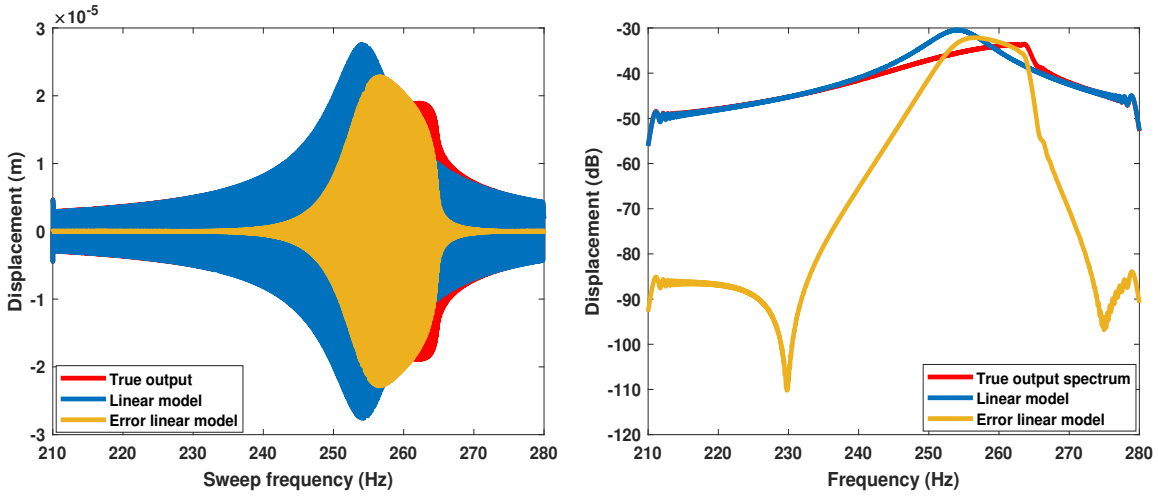

(a) (b)

Figure 4.9: *Estimated Linear model compared with original data and error: (a) time domain response of the SDOF, (b) corresponding displacement amplitude of the discrete time fourier transform of the SDOF.*

block of the SDOF system, which is of the form 4.8, is estimated based on and Output Error (OE) model function implemented in matlab. The Matlab OE function oe minimises the prediction error (difference between measured and modelled output) in mean-square sense in the time domain. More information on output error models and prediction error minimisation can be found in [227]. The results of the identified linear grey-box model are illustrated in Figure 4.9, where the true model data in red is compared with the estimated linear grey-box model in blue for both

time domain and spectrum. The error levels are also plotted in orange on each graph, error levels were evaluated based on a calculated difference between the true data and the modelled linear output. The results show low error level of around 40 dB below the true spectrum at the outer region of the resonance, however the error gradually increases around the resonance frequency region as observed in both spectrum and time domain result shown in Figure 4.9 where the linear identified grey-box model is unable to capture the true representation of the characteristics observed in the true data with an RMS error value of 69.9%. Results obtained from this linear grey-box identification reinforces the presence of nonlinearity in the system and the fact that a linear approach will not produce a satisfactory result.

4.3.4 Nonlinear Initialisation of the Duffing Oscillator Model

During the estimation of the linear grey-box model, the Output Error (OE) function was used to account for the quality of the estimated model. In this section, an initial estimate of the nonlinear

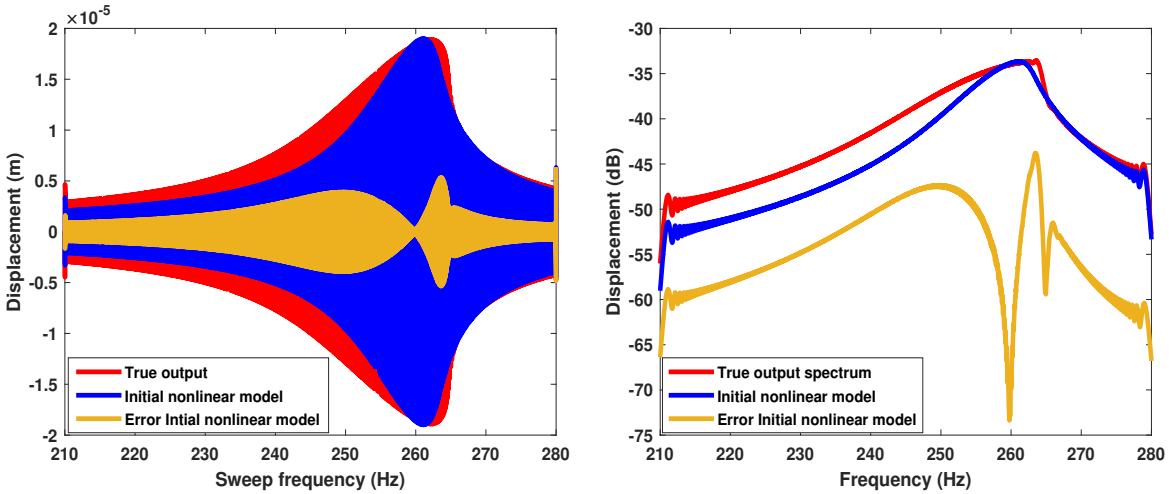

(a) (b)

Figure 4.10: *comparison of estimated initial nonlinear model against true nonlinear data. (a) Time domain data response (b) corresponding displacement amplitude spectrum of the discrete time fourier transform.*

model is estimated by cutting the feedback loop and solving a linear least squares problem to obtain the polynomial coefficients ($p_1,\ldots,p_{r_y},q_1,\ldots,q_{r_{\dot{y}}}$ and c) of the nonlinear block. The results of this estimation is referred to as the initial nonlinear model since the estimation uses the results

from the identified linear model and approximated derivative of the $G_{\text{Tustin}}(z)$. Initialisation of the nonlinear model conducted in this section is crucial to avoid the optimisation of the nonlinear model conducted in the next section from getting stuck in a local minimum. Figure 4.10 depicts a comparison of the estimated initialised nonlinear model with the true nonlinear data, where Figure 4.10a is the time domain data and 4.10b is the spectrum. Compared to the estimated linear

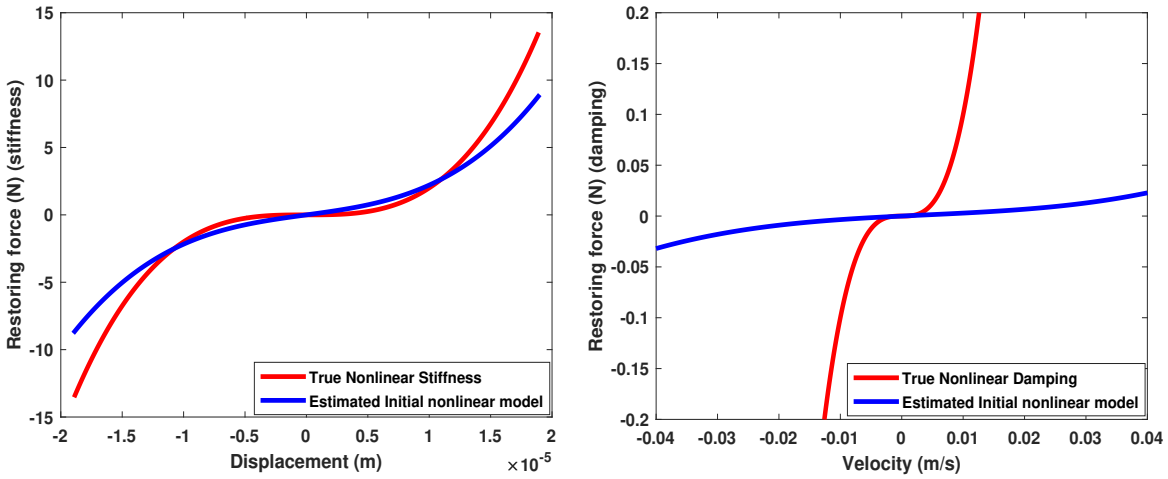

(a) (b)

Figure 4.11: *comparison of estimated initial nonlinear model against true nonlinear data. (a) stiffness curve (b) damping curve*

model illustrated in Figure 4.9, the error at the resonance region of Figure 4.10 is considerably lower, in addition, the estimated initial nonlinear model is able to capture a level of distortion characteristics illustrated at the resonance peak which was not captured by the estimated linear model. The time domain RMS error achieved by the estimated nonlinear initialised model is 31.8% which is significantly lower than the 69.9% value obtained by the linear model.

Unlike the black-box PNLSS identification method demonstrated in Chapter 3 where the fitting of the time domain and spectrum data in conjunction with the RMS error are used to judge the accuracy of the estimated model without any significant physics based interpretation. In the proposed grey-box PNLSS identification method implemented in this chapter, the time domain and spectrum are not only made available and used, it is also possible to extract the stiffness and damping characteristics of the estimated model in order to gain physics based understanding of

the estimated model. Figure 4.11 shows the comparison of the stiffness and damping curve of the estimated initialised nonlinear model with the true nonlinear data. While the time domain and frequency spectrum comparison illustrated in 4.10 show a reasonable fit, the stiffness and damping extracted from the estimated model shows less fit or correlation. This is more apparent in extracted damping curve in Figure 4.11b where only the linear region of the extracted curve has a perfect correlation with the original nonlinear damping curve. Judging from the fitness of the stiffness and damping curve and the RMS error value of 31.8%, it is possible to conclude that the initialised nonlinear model is not sufficient and thus requires further identification and minimisation of the error function.

4.3.5 Estimation of the Nonlinear Coefficients of the Duffing Oscillator

To estimate a parametric grey-box nonlinear model of the duffing oscillator, a weighted least squares cost function V_{LS} expressed in Equation 4.48 is defined through an Levenberg-Marquardt optimisation routine to evaluate the grey-box PNLSS model. To begin the optimisation routine the grey-box PNLSS model parameters obtained from the estimated initialised nonlinear model in the previous section were used as starting values. In this section, the optimisation is performed

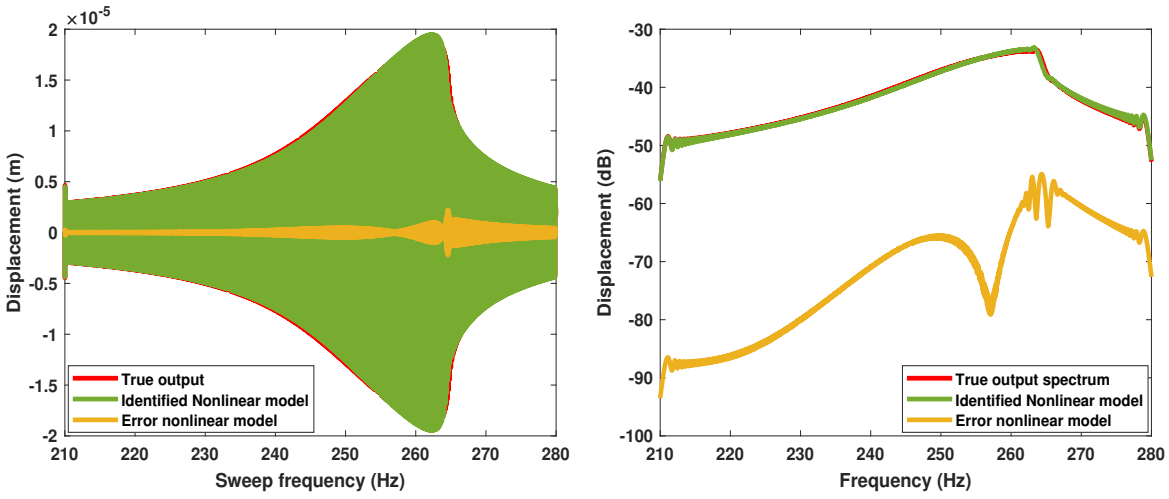

(a) (b)

Figure 4.12: *comparison of the identified nonlinear model against true nonlinear data. (a) time domain data response (b) corresponding displacement amplitude spectrum of the discrete time fourier transform.*

on the parameters of the grey-box PNLSS model which are the coefficients of the transfer function of the linear subsystem $a_1,\ldots,a_n,b_1,\ldots,b_n$ of elements in matrices A,B and E, in Equation 4.24, and the parameters of the nonlinear stiffness and damping curves, $p_1,\ldots,p_{r_y},q_1,\ldots,q_{r_{\dot{y}}}$, and c in matrices A,B and E, of Equation 4.24. For this optimisation, the Levenberg-Marquardt method is initialised with $\lambda = 100$ to make the optimisation procedure more robust, a fixed number of 300 iterations was selected to have a good trade off between the convergence and computational time. In Figure 4.12 a time domain and frequency spectrum comparison of the

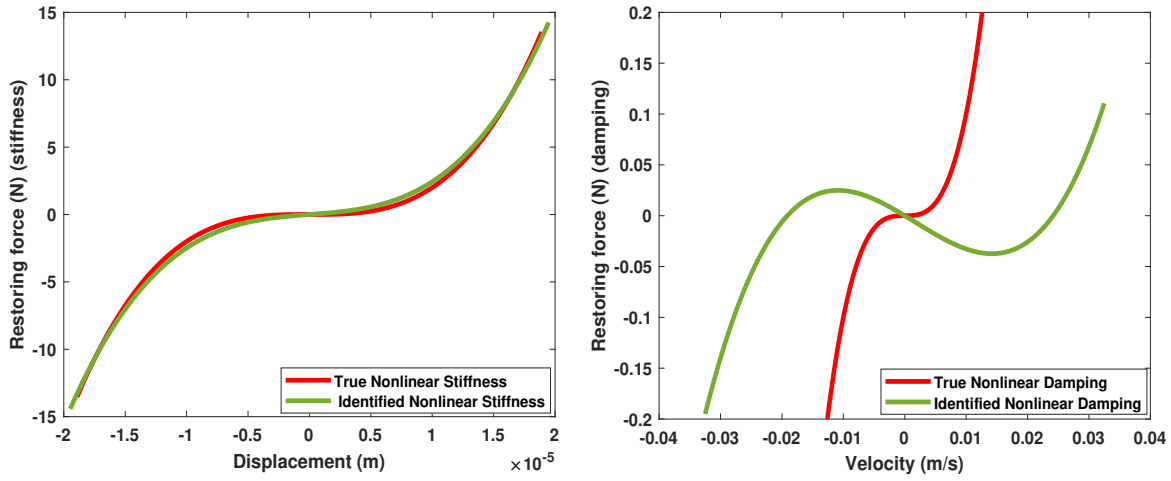

(a) (b)

Figure 4.13: *comparison of the identified nonlinear model against true nonlinear data. (a) nonlinear stiffness curve (b) nonlinear damping curve*

estimated nonlinear model based on optimisation with the true nonlinear data is illustrated. The obtained nonlinear model features lower error level ranging generally within 35dB below the true nonlinear spectrum data, similarly, compared to Figure 4.10a this new time domain estimate is able to capture the nonlinear distortions observed at the resonance peak better. The final RMS error obtained based on the nonlinear optimisation is 5.5%, this shows a significant error reduction compared to the initial estimated nonlinear model error of 31.8%. The corresponding nonlinear stiffness and damping curve obtained from this estimation are depicted in Figure 4.13, where a more accurate correlation is observed in this nonlinear stiffness curve compared to the one illustrated in Figure 4.11a. However the damping curve is non yet fully correlated, this could

be as an indication for further optimisation iteration to fully estimate the damping coefficients.

By plotting the normalised root mean squared error against the successful iterations of the LM optimisation, it is possible to observe the convergence behaviour of the models. From Figure 4.14, one can observe the advantage of making the extra effort in estimating a nonlinear initial model to use as starting values for the optimisation and estimation of the nonlinear model. The extra effort during the nonlinear initialisation pays itself back as shown in Figure 4.14, where the convergence of the nonlinear model show significantly better and faster performance compared to the linear model convergence curve. Starting from the linear model would require many optimisation

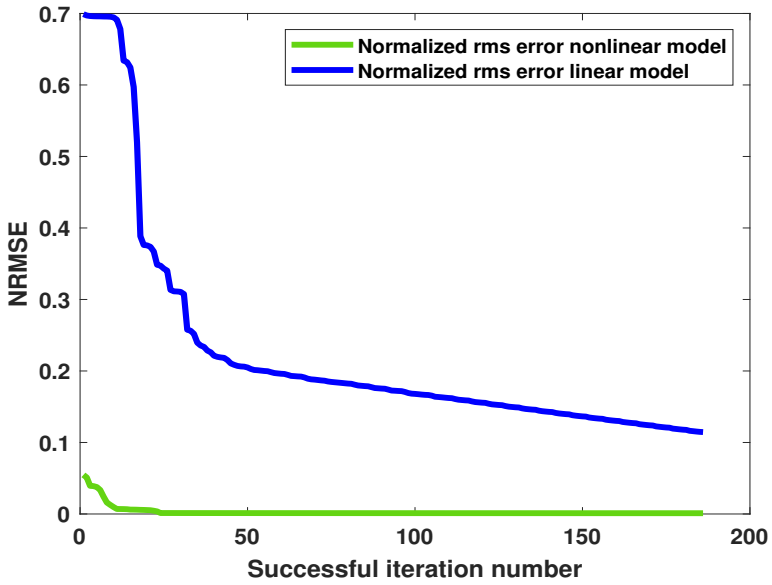

Figure 4.14: NRMS estimation error over successful Levenberg-Marquardt iterations.

steps/iterations before it would even achieve the same error of the nonlinear model which was based on using the initialised nonlinear model parameters as starting values for the optimisation. Achieving that same error is even not guaranteed, since the optimisation might get stuck in a local optimum before reaching the same error as that of the initial nonlinear model. Table 4.2 presents the identified coefficients values for the nonlinear parameters $p_1,\ldots,p_{r_y},q_1,\ldots,q_{r_y}$, for the simulated duffing oscillator example. The advantage of this proposed grey-box identification algorithm compared with the black-box PNLSS method implemented in Chapter 3 is that the coefficients of each nonlinear parameter in the grey-box PNLSS matrices A,B and E, in

Equation 4.24 can be tracked during the identification and optimisation. In Table 4.2, the relative error between the true nonlinear coefficients and the estimated coefficients for each nonlinear parameter for the linear, initialised nonlinear and final nonlinear models are calculated and reported. It is obvious from Table 4.2 that the coefficients of the nonlinear stiffness parameters

Nonlinear Parameters	$p_1(N/m)$	$p_2(N/m^2)$	$p_3(N/m^3)$	$q_1(Ns/m)$	$q_2(Ns/m^2)$	$q_3(Ns/m^3)$
True Coefficients	$7.04\cdot10^4$	$-2.38\cdot10^8$	$1.75\cdot10^{15}$	-3.66	-39.96	$7.92\cdot10^3$
Estimated Linear.	$4.90\cdot10^4$	$-1.33\cdot10^7$	$1.35\cdot10^{15}$	0.22	-1.36	$2.89\cdot10^2$
Rel. error	0.3049	0.9442	0.2277	1.0603	0.9659	0.9635
Initialised Nonlinear.	$1.63\cdot10^5$	$-1.33\cdot10^7$	$1.35\cdot10^{15}$	1.27	-1.36	$2.89\cdot10^2$
Rel. error	1.3167	0.9442	0.2277	1.3470	0.9659	0.9635
Estimated Nonlinear.	$-1.29\cdot10^4$	$-2.31\cdot10^8$	$1.75\cdot10^{15}$	-2.74	-40.14	$6.81\cdot10^3$
Rel. error	1.1835	0.0294	0.0028	0.2520	0.0045	0.1402
Optimised Nonlinear.	$7.16\cdot10^4$	$-2.31\cdot10^8$	$1.75\cdot10^{15}$	-2.97	-40.14	$6.81\cdot10^3$
Rel. error	0.0159	0.0294	0.0028	0.1885	0.0045	0.1402

Table 4.2: *True and estimated polynomial coefficients of the nonlinear stiffness and nonlinear damping curve of the grey-box PNLSS model. The relative estimation errors on the non-zero true coefficients are indicated in orange.*

p_2, and p_3 gradually decreases as from the linear model to the estimated nonlinear model. However, as errors for these coefficients decreases, the error for coefficient of p_1, which is the linear parameter of the polynomial function increases. The coefficients for q_1, q_2 and q_3, on the other-hand had a relative large error for the linear and initialised nonlinear model while a reduction is observed in error during the optimisation resulting in the values presented for the estimated nonlinear model. For both p_1, and q_1,, the error for estimated nonlinear coefficients are seen as the highest amongst others, further optimisation of these parameters could improve the overall identified nonlinear model.

4.3.6 Improving the Stiffness and Damping Estimates

While the estimated nonlinear model results presented in Figures 4.12 and 4.13 showed nearly perfect matching correlation with the true nonlinear data, the errors for some of the coefficients presented in Table 4.2 are still relatively high. To overcome this large error, further consideration of the linear part of the stiffness and the linear part of the damping either as part of the linear block or part of the nonlinear block was implemented in this section to observe if the error could

be further reduced. A feedback model structure as in Figure 4.5 with linear block

$$\tilde{G}(z) = \frac{G(z)}{1 + \beta_1 G(z) + \beta_2 G_{\text{Tustin}}(z) G(z)} \tag{4.50}$$

and a nonlinear feedback

$$\tilde{f}(\hat{y}(t), \hat{y}(t)) = f(\hat{y}(t), \hat{y}(t)) - \beta_1 \hat{y}(t) - \beta_2 \hat{y}(t) \tag{4.51}$$

has the same input/output behaviour for all $\beta_1 \in \mathbb{R}$ and $\beta_2 \in \mathbb{R}$

A static linear gain β_1 can be split off from the nonlinear stiffness and be taken into account in the linear block. Likewise, a static linear gain β_2 can be split off from the nonlinear damping and also be taken into account in the linear block:

$$\hat{y}(t) = G(z)\left(u(t) - f(\hat{y}(t), \hat{y}(t))\right) \tag{4.52}$$

Adding and subtracting $\beta_1 \hat{y}(t) + \beta_2 \hat{\hat{y}}(t)$:

$$\hat{y}(t) = G(z)\left(u(t) - f(\hat{y}(t), \hat{y}(t)) + \beta_1 \hat{y}(t) + \beta_2 \hat{\hat{y}}(t) - \beta_1 \hat{y}(t) - \beta_2 \hat{\hat{y}}(t)\right) \tag{4.53}$$

The $\hat{\hat{y}}(t)$ in the last term is equal to $G_{\text{Tustin}}(z)\hat{y}(t)$, since it is the output of the G_{Tustin} block which has $\hat{y}(t)$ as input:

$$\hat{y}(t) = G(z)\left(u(t) - f(\hat{y}(t), \hat{y}(t)) + \beta_1 \hat{y}(t) + \beta_2 \hat{\hat{y}}(t) - \beta_1 \hat{y}(t) - \beta_2 G_{\text{Tustin}}(z)\hat{y}(t)\right) \tag{4.54}$$

Transferring the last two terms from the right hand side to the left hand side, results in

$$(1 + \beta_1 G(z) + \beta_2 G_{\text{Tustin}}(z) G(z))\hat{y}(t) = G(z)\left(u(t) - f(\hat{y}(t), \hat{y}(t)) + \beta_1 \hat{y}(t) + \beta_2 \hat{\hat{y}}(t)\right) \tag{4.55}$$

and finally

$$\hat{y}(t) = \frac{G(z)}{1 + \beta_1 G(z) + \beta_2 G_{\text{Tustin}}(z) G(z)} \left(u(t) - (f(\hat{y}(t), \hat{y}(t)) - \beta_1 \hat{y}(t) - \beta_2 \hat{\hat{y}}(t))\right) \tag{4.56}$$

$$= \tilde{G}(z)\left(u(t) - \tilde{f}(\hat{y}(t), \hat{y}(t))\right) \tag{4.57}$$

which has the same form as (4.52), but with a linear block

$$\tilde{G}(z) = \frac{G(z)}{1 + \beta_1 G(z) + \beta_2 G_{\text{Tustin}}(z) G(z)} \tag{4.58}$$

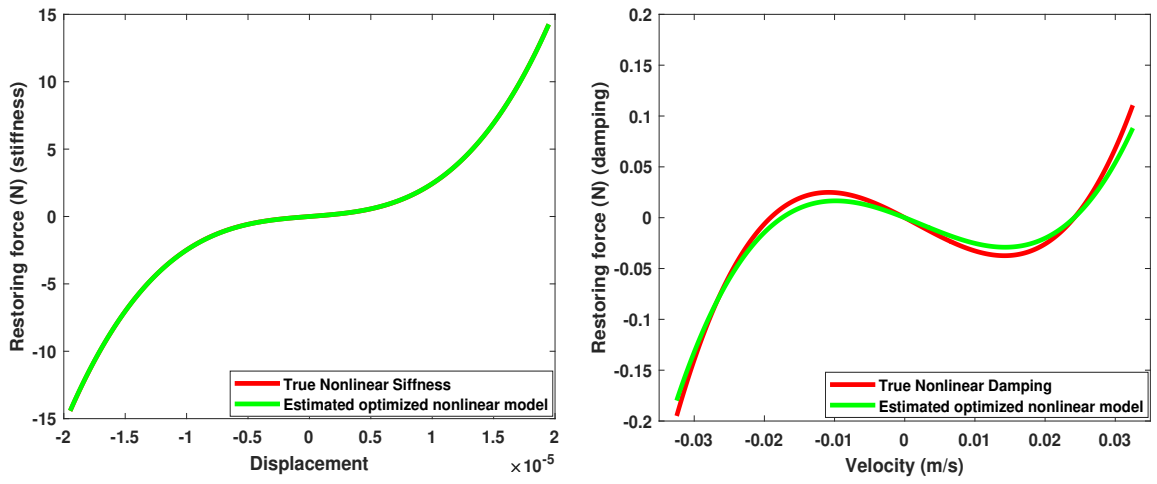

(a) (b)

Figure 4.15: *comparison of estimated optimised nonlinear model against true nonlinear data. (a) stiffness (b) damping*

and a nonlinear block

$$\tilde{f}(\hat{y}(t),\hat{y}(t)) = f(\hat{y}(t),\hat{y}(t)) - \beta_1\hat{y}(t) - \beta_2\hat{y}(t) \tag{4.59}$$

From this formulation it is possible to conclude that the static gains β_1 and β_2 can be adjusted to further improve the coefficients of the nonlinear stiffness and damping parameters presented in Table 4.2. Causing a further augmentation of the correlation between the true and estimated nonlinear curves. It is worth stating that the adjustment of the static gains parameters does not change the input/output behaviour of the model. Results obtained from these adjustment are the nonlinear stiffness and damping curves presented in Figure 4.15 and coefficients of the optimised nonlinear estimates presented in Table 4.2. From Figure 4.15, it is clear that the consideration of the linear terms as part of the nonlinear block certainly improves the newly estimated nonlinear stiffness and damping curve compared with the ones presented in Figure 4.13. The relative error values for the linear parts of the stiffness and damping polynomial functions have also reduced.

4.4 Validation of the Non-linear Feedback Model

To examine the domain of validity of the proposed grey-box PNLSS model, the estimated model of the Duffing oscillator demonstrated in Section 4.3 is validated on a newly generated sine-sweep

and multi-sine data sets. In the validation step, the final optimised nonlinear model parameters presented in Table 4.2 and Figure 4.15 was introduced to a simulated sine-sweep data generated at 3N RMS excitation level. It is important to note that no further optimisation was conducted in this step, only an evaluation of the final identified coefficients of the nonlinear model in the previous section was carried out by simulating these coefficients with the sine-sweep data input at 3N and comparing the modelled output with the original simulated data. This validation experiment was intended to measure the performance of the identified Grey-box PNLSS models under similar conditions based on the frequency and amplitude range of interest.

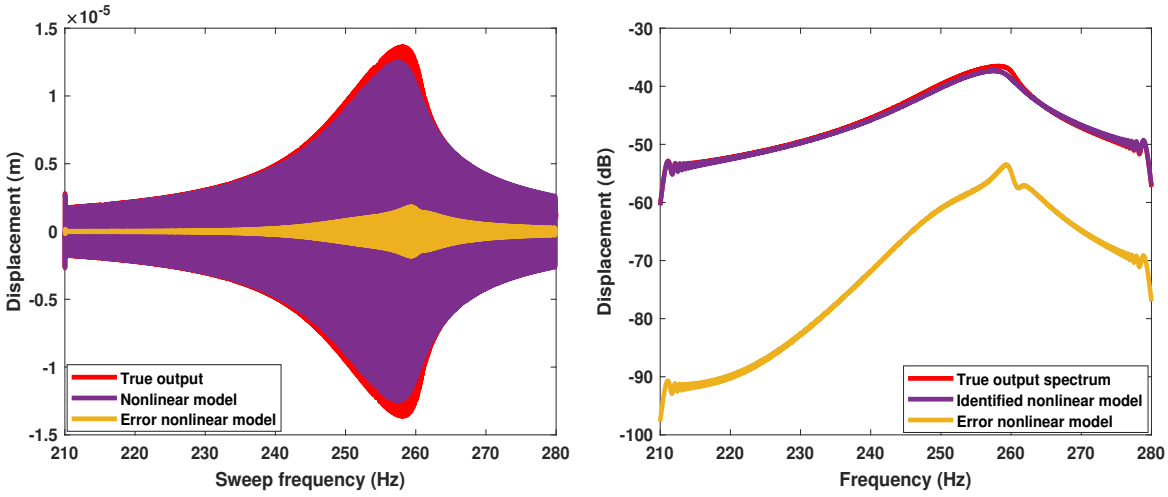

(a) (b)

Figure 4.16: *comparison of validated nonlinear model against true data. (a) time domain data response (b) corresponding displacement amplitude spectrum of the discrete time fourier transform.*

Results obtained from the sine-sweep validation experiment are presented in Figure 4.16, where the modelled validation output in purple is compared with the original simulated data in red for both time domain and spectrum output responses. The error obtained from the validation exercise is also plotted on the same Figure 4.16 in yellow, the validation results illustrated above feature a low error level difference generally lying between 35-40dB at both start and end frequencies and around 25dB at the resonance region. The Levenberg-Marquardt iterations used in constructing this validation model are presented in Figure 4.17. It is observed that the optimal model is reach after 26 successful iterations when using a nonlinear initialised model. Similar to

the estimation error presented in Figure 4.14, the significant difference in the NRMSE result of the linear model and nonlinear model ascertains the importance of initialising the nonlinear linear model before final estimation and validation of the nonlinear coefficients.

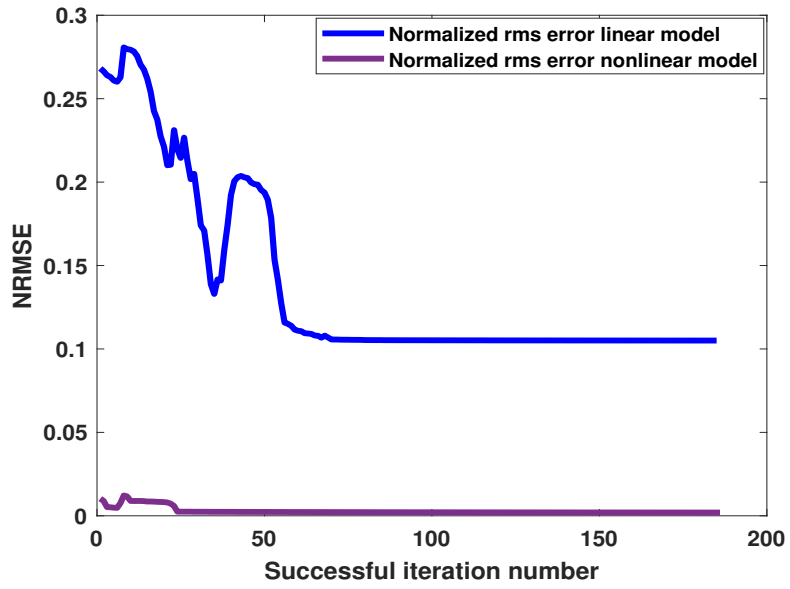

Figure 4.17: NRMSE validation error over successful Levenberg-Marquardt iterations.

4.4.1 Multi-sine Data Validation

The final test conducted on the proposed grey-box PNLSS identification algorithm is to assess the behaviour of the proposed identification method on a different type of signal often used in the field of nonlinear identification. In this case, multi-sine data sets was generated at three different excitation levels, one period and seven phase realisations of a full random-phase multisine with 5600 samples per realisation are used for generating the multi-sine validation signal. The multisine excites the frequencies between 210 Hz and 280 Hz with a frequency resolution of 2 Hz (the sampling frequency is 2800 Hz), this is done to mimic the similar frequency bandwidth that was used in the sine-sweep estimation data.The major advantage of the random-phase multisine is that it still has (asymptotically for sufficiently large N samples) all the nice properties of Gaussian noise, while it also has the advantages of a deterministic signal: the amplitude spectrum does not show dips at the excited frequencies [228].

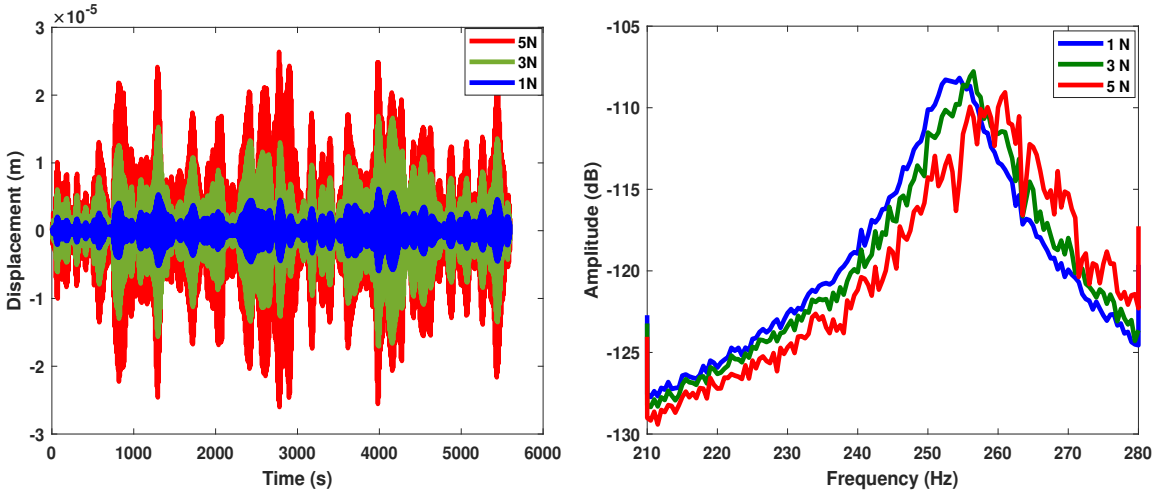

(a) (b)

Figure 4.18: *Comparison of simulated multi-sine time and frequency domain data at different force levels. (a) time domain data response (b) corresponding amplitude spectrum of the discrete time fourier transform.*

Three different amplitude levels are considered: 1N rms, 3N rms, and 5N rms. The time domain and frequency response function (FRF) results for the generated multi-sine data are presented in Figure 4.18. In the Frequency spectrum plotted in Figure 4.18b, a reduction in amplitude and frequency is observed which also corresponds to a nonlinear softening characteristics. To obtain comparable results that were achieved during the sine-sweep data estimation, the nonlinear identification was conducted on the 5N RMS data set. The same identification procedure implemented in Section 4.3, where the linear model was first estimated, followed by a nonlinear initialisation and nonlinear parameter estimation was used in estimating the nonlinear model for this multi-sine data. The time domain and spectrum results obtained from the nonlinear identification are presented in Figure 4.19, where the error obtained from each model is superposed over the original simulated multi-sine data at 5N rms. In Figure 4.19, a trend in the model error similar to the sine-sweep estimation is observed, where a large error is reported for the estimated linear model. Further refinement of the nonlinear estimation produces a significant error reduction through each estimated model with the optimal identified model being the optimised nonlinear model (in purple), where a significant difference of around (50dB) is noticed between the maximum magnitude spectrum of the true data and the error of the

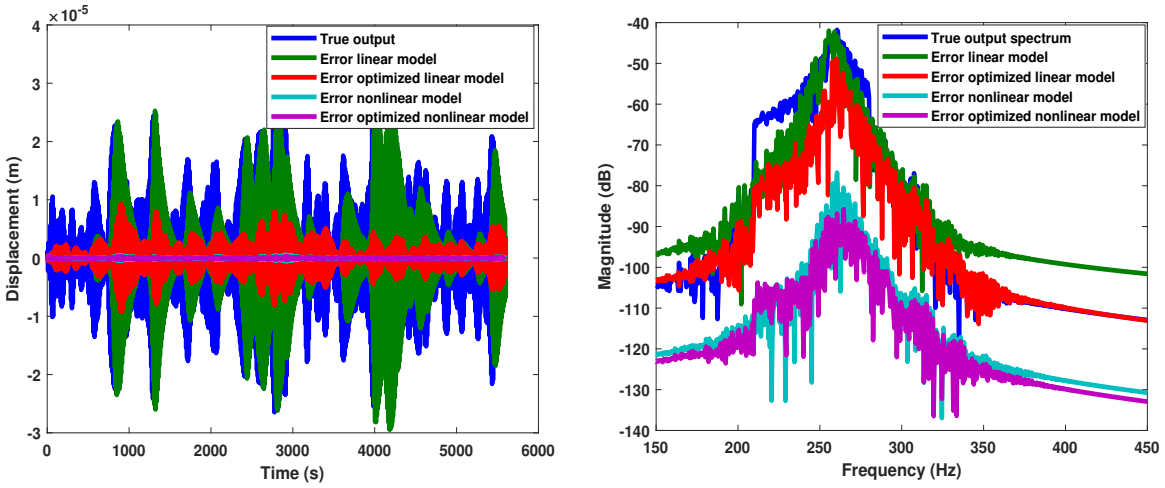

(a) (b)

Figure 4.19: *Comparison of multi-sine estimated model errors against true nonlinear data. (a) time domain data response (b) corresponding magnitude spectrum of the discrete time fourier transform.*

optimised nonlinear model.

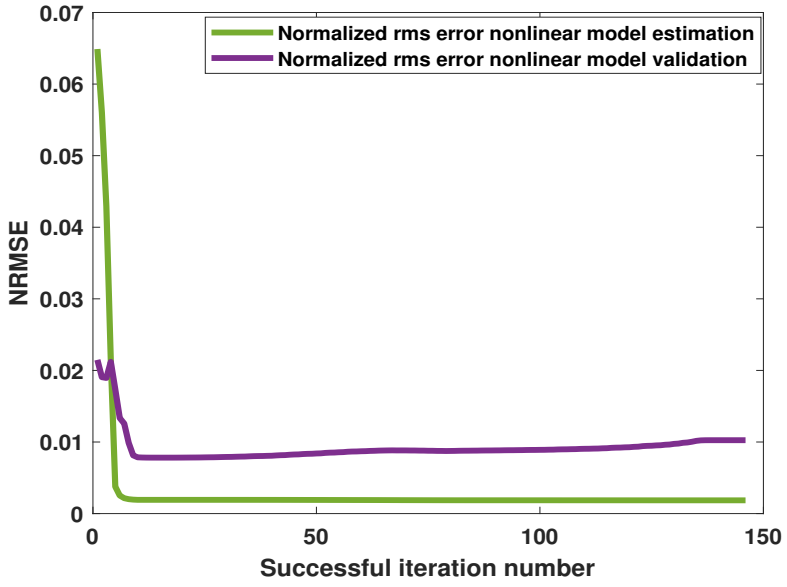

Figure 4.20: *NRMSE error over successful Levenberg-Marquardt iterations for the multisine data.*

The NRMSE against the Levenberg-Marquardt iterations for the multi-sine data identification is equally presented in Figure 4.20 for the estimation and validation models. Compared to the

sine-sweep data identification, it is observed for the multi-sine data that the optimal model is reached after the first 5 iterations. In addition, the final NRMSE fall within and below 1% for both estimation and validation models. Both Figures 4.19 and 4.20 agreeably demonstrates the significance and strength of the grey-box PNLSS model using a different type of excitation signal, where the achieved small RMS value indicates the predictive confidence of the proposed grey-box PNLSS model. From a user point of view, having minor errors between the true simulated data and the identified grey-box PNLSS models is in many cases acceptable, given that a good estimate of the maximum amplitude, the frequency of the response and other important features of the predicted responses are obtained. Most importantly, for this Duffing oscillator application, the results have shown a good degree of accuracy based on the various errors criteria discussed and presented in this chapter.

4.5 Conclusions

The main objective of this chapter was to introduce a nonlinear time domain grey-box PNLSS identification algorithm by revisiting the black-box PNLSS identification method implemented in Chapter 3. The underlying theoretical formulation and steps involved in the proposed grey-box identification method were highlighted and discussed in Section 4.2, an important assumption made during the formulation of the identification theorem is the notion that the nonlinearities in a system act as internal feedback forces to the underlying linear model of the system under consideration. The proposed identification method was demonstrated on a simulated Duffing oscillator example, where sine-sweep data was used for the nonlinear parameter estimation and validation. A further validation proof was also conducted using multi-sine data to check the validity of the identification method on broadband data.

The success of the grey-box PNLSS identification algorithm was judged based on the relative errors between each identified nonlinear coefficients and the original nonlinear coefficient used in generating the data as presented in Table 4.2. In addition, the RMS values of 0.2% and 1% achieved on the identified and validated grey-box PNLSS models were also used as supplementary measures for arbitrating the attained nonlinear model for the Duffing oscillator

example. One key feature demonstrated in this proposed grey-box identification algorithm is the ability to track the behaviour and estimation of each coefficient for each nonlinear parameter $p_1,\ldots,p_{r_y},q_1,\ldots,q_{r_{\dot{y}}}$, in the formulated grey-box PNLSS matrices A,B and E, in Equation 4.24. Having this coefficient tracking capabilities provides the possibility of plotting and visualising the evolution of the nonlinear stiffness and damping curve at each identification stage, such as the nonlinear initialisation and final estimation stages.

Compared to the exponentially increasing characteristics and very large number of the estimated nonlinear parameters attained using black-box PNLSS identification method implemented in Chapter 3, in this grey-box method, the estimated model has the advantage of being parameter-parsimonious where the number of estimated nonlinear coefficients is significantly reduced. Most importantly, once the model is estimated, the linear discrete-time transfer function G can be transformed to a continuous-time representation, allowing for obtaining meaningful parameters (e.g. the mass, linear spring constant, and linear damping coefficients). The estimated nonlinear block can be interpreted as the sum of a nonlinear stiffness and a nonlinear damping curve. These important features and advantages are not present or easily achieved when using the general unstructured nonlinear state space models.

While the competences of the proposed grey-box PNLSS identification method have been demonstrated in Section 4.3 of this chapter, future work is still required to advance the nonlinear identification capabilities. The numerical example demonstrated in this chapter was for used a single nonlinear mode or SDOF. Future research on this topic should include developing the Jacobian of the grey-box algorithm to accommodate multiple nonlinear modes, different types of nonlinearities and multiple nonlinear sources rather than a single localised source. Another improvement that could be benefited by this proposed method is the development of a method to calculate the confidence interval of the estimated nonlinear parameters and coefficients. Implementing the proposed method using noisy or imperfect data would be another avenue to challenge the strength of the proposed method and finally demonstration of the identification algorithm on measured data obtained from mechanical systems.

CHAPTER 5

Grey-box Identification of an Aerospace Structure.

Abstract

Complex shaped aerospace structures such deploy-able missiles are prone to exhibit some level of nonlinear phenomena due to their aerodynamically tailored design and application. Aside from the aerodynamic loads experienced by a missile during flight, a fundamental challenge is the inevitable concentrated structural non-linearities observed often around the jointed parts of the missile and connections to the air-frame. Activation of these non-linearities often affects the dynamic response of the missile and in some cases lead to structural failures. To obtain better understanding and improve the design, the nonlinear dynamic behaviour of a prototype missile is examined using the grey-box PNLSS identification method proposed in Chapter 4. The demonstration is conducted on measured data obtained from experimental campaign of the prototype missile.

5.1 Introduction

Based on the extensive review conducted on Chapter 2, it is now broadly acknowledged that nearly all engineering structures posses a degree of nonlinearity, at least in certain conditions of motion or operational environment. A large majority of these non-linearities are narrowed down to the design of the structure, nature of the joints design, material and geometric properties. For example, most aircraft components are designed and manufactured separately and later connected together through bolted connections or other joining means to create a complete assembled aircraft [229]. Effective characterisation of the mechanical properties such as stiffness and damping for jointed or assembled structures in a dynamic analysis remains a recurring challenge for most structural dynamicist [6]. Most assemblies or connections are made through the use of bolts, rivets, adhesives, pins and elastomers, the response of these elements under large external forces or compressive loads can often alter the global dynamic response of the assembly.

Further more, research on bolted joints and other types of nonlinear features have been proven to introduce large uncertainties in the stiffness and damping properties of a structure which can often render the response of the structure nonlinear, identifying and predicting the effect of these non-linearities at operational conditions also poses a challenge to present structural engineers dealing with complex nonlinear structures. Experimental identification of the nonlinearities arising from these jointed properties have been noticeable in many structural dynamic applications, for example in complex aerospace and mechanical structures [230], micro-mechanical systems with magnetic or friction forces [231], machineries with rubber isolation mounts and assembled structures with bolted interfaces [232]. Hence, the parametric estimation of these nonlinear behaviours from measured data would be of extreme benefit in obtaining better virtual response prediction of structure under consideration.

Extensive efforts have been devoted on the application of developed nonlinear identification methods to identify nonlinear parameters from experimental data, for example weak non-linearities was studied on a more complex aerospace structure in [29] where a strategy for non-linear modal identification of weak nonlinear effects on a large aircraft was presented. An

aluminium plate attached with two stores used to illustrate the behaviour of a wing and an engine suspended by a means of nonlinear pylon also displayed the presence of weak non-linearities during a vibration test, the results obtained illustrated some hardening characteristics as shown in [13]. A similar study was also carried out on a large helicopter with the identification of weak nonlinear softening behaviour on one of the vibration modes as shown in [177]. Other examples of case studies where non-linearity have been noticed in aerospace structures can be found in [233] where non-linearity was also detected at the elastomeric mounts supporting the four turboprop engines of the aircraft during the Ground Vibration Test (GVT) of the Airbus A400M aircraft designed for military purpose. The F-16 fighter aircraft also showed a nonlinear behaviour at wing-to-payload mounting interface of the aircraft when a similar GVT was conducted [10].

Despite the practical advancement and increasing interest in nonlinear identification from experimental data, only a selected range of methods have successfully been used to obtain parametric nonlinear models from experimental data. To continue this practical progression, this chapter addresses the nonlinear experimental identification of a prototype assembled missile. This involves the use of time domain grey-box PNLSS identification algorithm established in Chapter 4 and other nonlinear signal processing techniques to identify the type of non-linearity present in the assembled missile, the complete identification process i.e. (Detection, Characterisation and Parameter estimation) was achieved based on experimental data. Measured time series and frequency data driven by Sine-sweep test and random excitation were exploited to gain an useful insight to the dynamic behaviour and properties of the assembly. The validity and practical application of the proposed grey-box PNLSS identification method in Chapter 4 was mainly put to test in this chapter.

The structure of the chapter is as follows, Section 5.2 gives a brief description of the and of test structure under investigation. The experimental study followed by the linear identification based on measured data from low level random excitation and linear finite element modelling are presented in Section 5.3. Section 5.4 provides the initial nonlinear detection and time frequency analysis. The parametric nonlinear identification results based on the grey-box PNLSS identification algorithm are presented in Section 5.5. The conclusion of the study and the collective use of different analysis techniques in this chapter are summarised in Section 5.6.

Part of this chapter is based on the following conference papers:

S.B.Cooper, D.DiMaio, D.J.Ewins (2017) Nonlinear Vibration Analysis of a Complex Aerospace Structure. *In G. Kerschen (Ed.), Nonlinear Dynamics Volume 1: Proceedings of the 35th IMAC, A Conference and Exposition on Structural Dynamics 2017* (pp. 55-68).

S.B.Cooper, (2016) Nonlinear vibration analysis of a complex aerospace structure. *In proceedings of the Defence and Security Doctoral Symposium*. https://doi.org/10.17862/cranfield.rd.4288874.v2.

S.B.Cooper, M.Rosatello, A.T.Mathis, K.Johnson, M.R.W.Brake, M.S.Allen, A. A.Ferri, D.R.Roettgen, B.R.Pacini, R.L.Mayes (2017) Effect of Far-Field Structure on Joint Properties.*In M.S.Allen, R.L.Mayes, D.Rixen (Ed.), Nonlinear Dynamics Volume 4: Proceedings of the 35th IMAC, A Conference and Exposition on Structural Dynamics 2017* (pp. 63-77)

5.2 The Aerospace Test Structure

A Missile Test Structure (MTS) was designed and manufactured for a related piece of research in [234] as shown in Figure 5.1 which was extracted from the publication. The MTS, while not an exact scale replica of any particular missile system (for ease of manufacture and classification), has structural features that are typical of a full-size system e.g. multiple body sections, bolted joints, hanger and launch rail assembly. MTS is made up of 4 sections of aluminium tubing, a nylon nose cone, aluminium fins and hangers and a detachable aluminium launch rail. The approximate dimensions are: overall length 1200 mm, outside diameter 60 mm, overall mass 3 kg. Since most of the nonlinear phenomena experienced in mechanical vibrations are attributed to joints, friction and geometric non-linearities, the test structure has related features which can be used for investigating the effect of non-linearities caused by bolted joints and assembled multibody sections at high levels of vibration test.

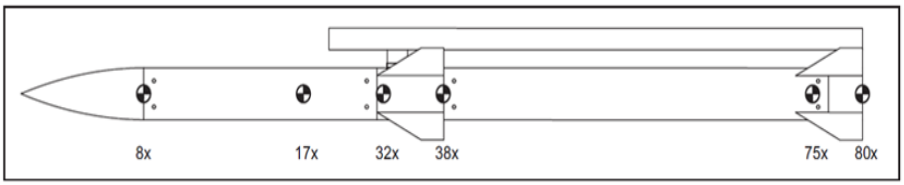

Figure 5.1: *Missile Test Structure.*

5.2.1 Linear Finite Element Model of the MTS

The use of pre-test simulation to plan modal test has been an active procedure used by many researchers and industrial engineers, to obtain a pre-test model an analytical or FE model of the structure is often required [169]. The advantage of starting from a FE model is the fact that the numerical results can be used in order to plan test strategy and to find optimal location for sensors, shakers and suspension, allowing the optimal control and observation of number of selected target modes. To generate the FE model of the MTS, a computer aided design of each individual part was drawn using the geometry sketch tool in ABAQUS commercial software. To keep the model simple and capable of describing the dynamic representation of the MTS, each bolted connection and joint was modelled and assembled together using tied kinematic constraint. Material properties of aluminium was selected for the tube, launch rail and fins, while material properties of nylon was selected for the nose. Figure 5.2 shows an illustrated of the CAD model for each part and the final assembly of the MTS.

5.2.1.1 Linear Finite Element Modal Analysis of the MTS

A detailed Finite Element (FE) mesh of the CAD model of the MTS was obtained using mesh generator in the commercial ABAQUS FE package, the result of generated mesh is presented in Figure 5.3. The model comprises about 720,000 nodes, and consists of mainly shell elements namely isotropic and orthotropic elements, the tubes and nose modelled using isotropic elements while the launch rail and fins were modelled with orthotropic elements. A linear FE modal analysis was conducted to extract the FE mode shapes. The linear FE analysis was conducted with the aim of getting better insight into the selection of appropriate measurement locations, sensor placement and the test excitation point. In addition, this initial FE analysis was used to

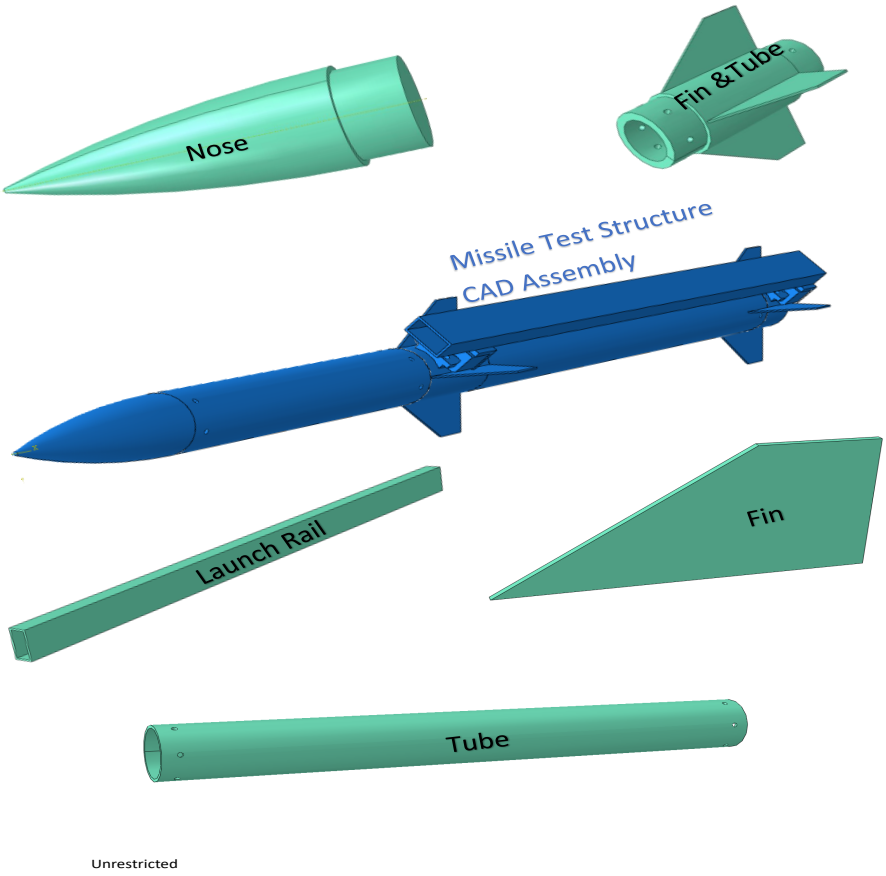

Figure 5.2: *Individual CAD parts and assembly of the Missile Test Structure.*

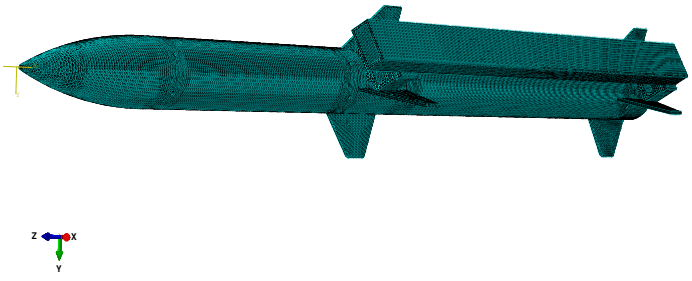

Figure 5.3: *Mesh model of the Missile Test Structure.*

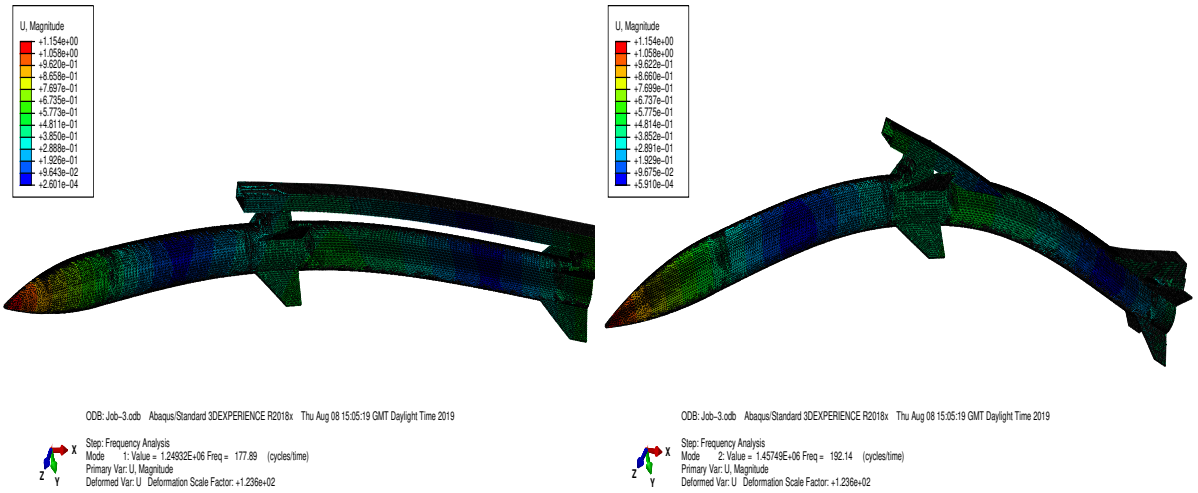

(a) (b)

Figure 5.4: *Linear FE Modes of the Missile Test Structure. (a) mode 1 (b) mode 2*

determine the number of expected modes in a given frequency range. Most importantly, since the test was being conducted on a test structure with multiple joints and localised non-linearities, the results from the FE mode shapes are used to quickly and reliably identify the frequency ranges where the joints and additional localised nonlinear source could be actively excited. Figure 5.4 shows two FE modes obtained at frequency range of 150Hz to 200Hz. Correlating the results of

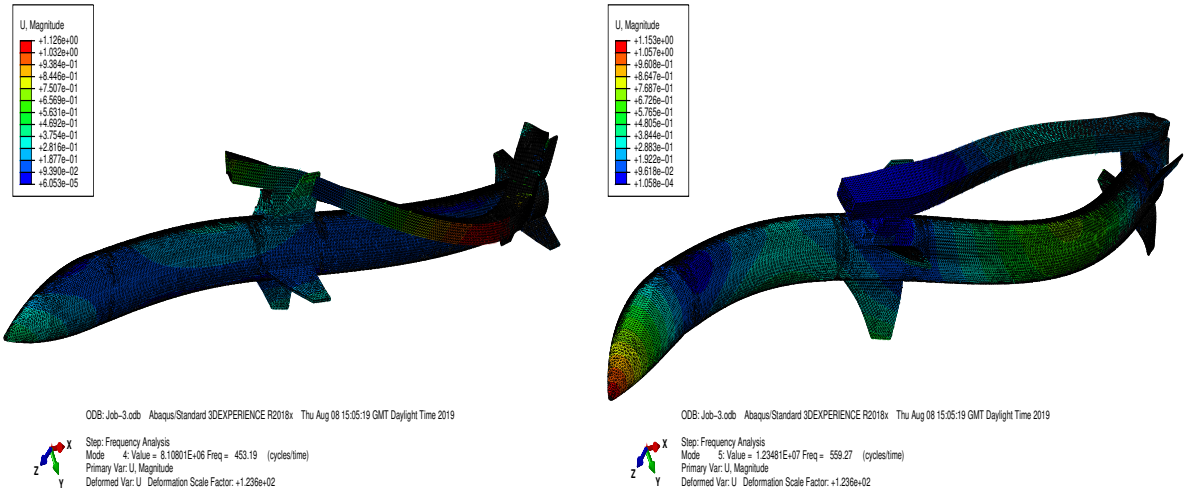

(a) (b)

Figure 5.5: *Linear FE Modes of the Missile Test Structure.(a) mode 4 (b) mode 5*

the linear FE model in very close quantitative agreement with the experimental observations, i.e. carrying out a formal linear model updating process, is not an objective of this chapter. However the results obtained from the linear FE modal analysis can be seen as satisfactory prerequisite for the modal tests and nonlinear identification. Of all modes of vibration highlighted by the FE model, only those that are prone to stimulate all joints and launch rail connections are further investigated in the nonlinear identification section of this chapter. Figures 5.5a and 5.5b illustrate two modes of vibration where the joints and local nonlinear sources are excited.

5.3 Experimental Test and Linear Modal Analysis of the MTS

To subject the MTS to a representative vibration environment the MTS was hung on a test frame using fishing lines, springs and light connection ropes as shown in Figure 5.6, the test setup was designed to replicate the usual boundary condition experienced by such device when attached to an air vehicle. The black frame was bolted on a seismic table to disallow any form of movement to the frame during the vibration test, the complete assembly was tested and examined to ensure that the level of vibration transferred to the missile test structure is reduced to a minimum or zero value. The assembled missile and hanger was instrumented with 15 accelerometers and a force transducer, the connection areas between the hanger and the missile were instrumented appropriately to capture any nonlinear phenomena exhibited by the bolted connection.

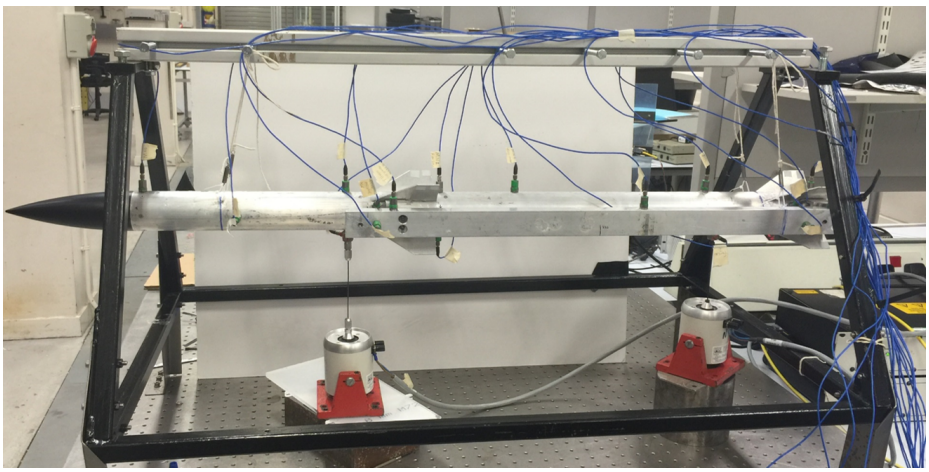

Figure 5.6: *Missile Test Structure Experimental Set-up.*

5.3.1 Low Level Test Campaign

The first measurements obtained from the experimental test comprised of several low random data which were acquired based on broadband excitation, the choice of broadband excitation was made based on its conventional use in modal testing. The use of broadband excitation also provides some early information on the behaviour of the structure and experimental configuration, the low level random test was performed using the Spectral Test module in LMS Test Lab [233], the test structure was excited close to the hanger attachment at the tail section as shown in Figure 5.6. The structure was excited using burst random excitation filtered in 120-550Hz. The FRFs and associated coherence functions obtained from the test was exploited to identify the linear modal properties of the test structure, the shape of the FRFs and ordinary coherence plots were also used as an indication to determine if the assembly was behaving linearly at the specified excitation level.

A selection of the Frequency Response Functions (FRF) and coherence functions obtained from the low level random excitation are plotted below in Figures 5.7a to 5.7d. The linear resonance frequencies and damping ratios were estimated using the frequency-domain identification algorithm (Polymax) method presented in [2], the PolyMAX method uses measured Frequency Response Functions (FRFs) as principal data. The measured FRF is is seen as the right matrix-fraction model which represents a pair of inputs and output. The corresponding resonance frequencies and damping ratio identified using the low level random data obtained from the missile test are presented in Table 5.1. The resonance peaks of the FRFs indicates that the structure is lightly damped across the selected bandwidths, the coherence function corresponding to each FRF or measured position are all close to unity for the whole excited frequency range.

5.4 Non-linear Detection and Analysis

Detection indicates that some effect attributed to non-linearity is observed, and it is deemed that the standard linear model cannot adequately represent the system response. There several techniques of detecting nonlinear behaviour from measured data, this however depends on the type of excitation signal used during the test campaign. Stepped sine and Sine-Sweep excitation

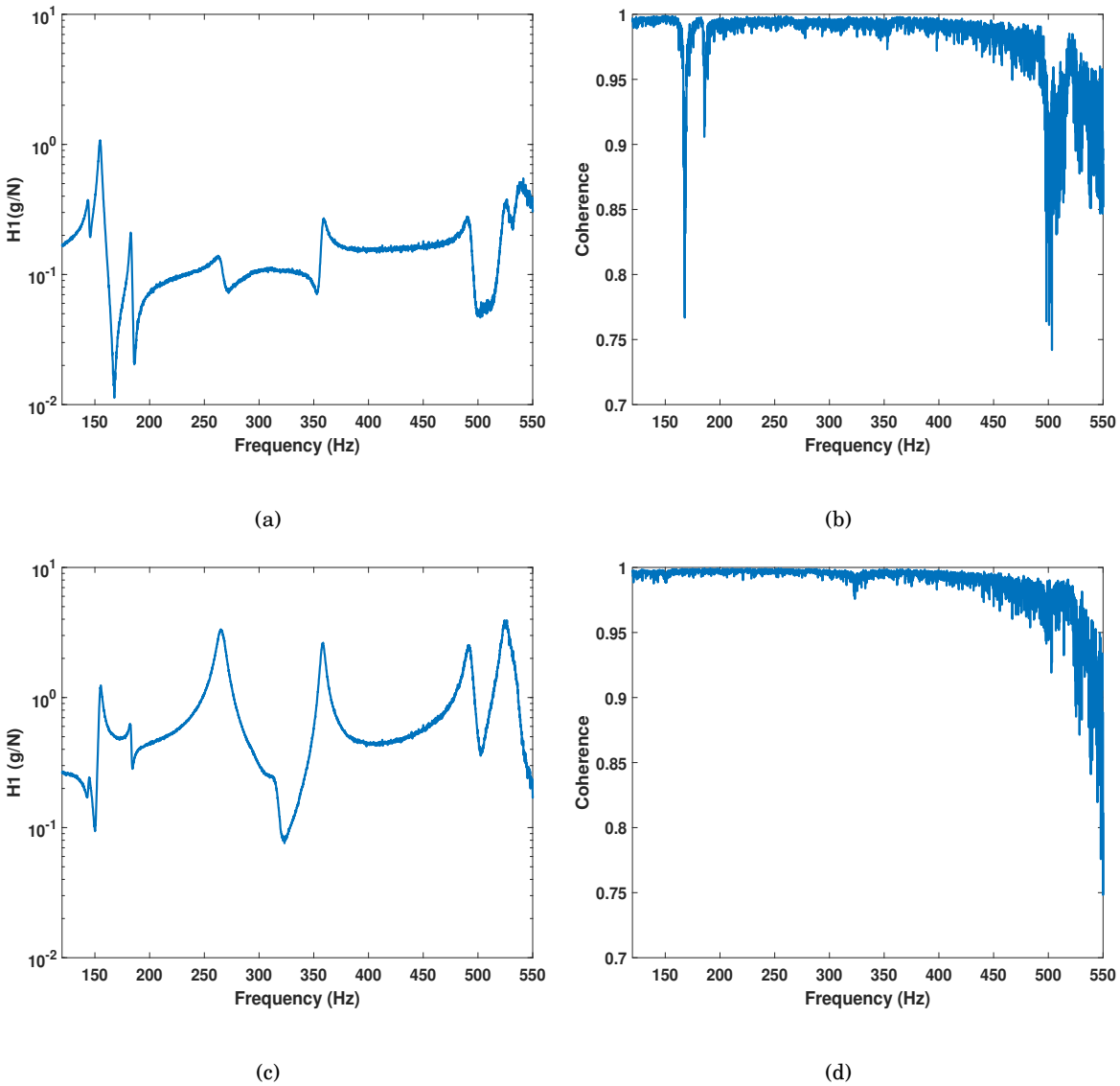

Figure 5.7: *FRFs and Coherence responses obtained from low-level broadband excitation.(a) and (b)FRF and coherence response for the centre tube of the Missile, (c) and (d) FRF and coherence response for the far-end of the Hanger.*

are predominantly suitable in determining if a structure has a nonlinear behaviour at higher excitation level, if linear, the structure would produce a pure sine wave in the output and if nonlinear, distortions are easily detected by visualising the output envelop of the sine wave.

Mode	Frequency (Hz)	Damping ratio (%)
1	144.38	0.75
2	154.90	0.94
3	183.04	0.52
4	253.57	1.63
5	292.17	1.72
6	315.41	1.34
7	358.05	0.69
8	492.44	0.72
9	524.85	0.75
10	539.21	0.71

Table 5.1: *Estimated resonance frequencies and damping ratios based on low-level random data*

5.4.1 Time Series and FRF Inspection

Visualisation of raw time series obtained from Sine-Sweep excitation can often reveal some level of nonlinear behaviour in the structure, any form of nonlinear distortions observed in the time response envelop is sufficient to prove the presence of non-linearity in the structure. In this research, Sine-Sweep test was conducted on the second, third and fourth mode of the assembly. Accelerations at every sensor locations on the MTS were measured between 0.5N and 15N. The Sine-Sweep test was conduct using the Multi-input Multi-output (MIMO) Sine-Sweep module in LMS Test Lab package , the input excitation force was uncontrolled however parameters such has the start and end frequencies, sweep type and sweep time were specified. To detect any form of nonlinear behaviour, the first observation is shown in Figure 5.8a and 5.8b where an absence of proportionality is noticed between the time responses from low to high excitation level. This indicates the breakdown of superposition principle, secondly, Figures 5.8b sweep-up shows clear skewness in the time responses as the excitation level increases from 1N to 5N. The skewness in the envelope of oscillation in Figure 5.8b where a sudden transition from low to high amplitude of vibration is observed can also be described as a jump phenomenon, this is also a useful technique for detecting nonlinear behaviour in the structure.

The final and most important observation from the time response envelope is the shift in the resonance frequency, a negative drop can be seen in the location of the resonance frequency between Figure 5.8 (a and b), where the resonance frequency has shifted / reduced from 250Hz

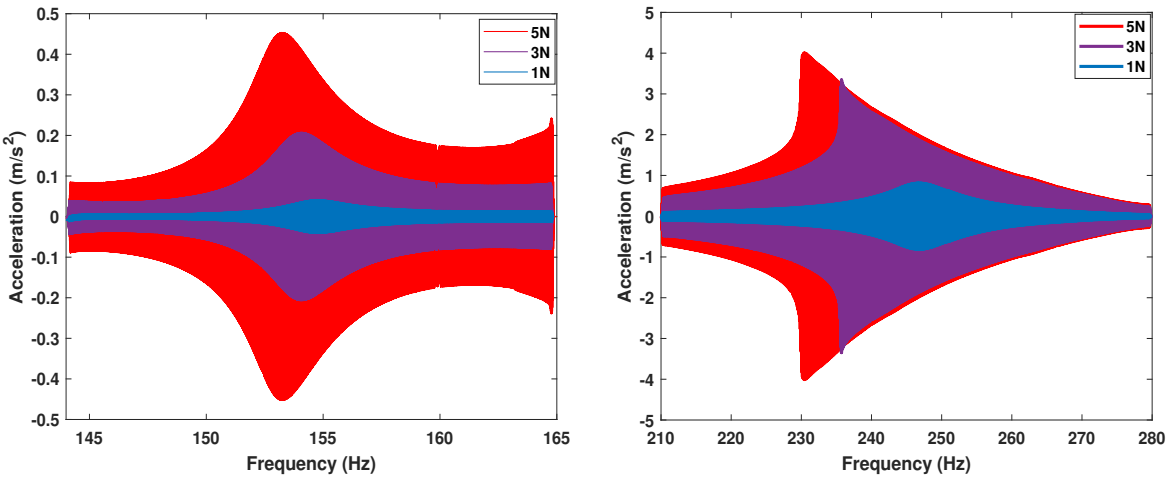

(a) (b)

Figure 5.8: *Nonlinearity detection based on envelope time series inspection.(a) measured time signals at different force levels for mode 2 (b) measured time signals at different force levels for mode 4*

to 230.2Hz due to the increase in the excitation level from 1N to 5N. Other forms of nonlinear behaviours which are observed in the time response envelope are peak distortion, non-smoothness and discontinuity of the sweep response at 5N compared to the response at 1N excitation level, indication of multiple solutions and bifurcation points are also observed around the resonance frequency for the response at 5N, all these observations are sufficient enough to detect the presence of non-linearity in the MTS assembly.

Another simplified method of detecting non-linearity in a structure from experimental measurement is based on the assumption that the FRF of a linear system is independent of the input amplitude. This assumption is often used by most researchers in the field of structural dynamics, it serves as a basic initial step in nonlinear identification and it associated with the homogeneity of the system [171]. For a nonlinear structure the FRF is dependent on the magnitude of the input force applied during the experimental test. The FRF cross correlation method presented in [235] is a simple method of quantifying non-linearity and it has been adopted in this section of the research to detect some non-linearities in the missile test structure. The first and most noticeable indicator of nonlinear behaviour is a lack of homogeneity in frequency response functions over different force inputs. By looking at Figure 5.9 it is immediately obvious that the structure

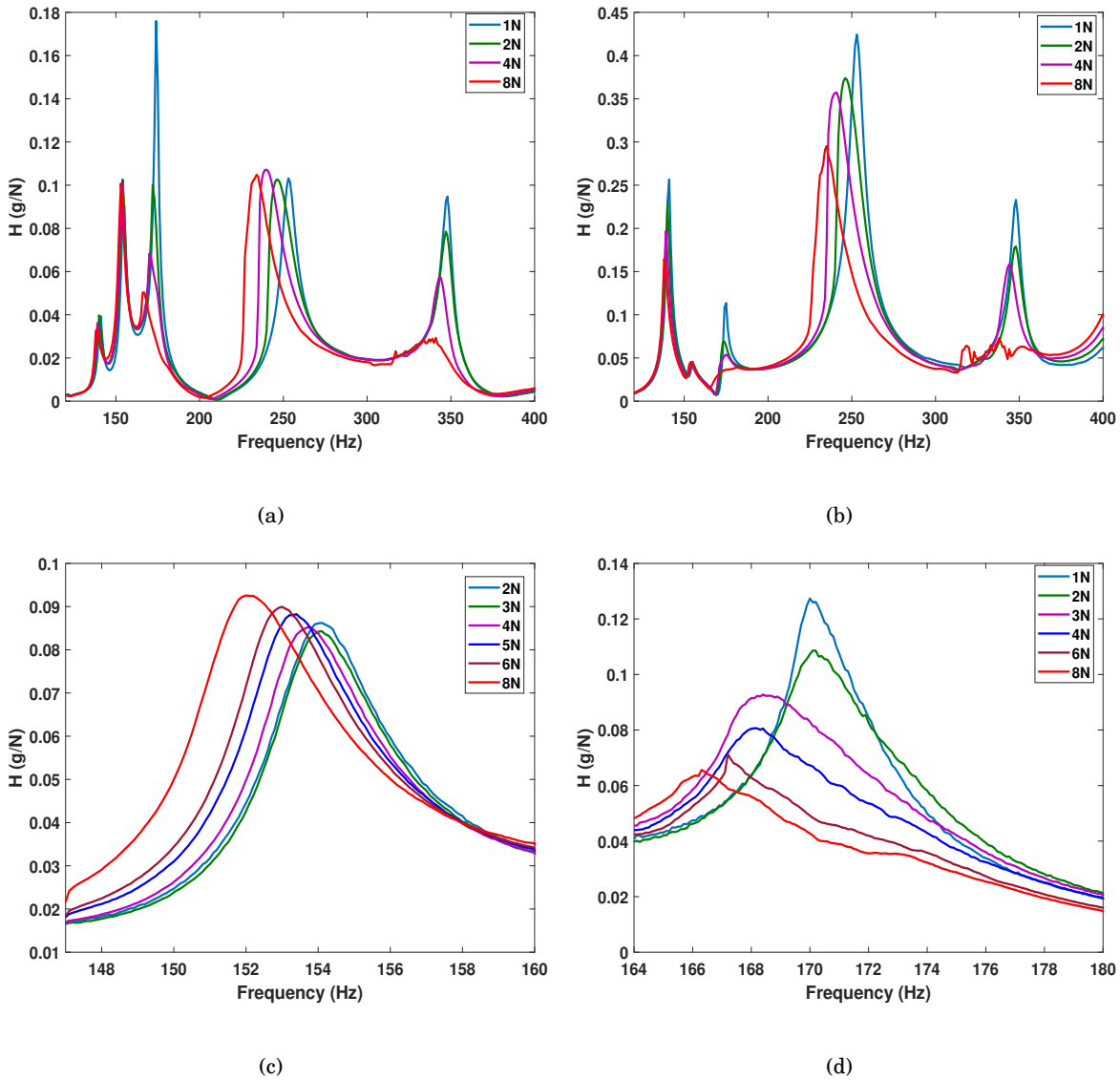

Figure 5.9: *Non-linearity detection based on FRF inspection. (a) MTS Nose, (b) (Hanger)*

behaves differently for different input forces, in contrast with established linear theory. The shifts in frequency and amplitude of the FRFs were here deemed not to be safely negligible, and we require a full identification of the non-linearities. A significant number of shifts was observed in the resonance frequency and response amplitude as shown in Figure 5.9a and 5.9b. The characteristics observed from the Sine-Sweep excitation FRFs shows that the assembly has a softening behaviour within the range of the input excitation levels.

5.4.2 Time Frequency Analysis using the short time Fourier transform

In Section 2.4.5 of Chapter of 2, time frequency analysis was mentioned as a nonlinear identification method available in the literature [6]. An important advantage of the time frequency methods is the ability to map a time-frequency-amplitude characteristic of a signal on a single plot. The mapping of these three parameters (time-frequency-amplitude) on a single plot can be used to study the general time-varying characteristics of a vibration signal. In this section, the *Short-Time Fourier-Transform* (STFT) is used to analyse and assess the the nonlinear characteristics and harmonics presented in the measured sine-sweep data obtained from the experimental campaign of the MTS. The principle of the STFT is derived from the discrete *fast Fourier transform* (FFT) that is used to estimate the frequency spectrum of the analysed signal. The Fourier transform (FT) used to map a time-domain signal to frequency domain is defined in [236] as:

$$X(\omega) = \int_{-\infty}^{\infty} x(t) e^{-j\omega t} dt \tag{5.1}$$

while the FT has been extensively adopted in structural dynamics, a specific limitation of the FT is the inability to capture non-stationary effects which are often observed in data acquired from nonlinear systems. This led to the improvement of the classical FT to develop a STFT for signal processing as described in [236]. To compute the STFT, the signal under consideration is first multiplied by a window $\omega(t-\tau)$ which is a short window of the original signal followed by a calculation of the FT of the signal based on the selected window $\omega(t-\tau)$ along the time axis. This yields a time-dependent representation of the form:

$$X(\omega, \tau) = \int_{-\infty}^{\infty} x(t) \omega(t-\tau) e^{-j\omega t} dt \tag{5.2}$$

Even-though the STFT has the disadvantage of not being able to adjust the length of the selected window, the STFT is still well used in modal analysis [237], structural dynamics [238] and in nonlinear identification [239].

Here, the displacement of the time-domain data used in generating the FRFs plotted in Figures 5.9a and 5.9b were used to compute the STFT spectrogram for three different force levels and different sensor location of the MTS. The STFT spectrogram for the measured sine-sweep data at four different location were also selected. In this chapter, the fixed time and frequency

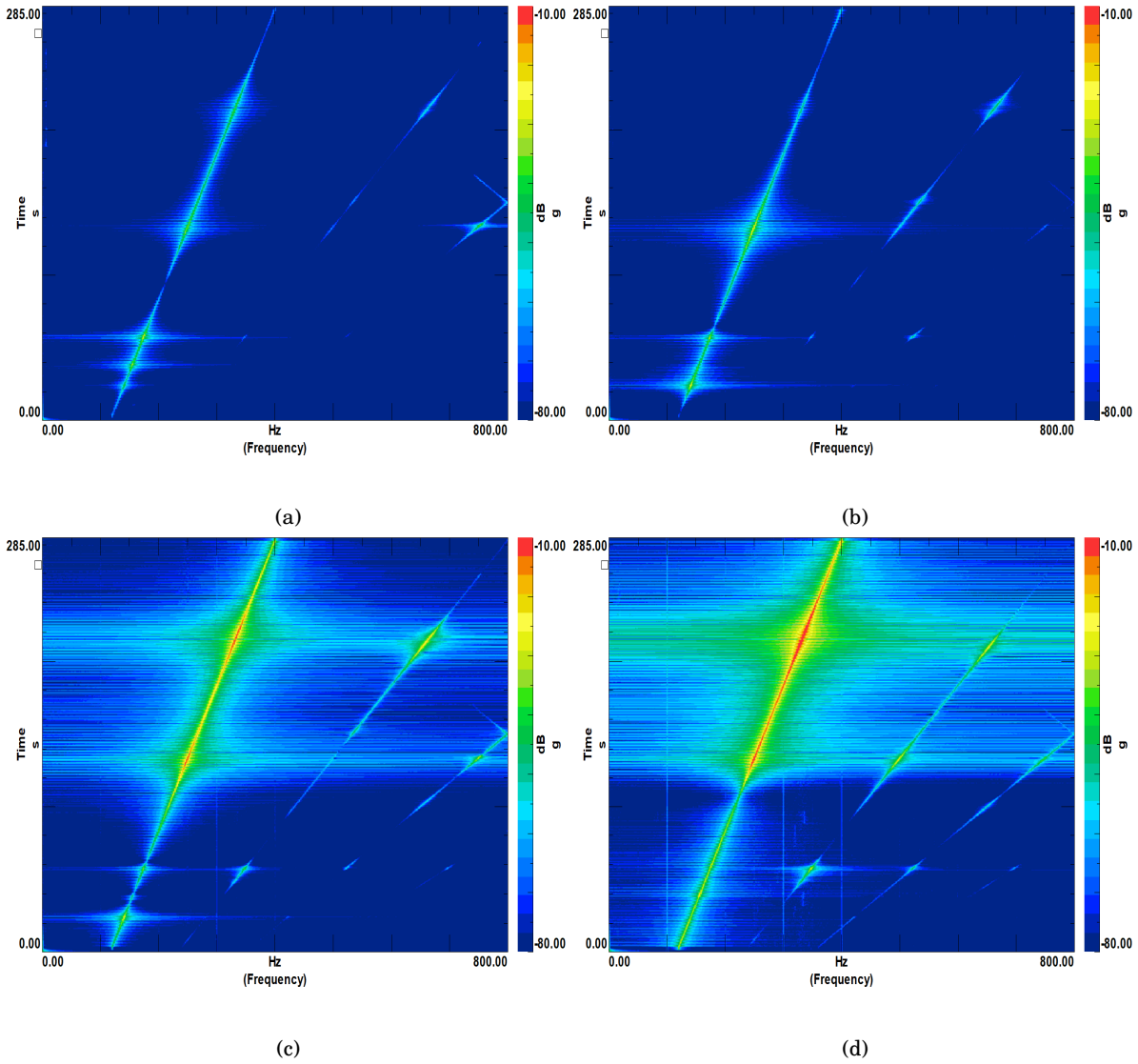

Figure 5.10: *Estimated spectrogram maps obtained for sweep frequency (120-400 Hz) at 1N. (a) and (b) spectrogram of 2 sensors located at the front and rear tube of the MTS. (c) and (d)spectrogram of 2 sensors located at connections between the tube and the launch rail.*

resolution limitation of the STFT was used as an advantages to locate and detect areas of the structure where the nonlinearity is more dominate based on computed STFT spectrogram. In Figure 5.10 (a-d) the STFT spectrogram at 1N is displayed respectively,where the spectrogram at Figure 5.10 (a and b) are the results obtained for the sensor located on the front and rear of the tube of the MTS. The spectrogram illustrated in Figure 5.10 (c and d) are the results obtained for the two sensors located on the connections between the tube and the launch rail. In Figure 5.10 (a and b), the spectrogram response mainly exhibits the fundamental harmonic

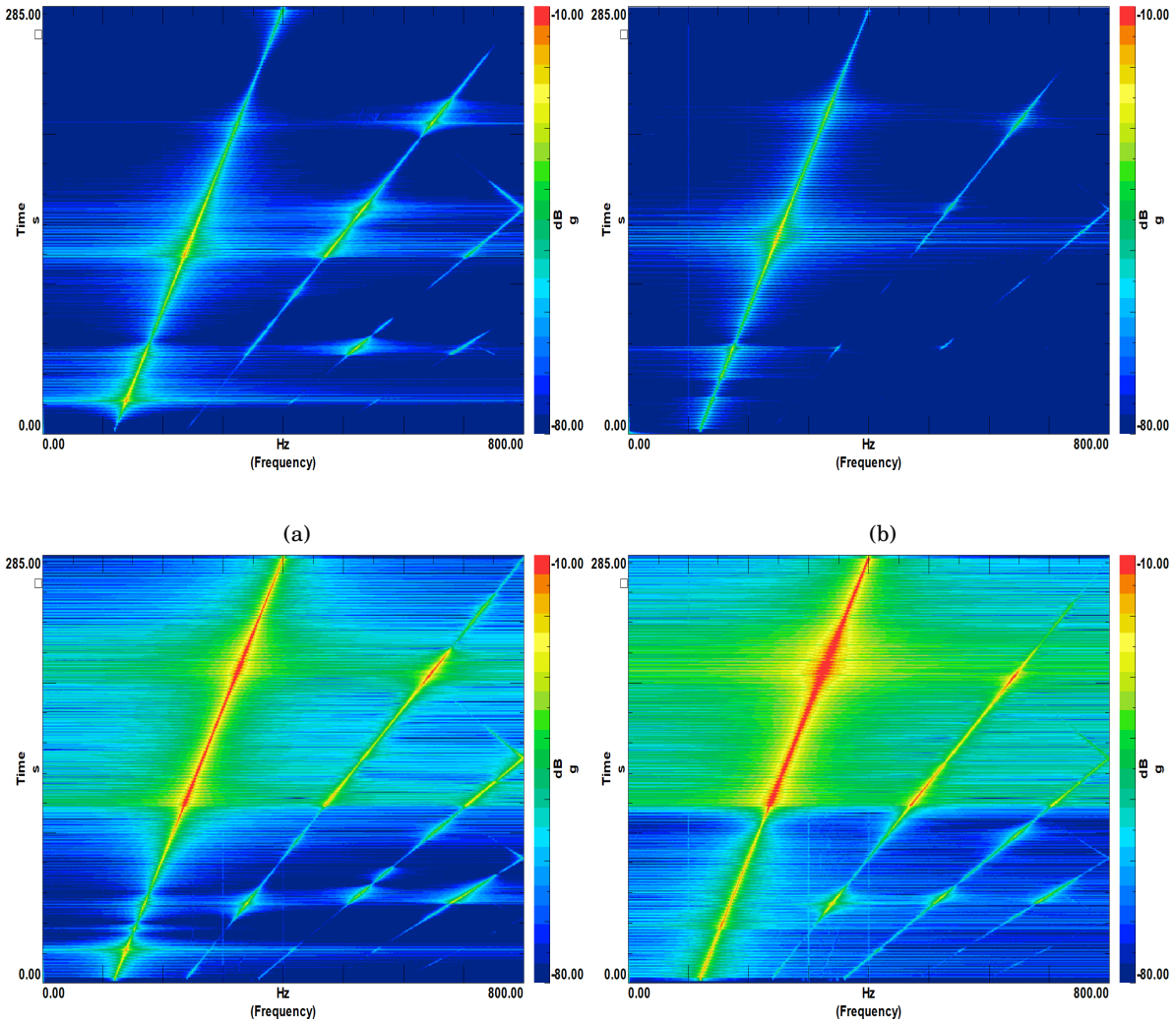

Figure 5.11: *Estimated spectrogram map obtained for sweep frequency (120-400 Hz) at 3N.(a) and (b) spectrogram of 2 sensors located at the front and rear tube of the MTS. (c) and (d)spectrogram of 2 sensors located at connections between the tube and the launch rail.*

component for the excited sweep frequency range. In addition, the level of the amplitude or energy observed at these sensor locations fall below -70dB, compared to 5.10 (c and d), where traces of other harmonics are beginning to appear at higher frequencies and higher amplitude levels are observed in the spectrogram. For increased excitation level at 3N, the spectrogram results for the same sensor locations are illustrated in Figure 5.11 (a-d), where Figure 5.11 (a and b) which represent the sensors on the tube have similar fundamental harmonic characteristics as that of the 1N excitation case. However, the spectrogram for the sensor location of the connections

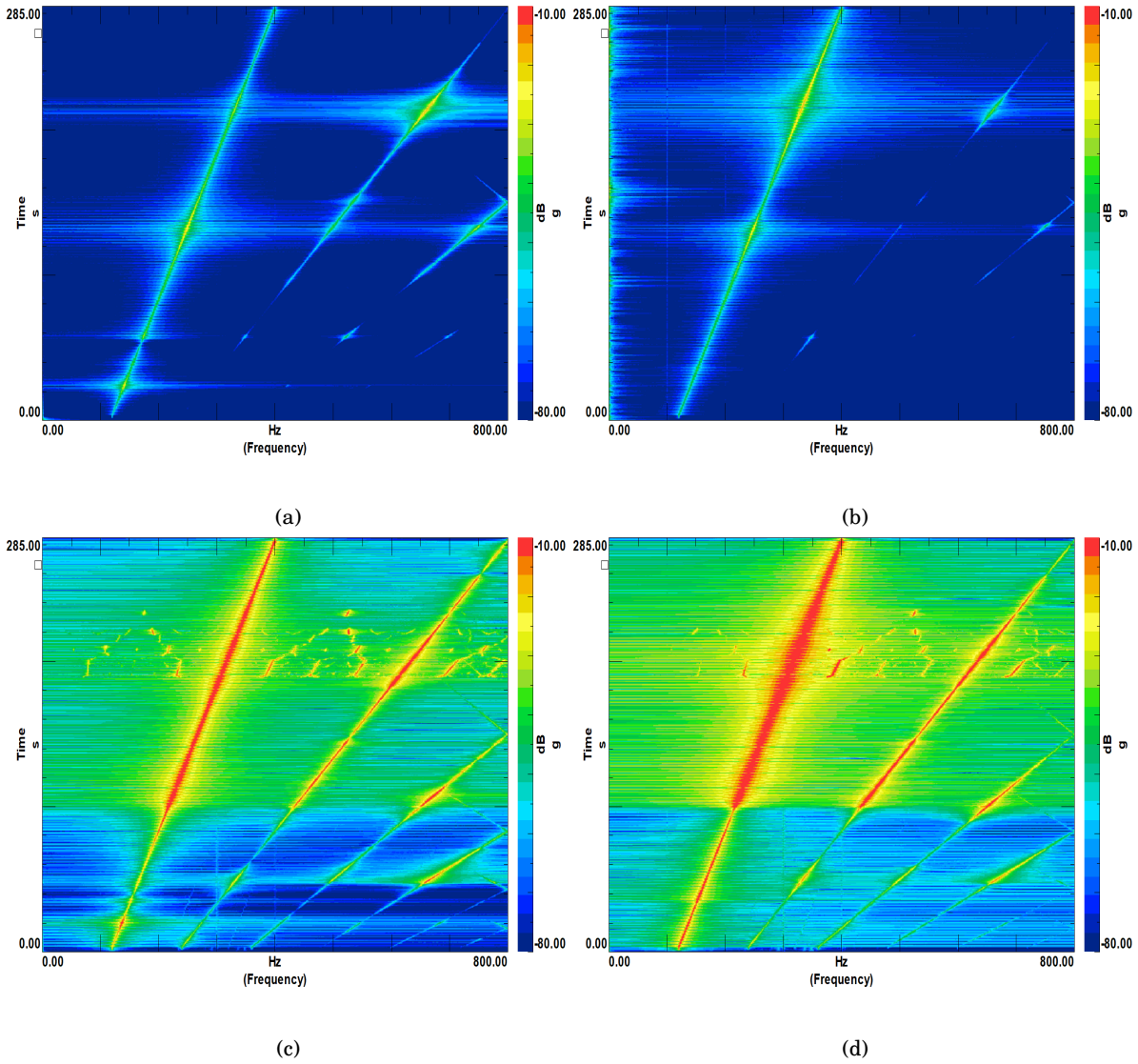

Figure 5.12: *Estimated spectrogram map obtained for sweep frequency (120-400 Hz) at 5N. (a) and (b) spectrogram of 2 sensors located at the front and rear tube of the MTS. (c) and (d)spectrogram of 2 sensors located at connections between the tube and the launch rail.*

between the tube and the launch rail (Figure 5.11 (c and d)) show evidence of nonlinearity through the appearance of strong harmonic components between 500 and 600 Hz with higher intensity amplitudes frequency lines.

This activation of the nonlinearity can be attributed to the opening of the connection between the launch rail and the tube of the MTS. The strengths of these harmonic components keep growing with the excitation level as presented in the STFT spectrogram in Figure 5.12 (a-d) for 5N excitation. At the highest excitation level (5N), the fundamental harmonic for the excited

frequency range still remain dominate for the sensor locations on the tube (Figure 5.12 (a and b)), indicating the absence of nonlinearities in those region of the structure. While the appearance of harmonic components on the spectra is stronger for the sensor location of the connections between the tube and the launch rail (Figure 5.12 (c and d)), indicating the presence of nonlinearities within that particular location of the structure. Based on the results obtained from this STFT analysis, it is evident that measured data obtained from these accelerometers locations (i.e connection between the tube and lunch rail) should be used for the grey-box nonlinear identification section.

5.5 Non-linear Identification Based on Grey-box PNLSS

In this section, the formulated grey-box PNLSS model identification method introduced and demonstrated on a simple SDOF Duffing oscillator system in Chapter 4 is applied as an identification tool to investigate the nonlinearities observed within the joints and bolted connection of the Missile Test Structure. Similar to the black-box PNLSS identification case study of the aero-engine in Section 3.5 of Chapter 3, the first step involved in this grey-box identification is to obtain a Best Linear Approximation (BLA) of the MTS. The next step is the derivation of a linear and nonlinear initialised model, required for the following step which is the final estimation of the nonlinear model which consist of the nonlinear parameters and coefficients. The nonlinear identification is conducted on measured data presented in Figure 5.8b which is obtained from a narrow band sine-sweep between 210Hz -280Hz, identification procedure and discussion of results are detailed in the following sections.

5.5.1 Best Linear Approximation of the Aerospace Test Structure

Using the insight gained from the STFT analysis, the relative acceleration between the two sensors located at the connection between the tube and launch rail was calculated and used for the nonlinear identification. To estimate the BLA of the MTS, measured sine-sweep input and the calculated relative acceleration at 3 different excitation levels were introduced to the Local Polynomial Method (LPM) [199] algorithm used in Section 3.5. Figure 5.13 shows the corresponding estimated FRFs and total distortions for the non-parametric BLA for the main frequency bandwidth of interest (210-280Hz), the FRFs and total distortion (= noise + non-linear) levels are based on excitation levels ranging from 1N to 5N. In Figure 5.13a, a shift in resonance peak and reduction in amplitude is observed across the estimated BLA FRFs which indicates a softening behaviour. The total distortions also increases as the excitation level changes from 1N to 5N, this result further confirms the presence of non-linearity in the measured data and thus require inclusion of non-linear terms in the grey-box state space modelling.

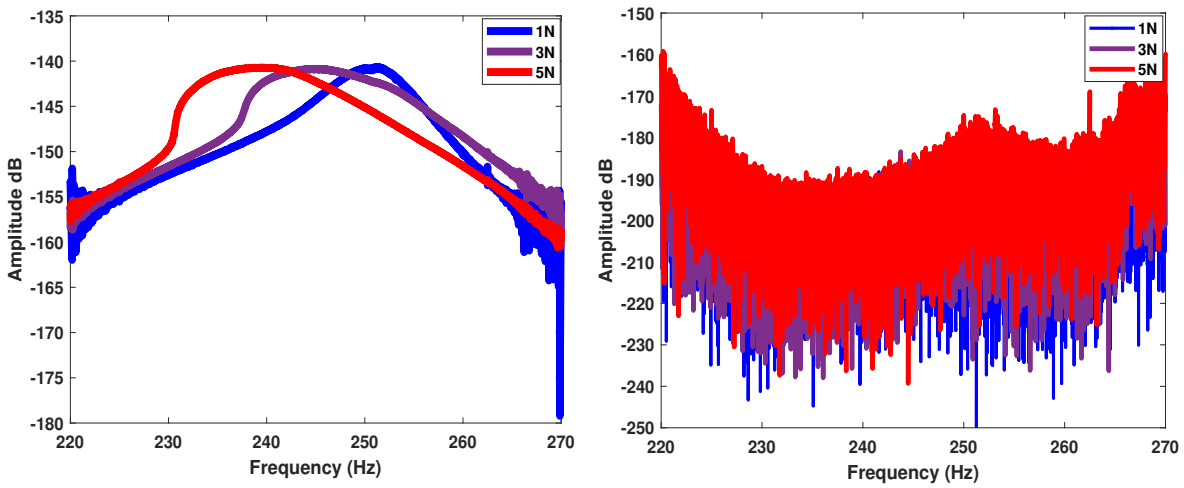

(a) (b)

Figure 5.13: *Estimated non-parametric BLA FRFs and total distortions for (mode 4). (a) amplitude of the discrete time fourier transform of the BLA FRF, (b) amplitude of the discrete time fourier transform of the nonlinear distortions*

5.5.2 Linear and Nonlinear Initialised Model

Before developing a nonlinear grey-box PNLSS model of the MTS, an underlying linear grey-box state space model of the system under consideration is required, in this chapter, the underlying linear grey-box state space model for the MTS is identified on the calculated relative displacement based on measured acceleration data at 5N. The higher level excitation data was used for deriving the underlying linear model based on the fact that the estimated model will be used for the initialisation of the nonlinear model. The Output Error function [227] implemented in Chapter 4 was used to model the prediction error between the measured data and the modelled output. The results of the identified linear grey-box model are illustrated in Figure 5.14, where the displacement from the measured data in red is compared with the estimated linear grey-box model in blue for both time domain and spectrum. It is evident from the both Figures 5.14 (a and b) that the identified underlying linear model is unable to model the nonlinear jump phenomena observed at the resonance region of the measured data. The results show high error level across the whole time domain data with an output RMS value of 90.6%.

Based on the feedback model structure described in Figure 4.3 and the assumption that the nonlinearities in a system can be seen as nonlinear feedback forces to the underlying linear

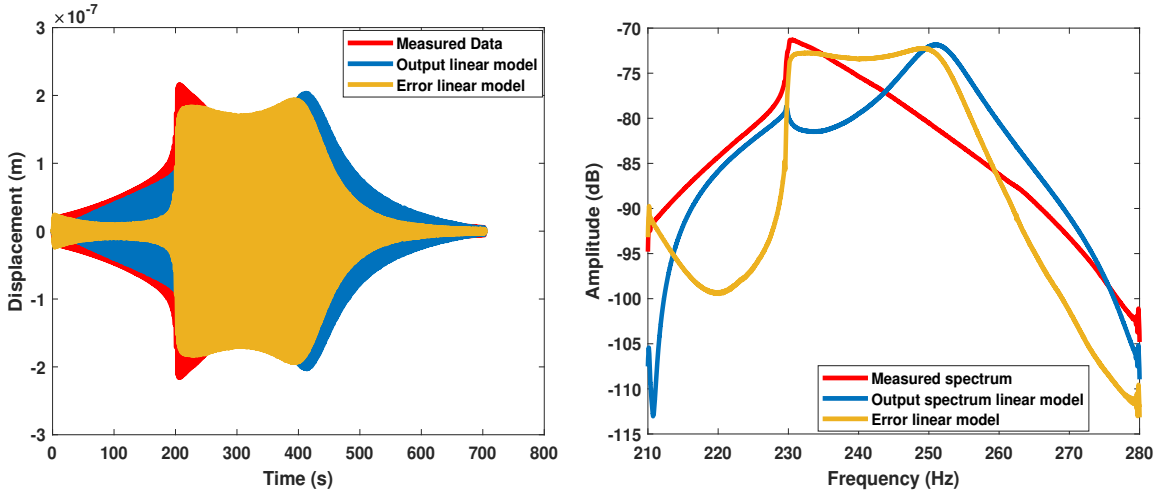

(a) (b)

Figure 5.14: *Estimated Linear grey-box model compared with measured data and error (mode 4). (a) time domain data response (b) corresponding displacement amplitude spectrum of the discrete time fourier transform*

model of the structure, an initialised nonlinear model of the MTS could be estimated. This was achieved by introducing polynomial degrees to the identified underlying linear model and the measured input force at 5N. The introduced polynomials are computed as a function based on relative displacement and velocity calculated from the measured accelerations. Finally, initial parameters and coefficients are estimated by solving a linear least squares problem.

Results obtained from the estimated initialised nonlinear model are illustrated in Figure 5.16, where a comparison of the estimated initialised nonlinear model with the measured nonlinear data is displayed. The error at the resonance region of this estimated model is significantly lower compared to the error at the resonance region of the estimated underlying linear model presented in Figure 5.14. This estimated initial nonlinear model is able to capture nearly all distortion characteristics illustrated at the resonance peak which was not captured by the estimated linear model. The time domain RMS error achieved by the estimated nonlinear initialised model is 15.3% which is greatly lower than the 90.6% value obtained by the linear model.

In addition, similar to the numerical demonstration in Chapter 4 it is also possible to extract the stiffness and damping characteristics of the estimated model in order to gain physics based understanding of the estimated model. Figure 5.15 shows the stiffness and damping curve of

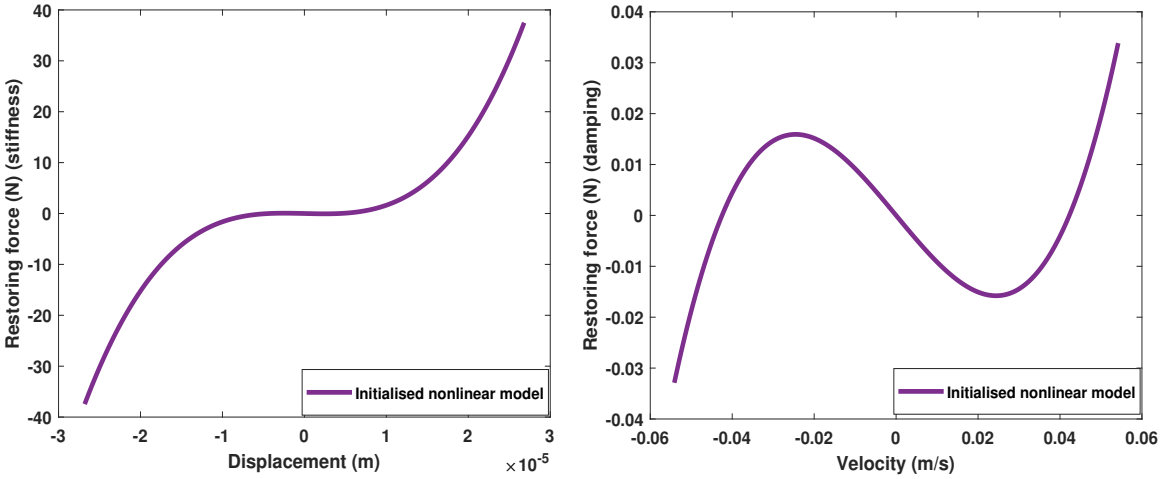

(a) (b)

Figure 5.15: *Estimated nonlinear initialised stiffness and damping curve (mode 4)*

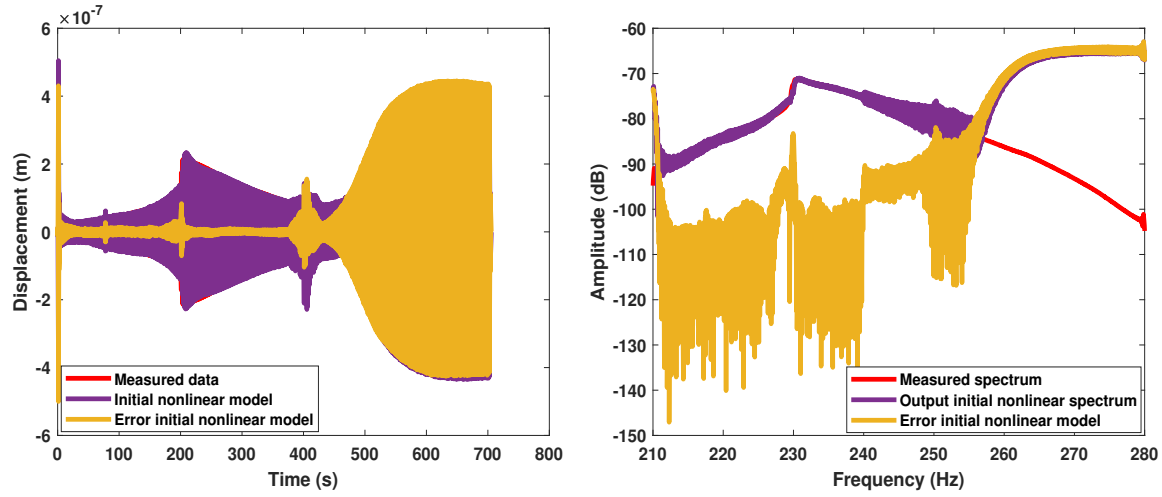

(a) (b)

Figure 5.16: *Comparison of estimated initial nonlinear model against measured data. (a) Time domain data (b) spectrum (mode 4)*

the estimated initialised nonlinear model. Unlike the numerical example in Chapter 4, where there were true parameters with stiffness and damping curves to compare with, it is not the case for this application where the algorithm is tested with real measured data and all manner of imperfections. However, both estimated stiffness and damping curve do have polynomial like characteristics or function and not any other type of function which shows good evidence that the

algorithm is able to fit the measured data well. It is worth stating that the nonlinear initialised model obtained in this section is important and will be used in the next section as initial starting parameters for the final nonlinear model estimation.

5.5.3 Estimation of a Full Nonlinear Model of the MTS

To estimate a final parametric grey-box nonlinear model for the missile test structure, a weighted least squares cost function VLS expressed in Equation 5.3 is defined through an Levenberg-Marquardt optimisation routine to evaluate the grey-box PNLSS model.

$$V_{WLS}(\theta) = \sum_{k=1}^{n_F} \epsilon^H(k,\theta) W(k) \epsilon(k,\theta) \tag{5.3}$$

Where $W(k) \in \mathbb{C}^{n_y \times n_y}$ is a user-chosen frequency domain weighting matrix. Here the parameters obtained from the initialised nonlinear model are used as starting values for the optimisation routine, the final estimation is then obtained by minimising the cost function. Due to the large size of data points being used for the optimisation, a unit weighting $W(k)$ data selection was applied to focus on the frequency bands around the resonance peak. This unit weight was chosen to speed up the optimisation process and also focus on the regions where nonlinear characteristics are observed. Final time domain and spectrum results obtained from the optimisation are presented in estimated in Figure 5.18, comparing this estimated nonlinear grey-box model with the initial estimated results in Figure 5.14, it is clear that there is a great improvement in the estimated nonlinear model compared to the initial linear model. The obtained nonlinear model features lower error level ranging generally within 40-45dB below the measured nonlinear spectrum data, similarly, compared to Figure 5.14a this time domain estimate is able to capture the nonlinear distortions observed at the resonance peak region. Although, a slight increase in error is observed towards the ends of the time data and spectrum plot, this increase in error can be associated with the weighting unit which was selected to focus more around the resonance frequency (215-245). However, the final RMS error obtained based on the nonlinear optimisation is 1.26%, this shows a significant error reduction compared to the initial estimated nonlinear model error of 15.3%.

The corresponding nonlinear stiffness and damping curve obtained from this estimation compared with the initial curves obtained from the nonlinear initialised model are presented in

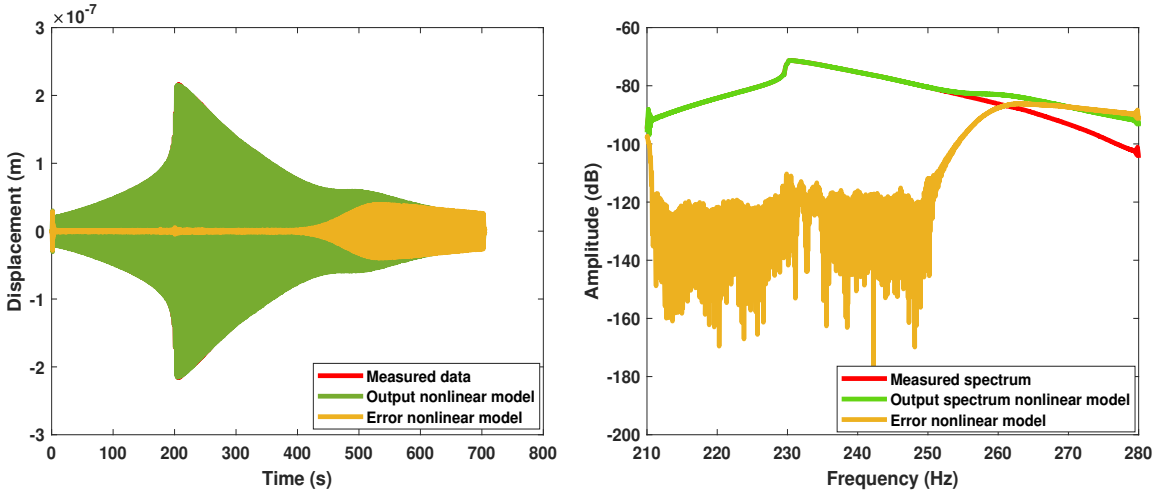

(a) (b)

Figure 5.17: *comparison of the identified nonlinear model against true nonlinear data for mode 4. (a) time domain data response (b) corresponding displacement amplitude spectrum of the discrete time fourier transform.*

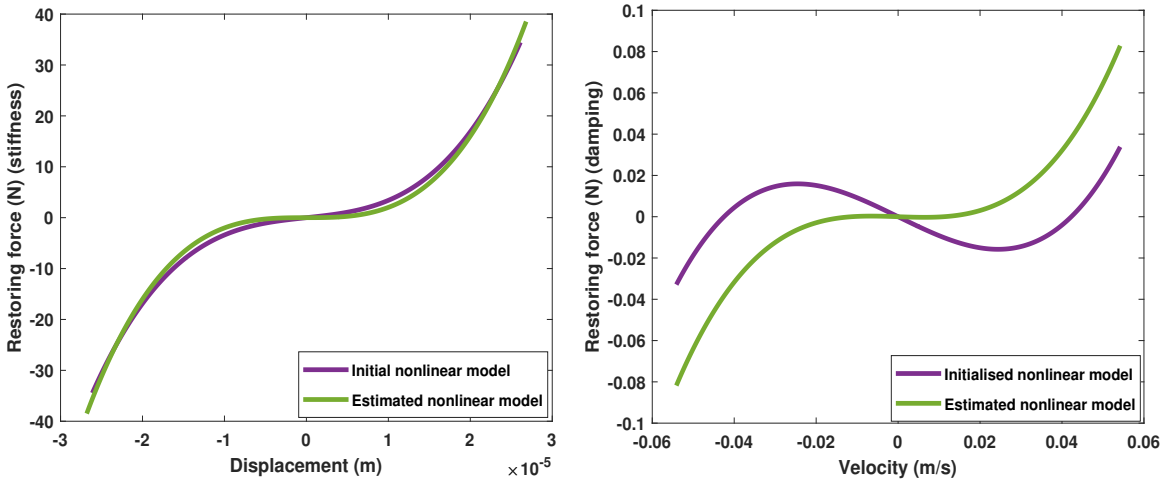

(a) (b)

Figure 5.18: *Final estimated nonlinear stiffness and damping curve (mode 4)*

Figure 5.18. While the parameters and coefficients estimated and tracked during the optimisation are recorded in Table 5.2. Compared with the numerical example of the grey-box identification demonstrated in Chapter 4, where there are true nonlinear parameters to compare the estimated results. In this case, there are no true parameters to compare with. However, judging from the

Stiffness Parameters	$x_1(N/m)$	$x_2(N/m^2)$	$x_3(N/m^3)$
Initialised nonlinear model	$1.72 \cdot 10^5$	$1.61 \cdot 10^6$	$1.48 \cdot 10^{15}$
Final nonlinear model	$2.24 \cdot 10^3$	$2.71 \cdot 10^6$	$2.08 \cdot 10^{15}$
Damping Parameters	$\dot{x}_1(Ns/m)$	$\dot{x}_2(Ns/m^2)$	$\dot{x}_3(Ns/m^3)$
Initialised nonlinear model	-0.97	0.11	$5.41 \cdot 10^2$
Final nonlinear model	-0.068	0.11	$5.41 \cdot 10^2$

Table 5.2: *Estimated nonlinear parameters of the Missile Test Structure for Mode 4*

coefficients presented in Table 5.2, the similarities and consistency in the estimated parameters and coefficients for both initialised and nonlinear model can be seen as a form of confidence in assessing the capabilities of the identification algorithm in an imperfect environment. The convergence behaviour of the initialised nonlinear and final estimated nonlinear models was also monitored by plotting the root mean squared error against the successful iterations of the Levenberg–Marquardt optimisation. Figure 5.19 shows the convergence plot obtained from the optimisation conducted on both models, this convergence plot can also be used as a form of measuring the performance of each model. In this case, from Figure 5.19, it is obvious that the nonlinear model performs better than the initialised nonlinear model with the optimisation starting with a lower NRMSE and also converges to the final error value faster. This better

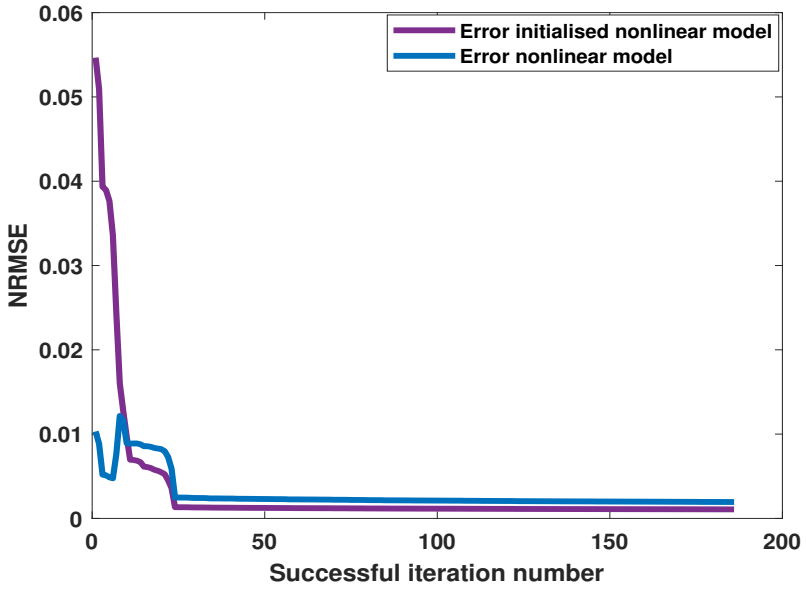

Figure 5.19: *NRMSE error over successful Levenberg-Marquardt iterations.*

performance is can be attributed to the fact the the starting parameters used for the optimisation was based on the optimised initialised nonlinear model. This validates the significance of the nonlinear initialisation step incorporated in this grey-box identification algorithm before progressing to the final nonlinear estimation through an optimisation procedure.

5.6 Conclusions

In this chapter, the capabilities of the grey-box PNLSS identification algorithm introduced in Chapter 4 is put to test by applying it to measured data obtained from test campaign conducted on a prototype missile test structure. The missile test structure had key features such as joints and multi-body sections which could be used to investigate the effect of nonlinearities in structures. To begin the application case study, a finite element model of the MTS was built to run a linear FE modal analysis, FE mode shapes obtained form the linear FE modal analysis were used to pre-test planing of the modal test. For the test, three different excitation signals were used to acquire acceleration data. First, data obtained from random excitation was used for the linear identification, dedicated narrow band sine-sweep data were then used for the nonlinear identification. The detection of nonlinearity was also achieved based on time-series and FRF inspection.

The success of the grey-box PNLSS identification of the MTS was judged based on the RMS errors between each identified nonlinear achieved on the identified grey-box PNLSS models and the measured data. Based on the RMS values of 15.3% and 1.26% obtained on the initialised and nonlinear models, it can be concluded that the PNLSS algorithm was able to successfully model the nonlinearities observed in the MTS . Corresponding coefficients estimated from both models and presented in Table 5.2 also show good comparisons. Future work is still required to advance the nonlinear identification capabilities. Another improvement that could be benefited by this application is the development of a method to calculate the confidence interval of the estimated nonlinear parameters and coefficients. In addition, the validity of this application could be strengthened by applying a different identification algorithm on the measured data and compare the estimated Using the identified nonlinear parameters to generate nonlinear

FE models and further cross validation with controlled test. could also be an area of future development.

CHAPTER 6

VALIDATION OF NONLINEAR VIBRATING STRUCTURES.

Abstract

The last three chapters have been centred on the development and applications of nonlinear identification methods in structural dynamics. However, predicting and validating the vibration response of identified non-linearities in structures remains a challenge. In addition, when non-linear effects are substantial or the need for simulating and predicting nonlinear vibration response in a virtual sense is of vital importance, current linear simulation tools generally prove to be unsatisfactory. In this chapter, an holistic approach to integrating test-based system identification and simulation for non-linear structures is presented.The benefit of the strategy presented shows the certainty and complementary role of simulation and experimental testing in achieving a validated nonlinear structural model. The proposed approach is demonstrated on a twin cantilever beam assembly structure coupled with a flexible arch shaped beam, where polynomial-type non-linearities are identified and validated.

6.1 Introduction

Non-linearities often originate from different sources in engineering structures. A large majority of these non-linearities are narrowed down to the design of the structure, the nature of the joints and material and geometric properties as briefly discussed in the literature review. Whilst great progress has been achieved in the identification of non-linearities as shown in the previous chapters and in [12, 6], adequate verification and validation of these nonlinear effects in a virtual domain still acts as a challenging task to present engineers dealing with complex nonlinear structures. In addition, the increasing use of industrial broad concept such as "digital twin" is introducing a revolution in the way engineering structures are being designed and validated, where the combination of simulations and experimental analysis are used to make important engineering decisions.

In the last two decades, the combined use of simulation models and experimental data to create a virtual prediction tool or design results has increased exponentially. For example, in linear structural dynamics, the correlation of Finite Element Methods (FEM) and Experimental Modal Analysis (EMA) have continuously been used as a validation technique for linear structures. However, today's engineering structures are being designed to meet stricter regulations requiring the use of light weight materials and multiple components which introduces a range of advanced mechanical behaviours some of which can be narrowed to have nonlinear effects. Hence, the accurate representation of experimental identified nonlinear features in a virtual duplicate such as a Finite Element model of the structure would be of extreme benefit as a predictive tool to help make engineering decisions. One of the ways of addressing this task is to consider an effective integration of experimental nonlinear identification and FE modelling of nonlinear structures.

Despite the advances in nonlinear system identification and developments in the numerical computation of nonlinear systems, there is little or no activity on the integration of experimental nonlinear identification and the validation of FE models of structures with identified non-linearities using measured and numerical data. The primary objective of this chapter is to explore the potential and ability of obtaining a validated nonlinear FE finite model of a structure by implementing developed experimental techniques and numerical tools available in the literature.

This chapter is preceded by an opinion paper in [36] where a new approach to modal testing was proposed for nonlinear structures. subsequently, a practical application of the proposed procedure was demonstrated on a wing-pylon structure in [169] with encouraging results. The promising results obtained from the first practical application of the procedure has led to further research on issues that were not addressed in the first case study. In this chapter, the engineering challenges encountered when two validated monolithic linear structures are coupled together to form a single assembled structure is addressed. This chapter demonstrates the procedures and technical contents required to uncover some new nonlinear phenomena exhibited by the assembled structure with specific attention on validating the FE model of the nonlinear structure.

The chapter is organised as follows: section 6.2 describes a brief overview of the proposed approach with the different phases required to obtain a validated FE model of a structure containing some nonlinear elements. In section 6.3, the test and simulation integration modular framework is applied on the cantilever beam assembly, where the first phase of the framework is conducted with the main focus on the derivation of an Underlying Linear Model (ULM) for the twin cantilever beams uncoupled and coupled with the arch shaped beam respectively using conventional modal analysis techniques. The nonlinear identification is also described in this section where the detection, characterisation and quantification of non-linearity is carried out using measured experimental data. In addition, the final phase of the procedure is addressed. The final phase of the frame work goes beyond nonlinear identification, it introduces the central role and importance of validating the finite element model of structure with the identified non-linearities using specifically controlled measured experimental data. Finally, discussions and conclusion of the holistic approach are drawn in section 6.4 with suggestions for future research on this aspect of nonlinear structural dynamics.

Part of this chapter is based on the following journal and conference papers:

S.B.Cooper, D.DiMaio and D.J.Ewins (2018) Integration of system identification and finite element of nonlinear vibrating structures. *Journal of Mechanical Systems and Signal Processing*,102,401-430.

S.B.Cooper,and D.DiMaio (2016) Experimental and Numerical Modelling of Nonlinear Complex Assembled Structures. *Proceedings of the 27th ISMA, An International Conference on Noise and Vibration 2016* (pp. 2597-2612).

S.B.Cooper, A.DelliCarri and D.DiMaio (2016) Model upgrading T0 augment linear model capabilities into nonlinear regions. *In G. Kerschen (Ed.), Nonlinear Dynamics Volume 1: Proceedings of the 34th IMAC, A Conference and Exposition on Structural Dynamics 2016* (pp. 203-217).

6.2 Integration of FE and test-based identification for nonlinear structures

Validation of linear FE models using modal test data is now widely practised in many areas of structural dynamics and design with the availability of several validation techniques such as the Modal Assurance Criterion (MAC), Coordinate Modal Assurance Criterion (COMAC), Frequency Domain Assurance Criterion (FDAC) and Frequency Response Assurance Criterion (FRAC) [1, 35]. These techniques are often used to validate a linear finite element model either through experimentally-measured Frequency Response Functions (FRF) or mode shapes or both. Based on the successful application of the combined use of EMA and FEM in linear structural dynamics, it is evident that the development of a similar validation procedure for nonlinear structures where the combined use of experimental and finite element techniques are used to obtain models proficient enough to describe the observed nonlinear characteristics. Hence in [36], a systematic approach was introduced to extend current modal testing and analysis techniques to a situation where nonlinear effects are captured and modelled.

The objective of the approach was to extend existing linear techniques with the addition of just as much nonlinear analysis as required to construct a model which is capable of predicting the nonlinear behaviour of such structure with a given accuracy. The approach is designed to integrate current modal analysis techniques with nonlinear identification methods and available nonlinear numerical algorithms in order to obtain a valid nonlinear FE model of the structure under consideration. It does not rely on any specific method but uses a collection of toolbox methods to obtain the final validated structural model. A schematic diagram extracted from [169] is presented in Figure 6.1 showing a step by step guide of the proposed approach. In principle, the integration framework is developed to be very flexible and generic. Meaning that the user can select any current state of the art developed tool box for the nonlinear identification and an appropriate numerical method for the computation of the periodic solution for the FE Model of the given structure.

Since the fundamental principle of integration was developed from a modal testing approach, it is important to stress that the whole procedure will only produce reliable results if a validated linear model of the test structure under consideration is available. As such, the integration comprises of three different phases, Phase I is referred to as linear model validation, Phase II is the nonlinear identification phase while Phase III is the nonlinear model validation phase. Phase I generally covers current industrial practice in linear structural dynamics which includes linear modal testing, model updating and model validation. PHASE II, described in Section 6.3, involves the nonlinear identification section of the overall approach.

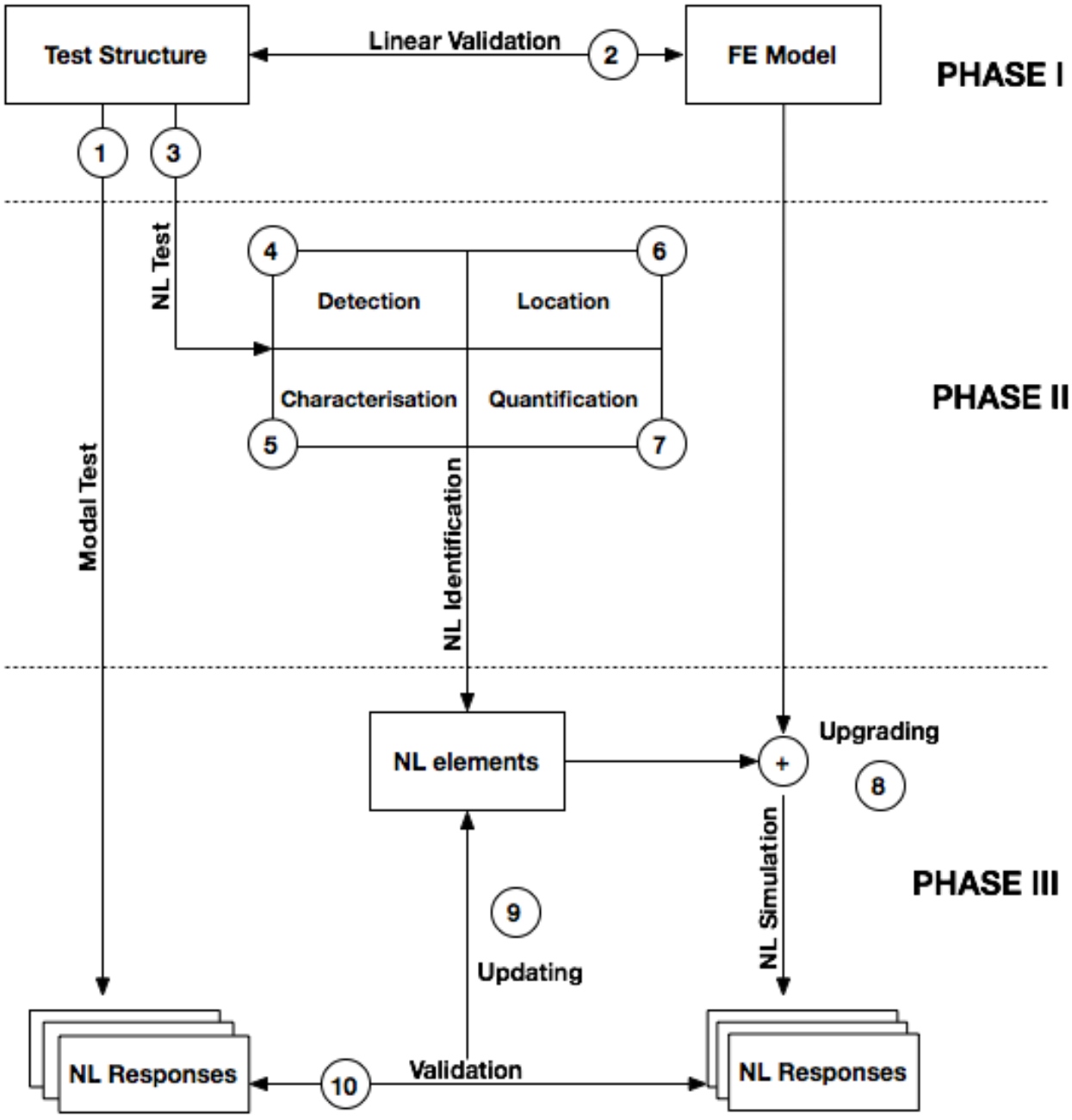

Figure 6.1: *Data flow scheme of FE and test-based identification integration procedure showing the steps in each phase Courtesy of Arnaldo DelliCarri, University of Bristol, United Kingdom.*

6.3 Demonstration on Cantilever Beam Assembly

6.3.1 Description of the Test Structure

The case study presented in this chapter was performed using a test rig intended to understand the effect of connecting two validated monolithic linear beam structures together to form a single assembled structure. In Figure 6.2a, the first sub assembled structure is made up of two cantilever steel beams assembled on the same rectangular steel base and the steel base is bolted on a seismic block to isolate and reduce any energy transfer that may occur through the base. A linearity test and validation was conducted on the linear model of the assembly to ensure that the structure behaves in such a manner to be called a linear structure. In Figure 6.2b, the two cantilever beams are connected together at their tips with a flexible curved beam. The ends of the curved beam are bolted to the tips of the two cantilever beams using M4 bolts as shown in Figure 6.2b. Table 6.1 presents the dimensions of each component in the assembly. The configuration of test rig in Figure 6.2 was chosen because, while fairly simple, it represents a typical assembled engineering structure that can easily generate some level of nonlinear behaviour when high levels of vibration excitation are introduced. The assembly was instrumented with 10 accelerometers and a force transducer; each accelerometer is given a node number as shown in Figure 6.2b.

Component	**Dimension (m)**
Cantilever Beam	0.3*0.025*0.012
Rectangular Steel Base	0.718*0.17*0.025
Curved Beam	0.18*0.012*0.0005

Table 6.1: Dimensions of the cantilever beam assembly

6.3.2 Linear model validation (phase I)

Phase I starts with a conventional modal test and procedures needed for a linear model validation. At this stage, only the fundamental linear properties of the structure are of interest. A first linear model validation is conducted on the first sub-assembly in Figure 6.2b where the two vertical steel beams are not connected. In addition, the sub-assembly was excited at different levels of excitation to check for linearity. A second linear validation was also conducted on the full

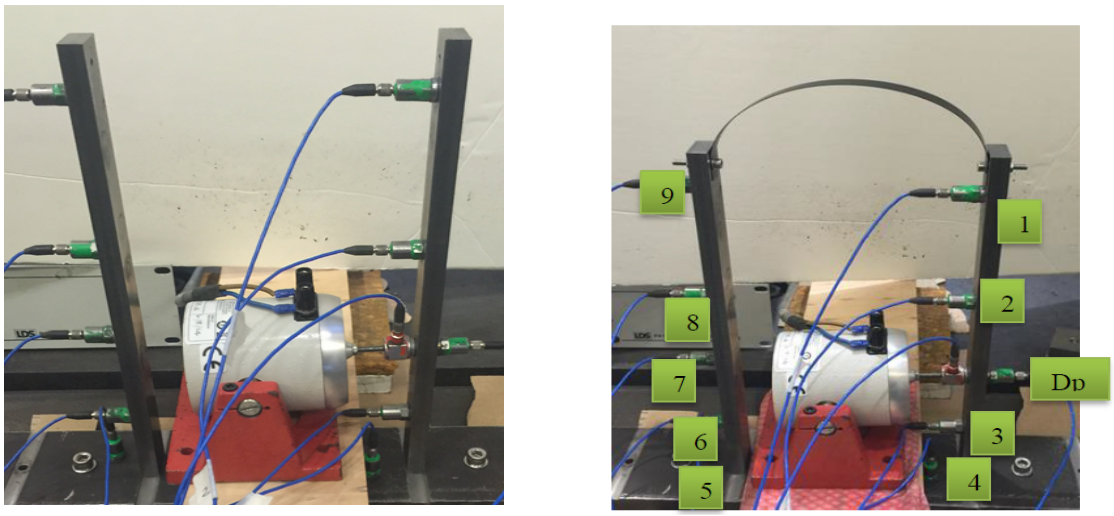

(a) linear assembly

(b) nonlinear assembly

Figure 6.2: *photograph of the cantilever beam structure.* .

assembled structure in Figure 6.2b. The main advantage of conducting the test is to extract the Underlying Linear Model (ULM) that is intended to represent the test structure under conditions where the non-linear features in the structure are effectively not activated. Separation of linear and non-linear effects is very challenging as both high and low level excitation can lead to either stiffness, damping or both types of non-linearity. In this phase, special attention is given to the level of input excitation applied to the structure. If signs of non-linear behaviour become apparent in this test phase, then special care is taken in the type of data used in validating the ULM.

6.3.2.1 Linear Modelling

The first measurements obtained from the experimental test conducted on the sub-assembly structure in Figure 6.2a comprised several low-level random data which were acquired based on burst random excitation. The choice of broadband excitation was made based on its conventional use in modal testing. The low-level excitation test was performed at 0.5N using the Spectral Test module in LMS Test Lab and the structure was excited close to the base of one of the beams as shown in Figure 6.2. The structure was excited using burst random excitation ranging between 20-1000Hz. The FRFs and associated coherence functions obtained from the test were exploited to identify the linear modal properties of the test structure. The linear natural frequencies and

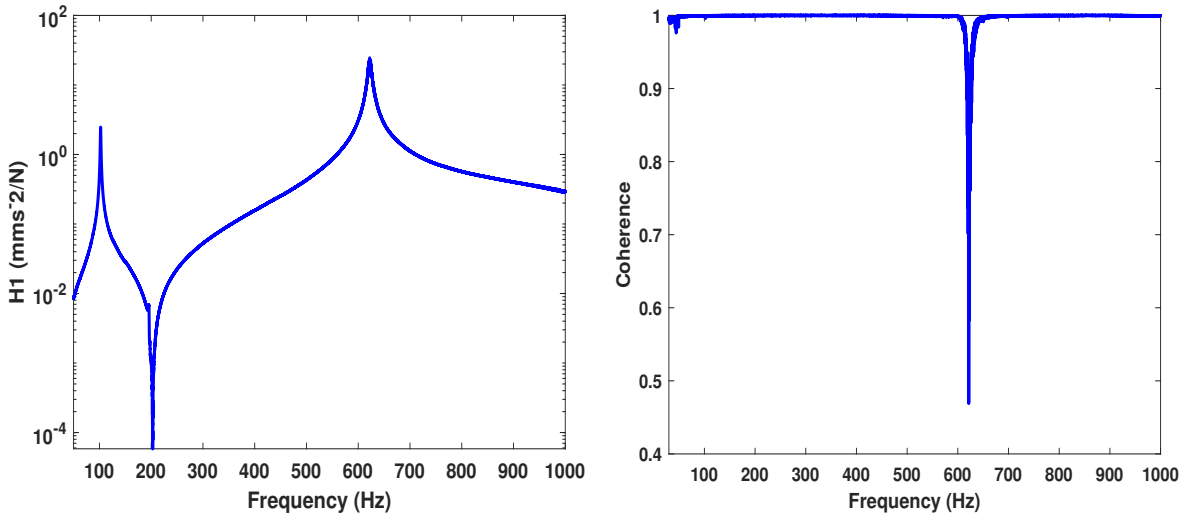

(a) (b)

Figure 6.3: *Linear acceleration response function and coherence measured at low-level excitation for the linear assembly. a (drive-point acceleration response) and b (Coherence)*

Mode	Frequency (Hz)	Damping ratio (%)
1	102.15	0.24
2	627.24	0.22

Table 6.2: Estimated linear resonance frequencies and damping ratios based on low-level excitation

modal damping ratios were estimated using the Polymax identification algorithm presented in [2].

The corresponding natural frequencies and damping ratios identified using the low-level random excitation are presented in Table 6.2. Figure 6.3 shows a selected FRF and coherence plot obtained from a low- level test: the resonance peaks of the FRF indicate that the structure is lightly damped across the selected bandwidths. The ordinary coherence function corresponding to each FRF or measured point are all close to unity except right at the second resonance of the whole excited frequency range. To check the behaviour of the sub-assembly, the structure was excited at several excitation levels using the same burst random excitation used in the previous test. The test was conducted to observe any frequency or damping shifts from the response of the structure. A selection of the FRFs and coherence functions obtained from the different levels

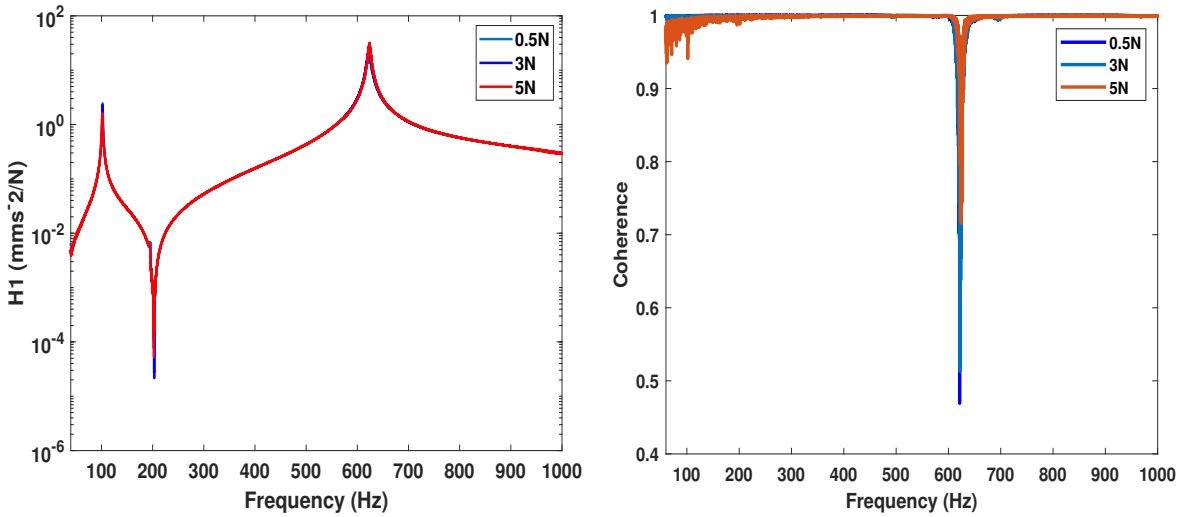

(a) (b)

Figure 6.4: *Comparison of acceleration response functions at three excitation levels for the linear assembly in figure 2a. (a) Magnitude and (b) coherence: (blue) measured form 0.5N, (d-blue) measured form 3N, and (red) measured from 5N excitation.*

of excitation test are presented in Figure 6.4. The results obtained from this test shows hardly any shift in the natural frequency or in the damping or distortion in the response curve and it is therefore possible to conclude that the sub-assembly is still behaving linearly within the excited range.

6.3.2.2 Linear Finite Element Model of the Sub-assembly

The test structure shown in Figure 6.2a was modelled mathematically using beam finite elements. In order to keep the model simple yet capable of describing the general dynamic behaviour, the whole structure was modelled using 2D beam elements. Since the structure was made out of steel beams, standard material properties for steel were selected for the initial FE modelling. The FE model was generated using the commercial ABAQUS FE package and a linear modal analysis was conducted to extract the FE mode shapes and natural frequencies over a bandwidth of 1000 [Hz]. Figure 6.5 shows the first four bending modes of the beam and the corresponding frequencies obtained from the linear FE modal analysis. It worth noting that due to the identical design of the cantilever beams, each beam has its individual first and second bending modes but

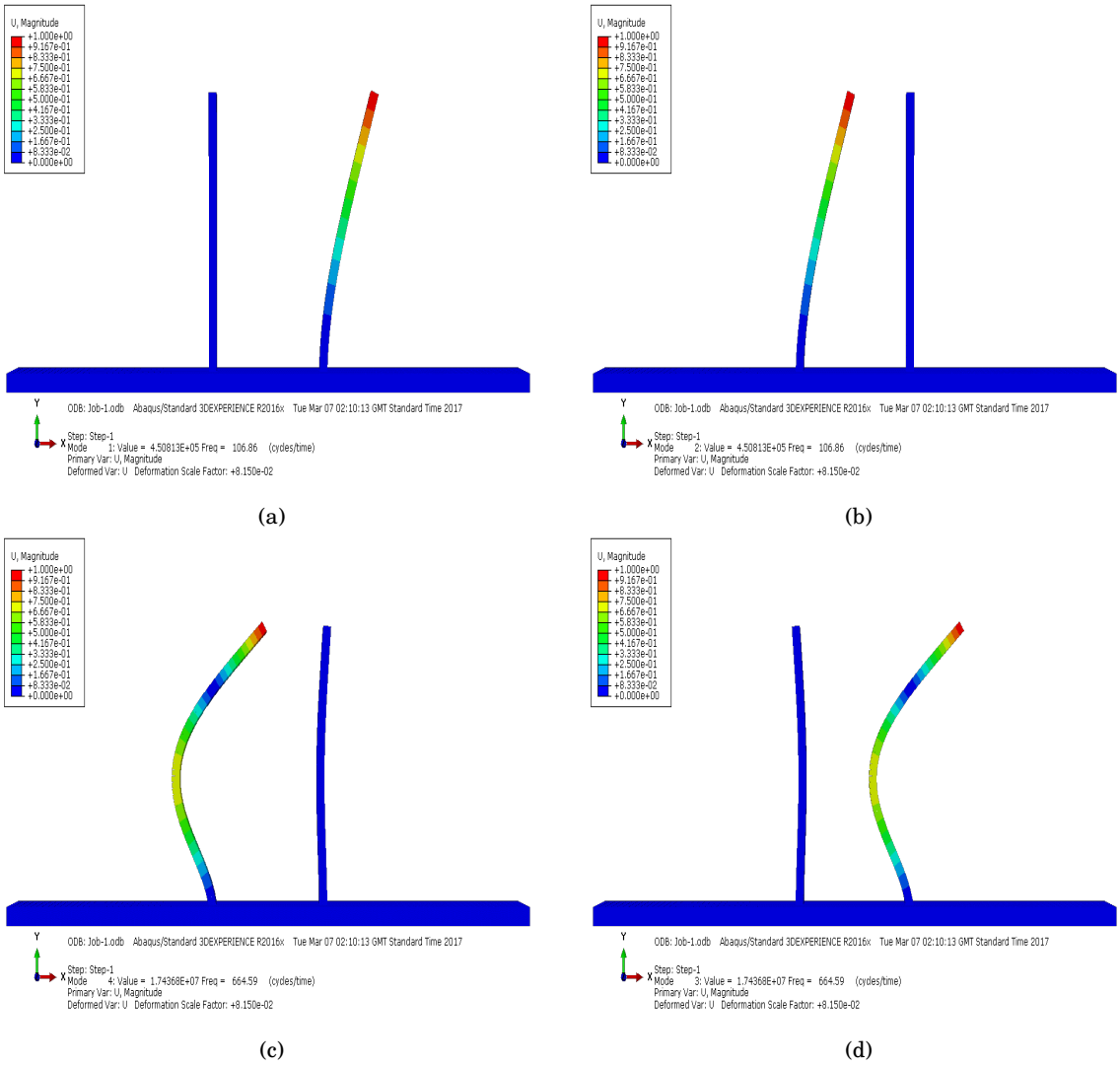

Figure 6.5: *Finite Element mode shapes of the cantilever beam for the linear assembly in Figure 6.2a. (a) Mode 1, (b) Mode 2, (c) Mode 3 and (d) Mode 4.*

with exactly the same natural frequencies. Hence a total of four mode shapes were obtained from the linear FE modal analysis.

6.3.2.3 Linear Model Updating

The initial FE model generated from ABAQUS was then correlated and updated using the experimental results obtained from the low-level random excitation modal test. The main objective in this step is to correct the FE natural frequencies and mode shapes over the frequency bandwidth of interest. The FE model updating was executed using FEM-tools software by Dynamic Design

Mode	FE Freq Before	Test Freq Hz	Diff (%) Before	MAC (%) Before	Updated FE Freq	Diff (%) After	MAC (%) After
1	105.21	102.11	3.04	82.7	102.33	0.21	98.4
2	105.21	102.11	3.04	82.7	102.33	0.21	98.4
3	641.29	627.24	2.24	79.1	627.81	0.09	96.5
4	641.29	627.24	2.24	79.1	627.81	0.09	96.5

Table 6.3: Updated FE Model Natural Frequencies and MAC Values for the linear-assembly in Figure 6.2a

Solutions (DDS). FEM-tools uses a Bayesian Parameter Estimation (BPE) technique to minimise the error for a given set of defined parameters, and the error minimisation is performed using an iterative process that modifies the distance between the FE and experimental results [240].

The updated natural frequencies and MAC values for the first 4 modes are presented in Table 6.3. In addition to the MAC correlation procedure, the system mass and stiffness matrices were also used to compute the FE frequency response for the first bending mode of the cantilever beam. Proportional damping was used for the simulation of the FE response and Figure 6.6 shows comparisons between the measured response at two levels of excitation (dots) and predicted responses using the linear FE model. Based on the results obtained from the MAC correlation, and the response curves in Figure 6.6, it is possible to conclude that a relatively successful linear FE model was obtained. The validated FE model can also be classified as an accurate representation of the test structure with an acceptable accuracy based on the good prediction of the FE response at low and high excitation levels

6.3.2.4 Underlying Linear Model

Since there are two different configurations of the test structure being used for this case study as shown in Figure 6.2 and the first sub-assembly in Figure 6.2 has been validated to an acceptable accuracy. This section is aimed at obtaining an Underlying Linear Model (ULM) of the proposed non-linear assembly in Figure 6.2b. The ULM is defined here as a model of the test structure where the non-linearities are negligible, meaning that the test structure is excited at nearly zero excitation so that any amplitude-dependent non-linear features within the structure are not

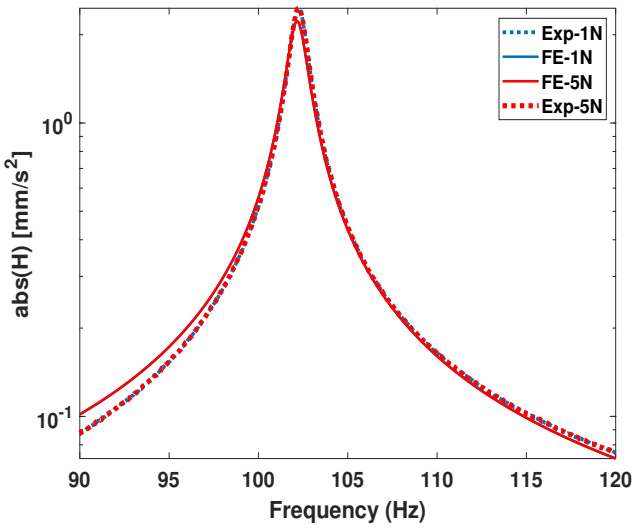

Figure 6.6: *Comparison between measured data and FE simulated response at the driving point for the first vibration mode of the linear assembly in Figure 6.2a.*

activated. The same experimental and linear FE procedures used for validating the linear model were also used to validate the second test structure configuration in Figure 6.2b. A selection of the FRF and coherence obtained from this test are illustrated in Figure 6.7 over a bandwidth of 1000 [Hz]. The natural frequencies and modal damping ratios were also identified using the same Polymax identification technique that was used in the linear modelling. Table 6.4 shows the list of frequencies and damping ratio obtained for this model. Comparing the linear FRF plots obtained from both structures, it is obvious that by connecting the two cantilever beams together with a flexible curve introduces new dynamics into the system where the new assembly can be regarded as a new structure. Also in Table 6.4 more natural frequencies and modal damping ratios are identified and compared with those identified from the two monolithic cantilever beams. By contrast, it is therefore important to create a new finite element model for this new assembled structure where each feature will be accurately represented.

6.3.2.5 Underlying Linear Finite Element Model

The updated FE model of the cantilever beams was improved by adding the geometry of the flexible curved beam. This was modelled with the exact dimensions presented in Table 6.1 using 2D beam elements. The bolted joint between each cantilever beam and the curved beam was

Mode	Frequency (Hz)	Damping ratio (%)
1	95.66	0.17
2	99.17	0.18
3	141.42	0.13
4	250.77	0.10
5	481.59	0.07
6	620.15	0.28
7	625.32	0.26
8	720.96	0.08
9	988.08	0.05

Table 6.4: Estimated Linear resonance frequencies and damping ratios based on low-level random data for the nonlinear assembly in Figure 6.2b

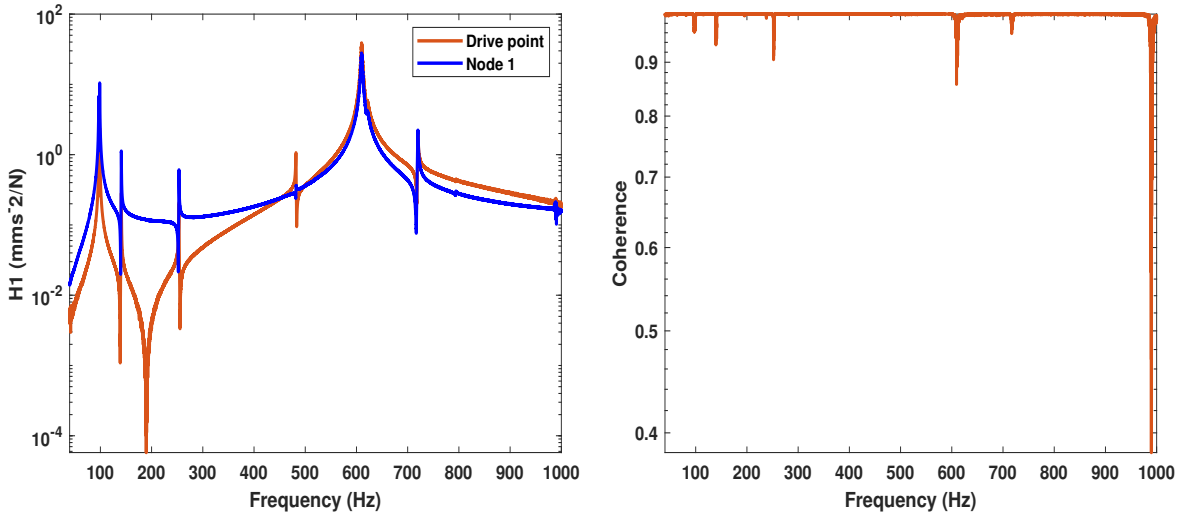

(a) (b)

Figure 6.7: *Acceleration response function and Coherence obtained from low-level broadband excitation performed on the non-linear assembly. (a) Acceleration response and (b) Coherence.*

modelled by means of linear springs in ABAQUS, where an initial stiffness coefficient of 500Nm was assigned to each connected Degree of Freedom (DOF) as a starting parameter to model the joints. For this FE model, standard material properties of steel were also used to model the curved beam and the material properties of the other components in the assembly were left unchanged since they were already updated. Similarly, a linear frequency analysis was conducted on this

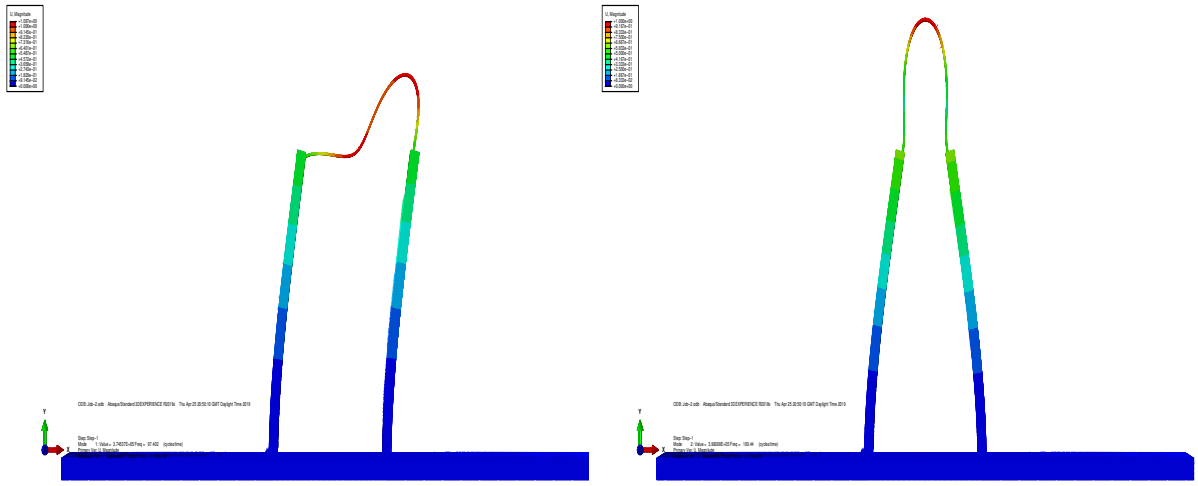

(a) (b)

Figure 6.8: *Linear Finite Element Mode shapes of the Non-linear Cantilever Assembly in figure 2b. (a) Mode 1 and (b) mode 2.*

version of the FE model to obtain the natural frequencies and mode shapes. Figure 6.8 illustrates the first two mode shapes and frequencies obtained from the analysis.

6.3.2.6 Underlying Linear Model Updating

The new FE model was also correlated and updated using the low-level burst random excitation modal test conducted on the complete assembly. In this model, the primary unknowns are the coefficients of the stiffness used in modelling the joints and the exact material properties of curved beam. FEM-tools software by Dynamic Design Solutions (DDS) [240] was used for the model updating. To start the updating process for this FE model, a sensitivity analysis was conducted on the coefficients of the linear springs to quantify the variation in the natural frequency of the model as a result of modifying the coefficients. The coefficients obtained for all combinations of responses and parameters were then stored in a sensitivity matrix and by analysing the matrix information, the sensitive and insensitive zones of the structure were obtained. The sensitivity coefficients are computed internally by FEM-tools using a finite difference method [240].

The updated FE frequencies were then compared against the measured natural frequencies. The second parameter that was selected for the updating process for this model was the Young's modulus of the curved beam, although there were no physical measurements obtained for this

Mode	FE Freq Before	Test (Hz)	Diff (%) Before	MAC (%) Before	FE Freq (Hz) After	Diff (%) After	MAC (%) After
1	102.66	95.66	6.63	81.3	96.49	0.86	98.1
2	106.87	99.17	6.89	84.7	99.55	0.38	95.7
3	157.35	141.42	11.41	73.9	141.71	0.21	96.4
4	284.21	250.77	11.65	68.5	248.25	-1.00	82.7
5	515.18	481.59	6.97	62.7	484.64	0.63	82.3
6	672.81	620.15	8.49	80.6	619.52	0.09	96.8
7	680.14	625.32	8.77	78.3	626.24	0.15	93.4

Table 6.5: Updated FE Model Natural Frequencies and MAC Values for the FE model of the nonlinear assembly in Figure 6.2b.

Components	Initial Material Properties	Updated Material Properties	Initial Stiffness	Final Stiffness
Cantilever Beam	Steel ($E = 210Gpa$, $\upsilon = 0.27$)	Steel (E = 195.4 Gpa, $\upsilon = 0.27$)		
Rectangular Base Beam	Steel ($E = 210Gpa$, $\upsilon = 0.27$)	Steel (E = 195.4Gpa, υ = 0.27 4)		
Curved Beam	Steel ($E = 210Gpa$, $\upsilon = 0.27$)	Steel (E = 195.4 Gpa, $\upsilon = 0.27$)	500Nm	397Nm

Table 6.6: Final Material Properties obtained from the model calibration

part of the structure due to light weight of the component. However, the data sheet provided by the manufacture indicated steel as its material property. Therefore margin of 5% was permitted for the variation in the material property values during this process and the updated natural frequencies and MAC values for the first 7 modes are presented in Table 6.5. In Table 5 the MAC percentage values were used as a form of quantifying the quality of the correlation between the FE model and the experimental data for each mode. A MAC value of 80% and above is often regarded as acceptable.

In this case, the majority of the MAC and frequency values are within acceptable figures, the final material property values and linear stiffness coefficients obtained from the updating process is presented in Table 6.6. In addition to using MAC to quantify the validation of this ULM, the frequency response for the FE model was also computed by extracting the mass and stiffness matrices from ABAQUS. The FRFs were computed using a new proportional damping matrix

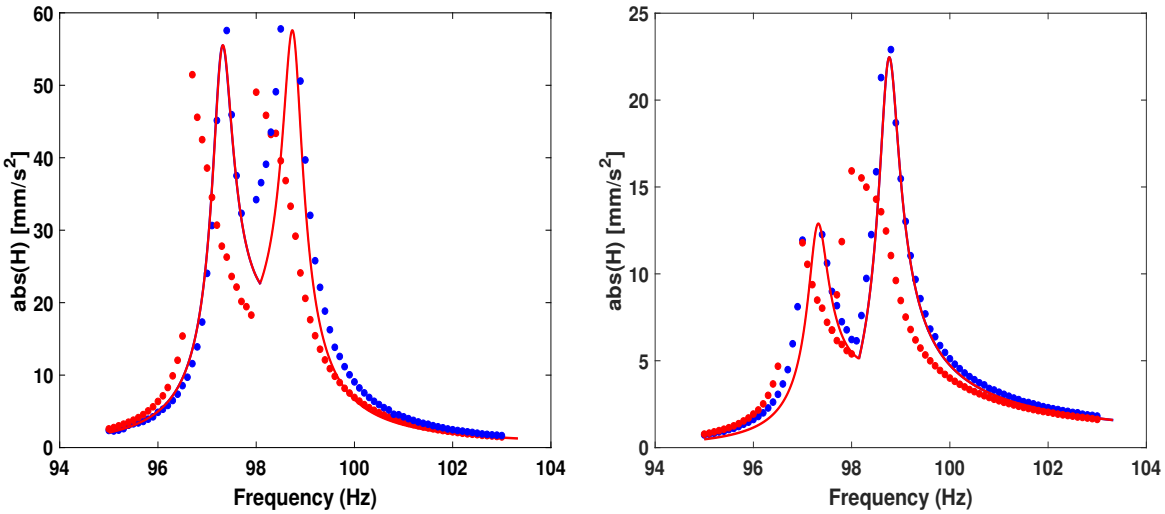

(a) (b)

Figure 6.9: *Comparison between measured data and FE simulated response at node 1 and driving point for the first and second modes of the nonlinear assembly. (a) node 1 and (b) drive point.*

calculated by using the FE mass and stiffness matrices and the identified modal damping ratios. Figure 6.9 shows the comparisons between the measured response (dots) and predicted responses at two levels of excitation using the linear FE model To quantify the correlation between the measured data and linear FE model, the Frequency Domain Assurance Criterion (FDAC) was used as tool for correlation. FDAC is a model validation technique discussed in [241] and [242] that extends the formula of the Modal Assurance Criterion to encompass Frequency Response Functions (or Acceleration Responses). It is particularly useful in this case, since it is insensitive to the relative scale factor of two responses and to the frequency shift that might affect them. While a successful correlation between linear FE model and the measured data at the low-level excitation of 0.5N (blue) was achieved, the results shown in Figure 6.9 illustrates that the same linear FE model could not be used to reproduce an acceptable frequency response of the structure at the higher excitation level of 5N (red).

6.3.2.7 Overview of Phase l Results

In view of the importance of FE and experimental modal analysis (EMA) in linear structural dynamics, conventional modal testing and model validation procedures have been applied to

Frequency Range	Excitation Level (N)	MAC {%}	Frequency Discrepancy {%}	FDAC {%}
95-98	0.5	98.1	0.86	97.4
95-98	5.0		10.16	77.1
98-103	0.5	95.7	0.38	98.6
98-103	5.0		13.13	76.3

Table 6.7: Validation Results Using FDAC Values for the FE model of the nonlinear assembly in Figure 6.2b.

both test structures in Figure 6.2 to obtain a valid linear FE representation of the structure at relatively low amplitudes of vibration. With this validation procedure, it is possible to describe the linear dynamic response of both test structures to an acceptable accuracy as shown in the MAC and FDAC values presented in Table 6.5 and 6.7 which are all above 80%. In Table 6.7, the percentage correlation of the FDAC at 0.5N for the selected frequency range are also above 95% and by common practice, they can be regarded to be within the acceptable range for linear validation techniques.

However, in practice, many non-linearities exhibit a degree of amplitude dependence and most of these become more prominent at higher levels of vibration rather than low levels. This is evident in Figure 6.9 where the validated underlying linear FE model of the non-linear test structure (Figure 6.2) at 0.5N could not successfully predict the response of the structure when the excitation was increased by a factor of 10. In addition, the FDAC values at 5N presented in Table 6.7 are below 80% with the frequency discrepancies between 10% and 14% and so it is obvious that the underlying linear FE model of the structure can only be used as a true representation of the structure within the validated excited range of 0.5N. In this case, the error between the predicted response and measured data of the non-linear structure at 5N is a clear indication of the presence of non-linearities in the test structure which are not represented in the validated underlying linear FE model. As such, it is important to conduct further analysis on the structure. This includes the identification of non-linearities and the non-linear model validation of the structure. All these are further investigated in Phases II and III.

6.3.3 Non-linear identification (phase II)

Referring to the chart in Figure 1, the second phase is primarily focused on non-linear identification of the structure using experimental data. The overall objective of this section is to locate and identify areas of the structure that exhibit any form of non-linear behaviour and, in addition, to build a model of the non-linearity present in the structure. Each non-linear element needs to be identified so as to be incorporated into the initial validated underlying linear FE model and this would ensure that the FE model is able to capture and to accommodate the described non-linear behaviour in the structure. In this Phase, new experiments are conducted under more strictly controlled excitation conditions. This is to ensure that the structure is vibrated at high amplitudes of normal operating conditions that would activate the non-linearities in the structure in service.

Special care and attention are taken into consideration during the measurements obtained in this phase: non-linear systems are sensitive to input data hence the exact excitation signals are specified and extra care are taken when deriving the response functions. The four stages recommended in [36] i.e (Detection, Characterisation, Location and Quantification) are adopted in this phase. This enables the use of different developed non-linear identification algorithms and techniques to characterise and estimate the non-linearity in the test structure. The location stage was not relevant in this chapter based on the assumption that the curved beam and the bolted joints are responsible for the non-linearity.

6.3.3.1 Detection of Non-linearity

The first step recommended in [36] for the experimental non-linear identification process is to consider if the structure exhibits some level of non-linear behaviour under different excitation conditions. This is often judged based on the absence of linear theory observed in the dynamic behaviour of the structure. In this case, Figure 6.9 already shows an early indication of non-linearity present in the structure both through the absence of proportionality in the measured data and the large error observed in the response prediction at high amplitudes of vibration. There are several techniques for detecting non-linear behaviour from measured data, this mostly depends on the type of excitation signal used during the test campaign.

Stepped and swept-sine excitations are predominantly suitable for investigating the response of non-linear structures at higher excitation levels. This is mainly due to their deterministic nature. If linear, the structure would produce a pure sine wave in the output and if non-linear, distortions are easily detected by visualising the output of the sine wave. Other techniques for detecting non-linearity from measured data are presented in [170, 171, 61]. Another intuitive method or indicator of non-linear behaviour is a lack of homogeneity in the frequency response functions over different excitation levels. The use of low-level and high-level random excitation is suitable for homogeneity testing on the FRFs and ordinary coherence.

Time Series and FRF Inspection.

Visualisation of raw time histories response data obtained from sine sweep excitations can be used to reveal non-linear behaviour in the response of the structure. In this chapter, swept sine tests were conducted on the first and second modes of the non-linear assembly in Figure 6.2b. Accelerations at selected locations of the assembly were measured at 0.5N, and 5N excitation levels. Figure 6.10 (a and b) shows selected plots of the measured acceleration against sweep frequency for the first and second modes of the assembly. Both sweep-up and sweep-down sine excitation test were conducted. This particular test was conducted using the Multi-input Multi-output (MIMO) Sine Sweep module in LMS Test Lab, given knowledge of the acquisition parameters and process functions, the sweep rate and instantaneous sweep frequencies were calculated.

The detection of non-linear behaviour in the response to the sine-sweep excitation is achieved here by visually inspecting the measured time histories. Symptoms of non-linearity are visible in the plots presented in Figure 6.10, in particular, Figure 6.10a, where a frequency shift is observed for both modes when the amplitude of vibration is increased from 0.5N (dark blue) to 5N (red). Skewness of the signal envelope in Figure 10b is also observed at 5N excitation around the resonance peak of mode 2, resulting to a jump phenomenon and the non-smoothness of this envelop. The comparison of frequency responses measured at different controlled excitation levels is another convincing way to detect non-linearity.

In Figure 6.11 stepped-sine FRFs are presented for each test concentrated around the mode

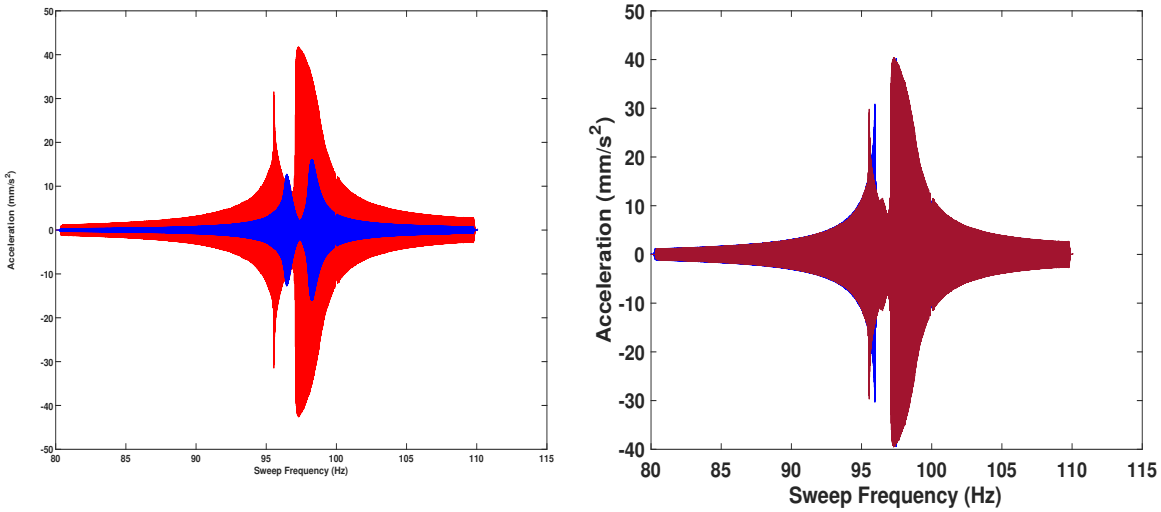

(a) (b)

Figure 6.10: *Sine-sweep acceleration data measured on node 1 of the non-linear assembly in Figure 6.2. (a) sine-sweep for mode 1, (b) sine-sweep for mode 2*

of interest, from the lowest (1N) to a high (5N) input levels of excitation. These stepped-sine FRFs only take into account the first harmonic and neglects all other higher-order harmonic components in both input and output [202]. Figure 6.11 (a) and (b) illustrate the breakdown of the principle of superposition coming from linear theory by comparing responses measured at mode 1 in ascending order from 1N to 5N. Similarly, measured FRFs obtained for mode 2 are illustrated in Figure 6.11 (c) and (d) between 1N and 4N where this principle is also violated. The shifts in frequency and amplitude observed in FRFs obtained for both modes 1 and 2 here are deemed not to be negligible, and will require further identification of the non-linearities. Finally, aside from the frequency and amplitude shifts, the resonant peaks lean to the left, causing a sudden transition (jump) down to a lower energy state when increasing in frequency, and a smaller transition (jump) up to a higher energy state when decreasing in frequency. This is most evident in the FRF obtained from mode 1 as illustrated in Figure 6.11 (a) and (b).

6.3.3.2 Characterisation of Non-linearity

The third step in the non-linear identification process is the characterisation of the non-linear system. This step seeks to characterise the aspects of motion that drives the non-linearity in

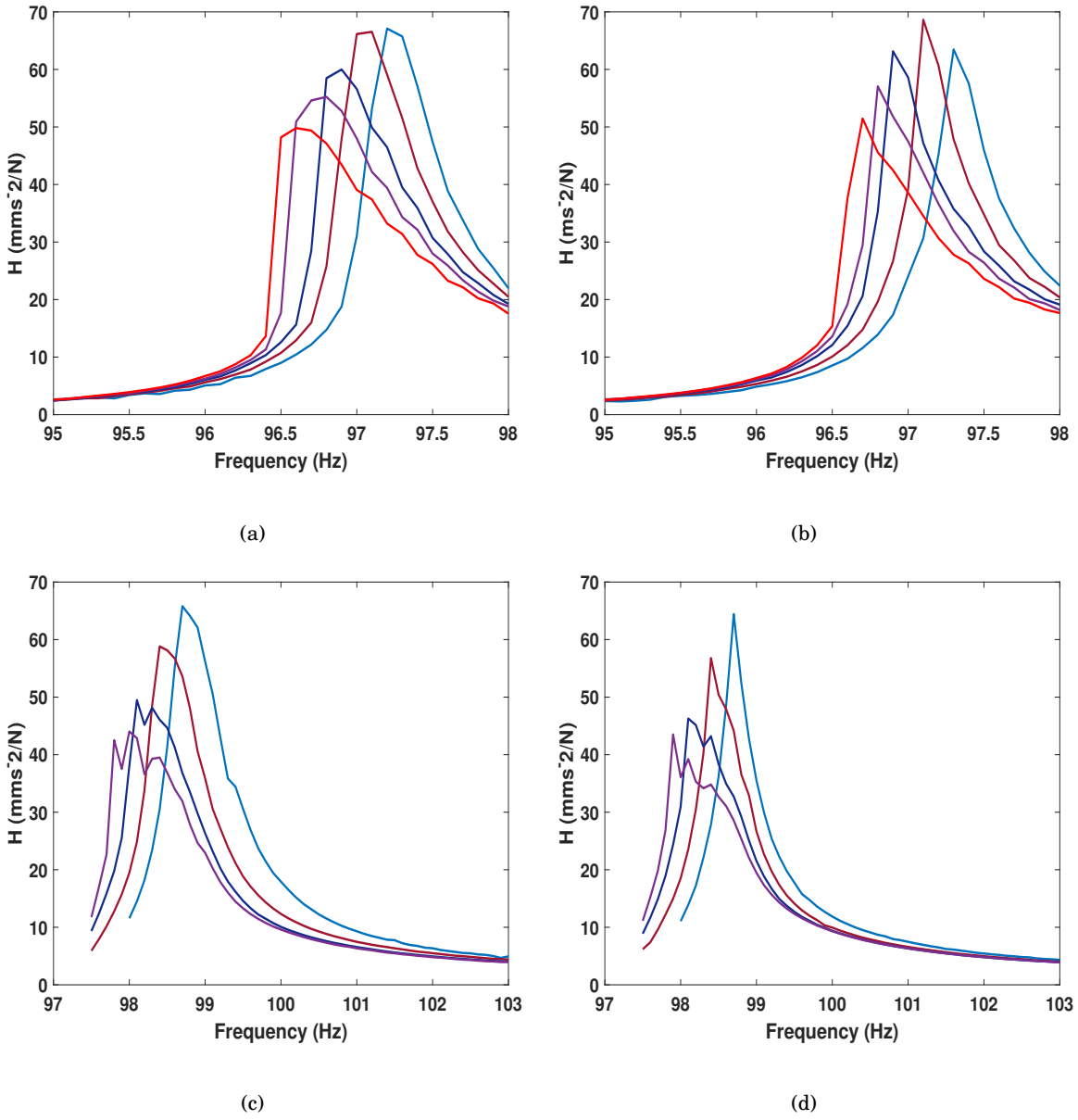

Figure 6.11: *Force controlled Stepped Sine acceleration response measured at Node 1of the non-linear assembly. (a) Mode 1 sweep up, (b) Mode 1 sweep down, (c) Mode 2 sweep up and (d) Mode 2 sweep down.*

the structure. Aside from identifying the characteristics that drives the non-linear behaviour, the selection of appropriate functional forms to represent the non-linearities in the structure is mainly achieved in this step. Non-linear characterisation also helps in determining the type of non-linearity in the structure and in addition seeks to provide answers to some major questions that arise when dealing with non-linear system. Some of the typical questions that arise are

listed below: a) What is the strength of the non-linearity? i.e is it weak or strong non-linearity b) What is the source of the non-linearity? i.e. is it stiffness or damping non-linearity or both c) What is the non-linear stiffness characteristic? i.e. is it hardening or softening d) What is the characteristic of the restoring force? i.e. is it symmetric or asymmetric.

Of all the characterisation methods available in the literature, the restoring force surface method has proven its ability to characterise the stiffness and damping properties of a non-linear structure directly from measured acceleration data. By presenting the restoring force surface results of a non-linear structure as a function of the displacement, velocity and acceleration in a three-dimensional plot, it is possible to visualise the nature of the non-linearity in the structure. The stiffness and damping properties of the non-linearity can also be visualised by taking a slice of the three-dimensional plot at zero values of the corresponding velocity and displacements. To this end, a modified version of the restoring force surface introduced in [120] was used to obtain qualitative information on the non-linear stiffness of the non-linear assembled test structure in this study.

Acceleration Surface Method.

In this section, the Acceleration Surface Method (ASM) for non-linear characterisation is discussed. This is a similar approach which has been used to provide some qualitative characterisation of the non-linear stiffness and damping at the wing-to-payload interfaces of the F-16 aircraft [243]. In this case, new Swept-Sine tests were conducted around the first and second modes at high level of excitation levels. The acceleration surface was computed using acceleration data measured at nodes 1 and 2 of the assembly. These nodes were selected to visualise the non-linear behaviour caused by the connection. The measured acceleration signals were integrated twice using the Trapezium rule and then filtered using a high pass filtering system designed in MATLAB to obtain the corresponding velocity and displacement signals. For more details on data signal processing obtained from sine excitation, the reader can refer to [61].

To visualise the form of stiffness non-linearities in the non-linear beam assembly connections, a cross section along the axis of the zero-velocity value of the acceleration surface plot in Figure 6.12 was plotted and is presented in Figure 6.13. This was computed separately for each mode in

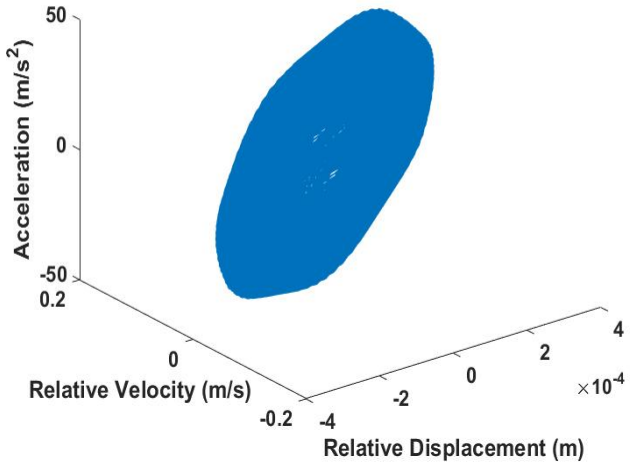

Figure 6.12: *Acceleration Surface plot across the non-linear connection.*

order to visualize the form of non-linearity exhibited by that specific mode. Figure 6.13a (left) shows the qualitative stiffness curve for mode 1 across node 1 and 2 while Figure 6.13b (right) illustrates the qualitative stiffness curve for mode 2 across nodes 1 and 2, these figures are mainly useful to understand the behaviour of the elastic non-linearities within the selected mode. The stiffness curves show the symmetric nature of the non-linearities in the assembly most especially for mode 2 within the excitation range. The stiffness curves for both modes have also revealed that an accurate representation of the non-linear behaviour in the structure should account for smooth and symmetric effects, the nature of the non-linearities in the system also indicates that the non-linear stiffness can be modelled using odd functions or a polynomial with odd powers.

6.3.3.3 Quantification of Non-linearity

Once the non-linearity has been characterised, the last step in the non-linear identification process is the estimation of the coefficients associated with the non-linear stiffness and damping properties. There are a number of techniques used for non-linear parameter estimation, examples of these techniques are the frequency domain feedback method [210], subspace identification methods [244] and [116], the reverse path method [142, 110], non-linear auto-regression and the RFS method [245]. Since the focus of this chapter is to estimate the non-linear stiffness and

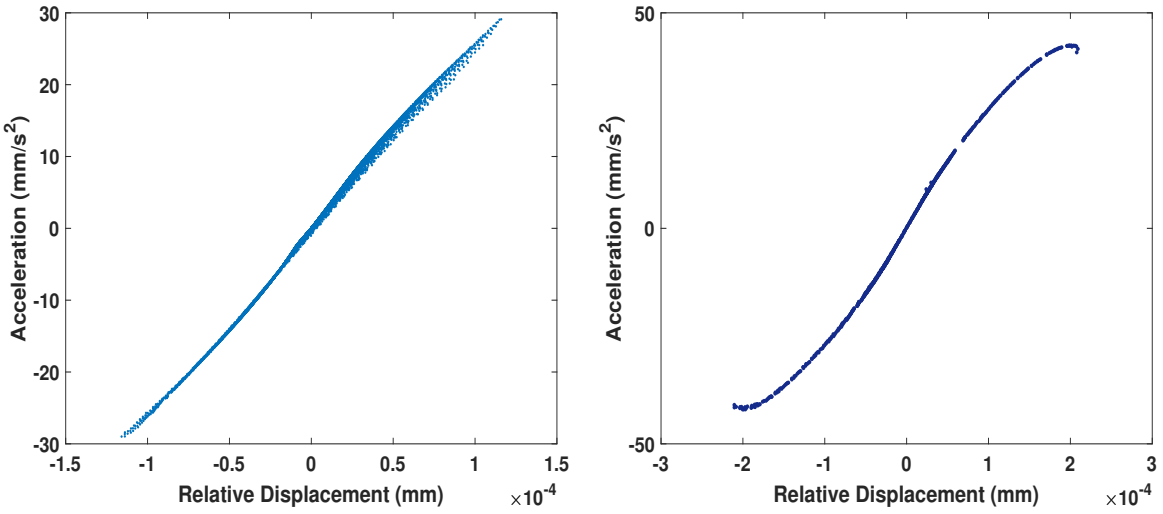

(a) (b)

Figure 6.13: *Qualitative Stiffness curve obtained across the beam connection of the non-linear assembly . Mode 1 (a), Mode 2 (b).*

damping properties caused by the complex assembly of the test structure, an alternative MDOF approach of the RFS method was adopted.

The initial extension of the RFS method for parametric estimation of MDOF system was introduced in [121] which was conducted in the modal space, however Al-Hadid and Wright proposed a useful form of estimating non-linear parameters using the physical coordinate representation of the non-linear forces while retaining a modal coordinate approach for the linear system [118]. Since the acceleration surface method was applied in the characterisation step, a direct parameter estimation of the RFS was adopted to estimate the initial stiffness coefficients of the characterised model. In addition the time-domain Hilbert transform (HT) approach (FORCEVIB) proposed in [246] for identifying instantaneous modal parameters was also adopted for the estimation of non-linear parameters.

Estimation of Non-linear Stiffness Coefficient.

The RFS method is very suitable for parameter estimation from sine excitation. However, its domain of applicability is generally limited to reduced-scale structures since it requires a rigorous writing of Newton's law of dynamics. Hence a simplified assumption of the structure is

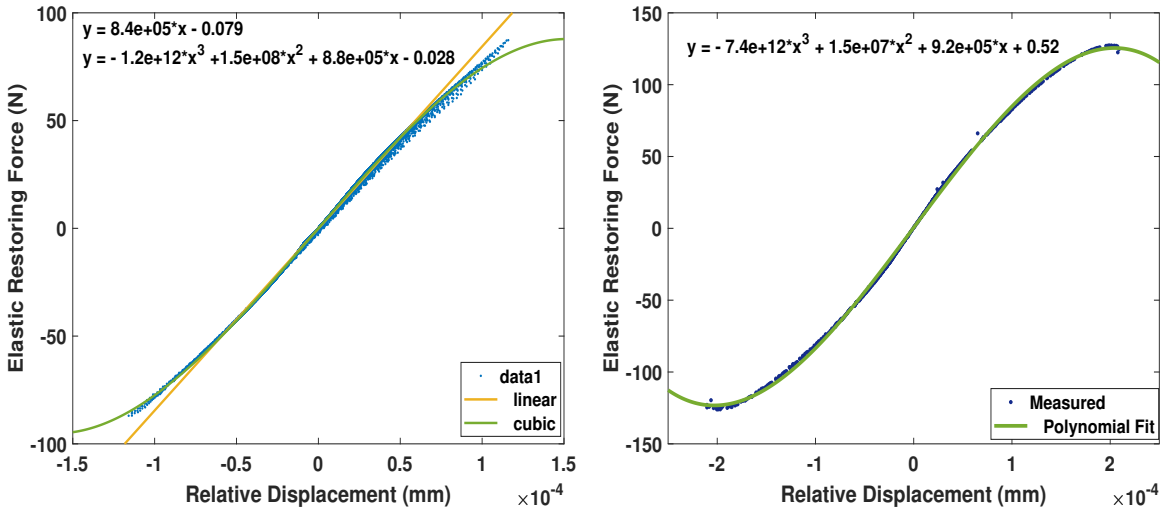

(a) (b)

Figure 6.14: *Measured vs Polynomial fit stiffness curve of the nonlinear assembly . (a) Mode 1, (b) Mode 2*

always considered, to estimate the coefficients of the non-linear characterised stiffness, a lumped parameter representation of the test structure was developed. The advantage of this approach is the fact that a new model of the parametric model of RFS can be reconstructed based on an appropriate polynomial order selection or curve fitting method that fits the measured RFS. A similar approach was introduced by Masri in [247] where a least squares method was used to estimate the mass required to obtain the coefficients of a polynomial model. Figure 6.14 presents the comparison between the measured stiffness curve and the polynomial model of the stiffness curve for modes 1 and 2.

The polynomial coefficients and effective mass value were obtained using the direct parameter and least square estimation approach discussed in the non-linear identification survey in [12], results of the polynomial fit are presented in Table 6 and the direct parameter approach is full explained in appendix B of [248].

$$MSE = 100\left(\frac{1}{N}\sum i\frac{(P_i - M_i)^2}{\bar{P}\bar{M}}\right) \tag{6.1}$$

It is worth noting that the curve fitting approach was used in this stage of the identification in order to estimate the required effective mass of the model, and the estimated mass value is

Property	Identified Model
Estimated Effective Mass	2.89 Kg
Actual Mass of Test Structure	3.62 Kg
NMSE_Mode l	3.05 %
NMSE_Mode 2	1.92 %

Table 6.8: Identified parameters

expected to be a sensible fraction of the actual test structure as stated in the Dynamic Testing Agency Hand book (DTA) and in [61]. To check the quality of the fit, the Normalised Mean Squared Error (NMSE) illustrated in Equation 6.1 was used to calculate the deviation between the measured stiffness and reconstructed polynomial model.

When applying the NMSE the deviations (absolute values) are summed instead of the differences, hence the NMSE is often used to show the most prominent differences between models. A model with a very low NMSE implies that the prediction error or residuals between the predicted model and the observed model is low and also shows that both the predicted and the measured model match closely well. As observed in Table 6 the NMSE for both modes 1 and 2 are below 5%, these results could also be used as a sign of accurate identification.

$$\begin{pmatrix} mode1 = -1.2e12x^3 + 1.5e8x^2 + 8.8e5x + 0.028 \\ mode2 = -7.4e12x^3 + 1.5e7x^2 + 9.2e5x + 0.52 \end{pmatrix} \tag{6.2}$$

Non-linear Identification based on Hilbert Transform.

Recently, the potential of the Hilbert Transform (HT) in the application to non-linear vibration system identification has attracted increasing interest [236, 127, 129]. A number of HT-based system identification algorithms, such as free vibration identification method (FREEVIB) [126] and forced vibration identification method (FORCEVIB) [246], have been successfully developed. However, both FREEVIB and FORCEVIB only consider the primary component (i.e., the fundamental quasi-harmonic solution) of system response. This type of simplification can often limit the proficiency of both algorithms when used in characterising the type of non-linearity present in a test structure. Hence in [249] Feldman developed a signal decomposition technique for system identification, named Hilbert Vibration Decomposition (HVD), where an initial vibration signal is decomposed into a sum of components with slowly varying instantaneous amplitude and frequency using a time domain analysis of the IF of the initial vibration signal.

In this chapter, the HVD and FORCEVIB methods were applied to characterise the instantaneous non-linear characteristics of the test structure using measured swept sine excitation. The non-linear estimation using the FORCEVIB algorithm was implemented in 4 different steps. (1) The HT of the measured vibration (and excitation) signals was obtained and their envelope and the IF were calculated, (2) The instantaneous modal parameters such as the modal frequency, modal damping, and modal mass value were calculated based on the signal envelop and IF, (3) low-pass filtering of the modal parameters and calculation of the scale factor functions around the selected extrema points of displacement and velocity of the measured signal; and scaling the smooth modal parameters and (4) Presentation of results in the form of the backbones, damping curves, average static force and average friction force characteristics.

Finally, curve fitting of the identified average non-linear characteristic was made to estimate the non-linear stiffness and damping coefficients. With the procedure described above, in this chapter the (IF) and (IA) of measured input and output vibration signals obtained from the test structure in Figure 6.2b was calculated. With the IF and IA extracted, the instantaneous modal parameters are obtained for each mode of vibration (modes 1 and 2) and the average non-linear elastic force and non-linear damping force are also calculated respectively. Final identified results are illustrated in Figure 6.15. In Figure 6.15(a) and (b), the stiffness and damping characteristics

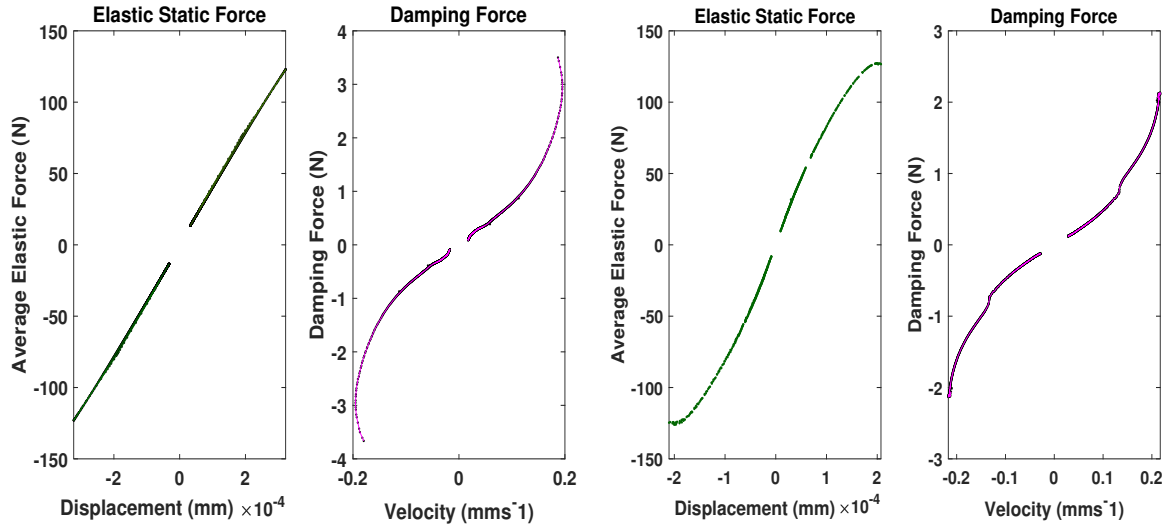

(a) (b)

Figure 6.15: *Hilbert Transform based Identified non-linear stiffness and damping curves for the non-linear assembly. (a) Mode 1, (b) mode 2*

for modes 1 and 2 of the non-linear test structure are shown, for mode 1 Figure 6.15a the stiffness curve is observed to have nearly a linear characteristics while the damping characteristics show more of a higher order polynomial trend. In Figure 6.15b, the HT identified stiffness and damping characteristics for mode 2 are observed to have a non-linear behaviour with a polynomial-like non-linear model.

Comparing both stiffness curves obtained from the RFS and HT based identification, one can detect the non-linear identical trend displayed by both curves which is a good correlation between both identification techniques. With the HT-based identification, neither low-pass filtering nor narrow band can cancel out noise from measured data. Hence, errors are bound to occur during the computation of the signal envelop and inverse Fourier components. As a consequence, further errors are generated in the identified stiffness and damping curves. This is most evident in Figure 6.15, where the FORCEVIB algorithm fails to produce results around zero velocity and displacement values. The estimated modal mass value obtained for modes 1 and 2 are 3.08 and 4.50. However, compared to some existing non-linear identification techniques which assume a prior knowledge of the type of non-linear stiffness and damping model before parameter estimation. The RFS and HT-based identification methods as non-parametric identification

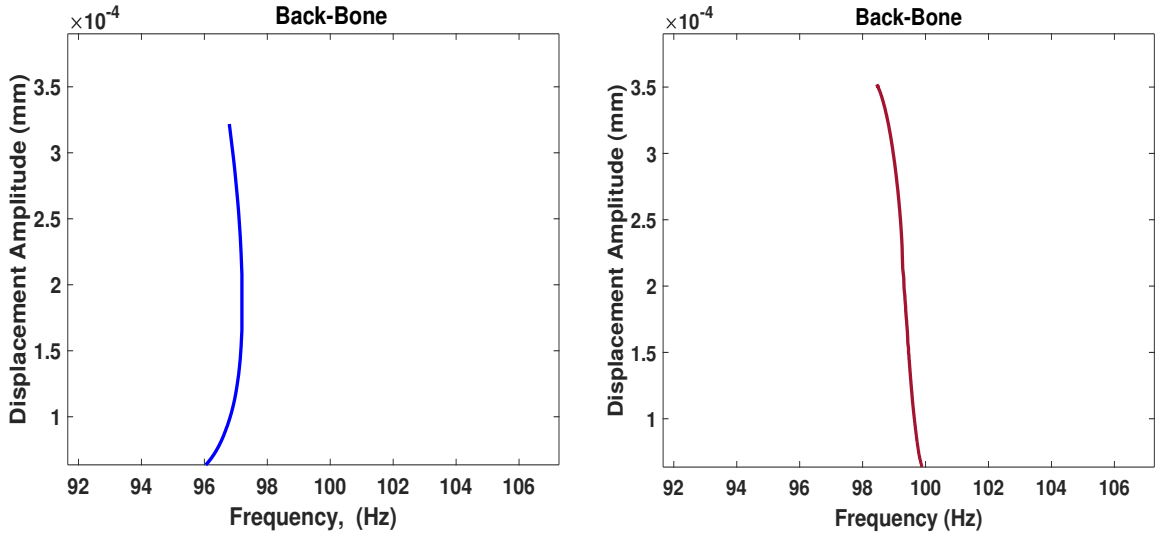

(a) (b)

Figure 6.16: *Experimental backbone curves identified from sine-sweep data for the non-linear assembly. (a) Mode 1, (b) Mode 2*

methods can directly characterise the non-linear stiffness and damping model from measured data, as shown in Figure 6.14 and Figure 6.15.

Aside from stiffness and damping estimation, the HT-based identification technique can also provide information about the backbone of a non-linear system. In [236] the procedure for constructing the Skeleton curve (backbone) as a function between the envelope and the modal frequency for a vibration mode from measured data is described. The backbone obtained from the time domain estimation of the modal parameters for modes 1 and 2 is presented in Figure 6.16. The obtained backbone has a typical non-linear form of softening stiffness characteristics. The instantaneous modal frequency and envelope obtained from the HT analysis are varying functions of time and have a fast oscillation about their smooth averaged values as discussed in [249]. As a result, the HT identified backbone with the presence of non-linearity will not always produce a smooth curve, but an oscillated curve (i.e. a curve varying in magnitude). Similar to the illustrated backbone curve, the HT identification method can also characterise the damping curve of a non-linear system as a function of the modal damping coefficients against vibration amplitude.

A damping curve is an essential feature of a non-linear structure where the system property

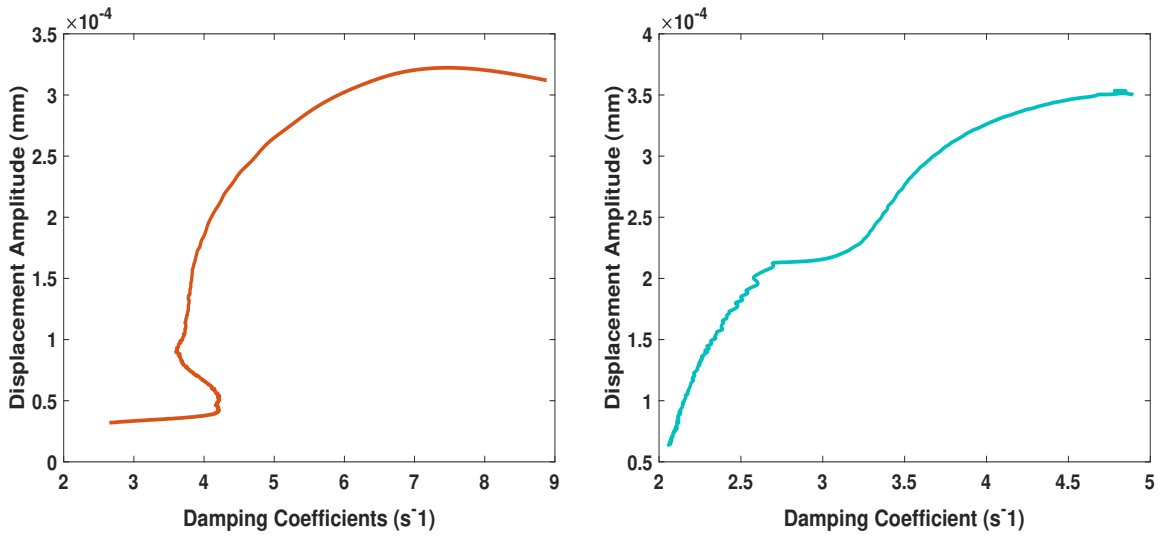

(a) (b)

Figure 6.17: *Experimental damping curves identified from sine-sweep data for the non-linear assembly. (a) Mode 1, (b) Mode 2*

often shows that the damping is amplitude-dependent. Figure 17 shows the damping curves obtained from the HT identification for modes 1 and 2, the damping curve illustrates the modal damping coefficients as a function of amplitude. For a linear structure, the damping characteristics which are not expected to change, hence the damping curve will normally turn out as a straight line. However, for a non-linear structure, where the modal damping depends on the vibration frequency the damping curve depicts the modal damping coefficients as a function of frequency. The obtained damping curve for modes 1 and 2 in Figure 6.17 display its non-linear characteristics at high vibration amplitude, indicating that the damping property of the structure increasingly becomes non-linear as the excitation force increases.

The use of HT-based identification can sometimes produce false results at the ends of its estimation due to the inefficiency in cancelling out noise from measured data which often leads to accumulation of further errors in the computation of the signal envelope and Fourier components. This is also evident in the estimated damping force characteristics illustrated in Figure 6.15. It is worth asserting that for both RFS and HT identification techniques, each stiffness and damping function, backbone cure and damping curve was obtained directly from measured data without any assumption of the forms of non-linearity present, classifying both as non-parametric.

6.3.3.4 Overview of Phase II

In this phase, experimental data measured on the nonlinear test structure in Figure 6.2 has been exploited using already developed nonlinear identification methods. Swept sine test data in conjunction with the acceleration surface method were used to detect and characterise the nonlinearities present in the structure. The nonlinear stiffness coefficients for modes 1 and 2 were estimated using a direct parameter estimation method and least squares fit to estimate the effective mass. The HT-based identification technique was also used to estimate the structure's instantaneous dynamic parameters (i.e. natural frequencies, stiffness and damping characteristics and backbone curves) and their dependence on the vibration amplitude directly from measured time signals.

The nonlinear model of the test structure was created by curve fitting the experimentally obtained restoring force characteristics, although the methods used in this nonlinear identification phase have been selected based on the swept sine excitation signal used during the test and also the ability to capture some interesting dynamic nonlinearities observed in this particular application. Other nonlinear identification methods based on random excitation applied in the first case study [169] could also be used to obtain similar results. Finally, the use of different identification methods to obtain similar nonlinear stiffness and damping characteristics also show the validity and reliability of the results achieved in this phase.

6.3.4 Non-linear FE modelling and validation (phase III)

Aside from identifying the non-linearities present in structures based on experimental data, engineers today also require the use or at least are willing to understand the effects of these identified non-linearities on the mechanical or physical response of a structure under certain operating conditions. Hence, this phase III was undertaken in the light of providing some level of solution to this challenge and also to integrate both the aspects of non-linear identification and numerical computation of non-linear systems together. Phase III can be said to be the least-developed phase of the proposed methodology. The steps are clearly defined in [169], but the ability to execute them is not as well developed compared to other Phases. In this phase, the non-linear characterised model identified in phase II is added to the stiffness and damping

properties of the validated underlying linear FE model.

This step is introduced in order to capture and describe the non-linear effects which are habitually amplitude-dependent as opposed to linear systems which are amplitude-independent. Non-linear identification only quantify the quantification of physical parameters which were not existing in the linear one. Therefore, in this phase the linear model must be upgraded with new physical laws that can describe the non-linear dynamics measured in the test structure. Hence, in this phase, the FE model is now referred to as a "non-linear FE model". Another motivation behind this phase is to exploit the non-linear FE model to understand new experimental measurements, discover new non-linear regimes of motion which were not noticed in the identification phase and finally, to conduct design modifications while retaining the knowledge of the non-linear characteristics present in the structure of interest.

The analysis conducted in this phase was carried out in three different consecutive steps which are model upgrading, model updating and model validation as per [12]. First, upgrading a model requires changes to be made to the equation of motion of a discretised (FE) model in order to accommodate previously identified non-linear characteristics in phase 2. The upgrading procedure is easily achievable through any commercial FE package that allows the introduction of customised elements (springs or dampers) between two interested degrees of freedom and also defines a customised non-linear force-displacement/velocity relationship between the connected DOF, as discussed in [12]. The second step involves updating the model. This task is often executed for linear structures where the parameters such as Young's modulus and Poisons ratio of the FE model are updated to match measured results.

In the case of a non-linear structure, updating the FE model involves modifying the coefficients of customised elements that were included in the validated underlying linear FE model in order to match the measured characteristics. The updating step in this phase is achieved iteratively where each updating loop requires the re-evaluation of the FE model and subsequent correlation with measured data until a low residual percentage error is achieved. Once the updating of the non-linear FE model has been successfully achieved, the model can then be used for prediction of new responses at different excitation levels and then validated with new measured data.

6.3.4.1 Non-linear Finite Element Model of the Assembly

The validated underlying linear FE model of the non-linear structure in phase I was used for the analysis in this phase. Details of the linear FE model can be found in section 6.3.2 of this chapter. The mass and stiffness matrices of the FE model of the assembly were extracted from ABAQUS simulation software into MATLAB for the numerical computation. To reduce the computational burden in this phase, it is often advisable to create a reduced model of the underlying linear FE model (ULM) of the test structure. The reduced model is defined here as a selection of interested physical DOFs and number of modes of the ULM while the rest of the DOF are transformed into modal coordinates to reduce the size of the system matrices and number of equations to solve numerically.

It is important that the reduced ULM must include selected DOFs from regions in the structure where the non-linear features are present or identified and also where the structure is being excited. In this section the reduced model FE model of the non-linear test structure was obtained using the Craig-Bampton model reduction technique presented in [250]. Figure 6.18 shows a schematic of the reduced FE model of the test structure and regions with the non-linear features. The dashed lines represent the linear FE model while the red-dots are the retained nodes. The validated underlying linear model in phase I had a total of 6542 DOFs, in this phase the model was reduced to 136 DOF. The non-linear connections were modelled by connecting each associated DOFs in the reduced FE model with the customised non-linear spring elements that describe the force-displacement or velocity relationship identified in phase II.

Figure 6.18 and Table 6.9 show a sample of the arrangement, order and magnitude of the non-linear spring elements that were added to the reduced FE model before numerical computation. It worth noting that the non-linear spring elements are made up of only higher order polynomial terms and do not contain linear terms. Proportional damping was introduced to obtain an appropriate linear damping matrix for the numerical model of the structure. Following the relation in the proportional damping equation the damping matrix was computed using

$$C_v = \alpha M + \beta K \tag{6.3}$$

where the coefficients α and β were computed using a least-square estimation. The damping

Nonlinear Element	Node Connection	DOF Connection	Model	Stiffness Coefficient N/m
1	Node_1-Node_7	Dof _1- Dof_21	x^3	-7.4e12
2	Node_1-Node_7	Dof_1 -Dof_21	x^2	1.5e7
3	Node_2-Node_15	Dof_4 -Dof_45	x^3	-7.4e12
4	Node_2-Node_15	Dof_4 -Dof_45	x^2	1.5e7
5	Node_7-Node_15	Dof_21 -Dof_45	x^3	-7.4e12
6	Node_7-Node_15	Dof_21 -Dof_45	x^2	1.5e7

Table 6.9: Non-linear Stiffness Elements included in the FE Model of the nonlinear assembly in Figure 6.2

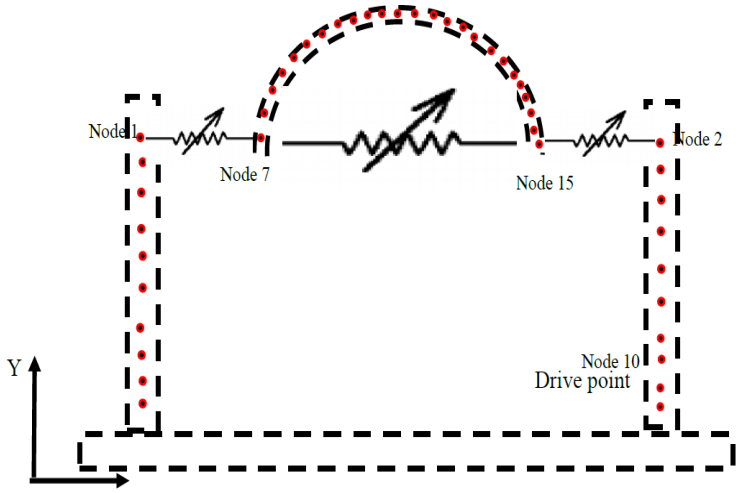

Figure 6.18: *Schematic diagram of the FE model with non-linear element..*

matrix was computed for the first 6 modes of the structure by setting the target modes in the least square estimation to the first 6 modal damping ratios obtained from the linear identification of the structure presented in Figure 6.2b and Section 6.3.2 of this chapter. In this context, the coefficients obtained from the least square estimation are $\alpha = 2.7195$ and $\beta = 1.8034e-6$.

6.3.4.2 Numerical Simulation and Experimental Correlation

As expressed in the introduction, a number of algorithms and numerical methods have been developed for computing the forced response of a non-linear system. In this section, the shooting method developed in [51] based on Newmark time integration was adopted in computing the

steady state Frequency Response of the new non-linear FE model. The equation of motion required to solve this type of numerical problem is written in the form:

$$M\ddot{x} + C\dot{x} + Kx + f_{nl}(x,\dot{x}) = F\sin\omega t \tag{6.4}$$

Where M, C and K denote the linear mass, damping and stiffness matrices obtained from the underlying linear FE model of the structure, $f_{nl}(x,\dot{x})$ represents the non-linear stiffness and damping terms which contain the coefficients and polynomial order of all the active non-linear DOFs in the system while $F\sin\omega t$ is the external periodic force at the harmonic frequency of interval ω. The forced response simulation was computed in a frequency range spanning the 1st and 2nd modes of the non-linear assembly, to assess the effect of each type of non-linearity (i.e. stiffness and damping) in the structure.

The numerical simulation was conducted in two stages. The first simulation was computed for the case where only the non-linear stiffness terms were included in the FE model while the non-linear damping terms were considered in the second stage. The simulation was computed for different forcing amplitudes ranging from $F = 1N$ to $F = 5N$. To clearly evaluate the effects of the non-linearities in the model, each amplitude response was normalised to its corresponding forcing amplitude with the relating law ($H = X/F$). The forced response simulation was computed for both the linear model (i.e. without the non-linear elements) and the non-linear model where the non-linear terms are included. The normalised responses are converted into accelerations vs frequency. Similarly, to validate the accuracy of steady-state frequency responses obtained from the numerical computation, experimental stepped-sine tests were conducted on the non-linear test structure in Figure 6.2b under forced controlled conditions.

The test was conducted for a range of different forcing amplitudes using the stepped-sine module in LMS Test Lab. The control strategy implemented in LMS Test Lab only accounts for the ability to control the first fundamental harmonic of the main forcing frequency which is often applied in many industrial vibration tests. The stepped-sine sweep test conducted included sweeps in both upward and downward frequency directions for the selected bandwidth with forcing amplitude ranging from 1N to 5N. To compare like for like, the results obtained from the numerical model were further post-processed to consider only the first harmonic response

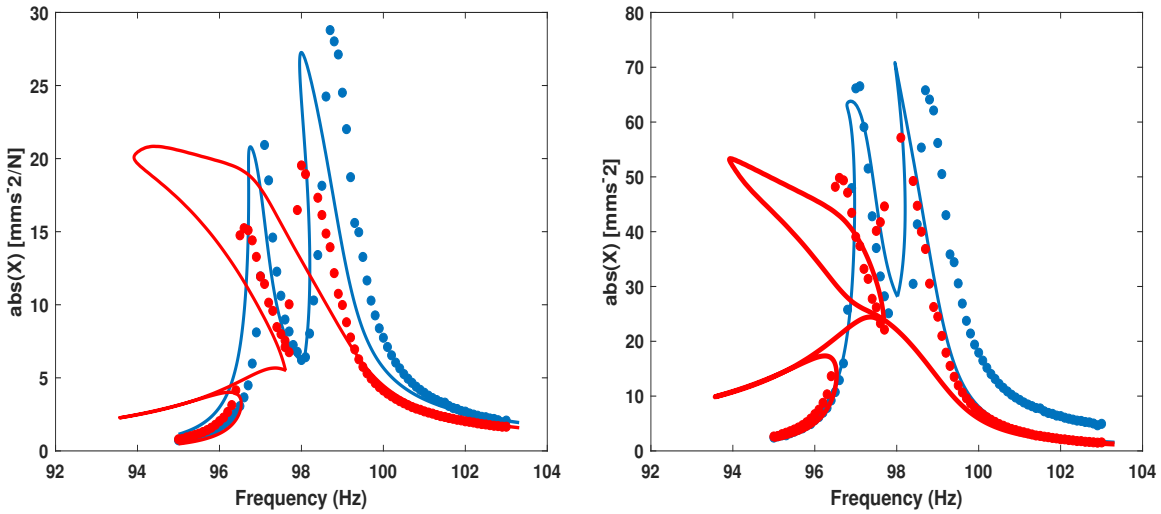

(a) (b)

Figure 6.19: *Comparison of measured and FE simulated acceleration responses for modes 1 and 2 of the non-linear assembly. (a) driving point and (b) node 1 at 2N (blue) and 5N (red) force levels. Dotted lines are from experiments, continuous lines are from upgraded FE model, before updating (using starting coefficients).*

in the simulation. Figure 6.19 shows the non-linear response comparison of the numerical and experimental results for the first 2 modes. Here the non-linear response is defined as a measured frequency response of the structure under controlled forcing condition with the first fundamental harmonic response of the structure.

The results comparing both experimental (dot) and numerical for the horizontal DOF of the driving point and horizontal DOF for node 1 at 2N (blue) and 5N (red) force levels are presented in Figure 6.19. As observed in Figure 6.19, while the shape of the numerical response of the upgraded FE model corresponds with the measured data obtained from the control test at low level excitation ,the model still fails to capture the exact measured points. However, the upgraded FE model now indicates that it includes the necessary parameters to describe the non-linear characteristics observed in the experimental measurements at least for the low force level (2N). At higher forcing level (red, 5N), large deviations are observed between the computed and measured response. This is mostly evident around the resonance peaks of both modes, where unusual phenomena (like a long back bone response) and loops are observed in the computed response.

In [169], a similar loop observed in Figure 6.19 b was also detected in the results obtained

for the non-linear response. The loops and unusual response behaviour probably indicates that the strength of the non-linear parameters in the model are too strong leading to the generation of multiple and unstable solutions around the resonance peaks. It is evident from Figure 6.19 that the non-linear FE model is still not able to capture the dynamics of structure at high forcing level, this also shows the breakdown of the results in the non-linear identification phase. Since both measured data and FE responses have the same non-linear behaviour (softening shape) at low force level, it is understandable that the coefficients of the non-linear parameters need to be updated to increase the accuracy of the upgraded FE model. At this stage, the updating process is only considered on the coefficients of the non-linear parameters since the polynomial model obtained from the non-linear identification already shows promising results as observed in Figure 6.19.

6.3.4.3 Non-linear FE Model Updating

In contrast to non-linear system identification, non-linear model updating in this chapter is aimed at generating improved numerical parameters which can be used to obtain predictions for alternative loading arrangements or modified structural configurations. The main objective here is to ensure that the non-linear stiffness and damping parameters in the updated FE model are physically meaningful when compared with measured data. In linear structural dynamics, model updating has received a significant level of attention with several developed updating methods and procedure as discussed in [251]. In contrast, model updating of non-linear structures has also received a small number development as illustrated in [6] and in [252] where major efforts are devoted to model updating of jointed structures. In this chapter, the parameters of the non-linear FE model are updated in order to minimize the difference between the numerical frequency response and the measured frequency response.

Based on the concept of frequency shifting and linear FE model updating, a technique to measure the closeness between measured and FE FRFs was proposed in [241], also known as FDAC. In the context of FRF-based updating procedures, FDAC helps in selecting the frequencies that should be used and also helps to choose the intervals where the FE model is close to the measured data. Since the objective of non-linear model updating stage of this chapter is to

minimise the error between the FE frequency response and the experimental frequency response, two main optimisation studies regarding the choice of objective functions were performed. The first objective function was the FDAC which is defined as the measure of the closeness between the measured frequency response and the FE frequency response at selected frequency intervals, while the second objective function represents the normalised root-mean-square as shown in Equations 6.5 and 6.6:

$$FDAC(\omega_a, \omega_x, j) = \frac{([H_a(\omega_a)]_j^T [H_x(\omega_x)]_j)^2}{([H_a(\omega_a)]_j^T [H_a(\omega_a)]_j)([H_x(\omega_x)]_j^T [H_x(\omega_x)]_j)} \tag{6.5}$$

$$\overline{RMSE}(\omega_a, \omega_x) = \frac{\sqrt{\frac{(\sum_{i=1}^{n}([H_a(\omega_a)]_j - [H_x(\omega_x)]_j)^2)}{N}}}{RMSE_1} \tag{6.6}$$

where j corresponds to the measured column of H, (ω_a) is the frequency at which H_a (numerical FE frequency response) is being calculated, (ω_x) is the frequency at which H_x (measured frequency response) was measured experimentally and N is the number of points used to interpolate the experimental data. In Equation 6.5, the FDAC values are restricted to the interval $[(0,1)$ or in percentages $(0\%, 100\%)]$ where a value close to 1 or 100% (in percentage form) means perfect correlation. In terms of FDAC objective function, the shift at a fixed frequency ω_a in the FE model is defined as the difference

$$\Delta\omega_{shift}(\omega_a) = \omega_x^* - \omega_a \tag{6.7}$$

where ω_x^* is the frequency at which FDAC reaches its maximum for all measured frequencies. One of the main advantage of the FDAC in linear model updating is its insensitivity to relative scale factor of the two responses and the flexibility in selecting frequency points to be correlated making it a useful method for frequency response 'shape' correlation. Taking the shape of the frequency response into consideration, the improved FDAC can be written in the form

$$FDAC(\omega_a, \omega_x, j) = \frac{([H_a(\omega_a)]_j^T [H_x(\omega_x)]_j)}{\left|[H_a(\omega_a)]_j\right| \left|[H_x(\omega_x)]_j\right|} \tag{6.8}$$

In this context, FDAC takes values in the range [(-1, 1) or (-100%, 100%)], where a value of FDAC near 1 or 100% means both frequency responses have a high shape similarity. Evaluating equation (6) for a given set of FE and measured responses within the same frequency bandwidth,

the FDAC value is obtainable. A perfect updated model will have only positive unitary values for all(ω_x) =(ω_a),and as a result, the criteria for the shape and equal frequency pairing of the FE model response will be given by a percentage value. The FDAC was selected for the final objective function based on its current existence in linear model updating for model correlation and model validation approach as discussed in [241, 242].

The non-linear FE model updating was performed using a gradient-based optimiser to calculate the sensitivities of the objective function with respect to the design variables. The fmincon algorithm in Matlab [253] is used to solve the error minimisation problem, gradients calculations are performed with a standard interior-point approach using Forward Finite Differences (FFD) method. To minimize the deviation between the FE and measured response, the non-linear stiffness parameters at the associated DOF of the FE model were updated, see Table 6.9 for the arrangement of the parameters and coefficients used in the updating process. The initial frequency response obtained from the upgraded FE model in Figure 6.19 showed that the coefficients of the non-linear parameters used for the numerical predictions were too high, hence large deviations were observed between the predicted and measured response as shown in Figure 6.19. With this knowledge, the non-linear terms ($i.e.x^3, x^2$) and coefficients in Table 6.9 were used as the design variables in the updating process.

The starting point (initial values of the design variables) were the coefficients of the polynomial terms identified in non-linear identification section, (see Table 6.9 for details) while each design variable was allowed to vary within ±0.6% of the starting value. The Matlab fmincon algorithm was used to find the coefficients of each cubic and quadratic term that minimises the objective function, a total of 15 iterations was achieved before obtaining the values that satisfies the local minimum of the objective function. The non-linear updating was performed near modes 1 and 2 using the non-linear frequency response obtained from 5N excitation level. Figure 6.20 shows the results obtained after the non-linear updating process. The estimated non-linear parameters obtained from the updated model, along with the initial non-linear parameters, are presented in Table 6.10. From this table, a significant improvement can be observed across the coefficients of the cubic terms while the coefficients of the quadratic terms remain unaffected.

In addition, the coefficients of the cubic terms connecting nodes 1 and 7 have reduced

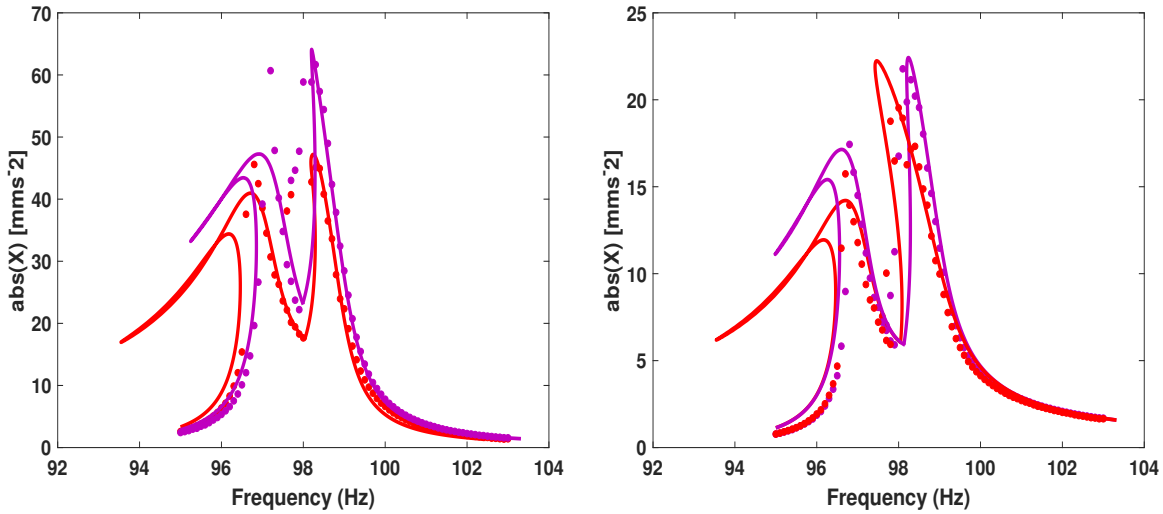

(a) (b)

Figure 6.20: *Comparison of Stiffness updated acceleration responses with measured data for modes 1 and 2. (a) node 1 and (b) driving point across two force levels. Dotted lines are from experiments, continuous lines are from the updated upgraded FE model.*

considerably compared with the coefficients connecting nodes 2, 7, and 15. This is probably related to the fact that the non-linear elements across node 2, 7 and 15 are more activated due to their closeness to the excitation source compared with the other non-linear element in the model. In general, the shape and data of the updated FE frequency response show very good agreement with the experimental response. This also indicates that the updated estimated coefficients are more accurate. The accuracy of the updated FE model was quantified by calculating the normalised ($I^2 - norm$) error of the discrepancies between the response of the updated model and the measured data. The frequency response for load case 4N and 5N was used in computing the norms:

$$E_H = \frac{\|H^a - H^x\|}{\|H^x\|} \times 100 \tag{6.9}$$

where H^a and H^a are the updated model and frequency response, and $\|\|$ corresponds to the ($I^2 - norm$) error. In addition, the value obtained for the objective function was also used to judge the accuracy of the updated model.

Table 6.11 presents values of the percentage error and objective functions for 4N and 5N levels of excitation While the shapes of the updated FE frequency response (i.e. 5N red) correlates

Nonlinear Element	Node Connection	DOF Connection	Model	Stiffness values before updating	Stiffness values after updating N/m
1	Node_1-Node_7	Dof_1x- Dof_21x	x^3	-7.4e12 (N/m^3)	-1.9e11 (N/m^3)
2	Node_1-Node_7	Dof_1x -Dof_21x	x^2	1.5e7 (N/m^2)	1.5e7 (N/m^2)
3	Node_2-Node_15	Dof_4x -Dof_45x	x^3	-7.4e12 (N/m^3)	-0.2e12 (N/m^3)
4	Node_2-Node_15	Dof_4x -Dof_45x	x^2	1.5e7 (N/m^2)	1.5e7 (N/m^2)
5	Node_7-Node_15	Dof_21x -Dof_45x	x^3	-7.4e12 (N/m^3)	-3.8e12 (N/m^3)
6	Node_7-Node_15	Dof_21x -Dof_45x	x^2	1.5e7 (N/m^2)	1.5e7 (N/m^2)

Table 6.10: Updated Non-linear Stiffness Coefficient

Excitation Level	Objective Function (FDAC)	Error (E_{H})
4N	87.3 %	12.4 %
5N	84.1 %	15.7 %

Table 6.11: Error and objective function values (%) for the Non-linear Stiffness updated FE model

well with the measured data, the percentage error and objective function values are slightly different when the same model is used to predict the response at 4N (pink) ,as shown in Table 6.11. This can be related to the characteristics of the non-linear features in the test structure, where the response amplitude decreases as the excitation force increases. This also relates to the evidence of non-linear damping in the response of the structure at higher excitation levels. It is worth noting that the updating was performed using the 5N excitation response before using the same updated parameters to predict the response at 4N.

Finally, while the updated and predicted FE responses show good agreement with the available set of measured data points most especially for modes 2, there is still a large percentage discrepancy between the FE response and measured data, most especially around the regions of the resonance peak of mode 1, where some interesting dynamics (like a long backbone response) which are not seen in the measured data is observed in the FE response. This is more evident around the resonance peak of mode 1as illustrated in Figure 6.20, where it is extremely difficult to select the true value for the new maximum vibration amplitude and resonance frequency due to long backbone response observed. As a result, it is evident that the non-linear FE model could

still be improved further to enhance its predictive capacity and also increase to the accuracy of the whole model by reducing the normalised error value.

6.3.4.4 Non-linear Damping Identification Based on Model Updating

The upgraded FE model in section 5.1 only included non-linear stiffness terms. In this section the aim is to further improve the accuracy of the non-linear FE model by including non-linear damping terms in the already updated non-linear FE model. The assumption here is based on the results obtained from the first updating process where the current non-linear FE model fails to predict the response amplitude of the structure to an acceptable value or at least to similar response shape observed in the experimental test. Estimation of non-linear damping parameters /coefficients remains a challenging aspect of non-linear system identification with little or no understanding. In phase II (section 4.3.2), the results obtained from the HT identification based on sine-sweep data showed the damping characteristics was non-linear, however obtaining a parametric model for the damping was not feasible.

Using the knowledge of the result obtained from the non-linear stiffness FE model updating, where the coefficients of the cubic terms had the highest level of convergence or improvement, it was obvious that a cubic non-linear spring element was an acceptable choice for modelling the stiffness. In this section, a similar arrangement used in the non-linear stiffness modelling was implemented in modelling the non-linear damping characteristics. The main difference here is that only cubic spring dampers were considered in the design variables for this updating process, the starting (initial values of the design variables) were set to $1Ns/m$, while each variable was allowed to vary between $(1-1000Ns^3/m^3)$ as a first start since there was no prior knowledge of the coefficients. The objective function was left unchanged Matlab fmincon algorithm was used to find the coefficients of each cubic term that minimizes the objective function, a total of 25 iterations was completed before obtaining the values that satisfies the local minimum of the objective function.

Table 6.12 presents the non-linear damping model updating arrangement and the estimated cubic coefficients after updating Similar to the stiffness updated model, the non-linear damping updating was conducted using the 5N (red line and dots) response. Of interest is also for the new

Nonlinear Element	Node Connection	DOF Connection	Model	Damping values before updating Ns^3/m^3	Damping values afterupdating Ns^3/m^3
7	Node_1-Node_7	Dof_1x-Dof_21x	x^3	1	4.2
8	Node_2-Node_15	Dof_4x-Dof_45x	x3	1	11.7
9	Node_7-Node_15	Dof_21x-Dof_45x	x3	1	23.9

Table 6.12: Updated Non-linear Damping Coefficient

upgraded and updated FE model to be able to predict the response of the structure at either higher or lower excitation levels. one more excitation 4N (pink) level was computed using the parameters from the newly updated FE model, measurement at the corresponding level of excitation were also obtained during the test. In Figure 6.21, the frequency response of the newly updated FE model is compared with measured data, a good agreement between both measured and predicted response is observed. To assess the improvement caused by the inclusion of cubic dampers in the FE model, the accuracy of the damping updated FE model was quantified by calculating the normalised ($I^2 - norm$) error of the discrepancies between the frequency response of the newly updated model and the measured data. These values were compared with the previous values listed in Table 6.11.

The corresponding errors and improvement are illustrated in Table 6.13. In Table 6.13, the objective function and error values obtained from the non-linear damping updating are presented for each excitation levels. From the table, one can observe a significant improvement of about 10% in the objective function values, also the normalised error values are now below 10%. This is more evident in the shapes of the non-linear frequency responses illustrated in Figure 6.21, compared to the initial responses illustrated in Figure 6.20 where a long backbone characteristic is observed in the first mode. The new non-linear FE responses with non-linear dampers do not show such particular behaviour, rather the new updated FE response show similar shape and agreement with measured data. Furthermore, the new updated non-linear FE frequency responses also illustrates the importance of including the non-linear dampers in the initial stiffness updated FE model through their good agreement with measured data at different excitation levels.

To validate the accuracy of all non-linear parameters and corresponding coefficients in the

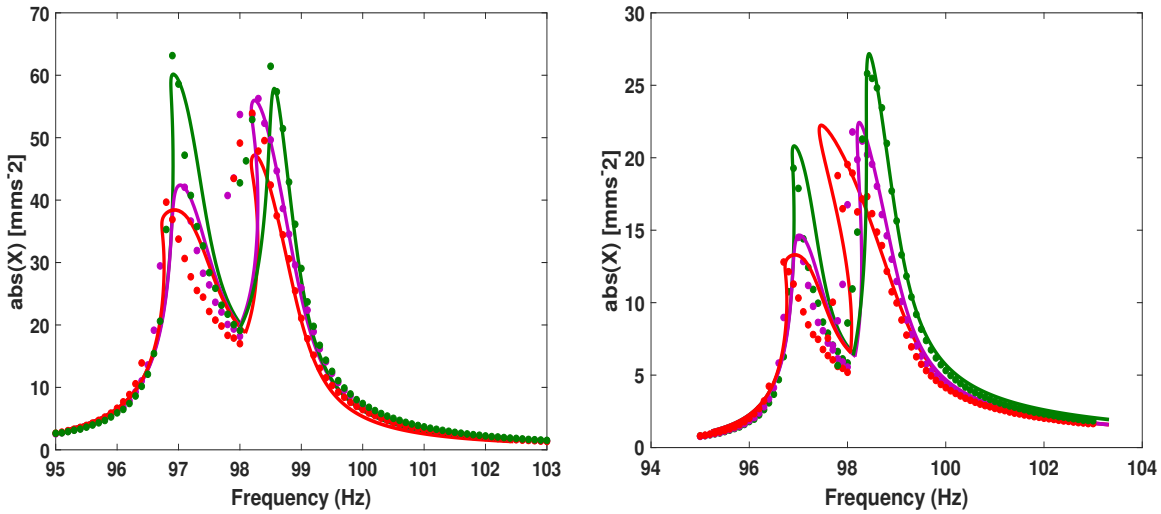

(a) (b)

Figure 6.21: *Comparison of Damping and Stiffness updated acceleration responses with measured data for modes 1 and 2.(a) Node 1 and (b) drive point across three force levels. Dotted lines are from experiments, continuous lines are from the updated upgraded FE model.*

non-linear FE, the model was used to predict the response of the structure and compared with measured data at 3N (green) as shown in Figure 6.21. The comparison of both responses at 3N in Figure 6.21 are in very good agreement with exact measured data points lying on the FE response, the equivalent objective function and normalised error values were also calculated and illustrated in Table 6.13 to quantify the validity and accuracy of the correlation between the FE response and measured data for this excitation case. The normalised error and objective function have been particularly useful in this case, since they are insensitive to the relative scale factor of two responses and to the frequency shift that might affect them.

In addition, both parameters do not require that the frequency responses be defined at the same frequency points, making them useful indicators for quantifying the accuracy and validity of the correlation between both numerical and measured Frequency responses. Table 6.13 illustrates the error distribution between the linear and non-linear model. In Table 6.13, while an improvement of around 10% is observed in the values of the objective function and normalised error for 4N and 5N excitation level, the values obtained for these parameters at 3N which was not used in the updating stage even show higher percentage accuracy of 97.2% for the

Excitation Level	Objective Function 1 (FDAC)	Error (E1_H)	Objective Function 2 (FDAC)	Error (E2_H)	Error Improvement
3N			97.2	2.8%	
4N	87.3 %	12.4%	96.8	3.2%	9.2%
5N	84.1 %	15.7 %	93.5	6.5%	9.2%

Table 6.13: Error distribution across the Upgraded non-linear FE model

objective function and 2.8% for the normalised error value, this could be as a result of the fact the non-linearity is not fully activated in at this excitation level compared to the higher levels.

Here, a model with a lower normalised error implies that the prediction error or residuals between the predicted model and the observed model is low and also shows that both the predicted non-linear FE model and corresponding measured data are in good agreement. Finally, the discrepancy between the measured and predicted maximum acceleration for the 3N and 4N load cases are within 1% and also much lower than the discrepancy obtained in linear model validation stage, the objective function values in Table 6.13 and correlation plots in Figure 6.21 also show that the shapes of the non-linear responses are well persevered within the excitation range for both the experimental and FE results. All these evidences are used as an indicator for a good validated non-linear model.

6.3.4.5 Validation of the Non-linear Model

The last step in phase three is validation of the non-linear model, this step is conducted to assess the predictive capabilities of the newly generated non-linear FE model and also evaluate the accuracy of the updated non-linear parameters in the presence of new data. This step can be achieved by performing the validation against a controlled structural modification or evaluating the predictive performance of other modes of the structure. In this case, the validation was conducted by comparing the predicted response of the third mode (141.3Hz) against newly measured force controlled stepped sine test. The new measured stepped sine test data were not used in the non-linear identification phase.

Figure 6.22 shows the newly computed non-linear FE response for mode 3 compared with stepped sine test data, the new non-linear response was generated using the updated non-linear

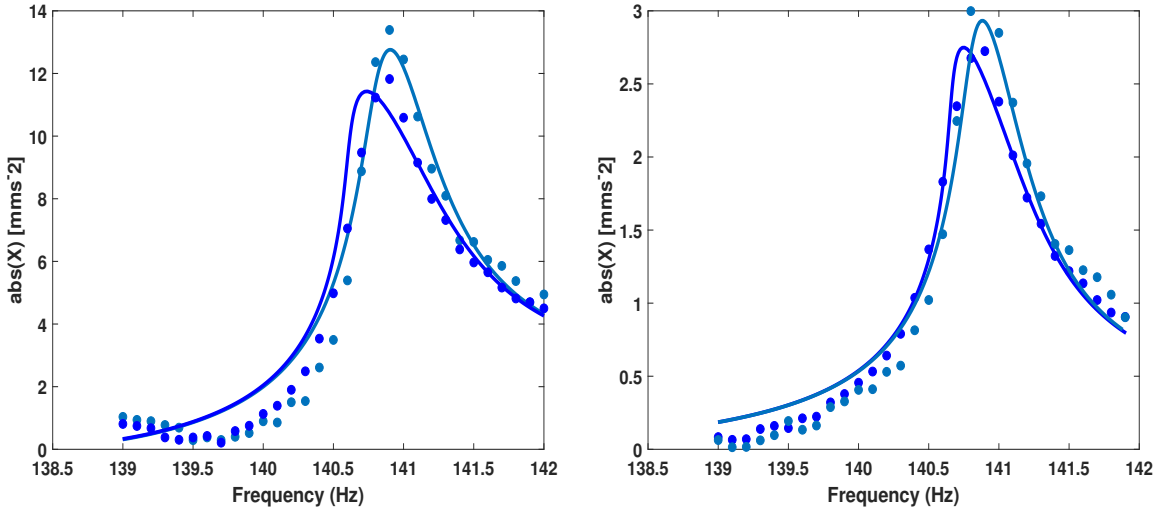

(a)

(b)

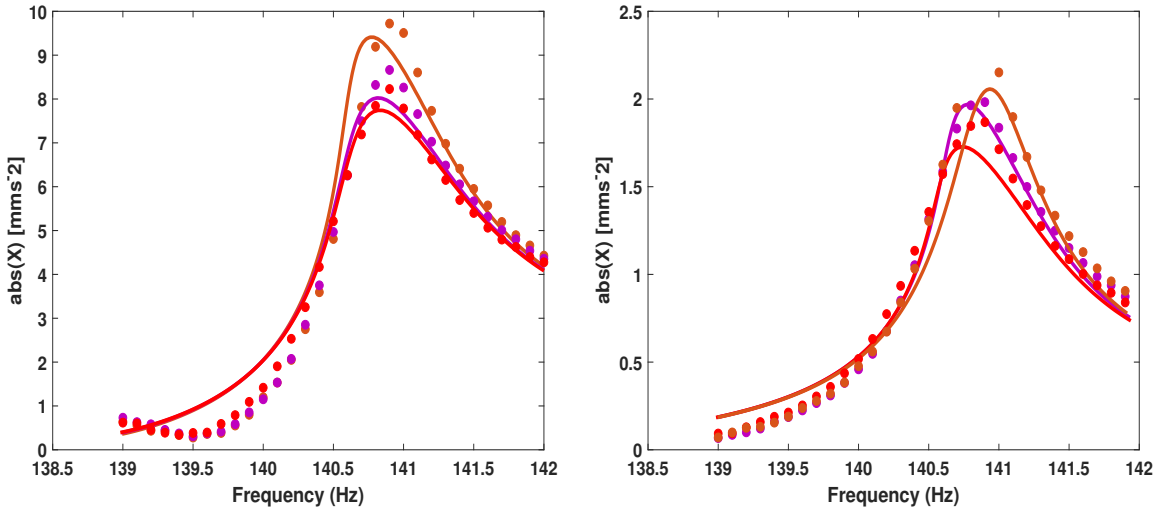

(c)

(d)

Figure 6.22: *Comparison of measured and FE predicted acceleration responses for mode 3 of the non-linear assembly. (a) Node 1 at 1N and 3N force level; (b) drive point at 1N and 3N ;(c) Node 1 at 4N, 6N and 7N force level; (d) drive point at 4N, 6N and 7N force level. Dotted lines are from experiments, continuous lines are from the predicted FE model.*

model obtained in Figure 6.21. Although the third mode indicates the presence of more damping non-linearity compared to the previous modes, the results presented in Figure 6.22 the predictive abilities of the non-linear FE model. While some discrepancies are observed between the computed responses and the measured data at the starting frequencies of the results in Figure 6.22, the

Excitation Level (N)	FDAC (%)	Error (%)
1	95.7	4.3
3	95.7	4.3
4	93.8	6.2
6	93.8	6.2
7	93.8	6.2

Table 6.14: Validation and Error Results Using FDAC and Normalised Error Values

overall shape and trend of the non-linear response was observed to be in good agreement with measured data. It is worth stating that the third mode (141.3Hz) is a local mode of the flexible curved beam which was not instrumented with accelerometers due to the light weight of the curved beam.

However the successfully correlation of the local mode on other measured points of the structure without changing any non-linear parameter shows a good predictive performance for the new non-linear FE model. The error between the computed acceleration response and measured data for the third mode was quantified by normalising the acceleration responses using the normalised error formulae in Equation 6.5 and the Frequency Domain Assurance Criterion (FDAC) as a good correlation indicator. Table 6.14 shows the FDAC percentages and the error distribution for the third mode of the structure.

6.4 Conclusions

In this chapter, a case study considering and accounting for the effects of non-linearities when performing model validation activities in structural dynamics is presented. Furthermore, we have provided a practical methodology for integrating already-existing linear model validation techniques with recent developments in non-linear system identification and numerical modelling to offer a pragmatic solution to the ongoing challenge in the area of non-linear structural dynamics. From the results, we can conclude that the finite element model validation of structures with local non-linearities is feasible to an acceptable degree of engineering accuracy. This is attributed to the progress in the area of non-linear system identification, increased development of numerical algorithms for computing the periodic solution of non-linear systems and finally, the ability to integrate the theoretical concepts and experimental knowledge of non-linear systems with the current validation techniques in linear systems.

The overall aim of the chapter has been to demonstrate a logical approach to validating finite element models of structures with localised non-linearities, based on knowledge obtained from the linear model validation of the structure of interest and measured data. The aim was achieved by following the 3 phases illustrated in Figure 1, Linear Validation, Non-linear Identification and Non-linear Model Validation. The methodology was also outlined in sequential steps making it possible to comment on the strengths and weaknesses of each step in each phase before moving on to the next phase. This kind of approach can be considered as a useful tool for industrial engineers that are confronted with similar challenges. Although the whole methodology still relies on careful and time-consuming FE and experimental procedures, the experimental validation of non-linear FE models can now be attempted using measured stepped-sine data.

Phase I, which is associated with the linear validation of the test structure, was executed using classic linear validation tools and methods such as EMA and MAC. This part of the methodology is already developed and does not require the derivation of new methods or technology. However, phases II and III which involve the experimental non-linear identification and non-linear model validation of the structure are executed using selected methods that were suitable for each step in the methodology. In phase III, periodic solutions of the non-linear FE model were computed

using the shooting method which was also used to gain insight into the dynamic response of the structure. These results were validated using experimental data obtained from force- controlled stepped-sine test data. The robustness of the non-linear FE model was validated by using the FE model to predict the response of the structure for different excitation levels which were subsequently correlated with measured data. The reliability of the validation was quantified by calculating the normalised error between the measured and model predicted response. In Table 6.13 and 6.14 the final error values all fall below 10%, which are all within the uncertainty quantification region.

Comparing the predicted FE response at 5N in Figure 6.21 and in Figure 6.9, it is obvious that the FE response in Figure 6.21 is in closer agreement with its corresponding measured data compared to the former. With this observation, one also measures the importance of upgrading the already-validated linear model in phase I with the identified non-linear elements in phase II, to develop the validated non-linear FE model presented in phase III. This type of sequential work flow is certainly more helpful in understanding the non-linear behaviour and predicting the non-linear response of the structure of interest. Regardless of the advances in non-linear system identification, there are still several challenges that need to be addressed in this area. One of the major challenges is the lack of reliable methods or algorithms to identify precisely the multiple non-linearities present in our current day design. In section 6.3.3.2, we used sine-sweep data for 2 modes to estimate a polynomial model for the physical stiffness representation of the non-linearity across the two cantilever beams.

However, at the end of the finite element model validation phase (phase III), a total of 9 non-linear elements were successfully identified of which 6 were quantified during the non-linear model updating stage and the other 3 remained unaffected. Hence, there is also a need to account for the sensitivity of each non-linear element in the FE model and also to rank their degree of significance in the FE model. Finally, it is also important to develop better algorithms and methods for quantifying the percentage correlation / error between non-linear FE responses and measured data, rather than the normalised error values which were used in this chapter. The reward in venturing into this research area of structural dynamics would help the community to acquire more knowledge and understanding in accurately predicting the actual vibration

amplitude of structures with non-linear features. Results from such research investment will not only benefit the academic community but would also be of great advantage to industrial partners to enable accurate prediction of fatigue life of structures with non-linear behaviour.

CHAPTER 7

CONCLUSION

The overall aim of the research presented in this doctoral thesis was to contribute to the development of methods and strategies for tackling the increasing challenge associated with the verification and validation of nonlinear phenomena encountered the design of vibrating structures. The scope of the work presented in this thesis was dedicated to the integration of two distinct competences (experimental testing and simulation), for the progression of current approaches to solving the on-going non-linear structural dynamic difficulties encountered when designing engineering structures. To accomplish the aim of the research presented in this thesis, three key objectives were highlighted and discussed in the introductory section of this thesis. These objectives are:

1. *Develop a black-box data-driven approach for detection and characterisation of nonlinearities for structures with multiple nonlinear sources and dynamic modes.*

2. *Propose an effective time-domain grey-box algorithm for experimental identification of nonlinear parametric models.*

3. *Demonstrate a pre-digital-twin framework for nonlinear vibrating structures using a white-box modelling approach.*

The first objective was addressed in Chapter 3 where an existing black-box oriented nonlinear state space method was used to develop a data driven identification approach for representation of the non-linearities observed in vibrating structures with multiple nonlinear sources and dynamic modes. A discrete-time PNLSS model was developed for the identification and validation of the non-linear phenomena using measured input and output data only without any prior nonlinear physics based knowledge of the structure under consideration. In addition, this chapter also investigated a specific challenge often encountered when deriving and using black-box models which is the choice between the flexibility and parsimony of the identified non-linear models. This challenge was addressed in Section 3.5.6 by conducting and validating a series of simulated experiments using seven different monomial combinations to derive the most suitable PNLSS model with the lowest number of parameters capable of reproducing the non-linearities observed across multiple vibration modes.

The developed data-driven identification approach was applied on experimental data obtained from the test campaign conducted on a large assembled aero-engine casing structure. The success of the identified PNLSS models were judged based on RMS errors between the data simulated from the PNLSS model and the true measured data, where RMS values of 1.58% and 1.44% were obtained on the identification and validation of the best PNLSS model illustrated in Figures 3.14 and 3.15. An important result obtained in this chapter is attributed to evidencing the flexible mathematical structure of black-box models, where different PNLSS models with monomial degree combinations ranging between orders (2 and 7) were introduced to the measured data for the aero-engine casing. Results obtained were presented in Tables 3.3 and 3.4, where a PNLSS model with monomial degree combination of (3, 5, 7) was identified as the most suitable model capable of reproducing the nonlinear behaviour observed on experimental data measured at a local bolted connection of the aero-engine casing. This result also strengthens and correlates well with current notion that odd polynomials are very useful for modelling nonlinearities originating from joints or bolted connections as evidence in the ref [232]. Three main contributions demonstrated in this chapter are highlighted as:

- *The developed black-box oriented PNLSS data driven identification approach proves that black-box models can still be considered as useful tools for identifying and interpreting*

non-linearities in structural dynamics.

- *The applicability of the identification approach was demonstrated on a large aerospace structure, where it was evident that a parsimonious PNLSS model was capable of describing observed complex nonlinear characteristics.*

- *Model errors between the measured data and final identified PNLSS models obtained from identification and validation cases studies were below 3%.*

To overcome two limitations of the developed PNLSS data driven identification approach presented in Chapter 4, the second objective of this doctoral thesis was achieved in Chapters 4 and 5. These two limitations being the very large number of estimated nonlinear parameters and the difficulty in extracting physics based meaningful quantified parameters. These disadvantages led to the introduction of a novel time domain grey-box state space identification method capable of identifying structural nonlinear stiffness and damping parameters. The proposed algorithm was based on combining the existing PNLSS method used in Chapter 3 with the existing concept of treating non-linearities as internal feedback forces to the underlying linear model of the system. These ideas were used to develop a grey-box state space identification algorithm. An important attribute of the proposed grey-box identification algorithm is that the formulation of the identification theorem is based on modifying the structure of the original black-box PNLSS matrices. Here, the a discrete-time PNLSS model equation (as in Equation 3.13) with nonlinear functions which depend on the states x and the input u is modified to a structured PNLSS state space of the form shown in (Equations 4.24 and 4.24). The resulting formulation contains nonlinear functions that depend on the model displacement and velocity, thus turning the black-box PNLSS model algorithm to the grey-box PNLSS model algorithm. The modifications made to the black-box PNLSS matrices were devoted to formulating a grey-box algorithm with the ability to extract physics-motivated reduced number of nonlinear parameters during the identification.

The proposed time domain grey-box PNLSS identification method was first successfully applied to a numerical single degree of freedom Duffing oscillator example in Chapter 4 where nonlinear stiffness and damping coefficients were identified. Similar to Chapter 3, the accuracy of each identified nonlinear parameter and coefficients was calculated based on the relative

error between the identified and the true coefficients as illustrated in Table 4.2. In addition, correlation and RMS error between the true and identified sine-sweep, nonlinear stiffness and damping curves presented in Figures 4.12 and 4.15 were also used to measure the confidence of the estimated parameters. To test the identification capabilities of the proposed grey-box state PNLSS identification method further and with all real-world imperfections. A practical application of the method on a larger scale was presented in Chapter 5. Here the non-linearities observed at the bolted connection of an aerospace structure was successfully identified and validated using measured sine-sweep and multi-sine data. Results obtained from this demonstration showed that the method can be confidently applied to measured data with an accuracy of 95% correlation between the measured and identified time-domain response. Three key findings drawn from the work presented in these two chapters are:

- *The proposed grey-box method is able to identify nonlinear models that has the advantage of being parameter-parsimonious, where the number of estimated nonlinear coefficients are minimal and posses physics-based interpretation of the model.*
- *Tracking the evolution of each identified nonlinear parameter and corresponding coefficient is a key feature embedded in the method, providing the possibility of visualising the nonlinear stiffness and damping curve.*
- *Application of the method on both simulation and experimental case studies yielded RMS model errors below 5%.*

While the last two objectives were centred around the development and application of nonlinear identification methods using experimental data, implementation of the identified nonlinear features in a virtual sense or development of early stage digital twin models of the identified nonlinear characteristics is of interest to practising engineers. To this end, the final objective of the research focused around the above interest is covered in Chapter 6. Where the importance of integrating two different research techniques, experimental tests and simulations, for effective modelling and validation of engineering structures exhibiting different nonlinear phenomena is demonstrated. The entire test and simulation integration is based on a coherent framework consisting of 10 different steps that permits the extension of current modal testing and analysis

procedure for linear structural dynamics to engineering structures with local non-linearities. The 10 steps listed in this framework are grouped into three phases. Phase I involves the use of classic linear tools to derive an Underlying Linear Model (ULM) of the structure. In Phase II, specific tests and measurements are conducted under controlled excitation for the identification and characterisation of nonlinear features, while Phase III is devoted to augmenting the underlying linear model with the identified nonlinear elements and validating the augmented model.

The integration strategy was successfully applied to an assembled multiple cantilever beam structure, where polynomial type non-linearities are identified and validated. The usefulness of integrating test and simulation in this way is in the complimentary roles that test and simulation can play when addressing some of the challenges experienced in nonlinear structural dynamics. An example is the aspect of using simulated models to develop the required experimental testing for a given engineering structure. Similarly, the experimental testing and data can be used to extract important modelling parameters such as damping and most importantly, cross validating the simulated model. The main contributions originating from this chapter are:

- *An integration strategy for experimental identification and simulation of nonlinear vibrating structures is presented and demonstrated on a test structure.*

- *Augmentation of validated linear simulation models with nonlinear elements to account for observed nonlinear behaviour was proven to be plausible.*

- *Implementation of nonlinear damping elements for improved nonlinear response prediction led to the reduction in the NRMSE between the test and simulation models from 15.7% to below 10%.*

In conclusion, in spite of the recent developments and contributions of this thesis, there is not yet a single or universal approach to addressing most of the challenges encountered in the field of nonlinear structural dynamics. This can partially be attributed to the individualistic nature of nonlinear systems. However, exploring a combination of the respective methods and analysis demonstrated in this thesis can be used to provide increasing insight and physics-based predictive capabilities outcome to some of these challenges. Most importantly, all methods and procedures

stated in this thesis have all been demonstrated on physical engineering structures of different sizes. This can be seen as a further progress in responding to industrial needs and applications.

7.1 Suggestions and Future Direction of the Research

The results presented in this thesis have shown significant progress towards addressing some of the nonlinear structural dynamics challenges encountered during the design and manufacturing of components subjected to vibrations and dynamic loads. While the results presented herein indicate a level of advancement, there is still more work and avenues for continuous research to develop these techniques and extend the applicability of currently available methods and framework to large-scale, complex real-world structures. Some future research topics relevant to the work presented in this thesis and nonlinear structural dynamics in general are listed and discussed below.

- *Spatial location and characterisation of distributed structural non-linearites*.

Majority of the work presented in this thesis have been devoted to challenges arising from localised non-linearites in engineering structures. But most engineering structures are made of multiple components and complex geometries causing non-linearities to originate from different parts of an assembled structure. Therefore, developing a robust method capable of locating and characterising structures with distributed non-linearities would be a meaningful advancement in this research domain. At the moment, most nonlinear identification methods are based on lumped parameter nonlinear modelling or assumed localised non-linearity as presented in the literature review. A proposed approach that could potentially be used to address this specific challenge is the use of nonlinear state-space models implemented in Chapter 3 and Chapter 4. The flexible and mathematical model structure of these state-space models could be seen as an advantage and in practice can be applied to structures with distributed non-linearities without any limitations. However, as demonstrated in Chapter 3, extracting physical interpretation of the system under consideration can be challenging or sometimes impossible. This challenge would need to be considered when developing new methods.

- *Ranking and assessment of nonlinear dynamic modes*.

In the literature review chapter, three steps (detection, characterisation and parameter estimation) were listed as prerequisite for a successful nonlinear identification. Whilst there are many available methods for detecting non-linearity, the question of whether the detected non-linearity should be considered or progressed to a full nonlinear identification remains unanswered. An example of this is illustrated in the practical case study of the aero-engine casing in Chapter 3, where three nonlinear consecutive modes were detected but not assessed quantitatively before progressing to full nonlinear identification. This can be narrowed down to the unique nature of nonlinear systems, where as currently described the the literature, some structures can be considered to possess characteristics of weak non-linearities while some can be strongly nonlinear. For this purpose, the development of techniques capable of ranking or assessing the strength of the non-linearity detected in a system would be of future benefit. Typical solution that could be offered to this particular challenge could start with examining the variation in the frequency and vibration amplitude of response under different dynamic loading for the structure under consideration. Then, a suitable variation score or ranking could be used to determine the strength of the detected non-linearity.

- *Development of robust identification methods for nonlinear damping mechanism*.

Modelling of damping mechanism has always been a known challenge in structural dynamics. While the research on estimation of linear damping parameters have received a significant attention, nonlinear damping on the other hand has so far received relatively little attention since most developed nonlinear identification method address only stiffness non-linearities. Another avenue to progress this research is the advancement of numerical and experimental methods through the use of nonlinear optimisation routine and tools such as the Levenberg-Marquardt method to properly account for characteristics of nonlinear damping (e.g., friction, joints, sliding contacts, micro and macro slips) as demonstrated in Chapter 4 and Chapter 6 during the identification and validation process.

- *Uncertainty quantification associated with verification and validation of structural non-linearites*.

A challenge that is often associated with the successful design of a structure is uncertainty, which can be represented through imprecision and system variability or through lack of awareness and inadequacy. For example, it is common in structural dynamics to observe the influence of noise, boundary conditions and experimental set-up on measured data, this can often cause scattering or dispersion within the band of accuracy of certain parameters used during an investigation. In addition, for simulations or computational modelling, uncertainties are not often considered even though a change in a simulation parameter can cause a substantial alteration on the response of the mechanical system under consideration. An important requirement frequently requested by engineers and researchers is a method or integrated strategy of identifying and accounting for such uncertainties during a design and validation exercise. Future research should therefore consider incorporating uncertainties for both experimental and simulation activities to attain better structural designs.

Nonlinear system identification in structural dynamics remains an active research topic, where the the development and use of individual toolbox philosophy is largely adopted by most researchers and industrial engineers. This toolbox adoption can partially be associated to the distinctive nature of nonlinear systems as proven in this thesis. Whilst a large percentage of this work has been focused on validation of nonlinear structures, the growing interest of the digital twin concept is set to disrupt the traditional ways of designing and validating structural models. A digital twin as defined in the introduction is a virtual representation or twin of the physical system. This means that the digital twin of a design would consist of a real-time description and monitoring of of the product, from product design to end of life. To achieve this, further developments beyond the integration of test and simulation models are required. The digital-twin will involve both test and simulation models as prerequisite but it will also entail connecting machine learning and other artificial intelligence tools together with real-time testing and Internet of Things (IOT) for exchange of data.

BIBLIOGRAPHY

[1] D.J.Ewins (2000) Modal Testing. Theory, Practice and Application, Research Studies Press Ltd, Hertfordshire, England, SG7 6AE.

[2] B.Peeters, H.VanderAuweraer, P.Guillaume, and J.Leuridan (2004) The PolyMAX frequency-domain method: A new standard for modal parameter estimation. *Shock and Vibration,* **11**(3-4), 395–409.

[3] P.Van Overschee, B. M. (1994) N4SID:Subspace algorithms for the identification of combined deterministic-stochastic systems. *Automatica,* **30**, 75–93.

[4] J.S.Juang, R. (1985) An eigensystem realization algorithm for modal parameter identification and model reduction. *Journal of Guidance, Control and Dynamics,,* **12**, 620–627.

[5] R.J.Allemang and D.L.Brown (1998) A unified matrix polynomial approach to modal identification. *Sound and Vibration,* **221**, 301–322.

[6] J.P.Noël and G.Kerschen (2017) Nonlinear system identification in structural dynamics: 10 more years of progress. *Mechanical Systems and Signal Processing,* **83**, 2–35.

[7] T.W.Clyne, W.P.Beaumont, and H.C.Zweben (2017) Comprehensive Composite Materials II.: Metal Matrix Composites, Elsevier, .

[8] V.V.Bolotin (1996) Delaminations in composite structures: its origin, buckling, growth and stability. *Composites Part B: Engineering,* **27**(2), 129–145.

[9] J.R.Ahlquist, J.M.Carreno, H.Climent, R.deDiego, and J.deAlba Assessment of Nonlinear Structural Response in A400M GVT. In *Proceedings of the 28th International Modal Analysis Conference (IMAC)* Springer.

[10] J.P.Noel, L.Renson, G.Kerschen, B.peeters, S.Manzato, and J.Debille Nonlinear dynamic analysis of an F-16 aircraft using GVT data. In *Proceedings of the International Forum on Aeroelasticity and Structural Dynamics (IFASD)*.

[11] K.Carney, I.Yunis, K.Smith, and C.Y.Peng Nonlinear-Dynamic-Behavior-Cassini-Spacecraft-Modal-Survey.. In *Proceedings of the 15th International Modal Analysis Conference (IMAC)*.

[12] G.Kerschen, K.Worden, A.F.Vakakis, and J.C.Golinval (2006) Past, present and future of nonlinear system identification in structural dynamics. *Mechanical Systems and Signal Processing,* **20**(3), 505–592.

[13] M.F.Platten, J.R.Wright, J.E.Cooper, and G.Dimitriadis (2009) Identification of a Nonlinear Wing Structure Using an Extended Modal Model. *Journal of Aircraft,* **46**(5), 1614–1626.

[14] A.Carrella and D.J.Ewins (2011) Identifying and quantifying structural nonlinearities in engineering applications from measured frequency response functions. *Mechanical Systems and Signal Processing,* **25**(3), 1011–1027.

[15] S.T.Trickey, L.N.Virgin, E. The stability of limit-cycle oscillations in a nonlinear aeroelastic system. In *Proceedings of the Royal Society of London* Series A pp. 2203–2226.

[16] Elshafey, A. A., Haddara, M. R., and Marzouk, H. (2010) Damage detection in offshore structures using neural networks. *Marine Structures,* **23**(1), 131–145.

[17] M.F.Platten, J.R.Wright, G. and E.Cooper, J. (2009) Identification of multi-degree of freedom non-linear systems using an extended modal space model. *Mechanical Systems and Signal Processing,* **23**(1), 8–29.

[18] M.B.Ozer, H.N.Ozguven, T. (2009) Identification of Structural Non-linearities Using Describing Functions.. *Mechanical System and Signal Processing,* **23**, 30–44.

[19] G.Dimitriadis (2002) Experimental Validation of the Constant Level Method for Identification of Non-Linear Multi-Degree-of-Freedom Systems. *Journal of Sound and Vibration,* **258**(5), 829–845.

[20] Software, S. I. Digitalization in industry: Twins with potential. (2019).

[21] Schleich, B., Anwer, N., Mathieu, L., and Wartzack, S. (2017) Shaping the digital twin for design and production engineering. *CIRP Annals,* **66**(1), 141–144.

[22] Wagg, D., Gardner, P., Barthorpe, R., and Worden, K. (2020) On Key Technologies for Realising Digital Twins for Structural Dynamics Applications. In *Model Validation and Uncertainty Quantification, Volume 3* pp. 267–272 Springer.

[23] M.Imregun (2009) Special Issue on Non-linear Structural Dynamics. *Mechanical Systems and Signal Processing,* **23**(1), 5–7.

[24] D.Goege (2007) Fast Identification and Characterisation of Non-linearities in Experimental Modal Analysis of Large Aircraft. *Journal of Aircraft,* **44**(2), 399–409.

[25] E.Petrov and D.J.Ewins (2004) State-of-the-art dynamic analysis for nonlinear gas turbine structures. *Journal of Aerospace Engineering,Proc.of the IMech E,* **218**, 199–211.

[26] S.H.Strogatz (1994) Nonlinear Dynamics and Chaos: With Applications to Physics, Biology, Chemistry, and Engineering., MAAddison-Wesley, Reading.

[27] U.Parlitz (2007) Complex dynamics of nonlinear systems. *Oscillations, Waves and Interactions,* pp. 405–434.

[28] G.Kerschen, V.Lenaerts, and C.Golinval, J. (2003) Identification of a continuous structure with a geometrical non-linearity. Part I: Conditioned reverse path method. *Journal of Sound and Vibration,* **262**(4), 889–906.

[29] U.Fuellekrug and D.Goege (2012) Identification of weak non-linearities within complex aerospace structures. *Aerospace Science and Technology,* **23**(1), 53–62.

[30] A.Carrella (2012) Nonlinear identifications using transmissibility: Dynamic characterisation of Anti Vibration Mounts (AVMs) with standard approach and nonlinear analysis. *International Journal of Mechanical Sciences,* **63**(1), 74–85.

[31] J.Sjoberg, Q.Zhang, L.Ljung, A.Benveniste, B.Delyon, P.Y.Glorennec, H.Hjalmarsson, and A.Juditsky. (1995) Nonlinear black-box modeling in system identification: A unified overview. *journal of Automatica,* **12**(31), 1691–1724.

[32] K.Worden, C.X.Wong, U. A. D. T. F.-B. D. and S.D.Fassois (2007) Identification of pre-sliding and sliding friction dynamics: Grey box and black-box models. *Mechanical Systems and Signal Processing,* **21**(1), 514–534.

[33] M.Eriten, M.Kurt, G. D. L. and A.F.Vakakis (2013) Nonlinear system identification of frictional effects in a beam with a bolted joint connection. *Mechanical Systems and Signal Processing,* **39**(1-2), 245–264.

[34] U.Ascher, J.Christiansen, and R.D.Russell (1979) A collocation solver for mixed order systems of boundary value problems. *Mathematics of Computation,* **33**, 659–679.

[35] D.J.Ewins (2000) Basics and state-of-the-art of modal testing. *Sadhana,* **25**, 207–220.

[36] D.J.Ewins, B.Weekes, and A.DelliCarri (2015) Modal Testing for Model Validation of Structures with Discrete Nonlinearities. *Journal of Philosophical Transaction,* **373**, 1–20.

[37] A.H.Nayfeh and D.T.Mook (2008) Nonlinear oscillations, John Wiley & Sons, .

[38] R.Rosenberg (1961) The normal modes of nonlinear n-degree-of-freedom systems. *Journal of applied Mechanics,* **29**(1), 7–14.

[39] A.F.Vakakis, L.I.Manevitch, Y. M. V. P. A. Z. (2001) Normal modes and localization in nonlinear systems, Springer, .

[40] S.W.Shaw and C.Pierre (1993) Normal modes for non-linear vibratory systems. *Journal of sound and vibration,* **164**(1), 85–124.

[41] Y.A.Kuznetsov (2013) Elements of applied bifurcation theory, Vol. 112, Springer Science & Business Media, .

[42] S.Sharma, E.B.Coetzee, M. S. and B.Krauskopf (2015) Numerical continuation and bifurcation analysis in aircraft design: an industrial perspective. *Philosophical Transactions of the Royal Society A: Mathematical, Physical and Engineering Sciences,* **373**(2051), 20140406.

[43] G.Gatti (2016) Uncovering inner detached resonance curves in coupled oscillators with nonlinearity. *Journal of Sound and Vibration,* **372**, 239–254.

[44] R.J.Allemang Survey of Nonlinear Detection and Identification Techniques for Experimental Vibrations.

[45] Y.Benhafsi, J.Penny, and M.I.Friswell (1995) Identification of damping parameters of vibrating systems with cubic stiffness nonlinearity. In *Proceedings of the 13th International Modal Analysis Conference* Vol. 2460, p. 623.

[46] T.Dossogne, J. and K.Gaëtan (2017) Identification of complex nonlinearities using cubic splines with automatic discretization. In *Nonlinear Dynamics, Volume 1* pp. 51–54 Springer.

[47] E.J.Dempsey and D.T.Westwick (2004) Identification of Hammerstein models with cubic spline nonlinearities. *IEEE Transactions on Biomedical Engineering,* **51**(2), 237–245.

[48] C.M.Richards and R.Singh (2001) Characterization of Rubber Isolator Nonlinearities in the Context of Single- and Multi-Degree-of-Freedom Experimental Systems. *Journal of Sound and Vibration,* **247**(5), 807–834.

[49] C.M.Richards and R.Singh (1999) Feasibility of identifying non-linear vibratory systems consisting of unknown polynomial forms. *Journal of Sound and Vibration,* **220**(3), 413–450.

[50] L.Renson, G.Kerschen, and B.Cochelin (2016) Numerical computation of nonlinear normal modes in mechanical engineering. *Journal of Sound and Vibration,* **364**, 177–206.

[51] S.Stoykov and S.Margenov (2014) Numerical computation of periodic responses of nonlinear large-scale systems by shooting method. *Journal of Computers Mathematics with Applications,* **67**(12), 2257–2267.

[52] E.J.Doedel, A.R.Champneys, T.F.Fairgrieve, Y.A.Kuznetsov, B.Sandstede, and X.Wang (1997) AUTO 97: Continuation and bifurcation software for ordinary differential equations (with HomCont).

[53] A.Dhooge, W.Govaerts, and YU.A.Kuznetsov (2003) Matcont: a matlab package for numerical bifircation analysis of odes. *ACM Trans. Maths. Software,* **29**(2), 141–164.

[54] H.Dankowicz and F.Schilder (2011) An Extended Continuation Problem for Bifurcation Analysis in the Presence of Constraints. *Journal of Computational and Nonlinear Dynamics,* **6**(3), 031003.

[55] B.K.Lee, L.Liu, and W.Chung, K. (2005) Airfoil motion in subsonic flow with strong cubic nonlinear restoring forces. *Journal of Sound and Vibration,* **281**(3-5), 699–717.

[56] K.Ekici, K.C.Hall, and E.H.Dowell (2008) Computationally fast harmonic balance methods for unsteady aerodynamic predictions of helicopter rotors. *Journal of Computational Physics,* **227**(12), 6206–6225.

[57] E.P.Petrov and D.J.Ewins (2003) Analytical Formulation of Friction Interface Elements for Analysis of Nonlinear Multi-Harmonic Vibrations of Bladed Disks. *Journal of Turbomachinery,* **125**(2), 364.

[58] V.Jaumouillé, J.J.Sinou, and B.Petitjean (2010) An adaptive harmonic balance method for predicting the nonlinear dynamic responses of mechanical systems—Application to bolted structures. *Journal of Sound and Vibration,* **329**(19), 4048–4067.

[59] T.Detroux, L.Renson, L.Masset, and G.Kerschen (2015) The harmonic balance method for bifurcation analysis of large-scale nonlinear mechanical systems. *Computer Methods in Applied Mechanics and Engineering,* **296**, 18–38.

[60] R.Brincker and C.Ventura (2015) Introduction to operational modal analysis, John Wiley & Sons, .

[61] K.Worden and G.R.Tomlinson (2001) Nonlinearity in Structural Dynamics: Detection, Identification and Modelling, Institute of Physics, Bristol and Philadephia.

[62] A.B.Stanbridge and D.J.Ewins (1999) Modal testing using a scanning laser Doppler vibrometer. *Mechanical systems and signal processing,* **13**(2), 255–270.

[63] D.DiMaio and D.J.Ewins (2011) Continuous Scan, a method for performing modal testing using meaningful measurement parameters; Part I. *Mechanical Systems and Signal Processing,* **25**(8), 3027–3042.

[64] J.P.Cusumano and B.W.Kimble (1995) A stochastic interrogation method for experimental measurements of global dynamics and basin evolution: Application to a two-well oscillator. *Nonlinear Dynamics,* **8**(2), 213–235.

[65] R.Wiebe, L.N.Virgin, and S.M.Spottswood (2015) Stochastic interrogation of competing responses in a nonlinear distributed system. *Nonlinear Dynamics,* **79**(1), 607–615.

[66] E.Bureau, F.Schilder, M.Elmegård, I.F.Santos, J.J.Thomsen, and J.Starke (2014) Experimental bifurcation analysis of an impact oscillator—Determining stability. *Journal of Sound and Vibration,* **333**(21), 5464–5474.

[67] D.A.W.Barton (2017) Control-based continuation: Bifurcation and stability analysis for physical experiments. *Mechanical Systems and Signal Processing,* **84**, 54–64.

[68] L.Renson, D.A.W.Barton, and S.A.Neild (2017) Experimental tracking of limit-point bifurcations and backbone curves using control-based continuation. *International Journal of Bifurcation and Chaos,* **27**(01), 1730002.

[69] I.D.Breslavsky, E.A.Strel'nikova, and K.V.Avramov (2011) Dynamics of shallow shells with geometrical nonlinearity interacting with fluid. *Computers Structures,* **89**(5-6), 496–506.

[70] A.S.K.Kwan (1998) A New Approach to Geometrical Nonlinearity of Cable Structures. *Computer Structures,* **67**, 243–252.

[71] R.Perez, X.Q.Wang, and M.P.Mignolet (2014) Prediction of displacement and stress fields of a notched panel with geometric nonlinearity by reduced order modeling. *Journal of Sound and Vibration,* **333**(24), 6572–6589.

[72] H.Cho, B.Jeong, M.F.Yu, A.F.Vakakis, D.M.McFarland, and L.A.Bergman (2012) Nonlinear hardening and softening resonances in micromechanical cantilever-nanotube systems originated from nanoscale geometric nonlinearities. *International Journal of Solids and Structures,* **49**(15-16), 2059–2065.

[73] D.M.Tang and E.H.Dowell (2004) Effects of geometric structural nonlinearity on flutter and limit cycle oscillations of high-aspect-ratio wings. *Journal of Fluids and Structures,* **19**(3), 291–306.

[74] M.Amabili and M.P.Paıduo (2003) Review of studies on geometrically nonlinear vibrations and dynamics of circular cylindrical shells and panels, with and without fluid-structure interaction. *Applied Mechanics Reviews,* **56**(4), 349.

[75] W.T.Royle Application of Perturbation Methods to Approximate the Solutions to Static and Non-linear Oscillatory Problems Thesis (2011).

[76] A.Gelb and W.E.VanderVelde (1968) Multiple-Input Describing Functions and Nonlinear System Design, McGraw-Hill Electronic Sciences Series, McGraw-Hill, New York,.

[77] W.F.Ames (2014) Numerical methods for partial differential equations, Academic press, .

[78] R.Bellman (1970) Methods of nonlinear analysis, Elsevier, .

[79] A.Hassan and T.D.Burton (1995) Extraneous solutions predicted by the harmonic balance method. *Journal of Sound and Vibration,* **182**(4), 523–539.

[80] D.W.Jordan and P.Smith (2007) Nonlinear ordinary differential equations: problems and solutions, Oxford University Press Oxford, UK, .

[81] S.Liao (2003) Beyond perturbation: introduction to the homotopy analysis method, Chapman and Hall/CRC, .

[82] S.H.Hoseini, T.Pirbodaghi, M.Asghari, G.H.Farrahi, and M.T.Ahmadian (2008) Nonlinear free vibration of conservative oscillators with inertia and static type cubic nonlinearities using homotopy analysis method. *Journal of Sound and Vibration,* **316**(1-5), 263–273.

[83] S.Liao (2004) On the homotopy analysis method for nonlinear problems. *Applied Mathematics and Computation,* **147**(2), 499–513.

[84] S.Liao (1995) An approximate solution technique not depending on small parameters: a special example. *International Journal of Non-Linear Mechanics,* **30**(3), 371–380.

[85] S.Liao (2005) A challenging nonlinear problem for numerical techniques. *Journal of computational and applied mathematics,* **181**(2), 467–472.

[86] B.J.Lazan (1968) Damping of materials and members in structural mechanics, Vol. 214, Pergamon press Oxford, .

[87] M.Aureli, M.E.Basaran, and M.Porfiri (2012) Nonlinear finite amplitude vibrations of sharp-edged beams in viscous fluids. *Journal of sound and vibration,* **331**(7), 1624–1654.

[88] O.Ozcelik and P.J.Attar (2014) Effect of non-linear damping on the structural dynamics of flapping beams. *International Journal of Non-Linear Mechanics,* **65**, 148–163.

[89] G.R.Tomlinson and J.H.Hibbert (1978) Identification of the dynamic characteristics of a structure with coulomb friction.

[90] C.J.Hartwigsen, Y.Song, M.D.McFarland, L.A.Bergman, and A.F.Vakakis (2004) Experimental study of non-linear effects in a typical shear lap joint configuration. *Journal of Sound and Vibration,* **277**(1-2), 327–351.

[91] W.J.Kim and Y.S.Park (1993) Non-linear Joint Parameter Identification by Applying the Force-state Mapping Technique in the Frequency Domain. *Mechanical System and Signal Processing,* **8**, 519–529.

[92] M.R.W.Brake (2017) The Mechanics of Jointed Structures: Recent Research and Open Challenges for Developing Predictive Models for Structural Dynamics, Springer, .

[93] D.J.Ewins (2016) Exciting vibrations: the role of testing in an era of supercomputers and uncertainties. *Meccanica,* **51**(12), 3241–3258.

[94] Yu.Wang, F.Li, X.Jing, and Y.Wang (2015) Nonlinear vibration analysis of double-layered nanoplates with different boundary conditions. *Physics Letters A,* **379**(24-25), 1532–1537.

[95] S.Maia, H.Lieven, and S.Lin, and, U. (1997) Theoretical and Experimental Modal Analysis, Research Studies Press, Taunton, Somerset.

[96] L.Perko (2013) Differential equations and dynamical systems, Vol. 7, Springer Science & Business Media, .

[97] S.Wiggins (2003) Introduction to applied nonlinear dynamical systems and chaos, Vol. 2, Springer Science & Business Media, .

[98] W.D.Iwan (1973) A generalization of the concept of equivalent linearization. *International Journal of Non-linear mechanics,* **8**(3), 279–287.

[99] T.K.Caughey (1963) Equivalent linearization techniques. *The Journal of the Acoustical Society of America,* **35**(11), 1706–1711.

[100] J.Kevorkian and J.Cole, a. A. (1982) Perturbation methods in applied mathematics. *Bulletin of the American Mathematical Society,* **7**, 414–420.

[101] R.E.O'malley (1991) Singular perturbation methods for ordinary differential equations, Vol. 89, Springer, .

[102] J.K.Kevorkian and J.D.Cole (2012) Multiple scale and singular perturbation methods, Vol. 114, Springer Science & Business Media, .

[103] J.C.Golinval, G.Kerschen, V.Lenaerts, F.Thouverez, and P.Argoul (2003) Working Group 3—IDENTIFICATION of Non-Linear Systems. *Mechanical systems and signal processing,* **17**, 177–178.

[104] F.Al-Bender, W.Symens, J.Swevers, and Brussel, H. (2004) Theoretical analysis of the dynamic behavior of hysteresis elements in mechanical systems. *International journal of non-linear mechanics,* **39**(10), 1721–1735.

[105] M.Juntunen and J.Linjama (2003) Presentation of the VTT benchmark. *Mechanical systems and signal processing,* **17**(1), 179–182.

[106] F.Thouverez (2003) Presentation of the ECL benchmark. *Mechanical Systems and Signal Processing,* **17**(1), 195–202.

[107] F.M.Hemez and S.W.Doebling, INVERSION OF STRUCTURAL DYNAMICS SIMULATIONS: STATE-OF-THE-ART AND ORIENTATIONS OF RESEARCH. Technical report, Los Alamos National Lab., NM (US) (2000).

[108] G.Kerschen, Y.S.Lee, A.F.Vakakis, D.M.McFarland, and L.A.Bergman (2005) Irreversible passive energy transfer in coupled oscillators with essential nonlinearity. *SIAM Journal on Applied Mathematics,* **66**(2), 648–679.

[109] D.E.Adams and R.J.Allemang (2000) A Frequency Domain Method for Estimating the Parameters of a Non-Linear Structural Dynamic Model through Feedback. *Mechanical Systems and Signal Processing,* **14**(4), 637–656.

[110] C.M.Richards and R.Singh (1998) Identification of multi-degree of freedom non-linear systems under random excitation by the reverse path spectral method. *Journal of Sound and Vibration,* **213**(4), 673–708.

[111] S.Bellizzi, R.Bouc, M.Defilippi, and P.Guihot (1998) RESPONSE SPECTRAL DENSITIES AND IDENTIFICATION OF A RANDOMLY EXCITED NON-LINEAR SQUEEZE FILM OSCILLATOR. *Mechanical Systems and Signal Processing,* p. 693–711.

[112] S.Meyer and M.Link (2003) Modelling and Updating of Local Non-Linearities Using Frequency Response Residuals. *Mechanical Systems and Signal Processing,* **17**(1), 219–226.

[113] K.Kimura, K.Yagasaki, and Sakata, M. (1983) Non-Stationary Response of A System With BiLinear Hysteresis Subjected To Non-White Random Excitation. *Sound and Vibration,* **91**(2), 181–194.

[114] L.Socha and M.Pawleta (2001) Are Statistical Linearisation and Standard Equivalent Linearisation the Same Methods in the Analysis of Stochastic Dynamic Systems?. *Journal of Sound and Vibration,* **248**(2), 387–394.

[115] Y.S.Lee, A.F.Vakakis, D.M.McFarland, and L.A.Bergman (2010) A global-local approach to nonlinear system identification: A review. *Structural Control and Health Monitoring,* **17**(7), 742–760.

[116] S.Marchesiello and L.Garibaldi (2008) A time domain approach for identifying nonlinear vibrating structures by subspace methods. *Mechanical Systems and Signal Processing,* **22**(1), 81–101.

[117] G.Kerschen, C.Golinval, J., and K.Worden (2001) Theoretical and Experimental Identification of a Non-Linear Beam. *Journal of Sound and Vibration,* **244**(4), 597–613.

[118] A.M.Al-Hadid and J.R.Wright (1989) Developments in the force-state mapping technique for non-linear systems and the extension to the location of non-linear elements in a lumped-parameter system. *Mechanical Systems and Signal Processing,* **3**(3), 269–290.

[119] M.A.Al-Hadid and J.R.Wright (1992) Estimation of mass and modal mass in the identification of non-linear single and multiple degree of freedom systems using force-state mapping approach. *Journal of Mechanical Systems and Signal Processing,* **6**(4), 383–401.

[120] S.F.Masri and T.K.Caughey (1979) A nonparametric identification technique for nonlinear dynamic problems. *Journal of Applied Mechanics,* **46**, 433–447.

[121] S.F.Masri, R.K.Miller, and A.F.Saud (1987) Identification of Nonlinear Vibrating Structures. *Journal of Applied Mechanics,* **109**, 918–922.

[122] C.Meskell, J.A.Fitzpatrick, and H.J.Rice (2001) APPLICATION OF FORCE-STATE MAPPING TO A NON-LINEAR FLUID–ELASTIC SYSTEM. *Mechanical Systems and Signal Processing,* **15**(1), 75–85.

[123] M.Haroon, D.E.Adams, and Y.W.Luk (2005) A technique for estimating linear parameters using nonlinear restoring force extraction in the absence of an input measurement. *Journal of vibration and acoustics,* **127**(5), 483–492.

[124] G.Dimitriadis and J.E.Cooper (1998) A method for identification of non-linear multi-degree-of-freedom systems. *Proceedings of the Institution of Mechanical Engineers, Part G: Journal of Aerospace Engineering,* **212**(4), 287–298.

[125] J.W.Kimm and S.Y.Park (1994) Non-linear joint parameter identification by applying the force-state mapping technique in the frequency domain. *Mechanical systems and signal processing,* **8**(5), 519–529.

[126] M.Feldman (1994) Nonlinear System Vibration Analysis Using Hilbert Transform-1. Free Vibration Analysis Method 'FREEVIB'.. *Mechanical Systems and Signal Processing,* **8**(2), 119–127.

[127] M.Feldman (2007) Considering high harmonics for identification of non-linear systems by Hilbert transform. *Mechanical Systems and Signal Processing,* **21**(2), 943–958.

[128] N.E.Huang, e. a. (1998) The empirical mode decomposition and the Hilbert spectrum for nonlinear and non-stationary time series analysis. *Proceedings of the Royal Society of London. Series A: Mathematical, Physical and Engineering Sciences,* **454**(1971), 903–995.

[129] C.Mao, Y.Jiang, D.Wang, X.Chen, and J.Tao (2015) Modeling and simulation of non-stationary vehicle vibration signals based on Hilbert spectrum. *Mechanical Systems and Signal Processing,* **50-51**, 56–69.

[130] G.E.P.Box, G.M.Jenkins, G.C.Reinsel, and G.M.Ljung (2015) Time series analysis: forecasting and control, John Wiley & Sons, .

[131] K.Peng, Z., Q.Lang, Z., C.Wolters, A.Billings, S., and K.Worden (2011) Feasibility study of structural damage detection using NARMAX modelling and Nonlinear Output Frequency Response Function based analysis. *Mechanical Systems and Signal Processing,* **25**(3), 1045–1061.

[132] B.Moaveni and E.Asgarieh (2012) Deterministic-stochastic subspace identification method for identification of nonlinear structures as time-varying linear systems. *Mechanical Systems and Signal Processing,* **31**, 40–55.

[133] R.W.K.Chan, J.K.K.Yuen, E.W.M.Lee, and M.Arashpour (2015) Application of Nonlinear-Autoregressive-Exogenous model to predict the hysteretic behaviour of passive control systems. *Engineering Structures,* **85**, 1–10.

[134] M.Schetzen (1980) The Volterra and Wiener theories of nonlinear systems.

[135] A.A.Khan and N.S.Vyas (1998) Non-linear Parameter Estimation Using Volterra And Wiener Theories. *Sound and Vibration,* **221**, 805–821.

[136] A.A.Khan and N.S.Vyas (2000) Nonlinear bearing stiffness parameter estimation in flexible rotor-bearing systems using Volterra and Wiener approach. *Probabilistic Engineering Mechanics,* **16**, 137–157.

[137] I.Tawfiq and T.Vinh (2003) Contribution to the Extension of Modal Analysis to Non-Linear Structure Using Volterra Functional Series. *Mechanical Systems and Signal Processing,* **17**(2), 379–407.

[138] M.Haroon, D.E.Adams, Y.W.Luk, and A.A.Ferri (2005) A time and frequency domain approach for identifying nonlinear mechanical system models in the absence of an input measurement. *Journal of Sound and Vibration,* **283**(3-5), 1137–1155.

[139] A.Suzuki, K.Kamiya, and K.Yasuda (2006) Identification technique for nonlinear boundary conditions of a circular plate. *Journal of Sound and Vibration,* **289**(1-2), 130–147.

[140] B.F.Feeny, C.M.Yuan, and J.P.Cusumano (2001) Parametric Identification of an Experimental Magneto-Elastic Oscillator. *Journal of Sound and Vibration,* **247**(5), 785–806.

[141] H.J.Fitzpatrick and J.A.Rice (1990) A Procedure For The Identification of Linear And Non-linear Multi-Degree-of-Freedom System. *Sound and Vibration,* **149(3)**, 397–411.

[142] C.M.Richards and R.Singh (2000) Comparison of Two Non-Linear System Identification Approaches Derived from "Reverse Path" Spectral Analysis. *Journal of Sound and Vibration,* **237**(2), 361–376.

[143] D.Laxalde and F.Thouverez (2009) Complex non-linear modal analysis for mechanical systems: Application to turbomachinery bladings with friction interfaces. *Journal of Sound and Vibration,* **322**(4-5), 1009–1025.

[144] T.J.Chalko, P.N.HarilosJ, and V.Gershkovich (1996) Non-linear curve fitting for modal analysis. *Environmental Software,* **11**(1-3), 9–18.

[145] W.Szemplinska-stupnicka (1978) The Modified Single Mode Method in The Investigations of The Resonant Vibarations of Non-Linear Systems. *Sound and Vibration,* **63**(4), 475–489.

[146] A.N.Robertson, a. K. and K.F.Alvin (1998) Identification of structural dynamics models using wavelet-generated impulse response data. *Journal of vibration and acoustics,* **120**(1), 261–266.

[147] T.P.Le and P.Argoul (2004) Continuous wavelet transform for modal identification using free decay response. *Journal of sound and vibration,* **277**(1-2), 73–100.

[148] M.Boltežar and J.Slavič (2004) Enhancements to the continuous wavelet transform for damping identifications on short signals. *Mechanical Systems and Signal Processing,* **18**(5), 1065–1076.

[149] D.Spina, C.Valente, and G.R.Tomlinson (1996) A new procedure for detecting nonlinearity from transient data using the Gabor transform. *Nonlinear Dynamics,* **11**(3), 235–254.

[150] H.Franco and R.M.O.Pauletti (1997) Analysis of nonlinear oscillations by gabor spectrograms. *Nonlinear Dynamics,* **12**(3), 215–236.

[151] J.K.Hammond and P.R.White (1996) The analysis of non-stationary signals using time-frequency methods. *Journal of Sound and vibration,* **190**(3), 419–447.

[152] S.Bellizzi, P.Guillemain, and R.Kronland-Martinet (2001) Identification of coupled non-linear modes from free vibration using time-frequency representations. *Journal of Sound and Vibration,* **243**(2), 191–213.

[153] W.J.Staszewski (2000) Analysis of non-linear systems using wavelets. *Proceedings of the Institution of Mechanical Engineers, Part C: Journal of Mechanical Engineering Science,* **214**(11), 1339–1353.

[154] R.Ghanem and F.Romeo (2001) A wavelet-based approach for model and parameter identification of non-linear systems. *International Journal of Non-Linear Mechanics,* **36**(5), 835–859.

[155] M.Feldman and S.Braun (1995) Identification of non-linear system parameters via the instantaneous frequency: application of the hilbert transform and Wigner-Ville techniques. In *PROCEEDINGS-SPIE THE INTERNATIONAL SOCIETY FOR OPTICAL ENGINEERING* SPIE INTERNATIONAL SOCIETY FOR OPTICAL pp. 637–637.

[156] D.Goege (2003) Automatic updating of large aircraft models using experimental data from ground vibration testing. *Aerospace Science and Technology,* **7**, 33–45.

[157] H.G.Lee and B.J.Dobson (1991) The direct measurement of structural mass, stiffness and damping properties. *Journal of sound and vibration,* **145**(1), 61–81.

[158] .Sheinman, I. (1994) Damage Detection and Updating of Stiffness and Mass Matrices Using Mode Data. *Computer Structures,* **59**(1), 149–156.

[159] R.Schmidt (1994) Updating Non-Linear Components. *Mechanical System and Signal Processing,* **8**(6), 679–690.

[160] G.Kerschen and J.C.Golinval (2005) Generation of Accurate Finite Element Models of Nonlinear Systems – Application to an Aeroplane-Like Structure. *Nonlinear Dynamics,* **39**, 129–142.

[161] V.Lenaerts, G.Kerschen, and C.Golinval, J. (2001) Proper Orthogonal Decomposition for Model Updating of Non-Linear Mechanical Systems. *Mechanical Systems and Signal Processing,* **15**(1), 31–43.

[162] G.Kerschen On the Model Validation in Non-linear Structural Dynamics Thesis (2002).

[163] G.Cybenko (1989) Approximation by Superpositions of a Sigmoidal Function. *Mathematics of Control, Signals, and Systems,* pp. 303–314.

[164] Abdessalem, A. B., Dervilis, N., Wagg, D., and Worden, K. (2019) Model selection and parameter estimation of dynamical systems using a novel variant of approximate Bayesian computation. *Mechanical Systems and Signal Processing,* **122**, 364–386.

[165] Dervilis, N., Simpson, T. E., Wagg, D. J., and Worden, K. (2019) Nonlinear modal analysis via non-parametric machine learning tools. *Strain,* **55**(1), e12297.

[166] Q.Chen, K.Worden, P.Peng, and T.Leung, A. Y. (2007) Genetic algorithm with an improved fitness function for (N)ARX modelling. *Mechanical Systems and Signal Processing,* **21**(2), 994–1007.

[167] F.L.Lewis and S.Jagannathant (1996) Identification of Nonlinear Dynamical Systems Using Multilayered Neural Networks. *Automatica,* **32**, 1707–1712.

[168] S.K.Doherty, J.B.Gomm, and D.Williams (1995) Experiment Design Consideration For Non-Linear System Identification Using Neural Network.. *Computers chem. Engng,* **21**(3), 327–346.

[169] A.DelliCarri, B.Weekes, D.DiMaio, and D.J.Ewins (2016) Extending modal testing technology for model validation of engineering structures with sparse nonlinearities: A first case study. *Mechanical Systems and Signal Processing,*.

[170] E.Zhang, J.Antoni, R.Pintelon, and J.Schoukens (2010) Fast detection of system nonlinearity using nonstationary signals. *Mechanical Systems and Signal Processing,* **24**(7), 2065–2075.

[171] A.Hot, G.Kerschen, E.Foltête, and S.Cogan (2012) Detection and quantification of nonlinear structural behavior using principal component analysis. *Mechanical Systems and Signal Processing,* **26**, 104–116.

[172] J.Schoukens, R.Pintelon, Y.Rolain, and T.Dobrowiecki (2001) Frequency response function measurements in the presence of nonlinear distortions. *Automatica,* **37**(6), 939–946.

[173] M.Simon and G.R.Tomlinson (1984) Use of the Hilbert Transform in modal analysis of linear and non-linear structures. *Journal of Sound and Vibration,* **96**(4), 421–436.

[174] V.Lenaerts, G.Kerschen, and J.C.Golinval (2003) Identification of a continuous structure with a geometrical non-linearity. Part II: Proper orthogonal decomposition. *Journal of Sound and vibration,* **262**(4), 907–919.

[175] K.S.Mohammad, K.Worden, and G.R.Tomlinson (1992) Direct parameter estimation for linear and nonlinear structures. *Journal of Sound and Vibration,* **152**(3), 471–499.

[176] P.Muhamad, N.D.Sims, and K.Worden (2012) On the orthogonalised reverse path method for nonlinear system identification. *Journal of Sound and Vibration,* **331**(20), 4488–4503.

[177] <Ordinary Differential Equations-App-A.pdf>.

[178] D.R.Roettgen and M.S.Allen (2017) Nonlinear characterization of a bolted, industrial structure using a modal framework. *Mechanical Systems and Signal Processing,* **84**, 152–170.

[179] J.Paduart, L.Lauwers, J.Swevers, K.Smolders, J.Schoukens, and R.Pintelon (2010) Identification of nonlinear systems using Polynomial Nonlinear State Space models. *Automatica,* **46**(4), 647–656.

[180] J.P.Noel, A.F.Esfahani, G. and J.Schoukens (2017) A nonlinear state-space approach to hysteresis identification. *Mechanical Systems and Signal Processing,* **84**, 171–184.

[181] A.Svensson and T.B.Schön (2017) A flexible state–space model for learning nonlinear dynamical systems. *Automatica,* **80**, 189–199.

[182] A.E.Fakhrizadeh, P.Dreesen, K.Tiels, J.P.Noël, and J.Schoukens (2018) Parameter reduction in nonlinear state-space identification of hysteresis. *Mechanical Systems and Signal Processing,* **104**, 884–895.

[183] R.Relan, K.Tiels, A.Marconato, P.Dreesen, and J.Schoukens (2018) Data driven discrete-time parsimonious identification of a nonlinear state-space model for a weakly nonlinear system with short data record. *Mechanical Systems and Signal Processing,* **104**, 929–943.

[184] J.Decuyper, Troyer, T., C.Runacres, M., K.Tiels, and J.Schoukens (2018) Nonlinear state-space modelling of the kinematics of an oscillating circular cylinder in a fluid flow. *Mechanical Systems and Signal Processing,* **98**, 209–230.

[185] L.Ljung and T.Söderström (1983) Theory and practice of recursive identification, MIT press, .

[186] P.Eykhoff (1974) System identification: parameter and state estimation.

[187] R.RMohler and W.J.Kolodziej (1980) An overview of bilinear system theory and applications. *IEEE Transactions on Systems, Man and Cybernetics,* **10**(10), 683–688.

[188] E.Sontag (1979) Realization theory of discrete-time nonlinear systems: Part I-The bounded case. *IEEE Transactions on Circuits and Systems,* **26**(5), 342–356.

[189] W.J.Rugh (1981) Nonlinear system theory, Johns Hopkins University Press Baltimore, .

[190] V.Verdult (2002) Non linear system identification: a state-space approach.

[191] J.A.K.Suykens, J.P.L.Vandewalle, and B.L.DeMoor (2012) Artificial neural networks for modelling and control of non-linear systems, Springer Science & Business Media, .

[192] J.A.K.Suykens, B.L.R.DeMoor, and J.Vandewalle (1995) Nonlinear system identification using neural state space models, applicable to robust control design. *International Journal of Control,* **62**(1), 129–152.

[193] R.Pintelon, J.Schoukens, G.Vandersteen, and K.Barbé (2010) Estimation of nonparametric noise and FRF models for multivariable systems—Part I: Theory. *Mechanical Systems and Signal Processing,* **24**(3), 573–595.

[194] R.Pintelon (2002) Frequency-domain subspace system identification using non-parametric noise models. *Automatica,* **38**, 1295–1311.

[195] D.W.Marquardt (1963) An Algorithm for Least-Squares Estimation of Nonlinear Parameters. *Society for Industrial and Applied Mathematics,* **11**(2), 431–441.

[196] R.Pintelon and J.Schoukens (2012) System Identification: A Frequency Domain Approach, Wiley-IEEE Press, .

[197] R.Pintelon, J.Schoukens, G.Vandersteen, and K.Barbé (2010) Estimation of nonparametric noise and FRF models for multivariable systems—Part II: Extensions, applications. *Mechanical Systems and Signal Processing,* **24**(3), 596–616.

[198] T.P.Dobrowiecki and Schoukens, J. (2007) Linear Approximation of Weakly Nonlinear MIMO Systems. *IEEE Transactions on Instrumentation and Measurement,* **56**(3), 887–894.

[199] J.Schoukens, G.Vandersteen, K.Barbé, and R.Pintelon (2009) Nonparametric Preprocessing in System Identification: a Powerful Tool. *European Journal of Control,* **15**(3-4), 260–274.

[200] T.Glad and L.Ljung (2000) Control Theory Multivariable and Nonlinear Methods, Taylor and Francis, London.

[201] S.B.Cooper, D.DiMaio, I.Sever, and S.Patsias An Experimental Case Study for Nonlinear Model Validation: Effects of Nonlinearities in an Aero-Engine Structure. In *35th International Modal Analysis Conference (IMAC)* Society for Experimental Mechanics.

[202] B.Weekes and D.J.Ewins (2015) Multi-frequency, 3D ODS measurement by continuous scan laser Doppler vibrometry. *Mechanical Systems and Signal Processing,* **58-59**, 325–339.

[203] Bertsimas, D., Tsitsiklis, J., et al. (1993) Simulated annealing. *Statistical science,* **8**(1), 10–15.

[204] Lynch, B. J. (2006) Optimizing with Genetic Algorithms. *Minesota supercomputing institute, Feb,*.

[205] B.R.Rich (1995) Clarence Leonard (Kelly) Johnson: 1910–1990: A Biographical Memoir. *Biographical Memoirs,* **67**, 221–241.

[206] Sjöberg, J. (2000) A nonlinear grey-box example using a stepwise system identification approach. In *Proceedings of the 11th IFAC Symposium on Identification, Santa Barbara, USA*.

[207] Ljung, L., Zhang, Q., Lindskog, P., and Juditski, A. (2004) Estimation of grey box and black box models for non-linear circuit data. *IFAC Proceedings Volumes,* **37**(13), 399–404.

[208] J.P.Noël, G.Kerschen, E.Foltête, and S.Cogan (2014) Grey-box identification of a non-linear solar array structure using cubic splines. *International Journal of Non-Linear Mechanics,* **67**, 106–119.

[209] Adams, D. and Allemang, R. (1999) A new derivation of the frequency response function matrix for vibrating non-linear systems. *Journal of Sound and Vibration,* **227**(5), 1083–1108.

[210] D.E.Adams and R.J.Allemang (1999) Characterisation of nonlinear vibrating systems using internal feedback and frequecy response modulation. *Journal of Vibration and Acoustics,* **121**, 495–500.

[211] K.Worden, D.Hickey, M.Haroon, and D.E.Adams (2009) Nonlinear system identification of automotive dampers: A time and frequency-domain analysis. *Mechanical Systems and Signal Processing,* **23**(1), 104–126.

[212] Marchesiello, S. and Garibaldi, L. (2008) Identification of clearance-type nonlinearities. *Mechanical Systems and Signal Processing,* **22**(5), 1133–1145.

[213] Noël, J.-P., Marchesiello, S., and Kerschen, G. (2014) Subspace-based identification of a nonlinear spacecraft in the time and frequency domains. *Mechanical Systems and Signal Processing,* **43**(1-2), 217–236.

[214] Glad, T. and Ljung, L. (2014) Control theory, CRC press, .

[215] Tocino, A. and Ardanuy, R. (2002) Runge–Kutta methods for numerical solution of stochastic differential equations. *Journal of Computational and Applied Mathematics,* **138**(2), 219–241.

[216] Gavin, H. (2001) Numerical integration for structural dynamics. *Department of Civil and Environmental Engineering, Duke University: Durham, NC, USA,*.

[217] Rong, Z., Yuewu, L., and Fuxin, Z. (2003) Numerical solutions for the transient flow in the homogenous closed circle reservoirs. *Acta Mechanica Sinica,* **19**(1), 40–45.

[218] Janiszowski, K. B. (1993) A modification and the Tustin approximation. *IEEE transactions on Automatic Control,* **38**(8), 1313–1316.

[219] Van Der Houwen, P., Sommeijer, B., and Kok, J. (1997) The iterative solution of fully implicit discretizations of three-dimensional transport models. *Applied numerical mathematics,* **25**(2-3), 243–256.

[220] Pintelon, R. and Schoukens, J. (2004) System Identification: A Frequency Domain Approach, Wiley, .

[221] Bozdogan, H. (1987) Model selection and Akaike's information criterion (AIC): The general theory and its analytical extensions. *Psychometrika,* **52**(3), 345–370.

[222] Sclove, S. L. (1987) Application of model-selection criteria to some problems in multivariate analysis. *Psychometrika,* **52**(3), 333–343.

[223] Al-Muthairi, N., Bingulac, S., and Zribi, M. (2002) Identification of discrete-time MIMO systems using a class of observable canonical-form. *IEE Proceedings-Control Theory and Applications,* **149**(2), 125–130.

[224] Ljung, L. (1995) Building models from frequency domain data. In *Adaptive Control, Filtering, and Signal Processing* pp. 229–239 Springer.

[225] Jain, P., Kar, P., et al. (2017) Non-convex optimization for machine learning. *Foundations and Trends® in Machine Learning,* **10**(3-4), 142–336.

[226] Westwick, D. T. and Schoukens, J. (2012) Classification of the poles and zeros of the best linear approximations of wiener-hammerstein systems. *IFAC Proceedings Volumes,* **45**(16), 470–475.

[227] Ljung, L. (1999) System identification. *Wiley Encyclopedia of Electrical and Electronics Engineering,* pp. 1–19.

[228] Schoukens, J., Vaes, M., and Pintelon, R. (2016) Linear system identification in a nonlinear setting: Nonparametric analysis of the nonlinear distortions and their impact on the best linear approximation. *IEEE Control Systems Magazine,* **36**(3), 38–69.

[229] Hernández, S., Menga, E., Moledo, S., Romera, L., Baldomir, A., López, C., and Montoya, M. C. (2017) Optimization approach for identification of dynamic parameters of localized joints of aircraft assembled structures. *Aerospace Science and Technology,* **69**, 538–549.

[230] P.Noël, J., L.Renson, and G.Kerschen (2014) Complex dynamics of a nonlinear aerospace structure: Experimental identification and modal interactions. *Journal of Sound and Vibration,* **333**(12), 2588–2607.

[231] D.A.Czaplewski, C.W.Dyck, H.Sumali, J.E.Massad, J.D.Kuppers, L.Reines, W.D.Cowan, and C.P.Tigges (2006) A soft landing waveform for actuation of a single pole single throw Ohmic RF MEMs switch. *Journal of Micromechanical Systems,* **15**, 1586–1594.

[232] D.J.Segalman, D.L.Gregory, M.J.Starr, B.R.Resor, M.D.Jew, J.P.Lauffer, and N.M.Ames, Handbook on Dynamics of Jointed Structures. Report, Sandia National Laboratories (2009).

[233] C.Croufer and A.Santangelo Modern Solutions for Ground Vibration and Modal Survey Testing$_{LMS}$. *In LMS Ground Vibration Test Workshop*.

[234] C.Roberts, D. (2016) Multi-axis vibration testing of an aerodynamically excited structure. *Journal of Vibration and Control,*.

[235] Kragh, K. A., Thomsen, J. J., and Tcherniak, D. (2010) Experimental detection and quantification of structural nonlinearity using homogeneity and hilbert transform methods. In *ISMA2010: International conference on Noise and Vibration Engineering*.

[236] M.Feldman (2011) Hilbert transform in vibration analysis. *Mechanical Systems and Signal Processing,* **25**(3), 735–802.

[237] Li, Z. and Crocker, M. J. (2006) A Study of Joint Time-Frequency Analysis-Based Modal Analysis. *IEEE Transactions on Instrumentation and Measurement,* **55**, 2335–2342.

[238] Nagarajaiah, S. and Basu, B. (2009) Output only modal identification and structural damage detection using time frequency & wavelet techniques. *Earthquake Engineering and Engineering Vibration,* **8**(4), 583–605.

[239] Neild, S., McFadden, P., and Williams, M. (2003) A review of time-frequency methods for structural vibration analysis. *Engineering Structures,* **25**(6), 713–728.

[240] FEMtools Dynamic Design Solutions (DDS) NV. (2007).

[241] R.Pascual, J.Golinval, and M.Razeto A frequency domain correlation technique for model correlation and updating. In *Proceedings -SPIE The International Society for Optical Engineering* pp. 587–592.

[242] W.Heylen and S.Lammens FRAC: A Consistent way of Comparing Frequency Response Functions. In *International Conference on Identification in Engineering*.

[243] T.Dossogne, J.P.Noel, C.Grappasonni, G.Kerschen, B.Peeters, J.Debille, and M.Vaes, J. Nonlinear Ground Vibration Identification of an F-16 Aircraft - Part II Understanding Nonlinear Behaviour in Aerospace Structures Using Sine-sweep Testing. In *International Forum on Aeroelasticity and Structural Dynamics*.

[244] J.P.Noel A Frequency-domain Approach to Subspace Identification of Nonlinear Systems Thesis (2014).

[245] S.F.Masri, J.P.Caffrey, T.K.Caughey, A.W.Smyth, and A.G.Chassiakos (2004) Identification of the state equation in complex non-linear systems. *International Journal of Non-Linear Mechanics,* **39**(7), 1111–1127.

[246] M.Feldman (1994) Non-Linear System Vibration Analysis Using Hilbert Transform-II. Forced Vibration Analysis Method 'FORCEVIB'.. *Mechanical Systems and Signal Processing,* **8**(3), 309–318.

[247] S.F.Masri, G.A.Bekey, and H.Sassi (1982) Non-parameter identification of a class of non-linear multidegree dynamic systems. *Journal of Earthquake Engineering Structural Dynamics,* **10**, 1–30.

[248] S.B.Cooper, D.DiMaio, and D.J.Ewins (2017) Integration of system identification and finite element modelling of nonlinear vibrating structures. *Journal of Mechanical Systems and Signal Processing,* **102**, 401–430.

[249] M.Feldman (2006) Time-varying vibration decomposition and analysis based on the Hilbert transform. *Journal of Sound and Vibration,* **295**(3-5), 518–530.

[250] D.J.Rixen (2004) A dual Craig–Bampton method for dynamic substructuring. *Journal of Computational and Applied Mathematics,* **168**(1-2), 383–391.

[251] J.E.Mottershead and M.I.Friswell (1993) Model Updating in Structural Dynamics: A Survey. *Sound and Vibration,* **167**(2), 347–375.

[252] R.M.Lacayo, B.J.Deaner, and M.S.Allen (2017) A numerical study on the limitations of modal Iwan models for impulsive excitations. *Journal of Sound and Vibration,* **390**, 118–140.

[253] S.Ebbesen, P.Kiwitz, and L.Guzzella (2012) A generic particle swarm optimization Matlab function. In *2012 American Control Conference (ACC)* IEEE pp. 1519–1524.